

Uniaxial and Viscoelastic Properties of SPI and SPI-Polysaccharide Gels

by

Haniye Abdi Kordlar

A thesis
presented to the University of Waterloo
in fulfillment of the
thesis requirement for the degree of
Master of Applied Science
in
Chemical Engineering

Waterloo, Ontario, Canada, 2022

© Haniye Abdi Kordlar 2022

Author's Declaration

This thesis consists of material all of which I authored or co-authored: see Statement of Contributions included in the thesis. This is a true copy of the thesis, including any required final revisions, as accepted by my examiners.

I understand that my thesis may be made electronically available to the public.

Statement of Contributions

Haniye Abdi Kordlar was the sole author of all Chapters which were written under the supervision of Dr. Christine Moresoli with the following content for chapter 3 to chapter 5:

Research presented in Chapter 3: This research was conducted at the University of Waterloo by Haniye Abdi Kordlar under the supervision of Dr. Christine Moresoli. Haniye Abdi Kordlar analyzed data from past publications and completed the writing of the chapter.

Research presented in Chapter 4: This research was conducted at the University of Waterloo by Haniye Abdi Kordlar under the supervision of Dr. Christine Moresoli. Haniye Abdi Kordlar completed the preparation of the gels, the design of the experiments, the visual observation of the gels, the data analysis and the writing of the chapter.

Research presented in Chapter 5: This research was conducted at the University of Waterloo by Haniye Abdi Kordlar and Jing Sy under the supervision of Dr. Christine Moresoli. Haniye Abdi Kordlar completed the preparation of the gels, the design of the experiments, the data analysis, and the writing of the chapter. Jing Sy conducted the experimentation of the uniaxial compression tests and the viscoelastic tests of the gels.

Abstract

Nowadays, consumption of soy-based products is increasing due to their appealing nutritional profile, affordability, health benefits, and potential to serve as a suitable substitute for dairy-based foods. Textural property is one of the most significant aspects to consider when evaluating the quality of soy protein gels. Textural characteristics of soy-based foods might be improved by using a good selection of ingredients, such as a source of soy protein, coagulants, or other additions like polysaccharides, as well as the experimental conditions, such as heating and coagulation temperature and duration. Variation in the temperature and duration of gelation along with the soy protein sources could result in the production of soy gels with a wide hardness range-from very soft to firm and hard gels.

The goal of this study was to assess the textural characteristics of citric acid-induced soy protein gels, with a particular emphasis on the type and concentration of soy protein sources and polysaccharides. This goal will be achieved by the use of uniaxial compression and viscoelastic properties. The uniaxial compression properties, e.g. fracture stress, fracture strain, and Young's modulus, could give insight about the gel strength, firmness, and hardness of a gel. On the other hand, the viscoelastic properties, e.g. storage and loss modulus, could provide information about the viscoelasticity and stiffness of a gel.

First, the kinetic of soy protein gelation was analyzed quantitatively for three soy protein sources, 11S, Soy Protein Isolate (SPI), and dried soymilk, under varied conditions, such as heating temperature. The results indicate that SPI gels had a moderate rate of gelation (it was somewhere between 11S and dried soymilk gelation rate) and might achieve higher stiffness (higher G'_0) than both dried soymilk and 11S. G'_0 is a storage modulus of a gel at the end of the gelation process at the coagulation temperature. As a result, SPI might be chosen as a soy protein source to produce gels with improved viscoelastic characteristics and increased stiffness. In addition, higher rate was observed when heating temperature was increased. Therefore, 95° C as a heating temperature was selected for the subsequent experimental works.

Second, by selecting the SPI as a source of soy protein, citric acid-induced SPI gel was generated. Citric acid was selected as it can generate soy protein gels with similar viscoelastic and textural properties of conventional tofu. The effect of different heating durations, citric acid concentrations, coagulation durations, citric acid states (liquid or solid), and citric acid addition methods on the strength of 8% w/v SPI gel were then visually investigated. The visual observations include analyzing the appearance of a gel (how watery or solid-like material is that) and the ability of a gel to be shaped and hold. According to the findings, the gel with the highest gel strength (deduced from pressing

the gel at $g.cm^{-2}$ for 10 minutes) was created with 0.3% w/v citric acid, when citric acid powder was added to the pre-heated SPI solution at 95° C for 30 minutes while constantly stirring, followed by coagulating at 80° C for 60 minutes.

Third, based on the Box-Behnken design, the 0.3% w/v citric acid-induced SPI-polysaccharide gels were created with 8% w/v SPI, 0-4% w/v inulin (I), 0-0.2% w/v starch (S), 0-0.1% w/v guar gum (G), and a mixture of those. The Box-Behnken design was used to assess the dependence of uniaxial and viscoelastic properties to the type and concentration of polysaccharides. Furthermore, starch, inulin, and guar gum can contribute to the SPI gel network and create a gel with higher firmness and viscoelasticity. Mechanical and rheological measurements were taken to determine the texture of SPI-polysaccharide gels. The mechanical and rheological properties analysis revealed that SPI gels containing only one type of polysaccharide (SPI-2% I, SPI-0.1% S, and SPI-0.05% G) can produce much tougher gels with higher gel strength, hardness, and stiffness and superior viscoelastic properties than SPI gel alone. Furthermore, inulin and starch may work synergistically, and their combination (SPI-4% I-0.1% S and SPI-2% I-0.2% S) could be employed to create gels with greater mechanical strength than SPI gel. Gels containing guar gum in combination with inulin, starch, or both, on the other hand, had significantly lower stress fracture point, Young's modulus, storage modulus, and loss modulus than SPI gel. So, inulin, starch, guar gum, or a combination of starch and inulin might be used to produce harder citric acid induced SPI gels with improved mechanical strength and viscoelasticity.

Acknowledgements

I would like to thank my supervisor, Prof. Christine Moresoli, for her guidance and support. She is a very good exemplar of the researcher and always inspires me to think more logically and precisely. I have learned a lot from her and knowledge in the field. Professor Moresoli always took the extra step to show her care to my current and future success.

I would like to thank Prof. Alexander Penlidis and Prof. Tizazu Mekonnen for being the readers of this thesis and giving me valuable comments and suggestions. I wish to thank Prof. Tizazu Mekonnen for his great advice and help in the project.

I would like to especially thank my friend and colleague who have helped and inspired me to enjoy being in Waterloo. My deepest thanks go to Ms. Jing Sy.

Finally, and the most important, I would like to express my deep appreciation to my husband, Mr. Ahmad Sajedi, and my family, Mrs. Nahid Aali, Mr. Masoud Mohammadian, and Mr. Hamed Abdi for their endless support, patience, understanding and their true love.

Dedication

To my mother, Nahid, and the soul of my father, Abdallah

&

my dear love Ahmad

Table of Contents

List of Figures	xiii
List of Tables	xxi
List of Abbreviations	xxv
List of Symbols	xxvii
1 Introduction	1
1.1 Research Motivation	1
1.2 Research Objectives	4
1.3 Thesis Structure	6
2 Background	8
2.1 Soybean	8
2.1.1 Soybean composition and processing	8
2.1.2 Soybean Proteins	9
2.2 Gel	13
2.2.1 Gel Formation	13
2.2.2 Soy Protein Gelation	13
2.2.2.1 Soy Protein Gelation by Thermal Treatment	14
2.2.2.2 Soy Protein Gelation by Salt Addition	15

2.2.2.3	Soy Protein Gelation by Acid Addition	17
2.2.2.4	Soy Protein Gelation by Enzyme Addition	18
2.2.3	SPI-Emulsion Gels	19
2.3	Hydrocolloids	20
2.3.1	Starch	21
2.3.2	Guar gum	22
2.3.3	Inulin	24
2.4	Cheese	25
2.4.1	Cheese Products and Regulations	25
2.4.2	Mozzarella Cheese	25
2.4.3	Paneer	26
2.4.4	Halloumi Cheese	27
2.4.5	Cheese Substitutes	27
2.4.6	Soy Cheese	29
2.5	Market Analysis of Plant Food Products	29
2.6	Uniaxial Properties	30
2.6.1	Properties and Definitions	30
2.6.2	Uniaxial compression properties of plant-based protein gels	31
2.6.3	Uniaxial compression properties and food texture	34
2.7	Rheological Properties	37
2.7.1	Properties and Definitions	37
2.7.2	Viscoelasticity	38
2.7.3	Determination of Viscoelastic Characteristics	39
2.7.3.1	Amplitude Sweep Test	39
2.7.3.2	Frequency Sweep Test	39
2.7.3.3	Temperature Sweep Test	40
2.7.4	Gelation Kinetics	41

2.7.5	Viscoelasticity of soy protein gel	42
2.7.5.1	Salt-Induced Soy Protein Gel	44
2.7.5.2	Acid-Induced Soy Protein Gel	44
2.8	Multi Comparison Tests	45
3	Gelation Kinetics	48
3.1	Overview	48
3.2	Methodology	50
3.2.1	Data Extraction	51
3.2.2	Estimation of the Gelation Kinetics Parameters by Least-Squares .	53
3.3	Gelation Kinetics and Storage Modulus	55
3.3.1	Effect of Temperature and Soy Protein Source on Gelation Kinetics	55
3.3.2	Effect of Coagulant Type and Concentration on Gelation Kinetics .	58
3.3.3	Effect of Soy Protein Isolate (SPI) Concentration on Gelation Kinetics	61
3.3.4	Gelation Kinetics of SPI and SPI-Emulsion Gels	62
3.3.5	Effect of Homogenization Pressure on Gelation Kinetics	64
3.4	Conclusion	66
4	Citric Acid-Induced SPI Gels	67
4.1	Overview	67
4.2	Materials and Methods	67
4.2.1	Materials	67
4.2.2	Soy Protein Isolate (SPI) Solution Preparation	67
4.2.3	Gel Preparation	68
4.2.4	Visual Observation of the SPI Citric Acid Gels	70
4.3	Results and Discussion	70
4.3.1	Heating Duration	70
4.3.2	Coagulation Duration	72

4.3.3	Citric Acid State	72
4.3.4	Citric Acid Addition Methododology	74
4.3.5	Citric Acid Concentration	75
4.4	Gel Shaping by Pressing	78
4.5	Classification of Gels	78
5	SPI Gels Containing Polysaccharides	81
5.1	Overview	81
5.2	Materials	81
5.3	Methodology	82
5.3.1	Gel Preparation	82
5.3.1.1	SPI or SPI-Polysaccharide Solution	82
5.3.1.2	SPI or SPI-Polysaccharide Gel	82
5.3.2	Initial Observations	83
5.3.3	Uniaxial Compression Properties	83
5.3.4	Viscoelastic Behaviour	84
5.3.5	Experimental Design	85
5.3.6	Statistical Analysis	87
5.4	Results and Discussion	87
5.4.1	Initial Observations	87
5.4.2	Uniaxial Compression Properties	90
5.4.2.1	Estimation of Young's Modulus	90
5.4.2.2	Uniaxial Compression Properties of SPI and SPI-P gels- Estimation Method Based on Mean of Replicates	95
5.4.2.3	Uniaxial Compression Properties of SPI Citric Acid Gels with Combinations of Polysaccharides	103
5.4.2.4	Quadratic Model Fitting	109
5.4.3	Viscoelastic Properties	117

5.4.3.1	Viscoelastic properties of SPI and SPI-P gels-Estimation Method Based on Mean of Replicates	117
5.4.3.2	Viscoelastic properties of SPI-Mixed polysaccharide gels	123
5.4.3.3	Quadratic model fitting	133
5.5	Effect of Polysaccharide Addition on SPI Citric Acid Gels	145
6	Conclusion and Recommendations	146
6.1	Conclusion	146
6.2	Recommendations	148
	Letters for Copyright Permission	150
	References	165
	APPENDICES	177
A		178
A.1	Calculation of Stress, Strain, and Young Modulus	178

List of Figures

1.1	Flow chart of project with steps and associated details. The project steps are outlined in the left column, and the brief specifics of what conditions/ingredients/methods were researched in each stage are mentioned in the right column. In this figure, “P” represents polysaccharide.	6
2.1	Schematic of a soybean oil body, which includes a matrix of triglyceride (in blue) enclosed by a layer of phospholipids (red) and oleosins (yellow) [42]. The permission to use the image was obtained. See Appendix 6.1.	10
2.2	Schematic diagram of glycinin molecule consisting of acidic, A, and basic, B, subunits [45]. The permission to use the image was obtained. See Appendix 6.2.	11
2.3	Proposed schematic representation of four steps of gelation of SPI during heating in an aqueous environment [55]. The permission to use the image was obtained. See Appendix 6.4.	14
2.4	Mechanism of soymilk gel formation [42]. The permission to use the image was obtained. See Appendix 6.1.	16
2.5	Schematic representation of the influence of NaCl concentration on the particle aggregation of SPI in the emulsion [54]. The permission to use the image was obtained. See Appendix 6.5.	17
2.6	Schematic representation of two emulsion-filled gels. a) oil droplets behave as active filler particles, b) oil droplets behave as inactive filler particles [69]. The permission to use the image was obtained. See Appendix 6.6.	20
2.7	Molecular structure of amylopectin (a) and amylose (b) of starch.	21
2.8	Molecular structure of guar gum.	23
2.9	Molecular structure of inulin.	24

2.10	Types of cheese substitutes [82]. The permission to use the graph was obtained. See Appendix 6.8.	28
2.11	The true stress-strain curve for a soft gel material. The fracture stress and fracture strain points are shown with filled circles, and the Young's modulus is calculated as the slope of the short dashed line. More information about the estimation of Young's modulus will be presented in Chapter 5.	32
2.12	The Force-Deformation of commercial firm and soft tofu [90]. The permission to use the image was obtained. See Appendix 6.14.	34
2.13	A typical TPA curve and the definition/calculation for each TPA characteristic [87]. The permission to use the image was obtained. See Appendix 6.15.	36
2.14	: G'' and G' as a function of shear stress showing linear viscoelastic region (LVR), yield stress, and flow point.	40
3.1	Experimental storage modulus reported by Koyama et al. (1995) [102] for 5% SPI at 70°C coagulated with 30 mM $CaSO_4$ or 20 mM Glucono δ -Lactone (GDL) at frequency of 1 Hz and amplitude of 25 μm . The permission to use the graph was obtained. See Appendix 6.9.	50
3.2	Temperature-sweep test results for the storage modulus (G') as a function of time obtained during temperature sweep at 1 Hz frequency and 1% strain for 75 $g.l^{-1}$ SPI and 3.5 $g.l^{-1}$ $CaSO_4$ concentration, containing different soy oil volume fractions (0% v/v: —; 1% v/v: ·····; 3% v/v: - - - - -; 5% v/v: - - - - -; 7% v/v: - - - - -) [68]. The permission to use the image was obtained. See Appendix 6.10.	51
3.3	WebPlotDigitizer screenshots for selecting plot type (a), aligning axis (b), and calibration (c) [109]	52
3.4	Left: published G' vs time profile for SPI-emulsion gels for the heating and incubation step reported by Zhao et al. (2020) (0% v/v: —; 1% v/v: ·····; 3% v/v: - - - - -; 5% v/v: - - - - -; 7% v/v: - - - - -) [68]. The bottom red rectangle in the left figure was digitized. Right: Generated digitized profile of G' vs time of the SPI-emulsion gels data from Zhao et al. (2020).	53
3.5	Observed and predicted G' vs time for set 2 of initial values (Table 3.2) for the gelation kinetics of SPI gel (0% oil volume fraction from Zhao et al. (2020) [68].	55

3.6	Estimated gelation kinetic rate constant (k) at three different temperatures for three sources of soy protein (11S (Kohyama et al. 1992 [101]), SPI (Kohyama et al. (1995) [102]), and dried soy milk (Chang et al. (2009) [15])).	57
3.7	G'_{sat} estimates for gelation kinetics according to temperature and two sources of soy protein (SPI, coagulant: $CaSO_4$ (Kohyama et al. (1995) [102], and dried soy milk, coagulant: GDL (Chang et al. (2009) [15])).	58
3.8	t_0 estimates of the gelation kinetics with GDL according to temperature for two different sources of soy protein (11S (Kohyama et al. (1992) [101] and dried soy milk (Chang et al. (2009) [15])).	58
3.9	G'_{sat} and k values for 5% (the unit was not mentioned) SPI-gels prepared with various concentration of $CaSO_4$. According to Kohyama et al. (1995) [102], the constant temperature was selected for the rheological set-up at frequency of 1 Hz and amplitude of 25 μm . Permission to use the data was obtained. See Appendix 6.9.	59
3.10	Estimated gelation rate constant (k) for 5% (units were not mentioned) SPI-gels prepared with two different coagulant (30 mM $CaSO_4$ or 20 mM GDL) and different temperatures. The rheological measurements were done at frequency of 1 Hz and amplitude of 25 μm [102].	60
3.11	G'_{sat} values for 5% (units were not mentioned) SPI-gels prepared with two different coagulant (30 mM $CaSO_4$ or 20 mM GDL) in different temperatures. According to Kohyama et al. (1995) [102], the constant temperature was selected for the rheological set-up at frequency of 1 Hz and amplitude of 25 μm .	61
3.12	Gelation mechanism of soy proteins with GDL or $CaSO_4$: (circles) protein molecules; (black areas) hydrophobic regions [102]. Permission to use the data was obtained. See Appendix 6.9.	62
3.13	Digitalized gelation curve for 75 $g.l^{-1}$ SPI-soy oil emulsion gels with 3.5 $g.l^{-1}$ $CaSO_4$ during heating (25°C to 90°C) and incubation (90°C) at frequency of 1 Hz and strain of 1% for 0% v/v, 3% v/v, and 7% v/v of oil. Details of the digitalized curve are presented in Table 3.8.	63
3.14	Experimental profile of G' with the time at different homogenization pressure for SPI soy oil emulsion gel with 4.5% (w/w) SPI, 4.5% (w/w) soy oil, and 2% GDL. Gelation process was done at frequency of 1 Hz and strain of 0.5% [13]. Permission to use the image was obtained. See Appendix 6.13.	65

4.1	SPI citric acid gels obtained with 0.2% $w.v^{-1}$ citric acid according to heating and coagulation conditions in Table 4.1.	71
4.2	Gels produced with 8% $w.v^{-1}$ SPI and 0.2% $w.v^{-1}$ citric acid and two coagulation duration at 95°C, as stated in Table 4.3.	73
4.3	Gels produced with 8% $w.v^{-1}$ SPI and 0.2% $w.v^{-1}$ citric acid for citric acid powder or solution, with and without SPI heating and two different coagulation temperatures for 10 minutes (Table 4.1)	74
4.4	Gels produced with 8% $w.v^{-1}$ SPI and 0.2% $w.v^{-1}$ citric acid with and without SPI heating, different coagulation conditions for 30 minutes duration and two methods of citric acid addition (Table 4.1).	75
4.5	SPI samples at 60 min coagulation duration with 0.2 - 0.4% $w.v^{-1}$ citric acid anhydrous.	77
4.6	0.3% $w.v^{-1}$ citric acid induced SPI gel, a) sectional view of a gel, b) shaped gel with apple cutter.	78
5.1	Schematic diagram for the preparation of SPI and SPI-Polysaccharide (SPI-P) solution.	82
5.2	Schematic diagram for the preparation of SPI and SPI-P citric acid gels.	83
5.3	SPI and SPI-P citric acid gels of cylindrical shape with diameter and height of 1 mm (compositions summarized in Table 5.1).	89
5.4	Stress-strain curve for gels (a) SPI, SPI-2I, SPI-0.1S, SPI-0.05G and (b) SPI-0.05G, SPI-4I-0.05G, SPI-0.2S-0.05G, SPI-4I-0.2S-0.05G citric acid gels. The median replicate curve of each gel was selected for Young's modulus, fracture stress, and fracture strain estimation. The average of replicates was also considered for the estimation of Young's modulus, fracture stress, and fracture strain.	92
5.5	Stress-strain curve for gels (a) SPI-0.1S, SPI-0.1S-0.1G, SPI-4I-0.1S-0.1G, SPI-4I-0.1S and (b) SPI-2I, SPI-2I-0.2S, SPI-2I-0.1G, SPI-2I-0.2S-0.1G citric acid gels. The median replicate curve of each gel was selected for Young's modulus, fracture stress, and fracture strain estimation. The average of replicates was also considered for the estimation of Young's modulus, fracture stress, and fracture strain.. . . .	93

5.6	Stress-strain curve for SPI-2I-0.1S-0.05G citric acid gel. The median replicate curve of each gel was selected for Young's modulus, fracture stress, and fracture strain estimation. The average of replicates was also considered for the estimation of Young's modulus, fracture stress, and fracture strain. . . .	94
5.7	The stress-strain curves for SPI citric acid gel.	95
5.8	The stress-strain curves for a) SPI-0.05G, b)SPI-4I-0.05G, and c) SPI-0.2 S-0.05G citric acid gels.	96
5.9	The stress-strain curves for a) SPI-4I-0.2S-0.05 G, b) SPI-0.1S , and c) SPI-0.1S-0.1G citric acid gels.	97
5.10	The stress-strain curves for a) SPI-4I-0.1S-0.1G, b) SPI-4 I-0.1S , and c) SPI-2I citric acid gels.	98
5.11	The stress-strain curves for a) SPI-2 I-0.2 S, b) SPI-2 I-0.1 G, and c) SPI-2I-0.2S-0.1G citric acid gels.	99
5.12	The stress-strain curves for SPI-2I-0.1S-0.05G citric acid gel a) first replicate, b) second replicate, and c) third replicate.	100
5.13	(a) Fracture Stress, (b) Fracture Strain, and (c) Young's modulus for SPI and SPI-2I, SPI-0.1S, and SPI-0.05G citric acid gels. The Young's modulus was estimated as a slope of a linear region of a stress-strain curve between strain $\frac{1}{3}$ and $\frac{2}{3}$ of the fracture strain. All properties were estimated from average and standard deviation of replicates. Data with a and b letters indicate the statistical differences according to Duncan's method ($p < 0.05$). The fracture point was detected for five replicates for SPI and SPI-0.1S citric acid gels, six replicates for SPI-0.05G citric acid gel, and seven replicates for SPI-2I citric acid gel. The error bars represents the standard deviation for the respective numbers of replicates.	102
5.14	The correlation between uniaxial compression properties, a) fracture stress (kPa) vs fracture strain (-), b) Young's modulus (kPa) vs fracture strain (-), c) Young's modulus (kPa) vs fracture stress (kPa).	106
5.15	Three dimensional (1) and contour (2) plots of fracture stress as a function of inulin concentration (x-axis) and starch concentration (y-axis) for different guar gum concentrations (level): -1 (a), 0 (b), and +1 (c).	112
5.16	Three dimensional (1) and contour (2) plots of Young's modulus as a function of inulin concentration (x-axis) and starch concentration (y-axis) for different guar gum concentrations (level): -1 (a), 0 (b), and +1 (c).	113

5.17	Three dimensional (1) and contour (2) plots of fracture stress as a function of (a) inulin concentration (x-axis) and guar gum concentration (y-axis) at 0.1% w/v of starch concentration (level 0) and (b) starch concentration (x-axis) and guar gum concentration (y-axis) at 2% w/v of inulin concentration (level 0).	114
5.18	Three dimensional (1) and contour (2) plots of Young's modulus as a function of (a) inulin concentration (x-axis) and guar gum concentration (y-axis) at 0.1% w/v of starch concentration (level 0), and (b) starch concentration (x-axis) and guar gum concentration (y-axis) at 2% w/v of inulin concentration (level 0).	115
5.19	A) Storage modulus (G') and loss modulus (G'') and (B) $\tan\delta$ of SPI, SPI-0.05G, SPI-0.1S, and SPI-2I gels at 25° C as a function of angular frequency. All gels contain 8%, w/v and 0.3%w/v citric acid. Three replicates were conducted for each gel typee and data are presented as mean of replicates \pm standard deviation.	119
5.20	Power law model parameter estimates of SPI, SPI-2I, SPI-0.1S, and SPI-0.05G citric acid gels. (a) G'_0 and (b) G''_0 . The superscript letters a and b indicate statistical differences ($p < 0.05$). The error bars represent the standard deviation, n=3. Estimated data based on the mean of replicates was used.	122
5.21	Storage modulus (G') and loss modulus (G'') of a) SPI-0.05G, b) SPI-4I-0.05G, c) SPI-0.2S-0.05G, and d) SPI-4I-0.2S-0.05G as a function of angular frequency.	125
5.22	Storage modulus (G') and loss modulus (G'') of a) SPI-0.1S, b) SPI-0.1S-0.1G, c)SPI-4I-0.1S-0.1G, and d) SPI-4I-0.1S as a function of angular frequency.	126
5.23	Storage modulus (G') and loss modulus (G'') of a) SPI-2I, b) SPI-2I-0.2S, c) SPI-2I-0.1G, d) SPI-2I-0.2S-0.1G as a function of angular frequency.	127
5.24	Storage modulus (G') and loss modulus (G'') of SPI-2I-0.1S-0.05G citric acid gel a) 1st replicate of centre point, sample 13, b) 2nd replicate of centre point, sample 14, and c) 3rd replicate of centre point, sample 15, as a function of angular frequency.	128
5.25	Storage modulus (G') and loss modulus (G'') of of control sample, SPI citric acid gel, as function of angular frequency.	129

5.26	The correlation between viscoelastic properties and viscoelastic-uniaxial compression properties, a) G'_0 (kPa.s ⁿ) vs G''_0 (kPa.s ⁿ), b) Fracture stress (kPa) vs G'_0 (kPa.s ⁿ), c) Young's modulus (kPa) vs G'_0 (kPa.s ⁿ).	130
5.27	Three dimensional (1) and contour (2) plots G'_0 as a function of inulin (x-axis) and starch (y-axis) concentration for different guar gum concentration (level -1 (a), 0 (b), and +1 (c)).	137
5.28	Three dimensional (1) and contour (2) plots G''_0 as a function of inulin (x-axis) and starch (y-axis) concentration for different guar gum concentration (level -1 (a), 0 (b), and +1 (c)).	138
5.29	Three dimensional (1) and contour (2) plots of G''_0 as a function of starch (x-axis) and guar gum (y-axis) concentration at different inulin concentration (level -1 (a), 0 (b), and +1 (c)).	139
5.30	Three dimensional (1) and contour (2) plots G'_0 as a function of starch (x-axis) and guar gum (y-axis) concentration for different inulin concentration (level -1 (a), 0 (b), and +1 (c)).	140
5.31	Three dimensional (1) and contour (2) plots G'_0 as a function of inulin (x-axis) and guar gum (y-axis) concentration for different starch concentration (level -1 (a), 0 (b), and +1 (c)).	141
5.32	Three dimensional (1) and contour (2) plots G''_0 as a function of inulin (x-axis) and guar gum (y-axis) concentration for different starch concentration (level -1 (a), 0 (b), and +1 (c)).	142
6.1	The copyright permission from Copyright Clearance Center for reusing figures/tables/data from reference [42].	150
6.2	The copyright permission from Copyright Clearance Center for reusing figures/tables/data from reference [45].	151
6.3	The copyright permission from Copyright Clearance Center for reusing figures/tables/data from reference [35].	152
6.4	The copyright permission from Copyright Clearance Center for reusing figures/tables/data from reference [55].	153
6.5	The copyright permission from Copyright Clearance Center for reusing figures/tables/data from reference [54].	154
6.6	The copyright permission from Copyright Clearance Center for reusing figures/tables/data from reference [69].	155

6.7	The copyright permission from Copyright Clearance Center for reusing figures/tables/data from reference [120].	156
6.8	The copyright permission from Copyright Clearance Center for reusing figures/tables/data from reference [82].	157
6.9	The copyright permission from Copyright Clearance Center for reusing figures/tables/data from reference number [102].	158
6.10	The copyright permission from Copyright Clearance Center for reusing figures/tables/data from reference [68].	159
6.11	The copyright permission from Copyright Clearance Center for reusing figures/tables/data from reference [101].	160
6.12	The copyright permission from Copyright Clearance Center for reusing figures/tables/data from reference [15].	161
6.13	The copyright permission from Copyright Clearance Center for reusing figures/tables/data from reference [13].	162
6.14	The copyright permission from Copyright Clearance Center for reusing figures/tables/data from reference [90].	163
6.15	The copyright permission from Copyright Clearance Center for reusing figures/tables/data from reference [87].	164
A.1	The stress-strain curve for replicate 2 of control sample. The stress and strain fracture points are shown with long dash line, and the Young's modulus could be calculated as a slope of a linear part of a curve before fracture (short dash line).	180

List of Tables

2.1	Amino acid composition for different subunits of glycinin and β -conglycinin [35]	12
2.2	The established Canadian cheeses types according to their moisture content [74]	25
2.3	Canadian regulation on moisture and milk fat content (wet basis) for the different types of mozzarella cheeses [74]	26
2.4	The textural properties of a commercial firm and soft tofu, as measured by Xu et al. (2016) [90].	37
2.5	Overview of rheological sweep tests for soy protein gels produced by salt or acid addition.	43
2.6	Summary of benefits and drawbacks of various Multi Comparison tests [105, 106, 107, 108]	47
3.1	Selected studies of the gelation kinetics of soy gel and soy emulsion gels. OC: Oil Content, OT: Oil Type	49
3.2	Estimated values for G'_{sat} , k , and t_0 by using three sets of initial values for the gelation kinetics of SPI gel (0% oil volume fraction from Zhao et al. (2020) [68]).	55
3.3	Effect of coagulation temperature on the estimated k and t_0 for 4% (unit was not provided) 11S globulin coagulated with 0.4% GDL. The constant temperature was selected for the rheological set-up at frequency of 2 Hz and amplitude of 125 μm [101]. Permission to use the figures was obtained. See Appendix 6.11.	56

3.4	Effect of coagulation temperature on the estimated k and G'_{sat} for 5% (no unit was provided) SPI coagulated with 30 mM $CaSO_4$. The constant temperature was selected for the rheological set-up at frequency of 1 Hz and amplitude of 25 μm [102]. Permission to use the figures was obtained. See Appendix 6.9	56
3.5	Effect of temperature on k , t_0 , and G'_{sat} for 4% w/v dried soymilk coagulated with 0.02 N (5 mM) GDL. The constant temperature was selected for the rheological set-up at frequency of 1 Hz and strain of 0.1% [15]. Permission to use the data was obtained.	57
3.6	Estimated k and G'_{sat} values for 5% SPI gels prepared with two different coagulants (30 mM $CaSO_4$ or 20 mM GDL) and different temperatures. The constant temperature was selected for the rheological set-up at frequency of 1 Hz and amplitude of 25 μm [102]. Permission to use the figures was obtained. See Appendix 6.9	59
3.7	Estimated rate constant (k) and G'_{sat} for SPI-gels coagulated with 30 mM $CaSO_4$ at 70°C and different SPI concentration [102]. Permission to use the data was obtained.	61
3.8	Estimated G'_{sat} , k , and t_0 for SPI-soy oil emulsion gels containing 0%, 3%, and 7% v/v soy oil from the temperature-sweep test (heating and incubation stages only) at frequency of 1 Hz and strain of 1% according to Zhao et al. (2020) [68]. SPI and $CaSO_4$ concentration were 75 $g.l^{-1}$ and 3.5 $g.l^{-1}$	63
3.9	G'_{sat} , k , and t_0 for SPI soy oil emulsion gels in different homogenization pressure with protein and oil concentration of 4.5% (w/w). 2% GDL was used during gelation process at frequency of 1 Hz and strain of 0.5 [13]. Permission to use the data was obtained.	65
4.1	Composition and naming convention of SPI citric acid gels. Mass and SPI concentration of SPI were 0.4 g and 8% $w.v^{-1}$	69
4.2	Descriptor of the visual observation of SPI citric acid gels	70
4.3	Mass of a liquid separated from the solid mass of 8% $w.v^{-1}$ SPI and 0.20% $w.v^{-1}$ citric acid gels with two coagulation durations at 95°C.	72
4.4	Mass of the solution separated from the solid mass of 8% $w.v^{-1}$ SPI citric acid mixtures with various citric acid concentration	76
4.5	Classification of citric acid-induced 8% $w.v^{-1}$ SPI gels according to visual observations.	80

5.1	Composition and coded value of the SPI and SPI-P citric acid gels. All gels contained 8% w/v SPI and 0.3% w/v citric acid.	86
5.2	List of the independent factors based on their concentration and mass for a 400 mL solution of SPI-P gels.	87
5.3	Box-Behnken design dependent variables.	87
5.4	Mass of SPI and SPI-P citric acid gels and extracted water after pressing at 10 g.cm^{-2} for 10 min. All gels contain 8% w/v SPI and 0.3% w/v citric acid.	88
5.5	Estimated Young's modulus. E_1 was estimated as a slope of a linear region of a stress-strain curve in a strain range of 0.2-0.3, E_2 was estimated as a slope of a stress-strain curve in a strain range of 1/3-2/3 of a peak. E_{1SPI} and E_{2SPI} are a modulus value for the control gel (SPI) in each method.	91
5.6	Fracture stress, fracture strain, and Young's modulus for SPI citric acid gels with and without polysaccharides. The Young's modulus was estimated as a slope of a linear region of a stress-strain curve between strain $\frac{1}{3}$ and $\frac{2}{3}$ of the fracture strain. The values are expressed as mean \pm standard deviation, for selected replicates (stress and strain fracture point was detected for: five replicates (*); six replicates (**); seven replicates (***)). Means within a column with different letters are significantly different ($p < 0.05$).	104
5.7	Fracture stress, fracture strain, and Young's modulus for SPI citric acid gels with and without polysaccharides. The Young's modulus was estimated as a slope of a linear region of a stress-strain curve between strain $\frac{1}{3}$ and $\frac{2}{3}$ of the fracture strain. The values estimated based on the median replicates were used.	108
5.8	Analysis of Variance (ANOVA) of the quadratic model for the fracture stress(σ_f), fracture strain (ϵ_f), and Young's modulus (E) as response variables and inulin concentration (X_1), starch concentration (X_2), guar gum concentration(X_3) as dependent variables. Estimated data based on the mean of replicates was used.	110
5.9	ANOVA of the quadratic model for the fracture stress(σ_f), fracture strain (ϵ_f), and Young's modulus (E) as response variables and inulin concentration (X_1), starch concentration (X_2), guar gum concentration(X_3) as dependent variables. Estimated data based on the median replicate was used.	117
5.10	Rheological properties of SPI and pea protein isolate gels containing starch, inulin, or guar gum, as reported in literature.	120

5.11	Estimated G'_0 , G''_0 , n' for SPI and SPI-P gels and corresponding $\tan\delta$ at angular frequency of 1 rad.s ⁻¹ . The values are expressed as mean \pm standard deviation, n=3. Means within a column with different letters are significantly different ($p < 0.05$).	124
5.12	Estimated G'_0 , G''_0 , n' , and n'' for SPI and SPI-P gels at angular frequency of 1 rad.s ⁻¹ . Estimated data based on median replicate was used.	132
5.13	ANOVA for quadratic model for G'_0 and G''_0 as response variables and inulin concentration (X1), starch concentration (X2), and guar gum concentration (X3) as independent variables. Estimated data based on the mean of replicates was used.	134
5.14	Maximum G'_0 estimates derived from equation 5.12.	136
5.15	Maximum G''_0 estimates derived from equation 5.13.	136
5.16	ANOVA for quadratic model for G'_0 and G''_0 as response variables and inulin concentration (X1), starch concentration (X2), and guar gum concentration (X3) as independent variables. Estimated data based on the median replicates was used	144

List of Abbreviations

ANOVA Analysis of Variance [xxiii](#), [xxiv](#), [86](#), [109](#), [110](#), [117](#), [133](#), [134](#), [144](#)

CLSM Confocal Laser Scanning Microscopy [22](#)

G Guar Gum [22](#), [23](#), [147](#), [148](#)

GDL Glucono δ -Lactone [xiv](#), [xv](#), [xxi](#), [xxii](#), [18–20](#), [23](#), [29](#), [44](#), [45](#), [48–50](#), [55–62](#), [64–66](#), [101](#), [103](#), [118](#), [120](#)

I Inulin [147](#), [148](#)

LVR linear viscoelastic region [xiv](#), [39](#), [40](#)

MCTs Multi Comparison Tests [45](#), [46](#)

MTgase microbial transglutaminase [18](#), [19](#), [29](#)

pI Isoelectric Point [9](#), [11](#), [16](#), [17](#)

PRESS Predicted Residual Error Sum of Squares [109](#)

RT Room Temperature [68](#), [75](#)

S Starch [147](#), [148](#)

SEM Scanning Electron Microscopy [103](#), [149](#)

SPI Soy Protein Isolate [x–xviii](#), [xxi–xxiv](#), [1–5](#), [7–9](#), [11](#), [14](#), [15](#), [18](#), [19](#), [22–25](#), [29](#), [40–42](#), [44](#), [45](#), [48–51](#), [53–65](#), [67–95](#), [101–105](#), [108](#), [110](#), [117–129](#), [132](#), [133](#), [145–149](#)

SSE Sum of Squared Errors [54](#)

Tgase transglutaminase [29](#)

WHC Water Holding Capacity [17](#), [48](#), [103](#)

List of Symbols

T Temperature, $^{\circ}C$ 49, 60

A_0 Original cross-sectional area, m^2 37

A Cross Sectional Area of a Sample, m^3 30

G^* Complex modulus, Pa 38

ϵ_f Fracture Strain 31, 84

ϵ Strain 30, 38

τ_f Flow stress or flow point, Pa 39

F Force, N 37

G'_0 Storage modulus at 1 rad/s (Pa) 42

G''_0 Loss modulus at 1 rad/s (Pa) 42

\hat{G}' Predicted storage modulus, Pa 53, 54

G'' Loss modulus, Pa xiv, xviii, xxviii, 7, 25, 38, 40–43, 48, 58, 62, 81, 85, 117–120, 123, 125–129, 145

G' Storage modulus, Pa xiv, xv, xviii, xxviii, 7, 25, 38, 40–44, 48, 50, 51, 53–55, 58, 62–65, 81, 85, 117–120, 123, 125–129, 145

G'_{sat} Saturated storage modulus, Pa xv, xxi, xxii, 41, 42, 50, 54–61, 63–66, 147

E_{inc} Incremental Young's modulus, $N.m^{-2}$ or Pa 31

k Rate constant, s^{-1} xv, xxi, xxii, 42, 50, 54–57, 59–61, 63–65

L_0 Original length of material, m 38

L Length of material after applied force, m 38

N Total numbers of observation 54

n'' Influence degree of ω on G'' 42

n' Influence degree of ω on G' 42

ω Angular frequency (rad/s) xxviii, 42

R_g Radius of gyration, mm 15

R_h Hydrodynamic radius 15

σ_f Fracture Stress, Pa 31, 84

σ Stress, $N.m^{-2}$ or Pa 30, 37

$\tan\delta$ Loss tangent xviii, xxiv, 7, 22, 23, 38, 39, 42–45, 81, 118–120, 124, 145, 148

t_0 Latent time, s xv, xxi, xxii, 41, 42, 50, 54–58, 62–65

t Time, s 50

τ_y Yield stress or yield point, Pa 39

E Young's modulus, $N.m^{-2}$ or Pa 31

Chapter 1

Introduction

1.1 Research Motivation

Over the years, there has been an increasing interest in the production of processed dairy cheeses, cheese analogues, and imitation cheeses, most likely due to their numerous potential benefits [1, 2]. Non-dairy substitutes, in particular, are gaining attention from food processors and consumers as a result of lactose intolerance in dairy milk, the increasing demand for low cholesterol- and saturated-fat foods, and growing consumer demand for plant-based dietary requirements [2, 3].

Consumption of soy-based products such as soy milk, tofu, and soy cheese has increased significantly among non-dairy options, possibly due to their appealing nutritional profile, affordability, and health benefits [4, 5]. Soymilk has a nutritional value containing 3.5% protein, 2% fat, 2.9% carbohydrate, and 0.5% ash, and is also high in vitamins and minerals [5]. It has a protein content approximately identical to cow's milk, while having lower fat and fatty acid, and higher fibre content when compared with cow's milk [6]. Tofu is a traditional soy curd manufactured primarily from soymilk obtained from soaked soybeans [3, 7]. However, due to the health benefits, producing tofu or soy-based cheese from other soy protein types, such as Soy protein isolates (SPI), is becoming more popular [7, 8]. SPI is usually made from defatted soy meal and contains fewer oligosaccharides, isoflavones, and trypsin inhibitors than soybean itself, which induce flatulence, phytoestrogens, and allergies, respectively [7]. In addition, SPI may help to lower the risk of heart disease [8]. SPI gel preparation is also simpler and more controllable process than soymilk gelation [7]. In most cases, the SPI gel is induced by heating the SPI solution with the desired soy protein content and introducing a coagulant. Citric acid can be added as a coagulant and

create a soy protein gel with comparable viscoelasticity and hardness as a conventional tofu product [9]. It is also a natural and organic acid and may impart a delightful sour flavor to the SPI gel [10].

Soy protein gels, e.g. tofu or SPI gel, are complex viscoelastic materials consisting of a protein network and entrapped water [11, 12, 13, 14]. Analyzing the soy protein gelation could consist of two critical steps: 1) analyzing the soy protein gelation kinetics and 2) evaluating the final properties and quality of the soy protein gel. Gelation kinetics could be attributed to the different gel formation steps and associated time and speed. The viscoelastic properties, namely storage modulus and loss modulus, can be related to the gel formation, induction, growth, and stabilization. The evolution of these properties during gel formation has been reported in the literature for various soy protein sources and conditions [7, 12, 15, 13]. While extensive experimental observations are available for a range of conditions and formulations, the analysis of the kinetics of gel formation and a comprehensive comparison of the various protein sources is limited.

When evaluating the final quality and acceptance of soy protein gels, one of the most important elements to examine is the texture. Soy protein gel texture can be assessed using small deformations, such as rheological measurements, or large deformations, such as mechanical measurements. The rheological properties could give insight into the gel's stiffness and viscoelasticity, while the mechanical properties, e.g. uniaxial compression properties, can provide information about the gel's hardness, firmness, and strength.

It was reported that inclusion of polysaccharide in the SPI gels could effectively influence and modify the textural properties, making gels with higher strength, hardness, elasticity, and better viscoelastic properties and stiffness [16, 17, 18, 19]. Protein and polysaccharide can interact with each other, resulting in the formation of protein-polysaccharide complexes with very different properties than the protein and polysaccharide alone [16, 17, 18, 20]. Hence, such interactions are gaining a lot of attention in the food industry and can be used widely to design and develop new food products [18, 16].

Starch is a polysaccharide found in corn, maize, wheat, rice, and other plants, and it serves as a reserve food store for the plant [19]. Starch is used in foods as a thickening, stabilizer, and gelling agent having a well-established role as a water binding and water holding agent in comminuted meats and plant-based protein gels [19, 16, 21]. It is also used in meat products as a filler and fat replacement [21]. As a texture modifier, starch was employed in several plant-based protein gel products such as pea protein [22, 23], faba protein [24], and soy protein [16, 25, 26], and its presence made plant-based protein gels stronger and firmer. Specifically, introducing starch to the SPI gels could improve its viscoelastic properties, gel hardness, strength, and water holding capacity [16]. It was

revealed that hydrogen bonds and hydrophobic interactions can occur between starch and soy protein, resulting in a gel with a more compact and denser network structure [16].

Guar gum is an uncharged hydrocolloid that is derived from the endosperm of guar beans and utilised as a thickening, stabiliser, and binder agent in the food industry [19, 27, 18]. Guar gum can generate high viscosity solutions at low concentrations and is entirely stable in the pH range of 2 to 10 [19]. Guar gum was found to be effective in improving the texture and gelling properties of pea protein and soy protein gels [18, 28], and has the potential to increase tofu yield while also possessing textural qualities (hardness, cohesiveness, springiness, chewiness, and guminess) and sensory acceptance comparable to commercial tofu manufactured with typical gypsum [27]. Guar gum was also discovered to influence the rheological properties of SPI gels, resulting in gels with greater rigidity and strength [18].

Inulin is a class of naturally occurring, and neutral polysaccharides produced by a variety of plants, the most common of which is chicory. Inulins are dietary and soluble fibres that belong to the fructan family and have a polymerization degree of 2 to 60 [17] and a chemical stability in a $pH > 5$ [29]. At high concentrations (for standard chicory inulin $> 25\%$), inulin could represent gelling characteristics, and a completely dissolved inulin in water can be simply added to foods as a fat replacer [30]. In the food industry, inulin has been employed as a fat substitute, texture modifier, coating material, and potential prebiotic source [17, 31, 32, 33]. Several studies have looked at the characteristics of plant-based protein gels containing inulin, such as pea protein [20], oat protein [34], and soy protein gels [17], and found that the addition of inulin made the protein gels stronger and more resistant to stress. Inulin could be involved in the protein gel matrices by forming hydrogen bonds and hydrophobic interactions with proteins, resulting in smaller pore sizes and more uniform gels [20]. The addition of inulin to SPI gel could result in changes to the textural, mechanical, and rheological properties of the gel, such as increased gel strength, stiffness, hardness, and rigidity [17].

While extensive research has been conducted on the effect of starch, guar gum, and inulin on the rheological and textural properties of SPI gels, comparative studies examining the effect of each on citric acid-induced SPI gel firmness (by analyzing the rheological and mechanical properties), using multiple types of hydrocolloids, and relating the rheological and mechanical properties of SPI-Polysaccharide gels to the polysaccharide interaction with protein and water is limited. As a result, the purpose of this study is to address the aforementioned questions. In a nutshell, the gelation kinetics of several soy protein sources will be examined in a comprehensive manner. Afterwards, a citric acid-induced SPI gel will be made to evaluate the effect of experimental conditions on the visual appearance of SPI gels, and finally, the mechanical and rheological properties of a citric acid-induced SPI

gel containing starch, guar gum, inulin, or a combination of them will be assessed.

1.2 Research Objectives

The main objective of this master’s research was to develop a citric acid-induced soy protein gel containing starch, guar gum, inulin, or a mixture of those and to characterize the gel’s viscoelastic and uniaxial compression properties. This could be accomplished by analyzing the gelation rate of soy protein, and then creation of soy protein gels with higher gel strength and hardness using hydrocolloids. A flow chart of the project is shown in Figure 1.1 which represents the main steps of this work.

As a starting point, four different studies on the gelation kinetics of soy protein systems were chosen to be analyzed. The gelation kinetics could provide useful information regarding the time it takes to initiate gelation, the rate of the process, the time it takes to finish gelation, and the final viscoelastic properties, namely storage modulus of the gel. By analyzing the gelation kinetics in various conditions and with different ingredients, we can determine which conditions and ingredients will result in a gel with higher rigidity and better viscoelastic properties, as well as how long it will take to achieve those properties and whether it is worthwhile to wait that long. Therefore, the gelation steps were quantitatively analyzed for the source of soy protein, the coagulant type, the coagulation conditions, the soybean oil volume fraction, and the homogenization pressure. This step’s primary objective was to investigate and evaluate the gelation kinetics of three different soy protein sources: SPI, 11S globulin, and dried soymilk, and selecting a proper coagulating temperature.

The second stage involved determining the experimental conditions for the production of the soy protein citric acid-induced gel based on visual evaluations. Citric acid can be added as a coagulant and create a soy protein gel with comparable viscoelasticity and hardness as a conventional tofu product [9]. SPI can be used as a source of soy protein because it could represent higher viscoelasticity and stiffness than other examined sources.

A variety of SPI gels were developed to achieve this goal, with different heating durations, citric acid concentrations, coagulation durations, citric acid states (liquid or solid), and citric acid addition method. The prepared citric acid-induced gels were examined visually, and the following conditions were chosen for the creation of SPI gel: 1) 0.3% w/v citric acid as this concentration created stronger, more shapable, and stable gels, when compared to other concentration, 2) adding acid as a powder while constantly stirring the solution because this method could slow down the gelation process and result in a more

uniform and stronger gel with higher water retention. 3) 30 minutes of heating at 95° C to thoroughly denature all soy protein subunits, and 4) 60 minutes of coagulation at 80° C to ensure that the gelation process was completed. Finally, by employing the indicated conditions for the production of citric acid-induced gels, the SPI gels containing potato starch, guar gum, or inulin were made to prepare gels with higher rigidity, hardness, and strength than only SPI gel. To begin, the rheological properties, mechanical properties, and firmness of SPI- starch, SPI-guar gum, and SPI-inulin gel were evaluated and were compared with that of the pure SPI gel. The SPI-Polysaccharide gels' characteristics were then connected to their structure and interactions with protein and water. Additionally, the feasibility of creating SPI gels containing multiple types of polysaccharides was explored, and the mechanical and rheological properties of the gels were investigated and characterized. The Box-Behnken design, a response surface methodology, was used to assess the dependence of uniaxial and viscoelastic properties to the type and concentration of polysaccharides.

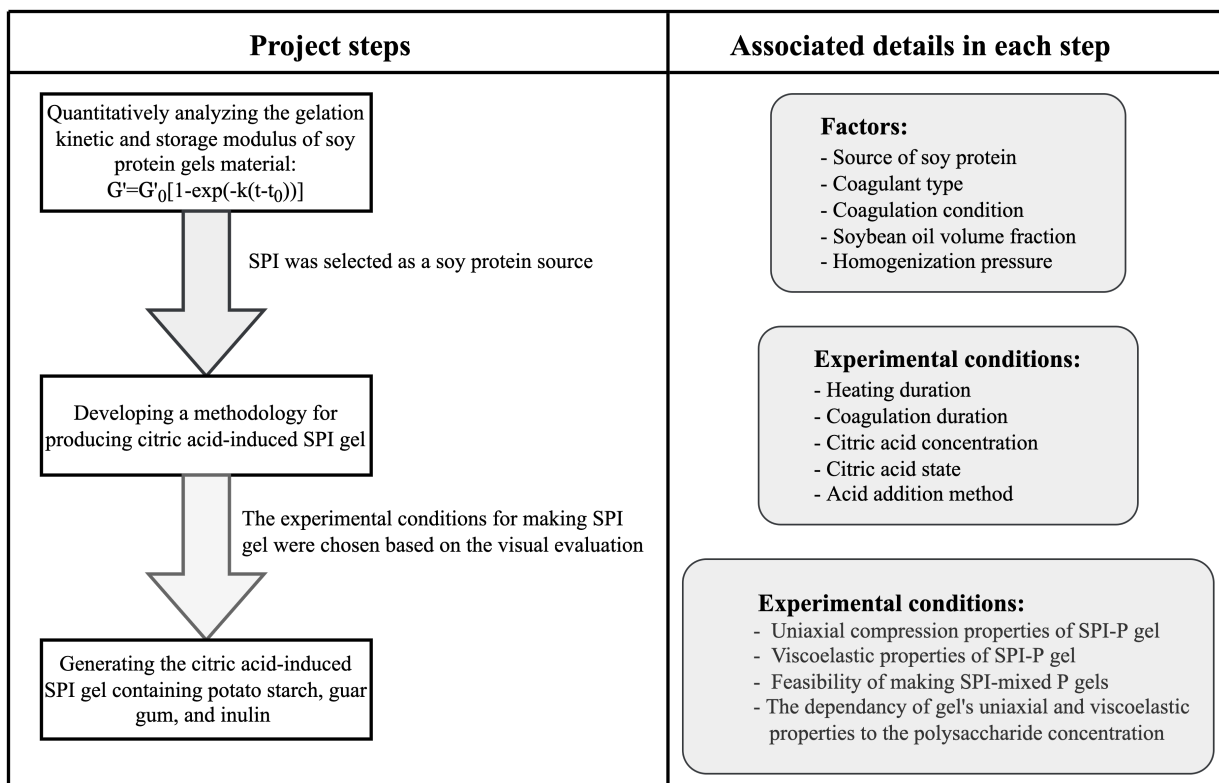


Figure 1.1: Flow chart of project with steps and associated details. The project steps are outlined in the left column, and the brief specifics of what conditions/ingredients/methods were researched in each stage are mentioned in the right column. In this figure, “P” represents polysaccharide.

1.3 Thesis Structure

The organization of the thesis consists of the following sections:

The background information is presented in Chapter 2. This chapter begins by introducing the composition and processing of soybean in section 2.1. In section 2.2, soy protein gel formation, thermal treatment, coagulation process, coagulant types, and gelation mechanism are explored in depth. The characteristics of the polysaccharides investigated in this study, starch, guar gum, and inulin, as well as their interactions with soy protein, are discussed in section 2.3. Cheese and cheese analogues are introduced in section 2.4, followed by a discussion of uniaxial and viscoelastic measurements and characteristics of soy protein gel in section 2.6 and 2.7. Finally, various multi-comparison tests and their

benefits/drawbacks were briefly introduced in section 2.8.

In chapter 3, the quantitative analysis of gelation kinetics of published soy protein gels is presented. For this purpose, section 3.2 presents the data extraction, data analysis, and empirical model evaluation. Then, in section 3.3 the effect of the source of soy protein, coagulant type, coagulation conditions, soybean oil volume fraction, and homogenization pressure on the gelation kinetics of soy protein gel is reported and discussed.

In chapter 4, the development of a methodology and the associated experimental conditions for the preparation of citric acid-induced SPI gels or curds is presented (section 4.2). In section 4.3, heating and coagulation duration, citric acid state (as liquid or solid), concentration, and addition method are reported and related to visual observations of the gels.

Chapter 5 consists of the experimental investigation of uniaxial and viscoelastic properties of citric acid-induced SPI gels containing three different polysaccharides. The experiments were conducted according to a Box-Behnken (B-B) design of experiments methodology to assess the dependence of rheological (G' , G'' , $\tan\delta$) and uniaxial mechanical properties (fracture strain, fracture force, Young's modulus) according to the type and concentration of polysaccharides (section 5.4).

Chapter 2

Background

2.1 Soybean

2.1.1 Soybean composition and processing

Soybean is utilized in many food applications and is one of the richest source of protein and oil. On a dry matter basis, soybean typically contains approximately 40% protein and 20% oil, and carbohydrate and ash are the remaining constituents of soybean seed [35].

The primary objective of soybean processing is to recover the oil component from the protein rich component, namely soybean meal. Soybeans must be washed, cracked, and flaked for this purpose. Processors crush soybeans to generate full-fat flakes, which are then extracted using organic solvents, primarily hexane, to produce oil and defatted flakes [36, 37]. The defatted soybean meal can be further processed to generate a variety of products such as soy flour, soy protein concentrate, and soy protein isolate (SPI). Gautam et al. (2020) [38] outlined the procedures of preparation and extraction for each kind in a review paper. Soy flour is obtained by heating dehulled soybeans and contains 50% protein. When compared to soy flour, soy protein concentrate is a fine soy protein that contains at least 70% protein. It can be extracted by three methods leaching, aqueous alcohol, and dilute mineral acid [39].

Soy protein isolates, with a minimum protein content of 90% on a dry basis, are traditionally prepared from defatted soy meal by using aqueous or mild alkali extraction (pH 7-10) of proteins and soluble carbohydrates. Then, centrifugation is used to remove the insoluble residues, which are primarily carbohydrate. Afterward, soy protein precipitates

at its **Isoelectric Point (pI)** (pH in the range of 4.5). The isoelectric point of a protein is the pH at which a protein carries no net electrical charge and hence is considered neutral [40]. Mechanical decanting separates the precipitated protein, which is subsequently washed and neutralized to a pH of around 6.8 before being spray-dried. **SPI** is a highly purified and protein-rich product (at least 90% protein content) as a result of the process [41]. Most of the soy off-flavor had been washed out during **SPI** processing, significantly improving the tastes of **SPI** products. It has also fewer soybean oligosaccharides, isoflavones, and trypsin inhibitors, all of which are flatulence factors, phytoestrogens, and allergens [12].

Soybeans are also processed into tofu. The first step in the preparation of tofu is the preparation of soymilk obtained by rinsing and soaking soybeans with water at 4° for around 12-14 hours. The hydrated soybeans are then drained, rinsed and placed in a high-speed blender with water. Following that, the soymilk is separated from the okara, the residue left after filtering the water-soluble fraction from ground soybean to make bean curd (tofu) or soymilk [7].

According to a review conducted by Peng et al. (2016) [42], soymilk can be divided into three parts: floating, soluble, and particulate fraction, with all lipids present in the floating fractions. These lipid droplets are originated from the oil bodies within the soybean structure, which are encapsulated by phospholipids and the protein oleosin (Figure 2.1).

2.1.2 Soybean Proteins

Soybean proteins can be classified into four categories based on their functions: storage proteins, metabolic enzymes, structural proteins, and membrane proteins [43, 44]. Approximately 65-80 wt% of soybean proteins are storage proteins. Glycinin (11S globulins), which belongs to the legumin protein family and β -conglycinin (7S globulins), which belongs to the vicilin, are the two primary storage proteins [43, 44]. Legumin is a protein substance analogous to the casein of milk, obtained from beans, peas, lentils, vetches, hemp (specifically edestin), and Vicilin is a globulin associated with legumin. The term 11S refers to the sedimentation coefficient, with a range of 10.5–13 versus the vicilin-like globulins (7S family) with coefficients of 7.0–9.0. Minor proteins present in soybean are involved in defence against micro- and macro-organisms, as well as nutrient mobilization. Some, such as the spherosome associated protein Gly m Bd 30K and soybean trypsin inhibitors, may also cause allergic reactions in humans and animals [35, 43, 44].

Glycinin is a hexamer, made up of two trimers linked together by electrostatic, ionic, hydrophobic, and hydrogen bonds. Each trimer is made up of three monomeric subunits that are linked by disulfide bonds and consist of acidic polypeptides with a molecular mass

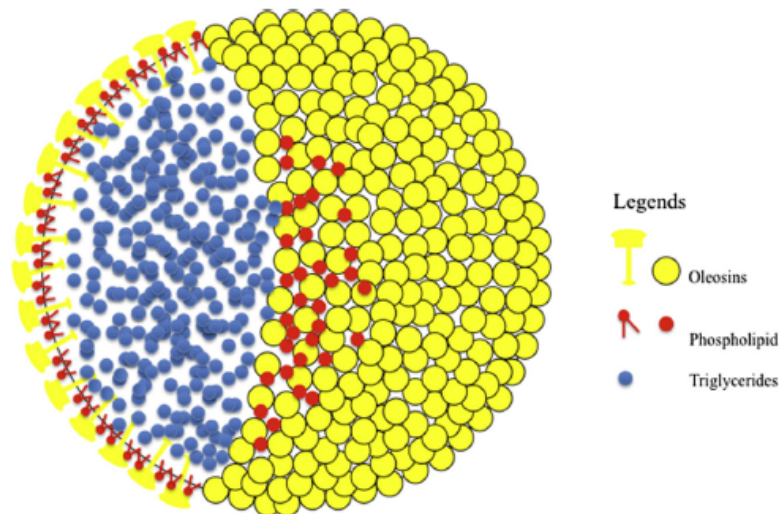


Figure 2.1: Schematic of a soybean oil body, which includes a matrix of triglyceride (in blue) enclosed by a layer of phospholipids (red) and oleosins (yellow) [42]. The permission to use the image was obtained. See Appendix 6.1.

of $30 - 40 \times 10^3 \text{ g.mol}^{-1}$ and basic polypeptides, with a molecular mass of $18 - 22 \times 10^3 \text{ g.mol}^{-1}$. The total molecular mass of Glycinin ranges between $320 - 375 \times 10^3 \text{ g.mol}^{-1}$. $A_{1a}B_2$, $A_{1b}B_{1b}$, A_2B_{1a} , A_3B_4 , and $A_5A_4B_3$ the primary monomeric subunits of glycinin, with A and B standing for acidic and basic subunits, respectively [35]. Figure 2.2 depicts the aschematic organization of acidic and basic subunits of glycinin.

β -conglycinin is made up of three subunits, α , α' , and β , all of which are tightly linked by hydrophobic and hydrogen connections. The molecular mass of β -conglycinin, α , α' , and β subunits are $150 - 200 \times 10^3$, 76×10^3 , 72×10^3 , and $53 \times 10^3 \text{ g.mol}^{-1}$, respectively, based on the ultracentrifugal analysis method [35].

At pH 7, the denaturation temperature of β -conglycinin and glycinin is approximately 75°C and 90°C , respectively [46]. As shown in Table 2.1, glycinin contains a greater number of sulfur-containing amino acid residues (methionine and cysteine) than β -conglycinin, allowing it to form more resilient gels [35].

The zeta potential of 7S and 11S globulins, which refers to the electrical charge at the surface of the hydrodynamic shear surrounding the colloidal particles [47], was measured by Liu et al. (2011) [48]. The zeta-potential of both 7S and 11S globulins shifted from positive to negative values when the pH was increased from 2.5 to 8.5, determining that

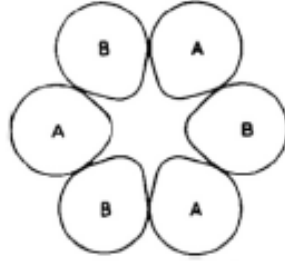


Figure 2.2: Schematic diagram of glycinin molecule consisting of acidic, A, and basic, B, subunits [45]. The permission to use the image was obtained. See Appendix 6.2.

the **pI** values of 7S and 11S globulin were pH 5.0 and pH 5.5, respectively [48]. The **pI** of 7S and 11S globulin subunits are also reported in the literature [49, 50]. Because the α and α' subunits of 7S contain more acidic amino acid residues, their **pI** values are lower than β subunit (**pI** values of α , α' , and β are pH 4.9, 4.8, and 5.4, respectively) [50]. SPI's **pI** value has been reported in the pH range of 4.0-5.0 [51].

Table 2.1: Amino acid composition for different subunits of glycinin and β -conglycinin [35]. The permission to use the table was obtained. See Appendix 6.3.

Amino acid	Number of amino acid residues per subunit							
	$A_{1a}B_{1b}$	$A_{1b}B_2$	A_2B_{1a}	A_3B_4	$A_5A_4B_3$	α	α'	β
Ala	27	28	31	18	22	23	23	22
Arg	27	29	29	33	36	38	43	29
Asn	37	36	40	33	33	37	37	33
Asp	17	16	18	24	30	28	27	21
Cys	8	8	8	6	6	1	1	0
Gln	48	49	51	45	48	52	45	33
Glu	41	38	37	42	55	79	77	37
Gly	35	31	34	40	37	29	24	18
His	8	6	4	15	15	20	6	8
Ile	26	24	23	17	21	28	30	26
Leu	33	31	33	34	37	41	45	42
Lys	24	18	18	18	27	38	31	21
Met	6	5	7	4	2	4	1	0
Phe	20	26	19	15	14	29	27	28
Pro	29	29	26	37	37	33	38	21
Ser	32	32	30	38	43	40	39	31
Thr	20	18	18	20	20	14	11	10
Trp	4	3	4	4	6	2	1	0
Tyr	11	10	11	15	15	13	13	12
Val	23	25	26	34	35	28	24	24
Total	476	462	467	492	539	577	543	416

2.2 Gel

2.2.1 Gel Formation

Gel materials exhibit both solid and liquid like behavior and are characterized by their viscoelastic properties. Gel formation is the phenomenon involving association or cross-linking of macromolecule chains to form a three-dimensional network that includes the entrapment of water molecules. The three-dimensional network formation generally requires external factors. Multiple external factors can be employed for the creation of gels.

Gels can be made from a variety of macromolecules, including polysaccharides and proteins. In the context of protein gels, the nature of the protein chain, its amino acid composition, and macromolecular structure will influence the gel formation and its material properties. In food products, protein gels include hard boiled eggs, gelatin, cheese, and tofu. Common to these protein gels are the forces existing between the protein chains that can be either attractive or repulsive. The balance between these forces determines the stability of the protein molecules in an aqueous solution. Hydrogen bonds, ionic attraction, van der Waals forces, disulfide bonds, and hydrophobic forces are examples of the molecular interactions which are involved in aggregation and gelation of proteins.

In this section, soy protein gels will be discussed with an emphasis on gel formation and gel material qualities in relation to various types of environmental conditions.

2.2.2 Soy Protein Gelation

In general, the gelation process begins with heating the protein solution to induce protein unfolding and create protein aggregates, followed by the addition of coagulant to create a three-dimensional gel network. Specifically, SPI will undergo four steps during the heating process (Figure 2.3). The first step corresponds to the dissociation of small aggregation of native soy protein particles. The second stage involves heating the protein solution to form spherical dense aggregates that grow in size over time until they reach a characteristic size (radii between 30 *nm* and 50 *nm*). If the protein concentration is low enough, for example, C=5 g/l at pH 6.0, the aggregation process can be stopped in this step [52, 53]. Then, for highly concentrated solutions, it is followed by the random association of elementary particles into self-similar aggregates. At the final step, the size of the aggregates increases during heating until they pass to a spanning network and form gels [52].

Coagulant will be introduced to the heated proteins to promote protein gelation; each can form various covalent or non-covalent interactions with the protein and water. Depend-

ing on the pH and ionic strength of the solution, protein molecules will have a positive or negative net charge. In the absence of salts or acids, an electrical double layer forms, causing repulsive forces to be generated between protein molecules. As a result, repulsive forces dominate in the protein-water mixture, preventing protein aggregation. The addition of coagulants to the aqueous phase, such as salts or acids, can diminish the thickness of the electrical double layer, thus lowering electrostatic repulsion between protein molecules through electrostatic screening. Consequently, the attractive connections prevail over the repulsive forces, causing protein molecules to flocculate in aqueous solution. [54].

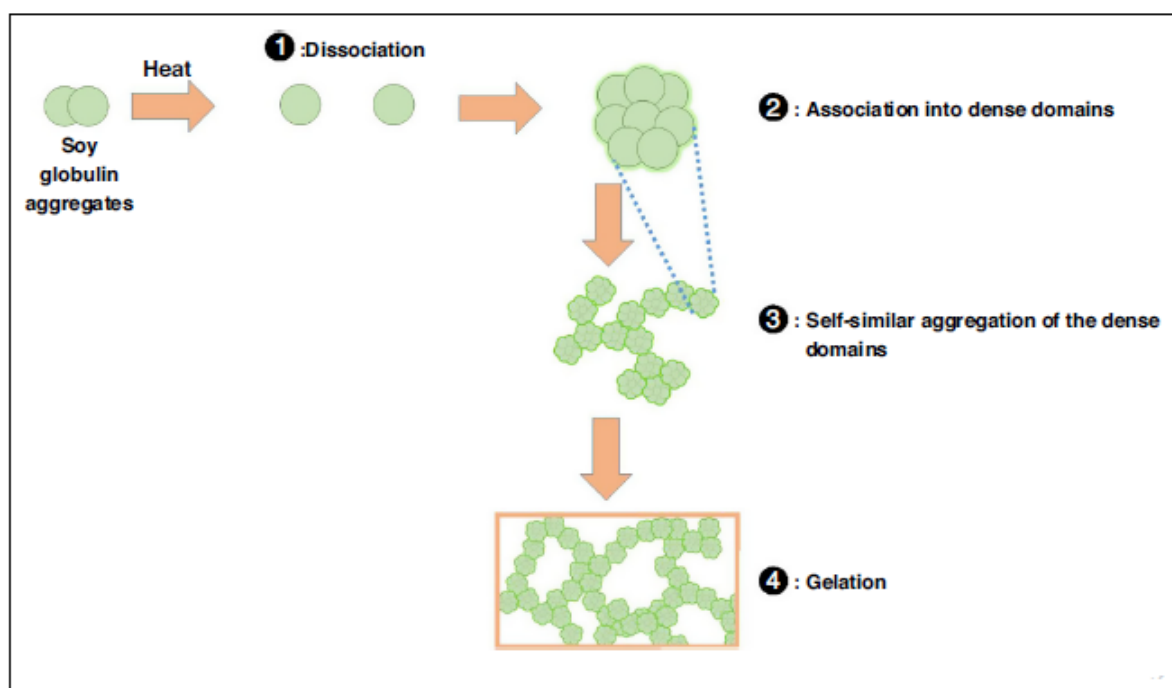


Figure 2.3: Proposed schematic representation of four steps of gelation of SPI during heating in an aqueous environment [55]. The permission to use the image was obtained. See Appendix 6.4.

2.2.2.1 Soy Protein Gelation by Thermal Treatment

Dissociation, association, self-similar aggregates, and gelation are the four stages that unfold and gelate proteins during heating, as discussed in section 2.2.2. Disulfide bonds and

non-covalent contacts, such as hydrophobic and hydrogen bonding, are the key interactions integrated in the heat-induced gel structure [56].

The temperature and duration of the heating process are two important factors that affect protein aggregation. Zhao et al. (2016) [57] evaluated the degree of denaturation of soy protein 7S and 11S globulins at temperatures ranging from 65 – 90° C for 5 to 15 minutes. According to the findings of this study, 7S globulin began to denature at 65° C and was totally denatured at 85° C, whereas 11S globulin was not susceptible to thermal denaturation below 75° C. Only at 90° C for 10 minutes or more could 11S globulin be completely denatured. Furthermore, increasing the heating period from 5 to 15 minutes resulted in more denatured 7S and 11S globulin.

The 7S and 11S globulin proteins were heated at 60°C, 80°C, and 100°C, and their hydrodynamic radius, R_h , and radius of gyration, R_g , which were determined through the dynamic light scattering, were compared to unheated samples in a study by Guo et al. (2012) [58]. The results revealed that as the temperature rose, aggregation of both proteins increased, with glycinin exhibiting a higher degree of aggregation (11S globulin)

He et al. (2016) [59] also commented that the basic polypeptides of 11S globulin and the β subunit of 7S globulin have a stronger tendency to combine and form protein particles during heating than the acidic polypeptides of 11S, the α' , and α subunits of 7S. The 7S and 11S globulins were isolated from soy flour in their study. The thermal aggregation behaviour of each component was studied using size exclusion chromatography after heating at 50 – 90° C for 10-60 minutes.

2.2.2.2 Soy Protein Gelation by Salt Addition

Shun-Tang et al. (1999) [60] looked into the role of Ca^{+2} in soymilk gelation. In general, after introducing calcium to the soymilk, lipid particles integrated into the soymilk gel network. Once Ca^{+2} is added, small molecules like phytate and other polyacid ions are consumed first. The excess Ca^{+2} can then form 7S-rich particles. Following that, the lipid particles are wrapped with the freshly generated 11S and 7S-rich particles made from soluble proteins. These micelles can then interact and associate with one another, as well as with the soymilk gel (Figure 2.4) [60].

Xu et al. (2015) [54] investigated the mechanism of *NaCl*-induced gels by varying the *NaCl* concentration for 1% (*w.v*⁻¹) SPI (Figure 2.5). The electrostatic repulsion interactions keep the protein particles apart in the absence of *NaCl*. As a result of the addition of 100 mM *NaCl*, protein particles have a greater proclivity for aggregation formation (a salting-out effect). In contrast, 400 mM *NaCl*, a relatively high concentration, increases

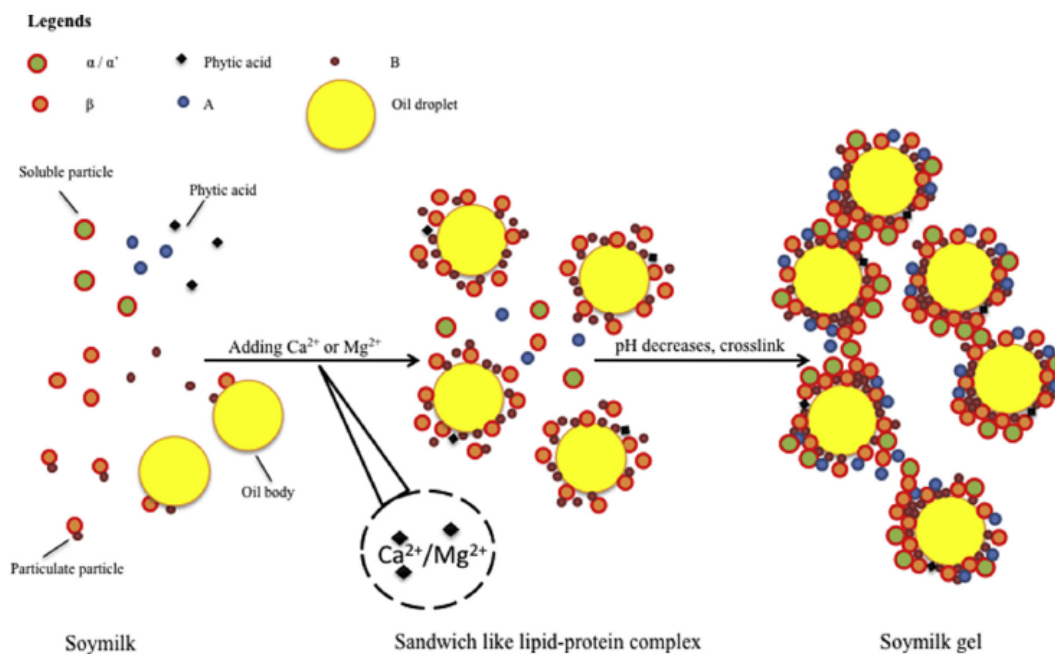


Figure 2.4: Mechanism of soymilk gel formation [42]. The permission to use the image was obtained. See Appendix 6.1.

electrostatic repulsive interactions between particles (a salting-in effect) and hinders effective aggregation [54].

The most frequent salts used for inducing soy protein gels in the manufacturing of tofu or tofu-type products are chloride-types (nigari-type), such as CaCl_2 and MgCl_2 , and sulfate-types, such as CaSO_4 and MgSO_4 . The different charges and charge density of the cations and anions of these salts affects their interaction with water and protein.

Tay et al. (2006) [61] investigated the effects of CaCl_2 , MgCl_2 , CaSO_4 , and MgSO_4 on different mixtures of 7S and 11S globulins in 7S:11S ratios ranging from 10:0 to 0:10 $w.v^{-1}$. As mentioned in section 2.1.2, each protein's molecular weight, pI, and thermal transition temperature are all distinct, resulting in a wide range of gel-forming properties. According to the findings of this study, increasing the ratio of 7S reduces aggregation and produces a liquid-like state. Among these four salts, CaCl_2 produced the strongest and most uniform curds, while MgSO_4 produced the weakest curd with products that remained nearly completely liquid for 7S:11S ratios of 2:8 to 10:0 [61].

Different gel characteristics will come from a mixture of salts. Wang et al. (2019)

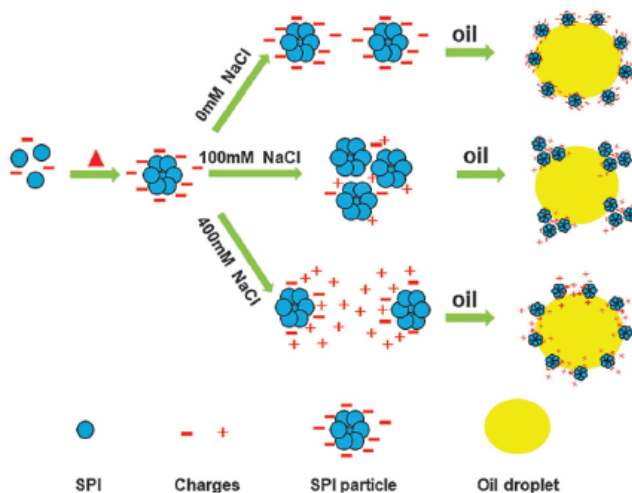


Figure 2.5: Schematic representation of the influence of NaCl concentration on the particle aggregation of SPI in the emulsion [54]. The permission to use the image was obtained. See Appendix 6.5.

[11] investigated the collaboration between different salts on the gel properties of SPI emulsion gels. An emulsion gel is essentially a complex colloidal material, typically referred to as a class of soft-solid matter that exists as both an emulsion and a gel [62]. The three salt combinations employed in this investigation were $CaSO_4$, $CaSO_4 - MgCl_2$, and $CaSO_4 - MgSO_4$. The results show that salts accelerate protein aggregation and that the aggregation power of these salts follows the order $MgCl_2 > MgSO_4 > CaSO_4$. The addition of 5 mM $MgSO_4$ to 20 mM $CaSO_4$ assisted in generating solid, compact, and homogeneous gels with high Water Holding Capacity (WHC), while using only $MgSO_4$ could not generate uniform and strong gels [61, 11].

2.2.2.3 Soy Protein Gelation by Acid Addition

As stated in section 2.2.2, lowering the pH of a solution containing proteins reduces the repulsion forces between the protein molecules as well as the protonation (addition of a proton) of protein carboxylic acid groups. As a result, depending on the pH value of a protein solution, aggregation or gelation in various stages can occur. According to section 2.1.2, the pI of 7S and 11S globulins are pH 5.0 and pH 5.5, respectively, implying that 7S globulins require a more acidic environment to aggregate or form gel.

The impact of pH on protein aggregation can be determined by analysing protein

particle sizes during acidification. The dynamic light scattering method, which measures the hydrodynamic volume of macro-molecules, is one of the most frequent methods for measuring the particle sizes of polymers/bio-polymers. The hydrodynamic volume is a volume of a polymer coil when it is in a solution. According to Chen et al. (2017) [52], the dynamic light scattering approach reveals that decreasing pH from 6.8 to 5.8 causes the gelation to occur in three steps. In the first step, dense almost spherical particles are generated, which then randomly associate into self-similar aggregates in the second step. Then, decreasing pH near to SPI pI caused growth of the self similar aggregates and led to the formation of a gel system spanning network at a critical gel time.

One of the most frequent materials used to make soft tofu is Glucono δ -lactone (GDL) [7]. GDL is an acid precursor, which means that once added to the protein solution, it will be hydrolyzed and produce acid. GDL works by releasing protons to neutralize the negative charges of soy protein aggregates, which are then coagulated through hydrophobic and electrostatic interactions to form a three-dimensional network [7]. Murekatete et al. (2014) [7] found that the gel point of SPI and soybean was reached quickly following the addition of 30 mM GDL, and the coagulation process began almost immediately at 20° C. The results indicate that acidification significantly improved the rate of protein gelation, and that even a low temperature, i.e. 20° C, could be an appropriate temperature for the acid addition step.

2.2.2.4 Soy Protein Gelation by Enzyme Addition

Enzymes can also produce protein gels. Enzyme gelation differs significantly from acid and salt gelation because enzymes generate gels by covalent interaction. The addition of an enzyme, such as microbial transglutaminase (MTgase), to the protein mixture causes the formation of an isopeptide bond between amide groups or ϵ -amino groups (in glutamine and lysine residues, respectively), and consequently, making the protein network [63, 64].

The mechanism of SPI coagulation with MTgase can be broken down into two phases. During the primary stage, the covalent linkage destabilized the spatial structure of SPI, exposing hydrophobic groups. The aggregation of SPI was then caused by covalent cross-links, hydrogen bonding, hydrophobic interaction, and disulfide bonds in the second stage [65].

Each subunit of glycine and β -conglycinin contains a different number of glutamine and lysine residues, as shown in Table 2.1. The glycine subunit has a higher total number of glutamine and lysine residues. As a result, glycine and β -conglycinin would have different interactions with MTgase. According to Tang et al. (2007) [66], glycinin has a

stronger tendency to cross-link with **MTgase** than β -conglycinin. In other words, glycinin is associated with the protein network and gel strength, whereas β -conglycinin is mostly incorporated into the viscous properties of gels.

2.2.3 SPI-Emulsion Gels

SPI-emulsion gels have attracted significant interest for the development of imitation cheeses [67]. Oil types used in the preparation of **SPI**-emulsion gel include liquid oils such as soybean oil and solid oils like palm stearin oil. The oil addition and emulsification steps can take place before or after the **SPI** solution has been heated. The emulsion solution is then converted to **SPI**-emulsion gels by adding coagulant, which is commonly done in conjunction with heating.

Zhao et al. (2020) [68] looked into the effects of heating before or after oil addition on the characteristics of $CaSO_4$ -induced **SPI** emulsion gels. The findings of this investigation showed that soybean oil addition to the protein mixture after heat treatment of the **SPI** solution can result in a more homogeneous and uniform microstructure. As a result, the hardness, water holding capacity, storage, and loss modulus were all improved.

Oil droplets can act as filler in the protein gel network. There are two types of fillers used in protein gels: active and inactive fillers (Figure 2.6). Proteins with predominantly hydrophilic surfaces cover active fillers (bound fillers). In other words, active fillers are protein-coated oil droplets that interact with other protein-coated oil droplets or protein networks in the continuous phase, implying that they are linked to the gel network and contribute to gel strength.

The concentration of oil, the pH of the solution, and the physical state of the oil are some of the factors that affect the role of the oil as either active or inactive filler. Murekatete et al. (2016) [12] investigated the effects of soybean oil on the rheological characteristics of $CaSO_4$ and **GDL**-induced **SPI** protein gels. A volume fraction of 5-35% soybean oil was added to the unheated **SPI** protein solutions. Following homogenization and heating of the soy protein solution, 30 mM $CaSO_4$ or **GDL** was added to the resulting mixture, which was then heated again, converting the solution to an emulsion gel. The viscoelastic properties obtained with temperature-sweep test revealed that oil droplets worked as active fillers when $CaSO_4$ was present, but were inactive fillers when **GDL** was present.

Gu et al. (2009) [38] identified the role of oil particles in distinct physical states. The emulsion preparation method was the same as above. Soybean and sunflower oil were used as liquid oils, and palm stearin was used as a solid oil, all with a volume fraction of 5-20%, and **GDL** was used as a coagulant. Gels without **GDL** with a pH of 6.9 and gels with

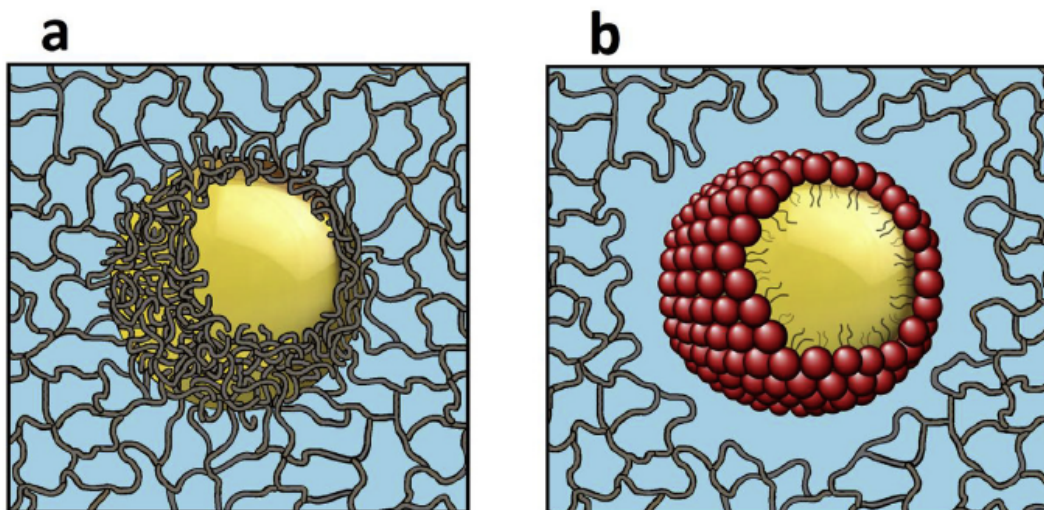


Figure 2.6: Schematic representation of two emulsion-filled gels. a) oil droplets behave as active filler particles, b) oil droplets behave as inactive filler particles [69]. The permission to use the image was obtained. See Appendix 6.6.

GDL with a pH of 4.5 were generated for further investigation. According to the findings, liquid oils behaved as active fillers in **GDL**-induced gels at sufficient low oil content or if pH of the solution was around 6.9, but behaved as inactive fillers when the oil content was high (10–20% v/v) or the environment was more acidic. Solid oil, on the other hand, was an active filler in all experimental conditions. Palm stearin and soy oil (or sunflower oil) have different physical states and melting points, which explains the differences of the gels produced (melting points of soy, sunflower, and palm stearin oil are -16°C , -17°C , and 44°C , respectively) [38].

2.3 Hydrocolloids

A colloid is a homogeneous system made up of molecules or particles that are nanoscale (1-100 nm) or mesoscale (from 100 nm to hundreds of microns) and dispersed through a medium. A colloidal system consists of two separate phases: a dispersed phase (or internal phase) and a continuous phase (or dispersion medium) [70]. A colloidal system may be solid, liquid, or gaseous. A hydrocolloid is a colloid system in which the colloid particles are dispersed in water and can exist in various forms, such as gel or sol, depending on the

amount of water available [70]. Hydrocolloids can perform a number of functions in food products, including thickening and gelling aqueous solutions, stabilizing foams, emulsions and dispersions, and the controlled release of flavors [71].

Proteins and polysaccharides are the most commonly used hydrocolloids in the food industry. Both can interact with each other, resulting in the formation of protein–polysaccharide complexes with very different properties than the protein and polysaccharide alone. Hence, such interactions are gaining a lot of attention in the food industry and can be used widely to design and develop new food products [18, 16]. Starch, guar gum, and inulin have been showed to have a considerable effects on the textural properties of plant-based protein gels. Starch was employed in several plant-based protein gel as a texture modifier, and its presence made plant-based protein gels stronger and firmer [22, 23, 24, 16, 25, 26]. Guar gum has been shown to improve the texture and gelling properties of pea protein and soy protein gels (increasing textural attributes: hardness, cohesiveness, springiness, chewiness, and guminess) [18, 28, 27]. Finally, inulin have been found to made the plant-based protein gels stronger and more resistant to the stress [20, 34, 17].

2.3.1 Starch

Starch is a mixture of two glucans, amylose and amylopectin, the content of which depends on the plant source. The average amylose and amylopectin contents are 20–30% and 70–80%, respectively [19]. The presence of a large number of hydroxyl groups in the starch molecule allows it to have a good hydrogen bonding interaction with water and protein. Figure 2.7 depicts the molecular structure of starch.

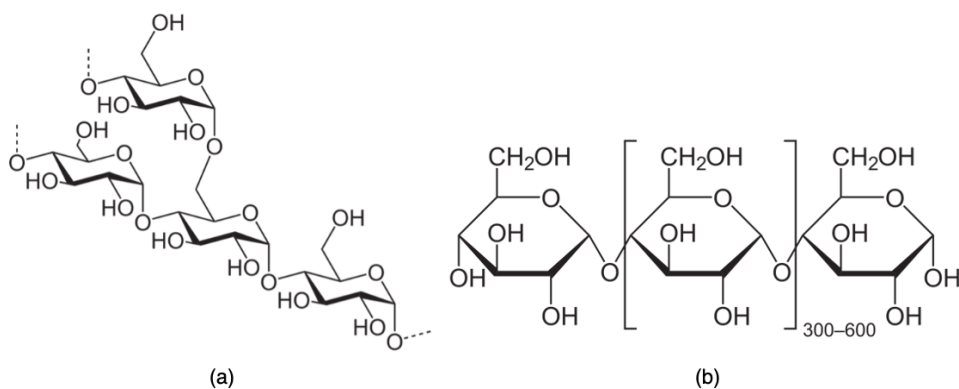


Figure 2.7: Molecular structure of amylopectin (a) and amylose (b) of starch.

Chu et al. (2019) [16] investigated the properties of the SPI-smilax china L. starch gel and the SPI-starch interaction. When the solubility of SPI gels (without starch) was measured in various buffers, it indicated that the physical and chemical interactions in the SPI gel occur in the following order: hydrophobic interaction > disulfide bonding > hydrogen bonding > electrostatic interaction. As a result, the hydrophobic and disulfide bonds are the two most important bonds in the formation of SPI gel. When starch was added, hydrogen bonding and hydrophobic interaction were significantly increased, and hydrogen bonding interactions exceeded disulfide bonding interactions. The hydroxyl content of starch could explain this result. Some SPI residues' side chains may form hydrogen bonds with carboxyl and amino groups, weakening the hydrophilicity of the residues and favouring hydrophobic interactions of some side chains, such that hydrogen bonding and hydrophobic interaction were enhanced after the addition of starch. The addition of starch had a minor effect on the disulfide interaction, indicating that covalent disulfide bonding occurs primarily between protein molecules rather than between protein and polysaccharide [16].

The addition of starch to SPI gels could significantly improve the functional properties of soy protein gel. Chu et al. (2019) [16] reported that increasing starch concentration from 0% to 1% resulted in more elastic and stiffer gels by increasing storage modulus by 3 times and decreasing $\tan\delta$ by approximately 30%. Furthermore, WHC and gel hardness were increased by 10 and 7.5 times, respectively. These findings support the role of starch as water binding and gelling agent.

2.3.2 Guar gum

Guar gum is an uncharged polysaccharide extracted from endosperm of guar beans used as a thickener, stabilizer, and binder agent in food products. Guar gum has the potential to increase tofu yield while also having sensory acceptability comparable to commercial tofu products made with traditional gypsum [19, 27, 18].

The structure of guar gum is shown in Figure 2.8. The main chain consists of D-mannose units, while the side chains are composed of D-galactose units in a 1:2 ratio of D-galactose to D-mannose. Guar gum has a high tendency to interact with water due to its side chains and can be completely hydrated in cold water. On the other hand, galactose substituents in galactomannans are clustered rather than evenly distributed along the chain backbone. Thus, the macromolecules may have sequences of 'smooth' mannose residues and 'hairy' galactose residues alternately [19, 72].

Confocal Laser Scanning Microscopy (CLSM) images of SPI and SPI-Guar Gum (G)

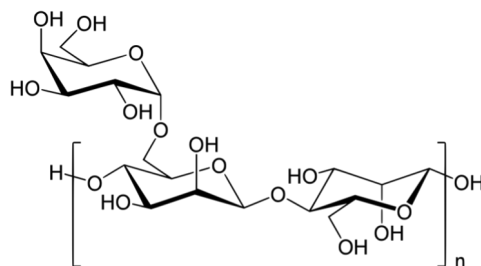


Figure 2.8: Molecular structure of guar gum.

gels collected by Chang et al. (2014) [18] indicate that the microstructure of SPI gel appears to be homogeneous and uniform, whereas coarse structure was formed by the addition of gum. The difference in microstructure between SPI and SPI-G gels could be attributed to the mechanism of SPI-G gel formation and the competition between protein aggregate gelation and phase separation between the protein aggregates and the polysaccharide molecules. In brief, the incompatibility between the protein and the polysaccharide caused the solution to phase separate into protein and serum phases after the addition of gums. Following that, GDL was added to the SPI-gum mixture, which reduced the pH of a solution and caused gels to form [18]. GDL is an acid precursor, which means that once added to the protein solution, it will be hydrolyzed and produce acid. GDL works by releasing protons to neutralize the negative charges of soy protein aggregates, which are then coagulated through hydrophobic and electrostatic interactions to form a three-dimensional network [7].

The effect of guar gum on the rheological and textural properties of tofu has been investigated. Chang et al. (2014) [18] reported that the final storage modulus and loss modulus of an 8% $w.w^{-1}$ SPI gel containing 0.3% $w.w^{-1}$ guar gum were approximately 2.8 and 2.6 times higher than that of only SPI, respectively, and the $\tan\delta$ of the SPI-guar gum gel was approximately 9% lower than the SPI sample. As a result of this study, adding guar gum to the SPI gel could improve the elasticity and rigidity of the gel. Li et al. (2015) [27] reported that introducing 0.075% $w.v^{-1}$ guar gum to $MgCl_2$ induced soy protein gel (protein content: 13% $w.w^{-1}$), increased the moisture content and yield of tofu by about 3% and 15%, respectively, with similar texture properties (hardness, springiness, cohesiveness, gumminess, and chewiness) as traditional tofu.

2.3.3 Inulin

Inulin is a class of naturally occurring polysaccharides produced by a variety of plants, the most common of which is chicory. Inulin belongs to the fructan's family of dietary and soluble fibres with a degree of polymerization between 2 and 60 mostly composed of linear fructose chains with β -linkages that end in a glucose unit [17]. As shown in Figure 2.9, inulin contains high numbers of hydroxyl groups, which may generate significant hydrogen bonding with water. Inulin has been considered as a fat substitute or texture modifier in food products [17].

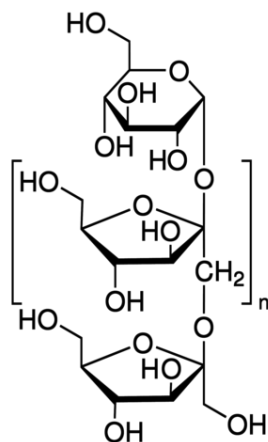


Figure 2.9: Molecular structure of inulin.

The mechanism of **SPI**-inulin interaction was described by Tseng et al. (2008) [73]. **SPI** was preheated at 95° C for 3.5 minutes to dissociate soy protein to facilitate its interaction between the hydrophobic cores of inulin and the denatured soy proteins, which led to the **SPI**-inulin gel formation.

The microstructure analysis of **SPI** gels and **SPI**-inulin gels revealed a particulate structure and slightly porous network structure in the **SPI** gels. In contrast, the **SPI**-inulin gels had smaller pore sizes, finer texture, and more compact protein aggregates. The inclusion of inulin appears to affect the soy protein aggregation pattern by increasing the aggregation tendency of unfolded protein molecules, most likely due to the excluded volume effect [73, 17]. This colligative effect is caused by the addition of concentrated weakly interacting neutral cosolutes and favours a decrease in the contact area between the protein surface and the surrounding solution [73].

The presence of inulin also affected the rheological and gelation properties of SPI-inulin gels. For example, the onset gelation time of SPI-4% *w.v*⁻¹ inulin was 40 seconds, which is shorter than the onset gelation time of SPI gel, which was 46 seconds. At 81° C, the *G'* and *G''* values of SPI gel containing 4% *w.v*⁻¹ inulin improved by around 18.2% and 17.7%, respectively, when compared to inulin-free SPI gels [17].

2.4 Cheese

2.4.1 Cheese Products and Regulations

According to Canadian regulations, cheese is defined as "the fresh or matured solid or semi-solid dairy food obtained by coagulating milk or milk products or any combination of these materials with the aid of bacterial culture, through the action of rennet and/or other suitable coagulating agents, and by partially draining the whey resulting from such coagulation" [74].

In Canada, cheeses are classified based on their moisture content. Five categories of cheese are established, as shown in Table 2.2: soft fresh cheese, soft cheese, semi-soft cheese, firm cheese, and hard cheese. This section will provide details of one semi-soft type of cheese, Mozzarella, two types of firm cheeses made by heat treatment, paneer and Halloumi, as well as imitation cheeses.

Table 2.2: The established Canadian cheeses types according to their moisture content [74]

Descriptor	Requirement
Soft Fresh Cheese	having a moisture on fat-free basis content of 80% or more
Soft Cheese	having a moisture on fat-free basis content of 67% and less than 80%
Semi-Soft Cheese	having a moisture on fat-free basis content of 62% and not more than 67%
Firm Cheese	having a moisture on fat-free basis content of 50% or more and not more than 62%
Hard Cheese	having a moisture on fat-free basis of less than 50%

2.4.2 Mozzarella Cheese

Mozzarella cheese (from the pasta filata family) is a soft, unripened, white, and lightly salted type of cheese. Mozzarella is prepared from milk, e.g. cow or buffalo milk, incubated

with a whey starter containing thermophilic bacteria, and then rennet addition to start milk coagulation. Cheese curds are produced, stretched and heated with salted boiling water, and then cooled by immersion in tap water [75].

Mozzarella cheese can be divided into two categories related to its final utilization: Pizza mozzarella (low-moisture) and Fresh mozzarella (high-moisture). Pizza mozzarella is a firm or semi-hard homogeneous cheese without holes that is mostly consumed after heating at a melting point, so stretchability and meltability are two important characteristics of these types of mozzarella cheese. Fresh mozzarella, a near-white soft cheese, is not aged, and can be consumed within hours of its making. Fresh mozzarella has a moisture content between 52-60% wet basis, and has a short shelf life, between 1 to 30 days [75].

In Canada, the fat and moisture content of mozzarella cheese is regulated and given in Table 2.4.

Table 2.3: Canadian regulation on moisture and milk fat content (wet basis) for the different types of mozzarella cheeses [74]

Mozzarella type	Maximum moisture (% $w.w^{-1}$)	Minimum milk fat content (% $w.w^{-1}$)
Mozzarella	52.0	20.0
Part skim mozzarella	52.0	15.0
Part skim pizza	48.0	15.0
Part skim pizza mozzarella	61.0	11.0
Pizza mozzarella	58.0	15.0

2.4.3 Paneer

Paneer is a soft cheese used in culinary dishes and snacks. The following are the steps involved in making paneer. Milk, such as cow or buffalo milk, is heated to 80 – 90° C for 5 minutes before cooled to around 70° C. As a coagulant, citric acid (wide concentration range of 0.1-5% $w.w^{-1}$) is added in this step [76, 77, 78, 79, 80]. Milk should be continuously stirred until two distinct phases, curd and whey, have formed. The milk (which now has two phases) will then be allowed to settle for 10 minutes before the whey is drained, and the curds are separated using a muslin cloth. The curds are pressed and cut to the desired size in the final step [80, 79].

2.4.4 Halloumi Cheese

Halloumi cheese is a semi-hard to hard, elastic and close textured cheese. It is traditionally produced in Cyprus from small ruminant's milk, the most frequent ones are goat and sheep's milk [81].

Halloumi is made by heating goat or sheep milk to a temperature of 30 – 33° C and adding rennet as a coagulant. Rennet is a complex set of enzymes produced in the stomach of ruminant mammals. The milk thickens after the addition of rennet, and two phases, curd and whey, are formed. The milk can be left undisturbed for 45-60 minutes to allow the curd to set. The curd is then cut into small pieces. The curd pieces are scalded in whey for 30 minutes at 40°C, and the whey should then be collected using muslin cloth. After pressing the curds, they are cut into blocks. The blocks are cooked for 1 hour at 94°C in collected whey. After that, the whey is drained and the cheese blocks (the pressed cooked curds) are placed in a brine solution [81]. Halloumi cheese is generally kept in brine in order to preserve the cheese for longer, and also keep the salty, acidic flavour of the cheese [81].

2.4.5 Cheese Substitutes

Cheese substitutes or imitation cheese are products that are intended to partially or completely substitute the milk components, fat and protein, with non-milk based ingredients [82]. There are two general types of manufacturing processes for producing cheese substitutes (Figure 2.10) [82]:

- **Manufacturing filled cheese:** Producing matured cheese by conventional methods with mixtures of liquid milk and vegetable oils or vegetable oil-butter fat (Figure 2.10).
- **Manufacturing cheese analogues:** Producing non-matured cheese by blending various raw materials, including fat and protein source other than those native to milk. The protein source of cheese analogues can be dairy, partially dairy, or synthetic. Butter oil, soy oil, artificial flavor, and enzyme modified cheese are other additives to these products (Figure 2.10).

Jeewanthi et al. (2018) conducted a comprehensive review on the variety of cheese analogues developed using soy proteins. According to this review paper, soy-based cheeses can be categorized into soft to hard based on their textural properties. Tofu, soy cream

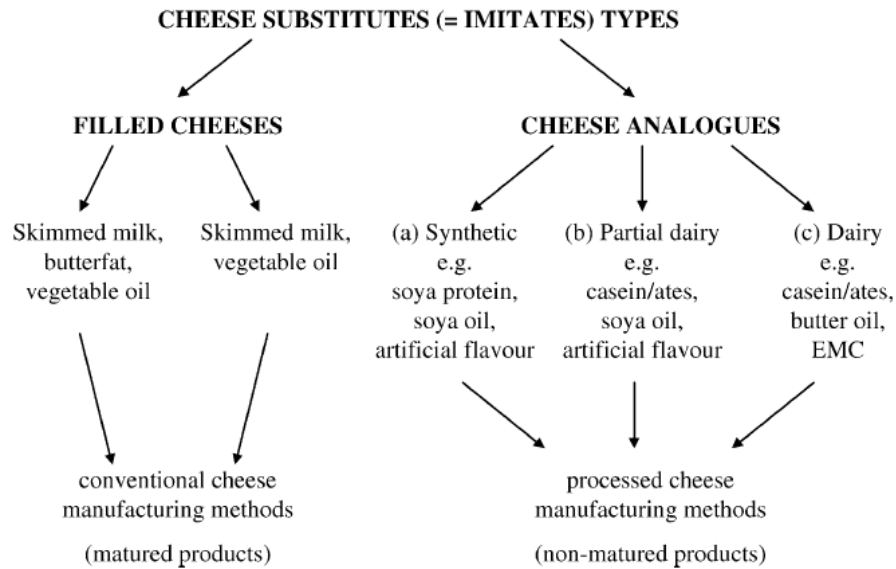


Figure 2.10: Types of cheese substitutes [82]. The permission to use the graph was obtained. See Appendix 6.8.

cheese, soy paneer, and soy mozzarella cheese are some examples of soft soy cheese types produced with soy protein or a combination of soy and milk. Gouda and cheddar cheese are also medium-hard-type of soy cheeses [3].

There is also soy paneer, a fresh, cheese-like product made by coagulating soymilk by itself or combined with cow and buffalo milk with calcium chloride, magnesium chloride, calcium sulfate, acetic acid, and citric acid. Citric acid is a most common coagulant and other ones are use not frequently. The level of combination will alter the physicochemical, texture, and rheological properties of soy paneer [3]. The combined milk is heated as it was discussed in section 2.4.3, and follows the same steps to convert to the soy paneer. The moisture and fat content of soy paneer should be higher than 50% (dry basis) but lower than 70% (wet basis) [3]. As mentioned in a review paper by Jeewanthi et al. (2018), for producing soy paneer, soymilk is combined with other milk types, e.g. cow and buffalo milk [3].

Soy mozzarella cheese is made by mixing soy curd or soymilk with milk or natural cheese curd in various proportions [1, 83, 84]. According to Kumar et al. (1997) [83], increasing the soy solids content in cow’s milk resulted in higher moisture content and lower fat and ash content in the final cheese. A mixture of 10% soymilk and 90% cow milk produced soy

mozzarella with high sensory properties and a longer shelf life [84]. The nutritional value of soy mozzarella cheese was improved by combining 10-20% soymilk with skimmed milk, but the meltability and stretchability were reduced [84, 83].

2.4.6 Soy Cheese

Tofu is a traditional soy-based product originated in China. Its texture ranges from soft to extra firm. Briefly, tofu is produced by soaking soybean, grinding, filtering (to recover soymilk and remove the solid component (okara)), heating the soymilk, coagulating, and pressing. Instead of soybean, SPI can also be used for preparing tofu [7].

As presented in section 2.2.2, common coagulants used for tofu preparation are salts ($CaSO_4$, $CaCl_2$, $MgCl_2$, $MgSO_4$), acids (GDL, citric acid), and enzymes (MTgase, transglutaminase (Tgase)). Tofu made with $CaSO_4$ and GDL is soft and smooth with homogeneous texture, whereas $MgCl_2$ and $CaCl_2$ produce coarse, hard, and granular tofu.

2.5 Market Analysis of Plant Food Products

The market analysis of plant-based products was investigated by Gaan et al. (2020) [85] during the years of 2018 to 2020. The data of this study was obtained from the Good Food Insight (GFI) industry, which led to an examination of retail sales data, new product development, investment analytics, scientific and technological improvements, consumer insights, and regulatory trends. GFI and the Plant Based Foods Association commissioned retail sales data from the market research firm SPINS.

Gaan et al. (2020) looked at the growth of plant-based foods in the United States and around the world, as well as at a detailed review of numerous categories. According to the findings of this study, retail plant-based food sales increased by 27% in the United States, which is 1.8 times faster than overall food sales growth. Plant-based milk, other plant-based dairy products (such as cheese and yoghurt), and plant-based meat were the top three most popular product categories in the United States in 2020. Between 2018 and 2020, global retail sales of plant-based meat and milk grew by about 24% and 4%, respectively. According to the research, people all around the world, particularly in North America, are showing a strong interest in purchasing plant-based foods. The most prevalent reasons for using plant-based products are health benefits, environmental sustainability, and animal welfare. Product price and taste, on the other hand, are the most critical factors preventing people from trying plant-based products [85].

2.6 Uniaxial Properties

Most of a gel’s functional properties, such as shape, cutting/slicing, and, in the case of food gels, eating characteristics, are linked to its large-deformation and fracture properties [86]. The large deformation of a gel involves changes in the geometry and sample size, and it mostly affects the structure of the gel significantly [86]. The mechanical behaviour of food gels under large-deformation conditions is correlated to textural properties, hence examining the mechanical properties could reveal valuable information on the food gel structure and texture [11]. A uniaxial test is a large deformation test in which the sample is compressed in one dimension but unconstrained in the other two [87]. Uniaxial compression consists of gradually applying load to a sample and measuring the deformation of the sample. The stress, defined as a force per unit area within the material that arises from externally applied forces, and the strain, defined as the ratio of a deformation or displacement to the original height of the material that results from an applied stress, can be determined from the measurement. In this section, the uniaxial compression properties will be defined, and their relationship with food gel material, specifically soy protein gels, will be introduced.

2.6.1 Properties and Definitions

During the uniaxial compression test, the applied force will compress the sample with a specific shape and dimension, and its deformation will be measured. The compression of the sample can be maintained until total rupture of a sample [88], or until a specific level of deformation is achieved, e.g. 80% deformation [89]. The shape and dimension of soft gel samples, which have a viscoelasticity property, might be affected during compression test [86, 90]. As a result, the stress and strain will fluctuate as a function of the sample size changes during compression, and these changes should be accounted for when calculating stress and strain [89]. In this situation, the result of a compression test could be reported either as a Force (N)-deformation (mm) curve or Stress (Pa)-Strain (-) curve, with the force-deformation curve transformed in the true stress ($\sigma(t)$)-strain ($\epsilon(t)$) curve using Equations 2.1 and 2.2, where $F(t)$, $L(t)$, $A(t)$ are the applied force, height of a sample, and cross-sectional area of a sample at time t , and A_0 and l_0 are the original surface area and height of a sample, respectively.

$$\sigma(t) = \frac{F(t)}{A(t)} \times \frac{L(t)}{L_0}, \quad (2.1)$$

$$\epsilon(t) = \ln \frac{L(t)}{L_0}, \quad (2.2)$$

The change in shape can be important and may be difficult for the instrument to capture these changes. It was reported that soft gel material may have a smooth fracture, and a maximum point or a plateau was detected during the fracture [89, 86, 90]. As a result, in order to capture the fracture area, the compression force must be small, and the equipment should be sensitive enough.

A typical stress-strain curve for a soft gel material is illustrated in Figure 2.11. As can be observed, the stress-strain curve increases until a maximum value is reached, after which the stress drops slightly. During the first stage, weak physical or chemical bonds could be unzipped or broken [86], then, by further increasing the applied force, more bonds will be disrupted, and the gel will be physically fractured (maximum point of the curve) [11]. The maximum point is defined as the fracture point or yield point, and the stress and strain values at this point are known as fracture stress (σ_f (Pa)) and fracture strain (ϵ_f) points. The Young's modulus (E) is usually defined as the slope of the linear portion of the stress-strain curve and reflects the initial change of the curve. The stress-strain relation of biopolymer gels or biological material are curves (Figure 2.11), and convex to the strain axis. The local slope gives the incremental Young's modulus, E_{inc} (Pa), which is strain or stress dependent [91]. In Figure 2.11, the fracture stress and fracture strain points are shown with the long dashed line, and Young's modulus can be calculated as the slope of the linear portion of the curve, e.g. in a strain range of $\frac{1}{3}$ to $\frac{2}{3}$ of the fracture strain, according to Canet et al. (2007) [92].

2.6.2 Uniaxial compression properties of plant-based protein gels

The mechanical properties of plant based protein food gels are influenced by the protein concentration [93, 94], protein type [7], coagulant type and amount [7, 11], and additives such as hydrocolloids [94, 95].

The effects of protein and coagulant (NaCl) concentration on the mechanical properties of pea protein isolate gel were evaluated by Zhu et al. (2021) [93]. The fracture stress of the gels increased as the protein concentration increased from 10% to 17% (the units were not mentioned). However, the fracture strain decreased, showing that the gel with a higher protein concentration gave superior gel strength but was less elastic. Similar changes were observed when the NaCl concentration was increased from 0.1% to 2% [93]. Increased pea isolate protein concentration and NaCl concentration resulted in stronger but less elastic gels. These observations may reflect the increased intermolecular interactions with higher

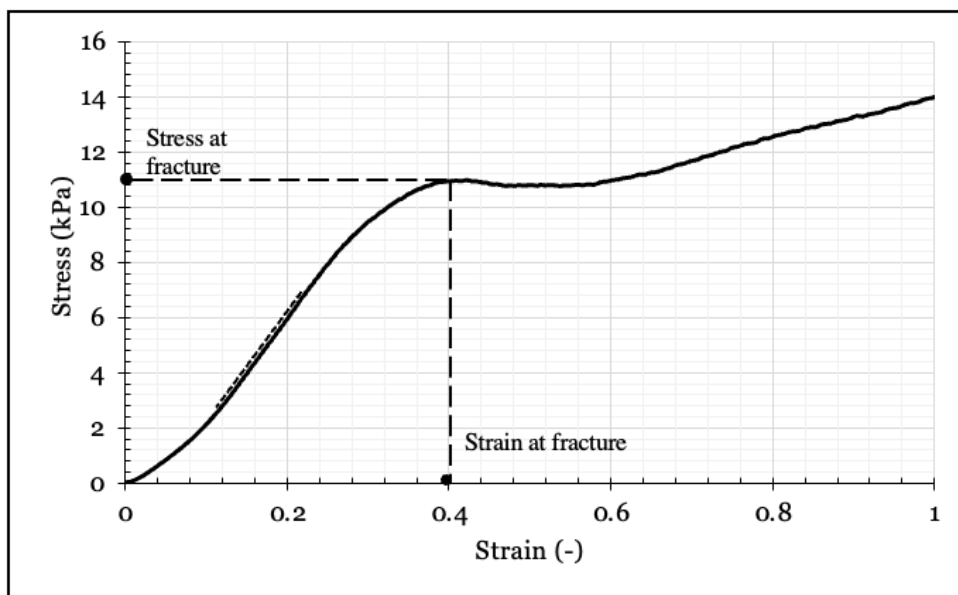


Figure 2.11: The true stress-strain curve for a soft gel material. The fracture stress and fracture strain points are shown with filled circles, and the Young's modulus is calculated as the slope of the short dashed line. More information about the estimation of Young's modulus will be presented in Chapter 5.

protein concentrations while higher NaCl concentration may have neutralised the surface charge of the proteins, making the gel stronger. On the other hand, the higher protein content may reduce protein mobility, resulting in lower gel elasticity [93].

In a study conducted by Chen et al. (2021) [94], the mechanical properties of transglutaminase induced SPI (7% or 9% $w.v^{-1}$)-chitin nanofiber gel were examined to analyze the impact of SPI concentration and chitin nanofiber addition. Comparing the fracture point of gels with 7% $w.v^{-1}$ and 9% $w.v^{-1}$ SPI revealed that 9% $w.v^{-1}$ SPI gel had higher fracture stress point and gel strength, while its fracture strain point could not be detected clearly. On the other hand, the presence of chitin nanofiber in SPI gels at both SPI concentrations resulted in a significant enhancement in the fracture stress point [94].

Wang et al. (2019) [11] evaluated the mechanical properties of 6% $w.v^{-1}$ SPI-emulsion gels coagulated with various salts, i.e., 35 mM $CaSO_4$, 30 mM $CaSO_4$ -5 mM $MgSO_4$ (or $-MgCl_2$), or 25 mM $CaSO_4$ -10 mM $MgSO_4$ (or $-MgCl_2$). The SPI gel produced by $CaSO_4$ with 5 mM $MgCl_2$ had the highest fracture stress, i.e., 1087.0 Pa, which was about 1.8 times that of the SPI gel coagulated with $CaSO_4$. However, the fracture stress dropped

by about 50% as the magnesium concentration increased from 5 mM to 10 mM. Similarly, the stress fracture of SPI gels created with 30 mM $CaSO_4$ -5 mM $MgSO_4$ was considerably higher than that of the SPI gels with 35 mM $CaSO_4$, while further addition of $MgSO_4$ reduced the fracture stress point of the gel. In contrast, the increase in magnesium content from 0 mM to 10 mM decreased the fracture strain for either $MgSO_4$ or $MgCl_2$ salt [11].

The comparison between the mechanical properties of 30 mM GDL- and $CaSO_4$ -induced 5% $w.w^{-1}$ SPI gel was carried out by Murekatete et al. (2014) [7]. In comparison to GDL-induced SPI gels, $CaSO_4$ -induced SPI gels were less deformable (lower fracture strain point) and had a higher gel strength (higher stress fracture point). In a study conducted by Murekatete et al. (2014), the difference between the gel properties obtained from two sources of soy protein, SPI and soybean, was also investigated. In both GDL and $CaSO_4$ -induced gels, the soybean gel showed stronger stress fracture despite having reduced deformability than the SPI gel [7]. The microstructure of the two gels was studied using cryo-scanning micrographs. It was observed that soybean gels had a more homogeneous and denser network with a smaller pore size than SPI gels, which could explain the higher strength of the soybean gel [7].

The addition of polysaccharides is another approach that can alter the mechanical properties of plant-based protein gels. For example, the mechanical properties of $CaSO_4$ -induced 7% $w.v^{-1}$ SPI gel containing konjac gum, gellan gum, and curdlan gum were studied by Zhao et al. (2020) [95]. Increasing the concentration of all three gums from 0% to 0.5% $w.v^{-1}$ resulted in SPI gels with superior deformability and stress fracture. The SPI gels containing 0.5% $w.v^{-1}$ konjac gum exhibited the highest fracture stress and fracture strain [95]. Xu et al. (2021) [20] investigated the variation of mechanical properties of 9% $w.v^{-1}$ pea protein isolate as a function of inulin concentration. Similar to the previous study, increasing inulin concentration from 0% to 7% $w.v^{-1}$ increased significantly the fracture force, also referred as gel strength (no information on the fracture strain and Young's modulus was provided). The observations of these two studies are different from the observations reported by Guo et al. (2014) for 8% $w.w^{-1}$ SPI-0.3% $w.w^{-1}$ gellan gum film gel produced with microbial transglutaminase as a coagulant. SPI gel alone exhibited higher fracture stress and fracture strain values when compared with SPI-gellan gum gel, while SPI-gellan gum had a higher Young's modulus [89].

The uniaxial properties of commercial soft tofu and firm tofu were evaluated by Xu et al. (2016) [90], and are depicted in Figure 2.12 showing three regions in the Force (N)-Deformation (mm) curve. Authors suggested that the first region, which is an initial elastic region corresponding to cell wall ¹ flexure, could reflect the protein backbone bending

¹A tough, flexible, and sometimes rigid layer of polysaccharides lying outside the plasma membrane of

followed by free water released from the network. The second region could be the result of elastic buckling followed by cell collapse and cell wall fusing. For fresh soft tofu, the second region was a fracture peak, whereas for firm tofu, it was a plateau. The higher elasticity of firm tofu, which resulted in a smooth breakage of its structure, could explain these variations. In the final region, cell walls may begin to touch because of densification, and the slope increases dramatically [10]. It could also be observed that firm tofu was fractured at a higher force and deformation, which consequently could represent a higher stress and strain fracture point.

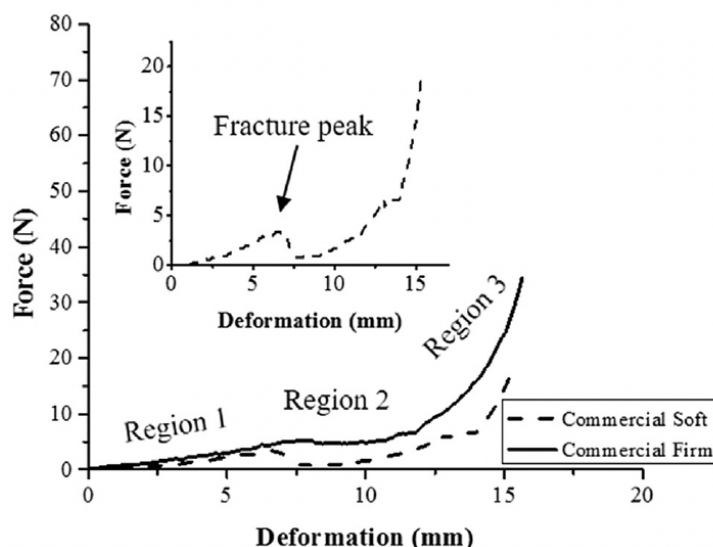


Figure 2.12: The Force-Deformation of commercial firm and soft tofu [90]. The permission to use the image was obtained. See Appendix 6.14.

2.6.3 Uniaxial compression properties and food texture

The mechanical behaviour of foods under large-deformation conditions can be related to some of their textural properties. For example, the fracture stress (or fracture force), fracture strain, and Young’s modulus obtained by uniaxial compression are associated with food texture, each with a different physical meaning. The fracture strain indicates the food gel’s deformation capacity while the fracture stress demonstrates the ”toughness”

the cells of plants, fungi, and bacteria. It provides the cell with both structural support and protection, and also acts as a filtering mechanism.

of the food, and the Young's modulus represents "firmness" or "hardness" of foods [96]. An alternative to uniaxial compression test for the characterization of the texture properties of food is the texture Profile Analysis (TPA), or two bite test, which is a double compression test [87].

In the TPA test, a food sample shaped to a specific dimension and shape is pressed twice in a reciprocating way at a steady pace using a plunger. The plunger moves in a semicircular motion, replicating the action of the human jaw during chewing. The plunger's surface area should be equal to or larger than that of the area of the food sample, and relative deformation of 90% or higher is commonly recommended [87].

A typical TPA curve is shown in Figure 2.13 with the associated texture properties definitions. Generally, 'hardness', 'fracturability' (or 'brittleness'), 'springiness', 'cohesiveness', and 'adhesiveness' are the primary parameters, and 'gumminess' and 'chewiness' are the secondary parameters that can be obtained from the TPA curve [87]. Each property is defined or calculated as follows [87]:

- Hardness: The height of the force peak on the first compression cycle (first bite).
- Fracturability (or brittleness): The force of the significant break in the curve on the first bite.
- Cohesiveness: The ratio of the positive force areas under the first and second compressions (A_2/A_1 in Figure 2.13).
- Adhesiveness: The negative force area of the first bite (A_3 in Figure 2.13) which also represented the work necessary to pull the compressing plunger away from the sample.
- Springiness (or elasticity): The distance that the food recovered its height during the time that elapsed between the end of the first bite and the start of the second bite.
- Gumminess: Could be calculated as hardness \times cohesiveness.
- Chewiness: Could be calculated as gumminess \times springiness.

The gel hardness of CaSO₄ induced SPI, SPI-konjac gum, SPI-gellan gum, and SPI-curdan gum was measured by Zhao et al. (2020) [95]. The findings indicate that the addition of all those polysaccharides improved the gel hardness of SPI gel significantly, and there was a positive correlation between the polysaccharide concentration and the gel

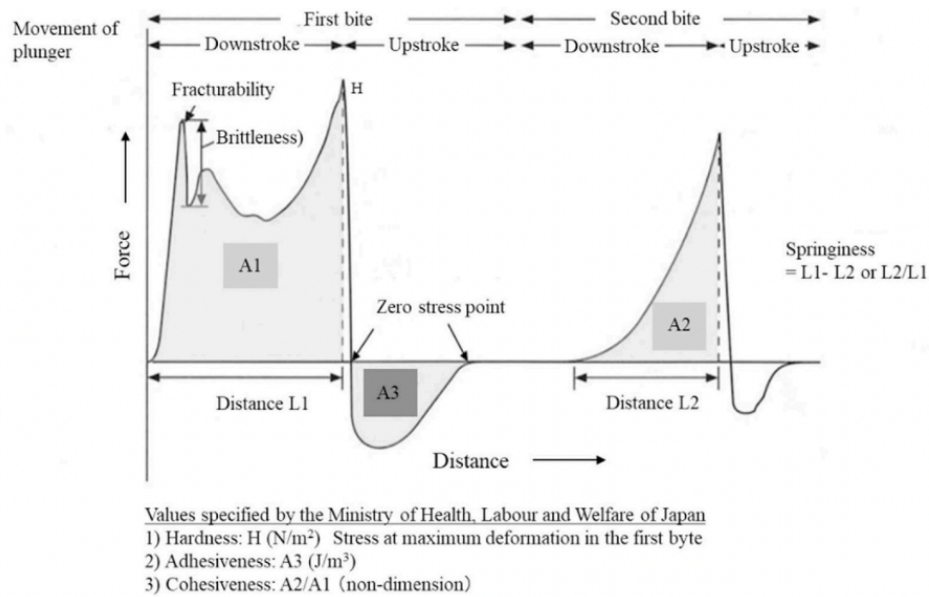


Figure 2.13: A typical TPA curve and the definition/calculation for each TPA characteristic [87]. The permission to use the image was obtained. See Appendix 6.15.

hardness [95]. Tseng et al. (2009) [17] investigated the influence of inulin addition on the textural attributes of an GDL induced SPI gel. The results imply that by the addition of 4% $w.v^{-1}$ inulin to the SPI gel, the gel hardness (g), and deformability (%) increased significantly by about 25% and 47%, respectively, and the gel's cohesiveness reduced by 5%. The abovementioned results have a pretty good consistency with the presented results in section 2.6.2, indicating that some of the textural properties, e.g. hardness, could positively be linked to the mechanical properties of a gel.

In the study conducted by Cao et al. (2017) [9], the textural properties were evaluated for the soybean gels coagulated with 0.12-0.18% $w.v^{-1}$ of various acids, i.e. citric acid, tartaric acid, and malic acid, and were compared with that of the 0.3% $w.v^{-1}$ GDL induced soybean gel. Tofu coagulated with 0.14% citric, malic, and tartaric acid had maximum hardness of 200.46, 188.32, and 176.98 g, respectively, which was comparable to GDL-cured tofu (189.41 g). However, at organic acid concentrations more than 0.14%, hardness reduced. The gumminess trends were in line with the hardness trends. Tofu gels cured with citric and l(-)-malic acid were more rigid and elastic than tofu cured with tartaric acid in terms of springiness.

Table 2.4 summarises the textural properties of firm and soft tofu, according to Xu et

al. (2016) [90]. It was discovered that firm tofu has higher textural characteristics than soft tofu. A firm tofu’s hardness was approximately 2.2 times that of a soft tofu. We also noticed in section 2.6.2 that firm tofu had greater mechanical strength and stress fracture point. This comparison of the uniaxial and TPA test findings suggests that there may be a correlation between food material hardness and stress fracture point, with a larger stress fracture point indicating that the gel is harder.

Table 2.4: The textural properties of a commercial firm and soft tofu, as measured by Xu et al. (2016) [90].

Tofu type	Hardness (N)	Springiness (mm)	Cohesiveness	Gumminess (N)
Firm	35	4	0.14	6
Soft	16	3	0.09	3

2.7 Rheological Properties

Rheology is the study of the deformation and flow of materials observed under defined conditions. The response to external deformation of the material relates to the internal structure and bonds of the material. In this section, important terms for the characterization of protein gels will be defined, viscoelasticity will be introduced, and their relationship to gels will be reviewed.

2.7.1 Properties and Definitions

Stress (σ) is the force applied to a material, divided by the cross-sectional area of the material subjected to the force.

$$\sigma = \frac{F}{A_0}, \quad (2.3)$$

where σ , F , and A_0 represent stress ($N/m^2, Pa$), force (N), and original cross-sectional area (m^2), respectively.

Depending on the position and direction of the applied force, two types of stress can be observed: shear stress and normal stress. Shear stress arises from the force vector component parallel to the cross-section of the material. Normal stress arises from the force vector component perpendicular to the cross-section of the material.

Strain (ϵ) is the deformation or displacement of the material that results from an applied stress.

$$\epsilon = \frac{L - L_0}{L_0} \quad (2.4)$$

In Equation 2.4, ϵ , L , and L_0 are strain, length after applied force (m), and original length (m), respectively. $L - L_0$ is defined as deformation, which means the change of the shape/size of a body over time and has units of length, while strain is unitless.

Depending on the stress that is applied, shear strain or normal strain will occur. Shear strain (shear deformation) occurs when the deformation of an object is in response to a shear stress (i.e. parallel to a surface). Normal strain occurs when the elongation of an object is in response to a normal stress (i.e. perpendicular to a surface).

Elasticity is the ability of a deformed material to return to its original shape and size when the force causing the deformation is removed. In elastic material, elasticity is the linear relationship existing between the stress and the strain.

Viscoelasticity is the property of a material that exhibits both viscous and elastic characteristics under stress and deformation conditions.

2.7.2 Viscoelasticity

Gels such as protein gels are viscoelastic materials and display both viscous and elastic characteristics. The elastic portion is described by the storage modulus, G' , which represents the ability of a material to store energy elastically and describes the solid-state behaviour of the material. The viscous portion is described by the loss modulus, G'' , which represents the ability of a material to dissipate stress through flow, and describes the liquid-state behaviour of the material. If G' is higher than G'' , the material is mainly elastic, and vice versa. The sum of the storage modulus and the loss modulus is called the complex modulus, G^* . G^* is the ratio of shear stress to the strain and can be defined by Equation 2.5 [97, 98].

$$G^* = G' + iG'' \quad (2.5)$$

The ratio between G'' and G' is called $\tan\delta$ (Equation 2.6) which shows the relative degree of energy dissipation or damping of the material [97].

$$\tan\delta = \frac{G''}{G'} \quad (2.6)$$

If $\tan\delta > 1$, the material is more viscous and represents more liquid like behaviour, if $\tan\delta < 1$, the material is more like solid and elastic, and if $\tan\delta = 1$, the material is at its

gel point indicating that the fluid has transitioned from fluid flow like behaviour to solid elastic behaviour. According to Ikeda et al. (2001), $\tan\delta$ values greater than or equal to 0.1 indicate "weak" gels, while values greater than or equal to 0.1 indicate "strong" gels (the storage modulus should be 10 times bigger than the loss modulus) [99].

2.7.3 Determination of Viscoelastic Characteristics

Viscoelasticity is determined by oscillatory tests, where the material is subjected to a controlled oscillation. Three factors are controlled in any given single test: the frequency of oscillation, the amplitude of oscillation, and temperature. A typical sweep test (continuous variation of a variable) holds two parameters constant while varying the third factor [97, 100]. In this section, the concept of linear viscoelastic region will be defined first, and the types of sweep tests will be described next.

2.7.3.1 Amplitude Sweep Test

During an amplitude sweep, the amplitude of the deformation - or the amplitude of the shear stress - is varied, while the frequency and temperature are kept constant. By using this test, we can obtain the linear viscoelastic region (LVR) of materials (Figure 2.14). The shear moduli of a material are independent of strain amplitude up to a given applied strain. Within this range, a material is said to be linear viscoelastic. Beyond that point, the structure of the material begins to break down, and the elastic modulus drops. A material that has a long LVR is indicative of a well-dispersed and stable system. In general, the LVR is shortest when the material is in its most solid form [97, 100].

Amplitude sweeps can also be used for determining the yield point and the flow point. As illustrated in Figure 2.14, the yield point (τ_y), sometimes also called yield stress, is the value of the shear stress at the limit of the LVR region. Beyond the yield stress, the material begins to flow. This point is also called the linearity limit. The flow point (τ_f), sometimes also called flow stress, is the value of the shear stress at the crossover point $G' = G''$. At higher shear, the viscous portion will dominate, and the sample will flow [97, 100].

2.7.3.2 Frequency Sweep Test

Dynamic (oscillatory) tests can measure time-dependent viscoelastic properties by varying frequency (deformation time), and the viscoelastic properties as a function of timescale

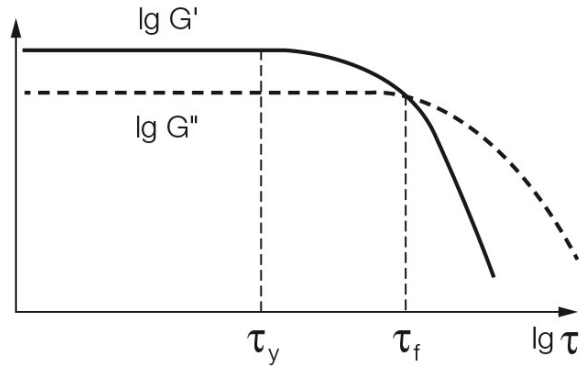


Figure 2.14: : G'' and G' as a function of shear stress showing LVR, yield stress, and flow point.

can be estimated [97, 100].

In a frequency sweep test, measurements are made over a range of frequency of the oscillation at a constant oscillation amplitude (stress or strain) and constant temperature. The strain should be in LVR as the material is stable in that region. The more frequency dependent the elastic modulus is, the more fluid-like is the material. The data at low frequencies describe the behaviour of the material at slow changes of stress (changes in stress take more time to occur, and make the frequency smaller) [97, 100].

2.7.3.3 Temperature Sweep Test

A temperature sweep test consists of constant frequency and amplitude oscillation conditions and changes of the temperature over time. Temperature sweeps are useful for measuring the temperature dependence of the viscoelastic properties, analyzing the gelation kinetics, gelation time, and the thermal transitions in food gels [97, 100].

In a temperature-sweep test for soy protein gels, the temperature gradually rises from $20 - 25^{\circ}\text{C}$ to $70 - 100^{\circ}\text{C}$ (heating step) and is maintained for about 10-30 minutes (incubation step). The temperature drops after the incubation process to reach the initial temperature (cooling step). G' and G'' are captured during the heating, incubation, and cooling steps. Zhao et al. (2020) performed a temperature-sweep test to investigate the gelation kinetics of CaSO_4 induced SPI gels. The heating step consisted of increasing the temperature from 25°C to 90°C for about 13 minutes, which induced protein gelation and network formation of SPI. The storage modulus after the heating step was about 6

time larger than the initial values. During the incubation step, the gel was relaxed for 10 minutes and its storage modulus increased by about 77% (1.8 times larger than the storage modulus before incubation). Finally, after 13 minutes of cooling, the storage modulus increased significantly. At the end of the cooling stage, the storage modulus became about 7 times higher, indicating that stronger bonds were formed in the SPI gel network. According to Zhao et al. (2020), hydrogen bond formation is more likely at lower temperatures [68].

2.7.4 Gelation Kinetics

The kinetics of gelation for soy protein gels has been conducted by observing the viscoelastic properties, G' and G'' over time under isothermal or non-isothermal circumstances, enabling the determination of the rate of gelation, the time required for the onset of gelation, and the final viscoelastic properties of the gel. Gelation kinetics were used to investigate the effect of coagulant type and concentration, protein source and concentration, incubation temperature, and additives.

Different temperature conditions can be used: constant temperature, semi-constant temperature, and temperature cycle. Typical constant temperature conditions consist of the addition of the coagulant to the protein solution at a constant temperature selected in the 50 – 90° C range, with the monitoring of the viscoelastic properties [101, 102, 15]. The semi-constant temperature conditions typically consist of the addition of the coagulants to the protein solution at room temperature. The solution is then placed in the rheometer and the temperature is increased to the desired incubation conditions, e.g. 60° C, and maintained constant for the desired duration [13]. The temperature cycle conditions typically consist of the addition of the coagulant to the protein solution at room temperature, and viscoelastic properties are monitored during the three phases of the cycle, heating, incubation, and cooling and their specific duration [7, 68].

Gelation kinetics experiments will consist of G' and G'' measurements according to time. Typically, G' is relatively constant at the beginning following the addition of coagulants. Then G' will increase after a few minutes/seconds, where the latent time (t_0) can be estimated, and then levelled off after a long time, indicating that G' has reached a constant value, known as the saturated storage modulus (G'_{sat}). Similar observations are obtained for the G'' . Equation 2.7 can be fitted into the collected data (G' or G'' vs time) [101, 102, 15, 13].

$$G'(t) = G'_{sat} \times [1 - \exp[-k(t - t_0)]] \quad (2.7)$$

In Equation 2.7, G'_{sat} , k , and t_0 are saturated storage modulus, rate constant, and latent time, respectively. These parameters can be estimated by the non-linear least square method. When t_0 tends to ∞ (measuring viscoelastic properties for a long time), then $\exp[-k(t - t_0)]$ goes to zero and G' reaches a constant value, G'_{sat} .

2.7.5 Viscoelasticity of soy protein gel

As indicated in section 2.2.2, soy protein gels are generated as a result of covalent and non-covalent interactions between protein, coagulant, and water molecules. The type and strength of the interactions can be related to the dependence of the storage and loss modulus on frequency. According to Murekatete et al. (2016), the dependency of G' and G'' to the angular frequency (ω) for the SPI and soymilk gels can be described by using equation 2.8 and 2.9, respectively [7],

$$G' = G'_0 \omega^{n'} \quad (2.8)$$

$$G'' = G''_0 \omega^{n''} \quad (2.9)$$

Where G'_0 (Pa) and G''_0 (Pa) are storage and viscous moduli at 1 rad.s^{-1} , respectively, and the exponents n' and n'' (both dimensionless) denote the influence of angular frequency on each specific modulus. The stronger the interactions in the gel network, the lower will be the dependence of G' and G'' on the frequency [7]. Identical n' and n'' values indicate that the created gel is strong and firm, whereas non-identical n' and n'' values indicate a weak gel formation and a soft gel was generated [7].

Table 2.5 represents some viscoelastic properties of acid- and salt- induced soy protein gels. As shown, the storage modulus of soy protein gels made with salt, acid, or a combination of the two is greater than the loss modulus ($\tan\delta < 1$), indicating that the material behaves like a gel. Furthermore, as compared to $CaSO_4$ induced SPI gel, GDL induced SPI gel may have a stronger elasticity (bigger G'). In the following sections, more information on the viscoelastic behaviour of salt- and acid- induced soy protein gels will be provided.

Table 2.5: Overview of rheological sweep tests for soy protein gels produced by salt or acid addition.

Sweep type	test	Gel preparation characteristics	Conditions	G' (Pa)	G'' (Pa)	$\tan\delta$	Ref.
Frequency		30mM $CaSO_4$ -induced 5% $w.w^{-1}$ SPI gel	strain: 0.5%, f: 1-100 Hz, T: 25° C	5000-8000	1000-1440	0.18-0.20	[7]
Temperature		0.05-0.1% $w.v^{-1}$ $CaCl_2$ and 0.14% citric acid-induced 6% $w.w^{-1}$ soybean gel,	strain: 0.5%, f: 1 Hz, T: 25–80° C	484-503	NR ^a	NR	[103]
Temperature		0.15% $w.v^{-1}$ $CaSO_4$ and 0.14% citric acid-induced 6% $w.w^{-1}$ soybean gel,	strain: 0.5%, f: 1 Hz, T: 25–80° C	609	NR	NR	[103]
Temperature		0.35% $w.v^{-1}$ $CaSO_4$ -induced 7.5% $w.v^{-1}$ SPI gel with 0-7% $w.v^{-1}$ soy oil,	strain: 1%, f: 1 Hz, T: 25 – 90° C	3500-5700	630-950	0.16-0.18	[68]
Frequency		30mM GDL-induced 5% $w.w^{-1}$ SPI gel,	strain: 0.5%, f: 1-100 Hz, T: 25° C	30000-45000	8000-13000	0.26-0.28	[7]
Temperature		0.14% $w.v^{-1}$ citric acid-induced 6% $w.w^{-1}$ soybean gel,	strain: 0.5%, f: 1 Hz, T: 25–80° C	434	NR	NR	[9]
Temperature		30mMv GDL-induced 5% $w.w^{-1}$ SPI gel	strain: 0.5%, f: 1 Hz, T: 25–85° C	2050-44300	430-9100	0.20	[12]

^aNot Reported

2.7.5.1 Salt-Induced Soy Protein Gel

$CaSO_4$ -induced soy protein gel, also known as gypsum tofu, produced a tofu that is soft and smooth with a uniform texture [7]. According to frequency-sweep tests results conducted by Murekatete et al. (2014), the storage modulus and $\tan\delta$ of $CaSO_4$ -induced SPI gel is in the range of 5000-8000 Pa and 0.18-0.20, respectively, and the dependency of G' to frequency was described by equation 2.10.

$$G' = 2,297.63 \times \omega^{0.105}, \quad G'' = 550.01 \times \omega^{0.109} \quad (2.10)$$

The storage and loss modulus of $CaSO_4$ -induced gel are somewhat frequency dependent, as expected ($n'=0.105$, $n''=0.109$), reflecting the predominance of physical bonds in $CaSO_4$ -induced SPI gel. The estimated n' and n'' are nearly identical, resulting in a strong gel [7].

Zhao et al. (2019) investigated the effects of combinations of $CaCl_2$ and $CaSO_4$ on citric acid-induced tofu properties, comparing them to $CaSO_4$ -induced gels (gypsum tofu). According to the temperature-sweep test, the salt combination and citric acid produced soy protein gels with final storage moduli that were nearly identical to gypsum tofu (G' at the end of cooling step at 25° C= 499.89 Pa for 0.35 g/100 mL $CaSO_4$, G' at the end of cooling step at 25° C= 502.44 Pa, 484.76 Pa, and 609.79 Pa for 0.14% $w.v^{-1}$ citric acid-induced tofu gels containing 0.10 g/100 mL $CaCl_2$, 0.05 g/100 mL $CaCl_2$, or 0.15 g/100 mL $CaSO_4$, respectively) [103].

According to the temperature sweep tests conducted by Zhao et al. (2020), increasing the soy oil volume fraction of $CaSO_4$ -SPI gel from 0 to 70 $ml.l^{-1}$ resulted in 62% and 51% enhancement in storage and loss modulus, respectively, and a small lowering of $\tan\delta$ from 0.18 to 0.16. These findings imply that the incorporation of soy oil, improved the elasticity, rigidity, and stiffness of $CaSO_4$ -induced SPI gel, and that soy oil behaved as active fillers in such gel environment [68].

2.7.5.2 Acid-Induced Soy Protein Gel

Murekatete et al. (2014) used the frequency-sweep test to determine the rigidity and investigate the interactions of GDL-induced SPI gels. The estimated storage modulus, loss modulus, and $\tan\delta$ of GDL-induced SPI gel are in the ranges of 30000-45000, 8000-13000, and 0.26-0.28, respectively. According to table 2.5 and presented data in section 2.7.5.1 (G' and $\tan\delta$ of $CaSO_4$ -induced SPI gel is in the range of 5000-8000 Pa and 0.18-0.20), the $\tan\delta$ of a GDL-induced SPI gel is much higher than that of a $CaSO_4$ -induced

SPI gel, implying that GDL may produce softer SPI gels. The frequency dependence of the measured viscoelastic properties of GDL-induced SPI gel is represented by Equation 2.11. Comparing the estimated n' and n'' values with that of the $CaSO_4$ induced SPI gel (Equation 2.10) suggests that GDL-induced gel is more frequency dependent than $CaSO_4$, and that the n' and n'' values are not identical (were not analyzed statistically), indicating weaker gel characteristics.

$$G' = 17,466.00 \times \omega^{0.129}, \quad G'' = 4,858.56 \times \omega^{0.133} \quad (2.11)$$

Other types of acid coagulants have recently sparked interest. Cao et al. (2017) showed that organic acids (citric acid, l(-)-malic acid, and tartaric acid) can be used to make different types of tofu (soft or firm). At an acid concentration of 0.14 g/100 mL, the final storage modulus values followed the order $G'_{Citric} > G'_{l(-)-malic} > G'_{Tartaric}$ (final storage modulus were 433.78, 264.43, and 129.79 Pa in tofu induced by citric, l(-)-malic, and tartaric acid, respectively, according to the temperature-sweep test). Interestingly, soymilk gels made with 0.14% *w.v*⁻¹ citric acid had almost the same storage modulus as 0.30% GDL-induced soybean gels [9].

According to temperature-sweep tests, Murekatete et al. (2016) found that increasing the soy oil volume fraction from 0 to 35% *w.v*⁻¹ reduced the elasticity and viscosity of the gel by approximately 90% and 95%, respectively. In an acidic environment, soy oil will act as an inactive filler that cannot effectively integrate into the GDL induced SPI gel network [12, 104]. On the other hand, increasing the soy oil volume fraction did not have considerable effect on the $\tan\delta$ value, and was approximately 0.20 for all GDL SPI gels.

2.8 Multi Comparison Tests

The researcher may need to understand subgroup differences among the various experimental and control groups. Differences between subgroups are referred to as "pairwise" differences. ANOVA does not allow for the testing of pairwise differences. The Multi Comparison Tests (MCTs), also known as a 'post-hoc test', is the only way to make this comparison. There are several MCTs available, each with its own way of controlling the significance level, relative power, and dealing with the error types I and II. Type I errors occur when H_0 is statistically rejected despite being true, whereas type II errors occur when H_0 is statistically accepted but H_0 is false.

MCTs are typically divided into two types: single-step and stepwise procedures. As the name implies, a single-step procedure assumes one hypothetical type I error rate. Almost

all pairwise comparisons are performed under this assumption. To put it another way, each comparison is independent. Fisher's least significant difference (LSD), Bonferroni, Scheffé, Dunnett, and Tukey tests are examples of single-step MCTs. The stepwise procedure handles type I error based on previously selected comparison results, which means it processes pairwise comparisons in a predetermined order and only performs each comparison when the previous comparison result is statistically significant. The stepwise methods include Duncan test, Ryan-Einot-Gabriel-Welsch Q (REGWQ), and Student-Newman-Keuls (SNK).

Bonferroni, Duncan's, Tukey, and LSD are the most common MCTs methods used in biochemical engineering [11, 57, 7, 13, 51]. Table 2.6 summarises the benefits and drawbacks of each test. Duncan's test, out of all the comparison tests listed in Table 2.6, would be a better fit for our study because it is effective in detecting statistical differences while accounting for Type I error, considers the number of treatments, can be used for dependent variables, is included in STATISTICA packages, and is suitable for small numbers of treatments. So, the minimum significant differences between means were determined by Duncan's multiple range test at a significance level of 0.05. Mechanical testing and frequency sweep testing each had seven and three replicates, respectively, with results expressed as means \pm standard deviation.

Table 2.6: Summary of benefits and drawbacks of various Multi Comparison tests [105, 106, 107, 108]

Test	Advantages	Disadvantages
LSD	<ul style="list-style-type: none"> - Simple - Available in many statistical packages - Powerful - Maybe used with unequal sample sized groups 	<ul style="list-style-type: none"> - α inflation - Multiple Type I errors - Unreliable results due to overestimation of differences among pairs
Bonferroni	<ul style="list-style-type: none"> - Preserve α - Available in many statistical packages - Reduces risk of Type I errors - Can test differences among experimental groups as well as between experimental and control groups - More rigorous than Tukey test 	<ul style="list-style-type: none"> - Weak statistical power - Not good for avoiding Type II error
Tukey HSD	<ul style="list-style-type: none"> - Considers number of treatments - Useful in confirmatory research when combinations of groups is not meaningful - Reduces risk of Type I error - Good for doing all pairs comparison - Good for high numbers of treatments 	<ul style="list-style-type: none"> - Observations must be independent within and among groups - Not good for small numbers of treatments
Duncan's	<ul style="list-style-type: none"> - Considers number of treatments - Good for small numbers of treatments - Powerful - Powerful in detecting statistical differences while considering Type I error 	<ul style="list-style-type: none"> - Not good for high numbers of treatments

Chapter 3

Gelation Kinetics

3.1 Overview

Gel formation characteristics are critical considerations when developing formulations for food gel materials. Among gel characteristics, viscoelastic properties can provide insights and assist with the understanding of interactions between the constituents and their role in the gel formation and ultimately the final gel, namely the strength, microstructure, water holding capacity (WHC), and sensory attributes.

The gelation kinetics can be observed by monitoring the evolution over time of the viscoelastic properties, storage modulus (G') and loss modulus (G''), of the gel formulation. Gelation kinetics can be investigated by conducting temperature sweep experiments where the temperature profile and heating rates are controlled while the evolution of (G') over time and temperature is captured. In this work, four different studies of the gelation kinetics of soy protein systems (Table 3.1), were selected to illustrate the effect of the source of soy protein, coagulant type, coagulation conditions, and the benefits of empirical models for the analysis of the experimental profile of the change of (G') over time.

Specifically, the source of soy protein includes Soy Protein Isolate (SPI), 11S soy globulin, and dried soymilk, coagulants include $CaSO_4$, a salt coagulant, and GDL an acid coagulant, soybean oil for producing soy emulsion gels and pressure for processing.

Table 3.1: Selected studies of the gelation kinetics of soy gel and soy emulsion gels. OC: Oil Content, OT: Oil Type

Soy Protein	Coagulant	Soybean Oil	Rheology	Temperature condition	Frequency (Hz)	Strain amplitude
4% 11S globulin [101]	0.4% GDL	-	Rheograph Sol (Toyoseiki Seisakusho), a Parallel plate (internal dimensions 2.6 mm \times 15 mm \times 45 mm)	Constant T (section 2.7.4), cell and 10 ml protein solution were preheated to 5°C below the desired T . Then, the T was reached to the desired T (50 – 90°C) and GDL was added	2	125 μ m
5% SPI [102]	20 mM GDL or 30 mM $CaSO_4$	-	Rheograph Sol (Toyoseiki Seisakusho), a Parallel plate (internal dimensions 2.6 mm \times 15 mm \times 45 mm)	Constant temperature (section 2.7.4) (50 – 90°C) and 10 ml of SPI solution	1	25 μ m
4% Dried soymilk [15]	0.02 N (5 mM) GDL	-	Controlled stress rheometer (Carri-Med CSL-100), a double-cylindrical	Constant T (section 2.7.4), 3.5 ml soymilk preheated outside the rheometer to the desired T (55 – 80°C), after addition of GDL, protein solution was loaded to the rheometer cell which was preheated to same T	1	0.1%
4.5% SPI [13]	2% GDL	OC: 4% w/w, OT: soybean oil	DHR-2 rotary rheometer, a parallel plate with diameter of 40 mm and gap of 1 mm	Semi-constant T (section 2.7.4), GDL was added to 10 g soymilk at 5°C, then was mixed and loaded to the rheometer cell with same T . The T then was set to 60°C	1	0.5%
75 $g.l^{-1}$ SPI [68]	3.5 $g.l^{-1}$ $CaSO_4$	OC: 10, 30, 50, and 70 g/l, OT: soybean oil	AR-G2 Rheometer, a parallel plate with diameter of 40 mm	Semi-constant T (section 2.7.4), After addition of coagulant samples were loaded to the rheometer. Samples were heated from 25° C to 90° C at a heating rate of 5° C/min, followed by incubation at 90° C for 10 min and subsequently cooled to 25° C at a cooling rate of 5° C/min.	1	1%

3.2 Methodology

The methodology employed for the analysis of the kinetics of gelation was based on the changes over time of the storage modulus parameter G' and the empirical model, discussed previously in section 2.7.4, and described by Equation 2.7.

$$G'(t) = G'_{sat} \times [1 - \exp[-k(t - t_0)]]$$

The representation of each set of experimental data (G' vs t) with Equation 2.7 is characterized by its set of parameters G'_{sat} , k and t_0 for a given protein concentration, coagulant type and concentration and operating conditions.

Published experimental data of G' presented in a table or figure format were used. When presented in a figure format (5% SPI at 70° C coagulated with 30 mM $CaSO_4$ or 20 mM GDL at frequency of 1 Hz and amplitude of 25 μm (Figure 3.1) and 75 $g.l^{-1}$ SPI and 3.5 $g.l^{-1}$ $CaSO_4$ concentration with different soy oil volume fractions (Figure 3.2)), digitalization of the figure was required and details will be presented in the next section.

Once digitalized values of G' were generated, the parameters G'_{sat} , k and t_0 were estimated by least squares method and this will also in what follows.

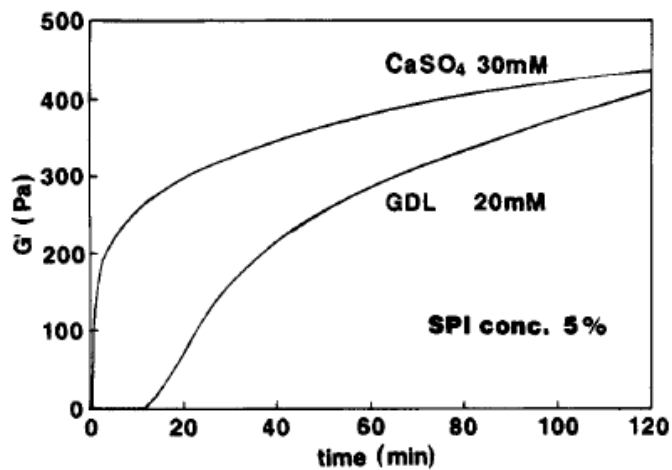


Figure 3.1: Experimental storage modulus reported by Koyama et al. (1995) [102] for 5% SPI at 70°C coagulated with 30 mM $CaSO_4$ or 20 mM GDL at frequency of 1 Hz and amplitude of 25 μm . The permission to use the graph was obtained. See Appendix 6.9.

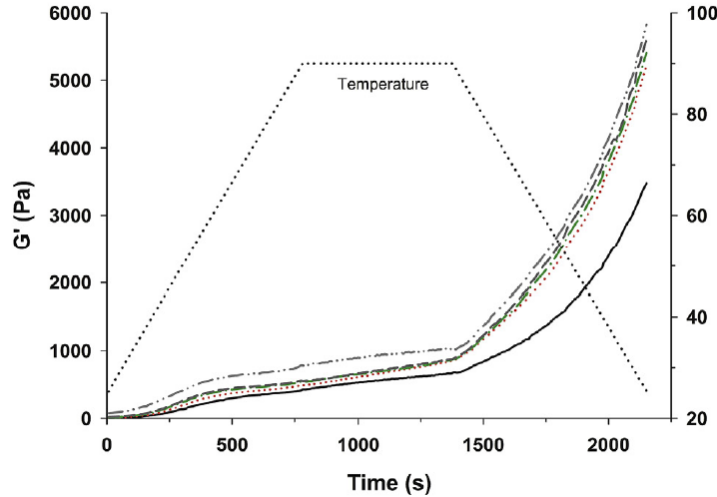


Figure 3.2: Temperature-sweep test results for the storage modulus (G') as a function of time obtained during temperature sweep at 1 Hz frequency and 1% strain for 75 g.l^{-1} SPI and 3.5 g.l^{-1} CaSO_4 concentration, containing different soy oil volume fractions (0% v/v: —; 1% v/v: ·····; 3% v/v: -·-·-·; 5% v/v: - - - -; 7% v/v: - · - · - ·) [68]. The permission to use the image was obtained. See Appendix 6.10.

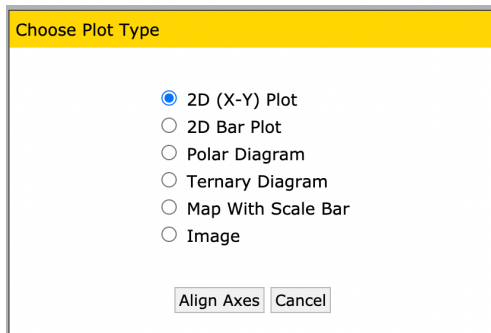
3.2.1 Data Extraction

When gelation kinetics were reported in a Figure format, the corresponding numerical data were generated with WebPlotDigitizer, <https://apps.automeris.io/wpd/>. This method was used for the study conducted by Kohyama et al. (1992) for 11S globulin gels [101], Kohyama et al. (1995) for SPI gels [102], Chang et al. (2009) for dried soy milk gels [15], and Zhao et al. (2020) for SPI soybean oil gel emulsions [68].

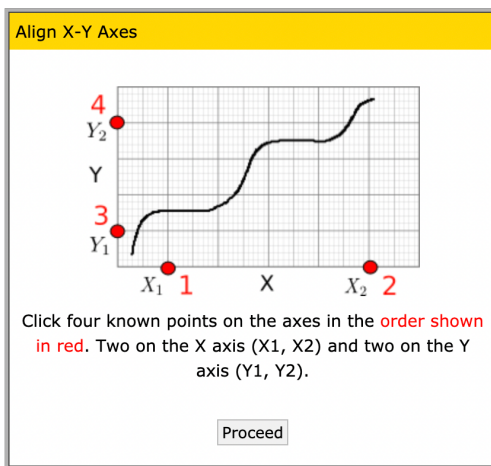
Specifically, the first step was the uploading of the figure in the WebPlotDigitizer website. The 2D (X-Y) plot was selected as a plot type, and then the X and Y axis were aligned. At the final step, the X and Y axis were calibrated by choosing two points on the axis and selecting Log scale, if necessary (Figure 3.3). This process helped determine and extract data from figures with much lower error compared to visual extraction.

An example of the above approach is illustrated in Figure 3.4 for the gelation kinetic of SPI-emulsion gels published by Zhao et al. (2020) [68], and the data extracted by WebPlotDigitizer (the digitized part is illustrated in Figure 3.4)

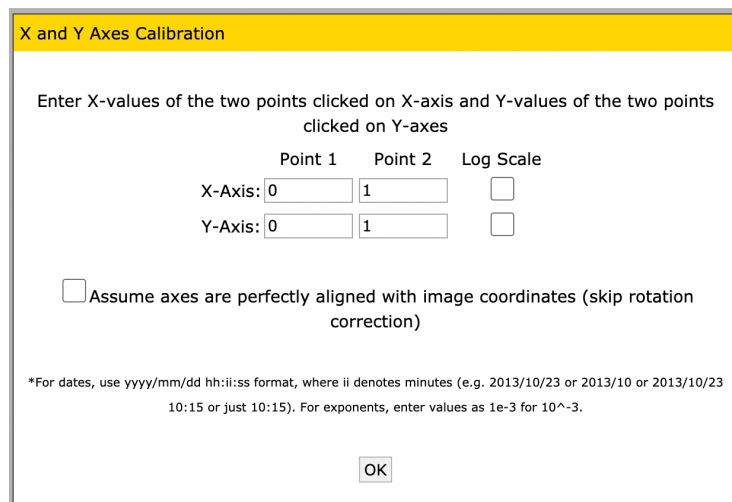
Figure 3.4 represents the gelation kinetic of SPI-emulsion gels according to Zhao et



(a)



(b)



(c)

Figure 3.3: WebPlotDigitizer screenshots for selecting plot type (a), aligning axis (b), and calibration (c) [109]

al. (2020), and the gelation kinetics obtained by WebPlotDigitizer (does not include the cooling step).

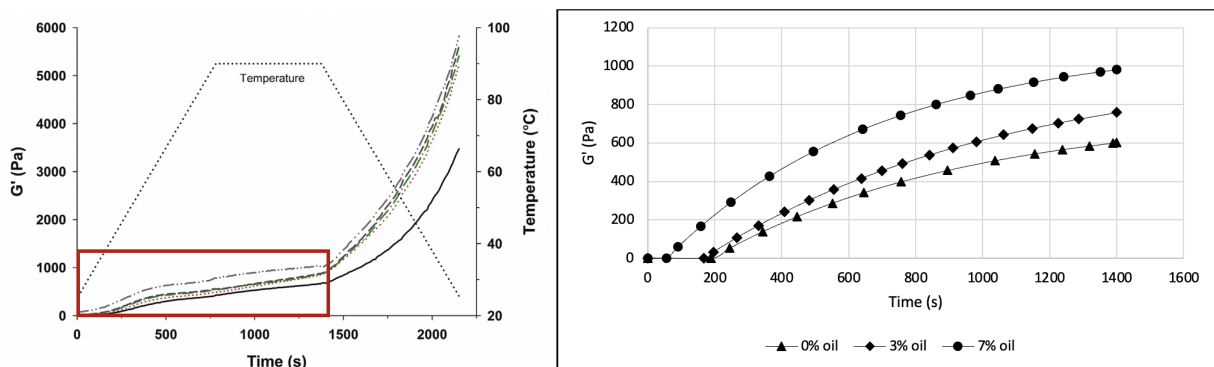


Figure 3.4: Left: published G' vs time profile for SPI-emulsion gels for the heating and incubation step reported by Zhao et al. (2020) (0% v/v: —; 1% v/v: ·····; 3% v/v: -·-·-·; 5% v/v: ----; 7% v/v: -·-·-·-·) [68]. The bottom red rectangle in the left figure was digitized. Right: Generated digitized profile of G' vs time of the SPI-emulsion gels data from Zhao et al. (2020).

3.2.2 Estimation of the Gelation Kinetics Parameters by Least-Squares

The gelation kinetics parameters were estimated by least squares using Excel and the Solver function. A least squares method is a mathematical regression method to determine the best fit for a set of data, providing a visual demonstration of the relationship between the data points. The purpose of the method is to generate a line or a curve that minimizes the sum of the squares of the errors that are generated by the results of the associated equation, such as the squared residuals resulting from differences in the observed value, and the value anticipated, based on the equation.

By considering G' as an observed storage modulus and \hat{G}' as an estimated storage modulus value, which was calculated from Equation 2.7, the residual or error for each observation follows Equation 3.1:

$$Residual = G' - \hat{G}' \quad (3.1)$$

The **Sum of Squared Errors (SSE)** then follows Equation 3.2. The purpose of defining the **SSE** is to minimize the sum of errors (or residuals) between the observed and the estimated values to find the best model that fits the data. In Equation 3.2, N is the total number of observations.

$$SSE = \sum_{n=1}^N (G' - \hat{G}')^2 \quad (3.2)$$

The time (independent variable) and G' (dependent variable) were obtained by using WebPlotDigitizer as discussed previously (first step). As an example, consider the results obtained by Zhao et al. (2020) for **SPI** soybean oil emulsion gels [68]. When using Excel for minimizing the **SSE**, an initial value to G'_{sat} , k , and t_0 is required. Considering the extracted data obtained from Zhao et al. (2020) for gelation kinetic of **SPI** gel (0% oil volume fraction), the following values obtained by visual inspection were selected as initial values. Three different sets of initial values were considered. Set 2 represents the values obtained by visual inspection, whereas set 1 and set 3 were calculated as 20% lower and higher than set 2, respectively.

1. $G'_{sat} = 560 \text{ Pa}$, $k = 0.0010 \frac{1}{s}$, and $t_0 = 160 \text{ s}$
2. $G'_{sat} = 700 \text{ Pa}$, $k = 0.0013 \frac{1}{s}$, and $t_0 = 200 \text{ s}$
3. $G'_{sat} = 840 \text{ Pa}$, $k = 0.0015 \frac{1}{s}$, and $t_0 = 240 \text{ s}$

Minimizing the **SSE** was obtained for three different sets of initial values to ensure that the estimated parameters remained constant and were independent of the initial values.

By considering the three sets of initial values, the \hat{G}' and residuals were estimated with Equation 2.7 and 3.1, respectively. Then, by computing the **SSE** and using the Solver function in Excel, the values of G'_{sat} , k , and t_0 were estimated.

As shown in Table 3.2, the estimated model parameters are similar for each set of initial values. Figure 3.5 represents the observed G' curve (based on the extracted values by WebPlotDigitizer) and predicted G' curve (R^2 was 0.96).

Table 3.2: Estimated values for G'_{sat} , k , and t_0 by using three sets of initial values for the gelation kinetics of SPI gel (0% oil volume fraction from Zhao et al. (2020) [68]).

Parameters	Initial Sets		
	1	2	3
G'_{sat} (Pa)	757	757	757
k (s^{-1})	0.0013	0.0013	0.0013
t_0 (s)	186	186	186

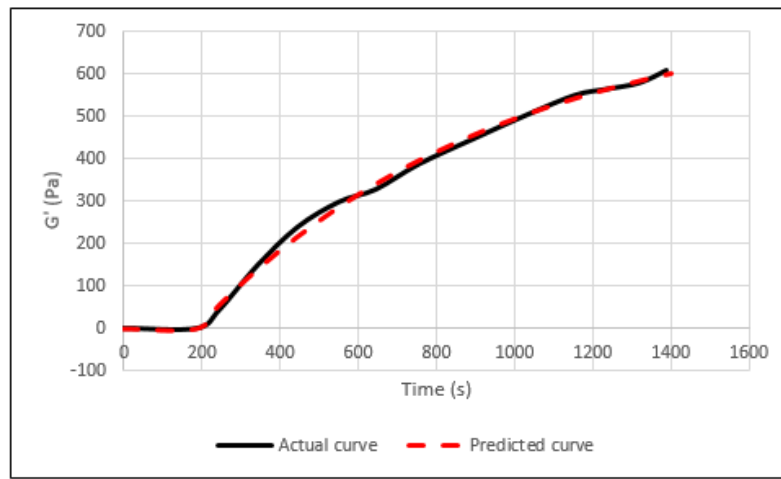


Figure 3.5: Observed and predicted G' vs time for set 2 of initial values (Table 3.2) for the gelation kinetics of SPI gel (0% oil volume fraction from Zhao et al. (2020) [68]).

3.3 Gelation Kinetics and Storage Modulus

3.3.1 Effect of Temperature and Soy Protein Source on Gelation Kinetics

One of the critical factors influencing the properties of protein gels is the coagulation temperature. In this section, the role of temperature on the gelation kinetics with GDL and three different sources of soy protein will be discussed. The source of soy proteins includes soybean 11S (Kohyama et al. (1992) [101]), SPI (Kohyama et al. (1995) [102]), and dried soy milk obtained during touhua preparation (similar to packed tofu) (Chang et al. (2009) [15]). Table 3.1 shows the amounts and types of ingredients for each study.

The estimated kinetic parameters, k , t_0 , and G'_{sat} , are presented in Table 3.3, 3.4, and 3.5.

Table 3.3: Effect of coagulation temperature on the estimated k and t_0 for 4% (unit was not provided) 11S globulin coagulated with 0.4% GDL. The constant temperature was selected for the rheological set-up at frequency of 2 Hz and amplitude of 125 μm [101]. Permission to use the figures was obtained. See Appendix 6.11.

Parameters	Temperature ($^{\circ}C$)				
	50	60	70	80	90
k (s^{-1})	0.0003	0.0055	0.0138	0.0244	0.0692
t_0 (s)	152	68	35	17	0

Table 3.4: Effect of coagulation temperature on the estimated k and G'_{sat} for 5% (no unit was provided) SPI coagulated with 30 mM $CaSO_4$. The constant temperature was selected for the rheological set-up at frequency of 1 Hz and amplitude of 25 μm [102]. Permission to use the figures was obtained. See Appendix 6.9

Parameters	Temperature ($^{\circ}C$)				
	50	60	70	80	90
k (s^{-1})	0.0011	0.0018	0.0017	0.0021	0.0024
G'_{sat} (Pa)	516	454	393	300	176

As expected, increasing the temperature increased the gelation rate constant, k , which supports faster gelation rate. The magnitude of the rate constant is more significant for 11S globulin, increasing by about 230%, while the magnitude of the rate constant of SPI and dried soymilk increased by only 1.2% and 2.3%, respectively, for a similar temperature increase. Dried soymilk had the smallest rate constant of the three soy protein sources (Figure 3.6). This suggests that the soy protein source may impact the gelation kinetics. It is important to highlight that the rheological equipment, set-up, operating conditions, and coagulant type differed according to the study and may have influenced the gelation kinetics.

Increasing temperature reduced t_0 , and resulted in a shorter gelation time [101, 15] such that at 90 $^{\circ}C$, 11S globulin gelation occurred immediately when GDL was added to the protein mixture ($t_0 \sim 0$) [101]. The estimated latent time was reduced by about 84-88% in a temperature range of 50 – 80 $^{\circ}C$, and was much lower than that of soymilk, and

Table 3.5: Effect of temperature on k , t_0 , and G'_{sat} for 4% w/v dried soymilk coagulated with 0.02 N (5 mM) GDL. The constant temperature was selected for the rheological set-up at frequency of 1 Hz and strain of 0.1% [15]. Permission to use the data was obtained.

Parameters	Temperature ($^{\circ}C$)					
	55	60	65	70	75	80
k (s^{-1})	0.0003	0.0004	0.0005	0.0006	0.0008	0.0009
t_0 (s)	738	486	270	246	162	102
G'_{sat} (Pa)	79	83	91	119	153	121

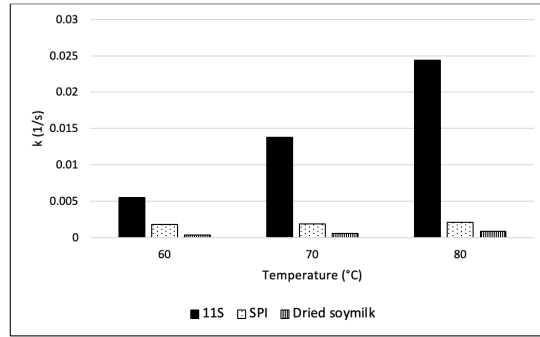


Figure 3.6: Estimated gelation kinetic rate constant (k) at three different temperatures for three sources of soy protein (11S (Kohyama et al. 1992 [101]), SPI (Kohyama et al. (1995) [102]), and dried soy milk (Chang et al. (2009) [15])).

more pronounced at lower temperatures. Comparing the estimated G'_{sat} of SPI and dried soymilk in the temperature range of 55–80 $^{\circ}C$ reveals that a 2-5% higher G'_{sat} was observed for SPI gel (Figure 3.7). 11S also created gel with G'_{sat} between SPI and dried soymilk (G'_{sat} of 11S gel was reported for two temperatures: at 60 $^{\circ}C$, $G'_{sat} = 249$ Pa, and at 80 $^{\circ}C$ $G'_{sat} = 156$ Pa). G'_{sat} was affected differently by changes in temperature where temperature increase resulted in a 65% reduction of G'_{sat} for SPI [102], whereas G'_{sat} increased to about 93% to reach a maximum value at 75 $^{\circ}C$, then decreased to 121 Pa for dried soymilk [15]. This disparity could be attributed to the type and concentration of the protein source and the type and concentration of the coagulant and preparation methods (Table 3.1).

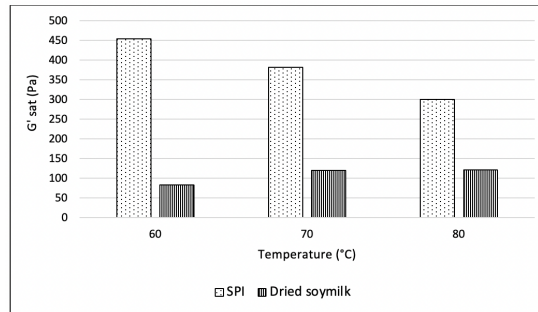


Figure 3.7: G'_{sat} estimates for gelation kinetics according to temperature and two sources of soy protein (SPI, coagulant: $CaSO_4$ (Kohyama et al. (1995) [102], and dried soy milk, coagulant: GDL (Chang et al. (2009) [15])).

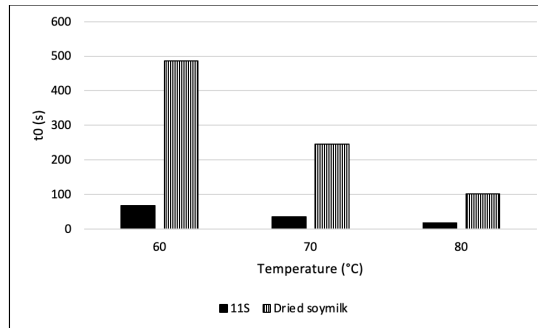


Figure 3.8: t_0 estimates of the gelation kinetics with GDL according to temperature for two different sources of soy protein (11S (Kohyama et al. (1992) [101] and dried soy milk (Chang et al. (2009) [15])).

3.3.2 Effect of Coagulant Type and Concentration on Gelation Kinetics

The level of coagulant will affect protein gel characteristics which can be captured by monitoring differences in their rheological properties. As discussed in section 2.2.2, increasing coagulant concentration may increase the storage and loss modulus until a maximum is reached, G'_{sat} , at which point the coagulant level may have a detrimental effect on the gelation. In fact, a large amount of coagulant may produce large aggregates and lumps, lowering G' and G'' . Consider the gelation kinetics of SPI (Figure 3.9), where the maximum $G'_{sat}=480$ Pa, is observed at a concentration of 35 mM $CaSO_4$.

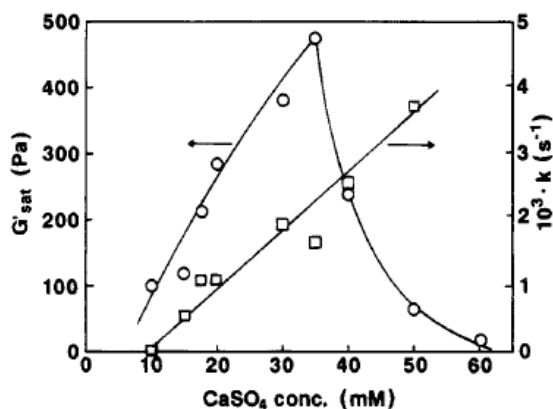


Figure 3.9: G'_{sat} and k values for 5% (the unit was not mentioned) SPI-gels prepared with various concentration of $CaSO_4$. According to Kohyama et al. (1995) [102], the constant temperature was selected for the rheological set-up at frequency of 1 Hz and amplitude of 25 μm . Permission to use the data was obtained. See Appendix 6.9.

The gelation kinetics of soy protein is generally affected by the type of coagulant. Kohyama et al. (1995) [102] compared 30 mM $CaSO_4$ and 20 mM GDL-induced SPI gels with the same SPI content at different temperatures (Table 3.6 and Figure 3.1).

Table 3.6: Estimated k and G'_{sat} values for 5% SPI gels prepared with two different coagulants (30 mM $CaSO_4$ or 20 mM GDL) and different temperatures. The constant temperature was selected for the rheological set-up at frequency of 1 Hz and amplitude of 25 μm [102]. Permission to use the figures was obtained. See Appendix 6.9

Coagulant	Temperature ($^{\circ}C$)							
	60		70		80		90	
	k	G'_{sat}	k	G'_{sat}	k	G'_{sat}	k	G'_{sat}
$CaSO_4$	0.0018	454	0.0017	381	0.0021	300	0.0024	176
GDL	2.6×10^{-4}	448	4.1×10^{-4}	393	4.9×10^{-4}	363	9.1×10^{-4}	241

According to Figure 3.10, the estimated rate constants (k) for $CaSO_4$ induced SPI gels was roughly 2.6-7 times greater than that of GDL induced gels, implying a faster gel formation with $CaSO_4$ as a coagulant. The rate of gelation of the GDL induced gel, on the other hand, was more sensitive to temperature increases. The estimated k for GDL-

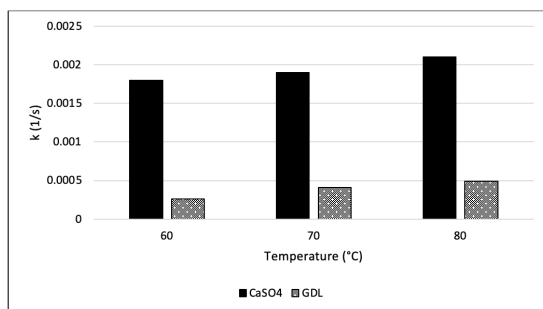


Figure 3.10: Estimated gelation rate constant (k) for 5% (units were not mentioned) SPI gels prepared with two different coagulant (30 mM $CaSO_4$ or 20 mM GDL) and different temperatures. The rheological measurements were done at frequency of 1 Hz and amplitude of 25 μm [102].

induced gels increased by around 3.5 times when the temperature was raised from 60° C to 90° C, but only by 1.3 times for $CaSO_4$ induced gels.

The estimated G'_{sat} for GDL induced SPI gels was roughly 3-36% higher than for $CaSO_4$ induced SPI gels (except at $T = 60^\circ C$), as indicated in Figure 3.11. With increasing temperature, the difference in G'_{sat} was more significant. $CaSO_4$ induced SPI gel is more sensitive to temperature as increasing temperature from 60° C to 90° C reduced G'_{sat} by 61%, whereas for GDL induced gels, G'_{sat} decreased by 46%. Moreover, $CaSO_4$ induced SPI gels had an estimated latent time around 0 at 70° C, which was much smaller than GDL induced SPI gels.

The difference between these two coagulants reflects their different gelation mechanisms (section 2.2.2). The hydrophobic regions of protein molecules are initially hidden inside the native state and are exposed to the outside by heat denaturation. The formation of protons induced by GDL or Ca^{+2} ions neutralizes the net charge of the denatured soy protein, which is negatively charged. The different net charges of H^+ and Ca^{+2} may affect soy protein network formation and, as a result, the gelation kinetics of Ca^{+2} and GDL induced SPI gels. As depicted in Figure 3.12, H^+ could only interact with one negative side of a protein particle, while Ca^{+2} can create bond and entangle protein particles through two positive charges [102]. It is worth noting that the concentrations of $CaSO_4$ and GDL were also different.

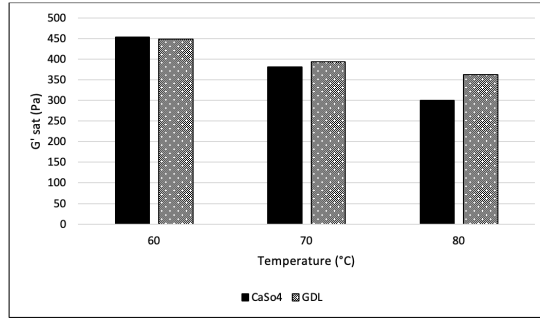


Figure 3.11: G'_{sat} values for 5% (units were not mentioned) SPI-gels prepared with two different coagulant (30 mM $CaSO_4$ or 20 mM GDL) in different temperatures. According to Kohyama et al. (1995) [102], the constant temperature was selected for the rheological set-up at frequency of 1 Hz and amplitude of 25 μm .

3.3.3 Effect of Soy Protein Isolate (SPI) Concentration on Gelation Kinetics

The estimated G'_{sat} (Table 3.7) for gels prepared with different concentrations of SPI and 30 mM $CaSO_4$, at 70°C (Kohyama et al. (1995) [102]) increased roughly 13 times as SPI concentration increased from 2% to 7% (units were not mentioned). By increasing the protein concentration, more protein molecules will be involved in the gel network, contributing to a higher saturated storage modulus.

Table 3.7: Estimated rate constant (k) and G'_{sat} for SPI-gels coagulated with 30 mM $CaSO_4$ at 70°C and different SPI concentration [102]. Permission to use the data was obtained.

Parameter	SPI concentration					
	2%	3%	4%	5%	6%	7%
k (s^{-1})	0.0006	0.0029	0.0035	0.0025	0.0013	0.0008
G'_{sat} (Pa)	68	164	284	367	686	917

As the SPI concentration increased from 2% to 4%, the estimated rate constant increased by about 6 times (Table 3.7). The estimated k values decreased to 0.0008 (s^{-1}) after reaching a maximum at 4 % SPI (the unit was not mentioned). This reduction could probably be due to the lack of coagulant content for higher protein concentration.

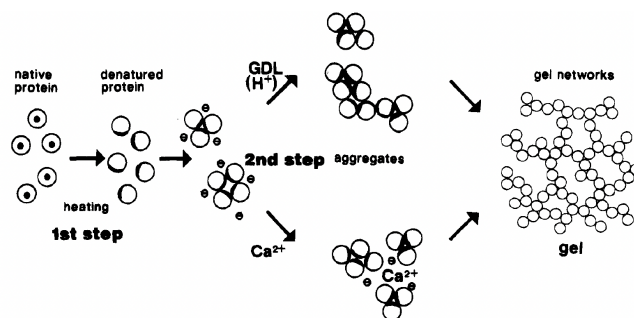


Figure 3.12: Gelation mechanism of soy proteins with GDL or $CaSO_4$: (circles) protein molecules; (black areas) hydrophobic regions [102]. Permission to use the data was obtained. See Appendix 6.9.

According to Kohyama et al. (1992) [101] and Chang et al. (2009) [15], increasing protein content while using a fixed amount of coagulant increased the latent time (t_0), delaying the initiation of the gelling.

3.3.4 Gelation Kinetics of SPI and SPI-Emulsion Gels

The addition of oil can alter the rheological properties and gelation kinetics of soy protein gels, as discussed previously in section 2.2.3. Liquid oils, such as soy oil, can participate in the protein network of salt-induced soy protein gels and act as active fillers, increasing the G' and G'' , while decreasing these properties for acid-induced soy protein gels [7, 68, 38, 110]. Some studies have shown that oils which are solid at room temperature, such as palm stearin oil, act as completely active fillers, regardless of whether soy protein gels have been induced by acid or salt [7, 68, 38, 110]. This result could be attributed to the crystalline characteristics of palm stearin oil and the stronger interactions between protein and oil for solid oil compared to liquid oil at acidic pH [38].

Zhao et al. (2020) [68] performed a rheological temperature-sweep test with a strain of 0.01 (1%) and a frequency of 1 Hz to investigate the gelation kinetics of SPI-soy oil emulsion gels coagulated with $CaSO_4$. The SPI and $CaSO_4$ concentration were set to 75 $g.l^{-1}$ and 3.5 $g.l^{-1}$ and soy oil content of 0-7% v/v. The evolution of G' for the incubation and heating and cooling phases (Figure 3.2) consists of a slow increase of G' during the incubation and heating stages followed by a sharp increase during the cooling stage.

The estimated gelation kinetics parameters (Table 3.8) and the corresponding digitized G' profiles over time (Figure 3.13), and experimental data (Figure 3.2), indicate that

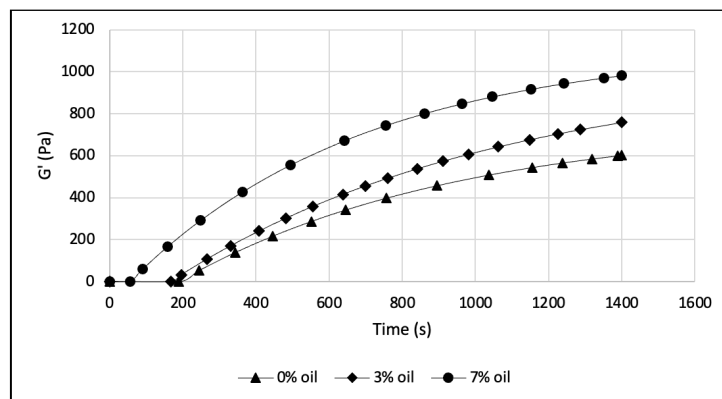


Figure 3.13: Digitalized gelation curve for 75 g.l^{-1} SPI-soy oil emulsion gels with 3.5 g.l^{-1} CaSO_4 during heating (25°C to 90°C) and incubation (90°C) at frequency of 1 Hz and strain of 1% for 0% v/v, 3% v/v, and 7% v/v of oil. Details of the digitalized curve are presented in Table 3.8.

Table 3.8: Estimated G'_{sat} , k , and t_0 for SPI-soy oil emulsion gels containing 0%, 3%, and 7% v/v soy oil from the temperature-sweep test (heating and incubation stages only) at frequency of 1 Hz and strain of 1% according to Zhao et al. (2020) [68]. SPI and CaSO_4 concentration were 75 g.l^{-1} and 3.5 g.l^{-1} .

Oil volume fraction (% v/v)	G'_{sat} (Pa)	k (s^{-1})	t_0 (s)
0	756	0.0013	186.1
3	1011	0.0011	167.2
7	1118	0.0015	55.2

* The presented data are obtained from Solver function of Excel.

increasing the oil volume fraction from 0% to 7% v/v increased G'_{sat} by 48% (Figure 3.8). The changes in estimated G'_{sat} could reflect the hydrophobic interaction between the oil and proteins. Oil may act as an active filler, and become actively incorporated within the soy protein network. Subsequently, the oil and protein interaction causes an increase in the G' and G'_{sat} values.

According to Table 3.8, as the oil volume fraction increased, the induction time (t_0) decreased. The smaller t_0 estimated at higher oil content can reflect favorable interactions between oil and protein. The estimated gelation rate constant (k) remained relatively constant for these conditions.

By comparing the gelation kinetics estimates for SPI gels and SPI soy oil emulsion gels

obtained with $CaSO_4$, one can conclude that the SPI soy oil emulsion gels had higher G'_{sat} with shorter latent time estimates than the SPI gels.

3.3.5 Effect of Homogenization Pressure on Gelation Kinetics

The preparation of emulsion gels requires the creation of an emulsion with finely dispersed oil droplets which is strongly dependent on the operating conditions. Bi et al. (2020) [13] investigated the effect of high-pressure homogenization during the preparation of SPI soy oil emulsion GDL gels with a 4.5% (w/w) soy oil. SPI was dissolved in deionized water, followed by oil addition and high-pressure homogenization. All the emulsions were homogenized at the pressure of 5 MPa, as a pre-processing step, and then emulsion solutions were treated at 5, 10, 20, 40, 60, or 80 MPa. Subsequently, 2% (w/w) GDL was added to the emulsion solutions at room temperature, and samples were transferred to the rheometer. During the rheological measurements, the temperature was raised from room temperature to the coagulation temperature, $60^\circ C$, and then kept constant (semi-constant temperature. Figure 3.14 depicts the experimental G' values over time of this study.

The estimated gelation kinetic parameters, presented in Table 3.9, G'_{sat} increased by 81% when the homogenization pressure increased from 5 MPa to 80 MPa. The estimated t_0 decreased by 4% while the estimated rate constant, k , remained constant [13].

The increase in homogenization pressure may have disrupted the covalent cross-linking of the protein disulfide bonds, increasing protein denaturation and the exposure of hydrophobic groups, which then increases the number of active sites available for protein gel formation. The increased pressure may also have reduced the size of the oil droplets, thus enhancing the contact area between oil and other constituents. The estimated t_0 was 4% smaller by increasing the homogenization pressure, while the estimated rate constant, k , remained constant [13].

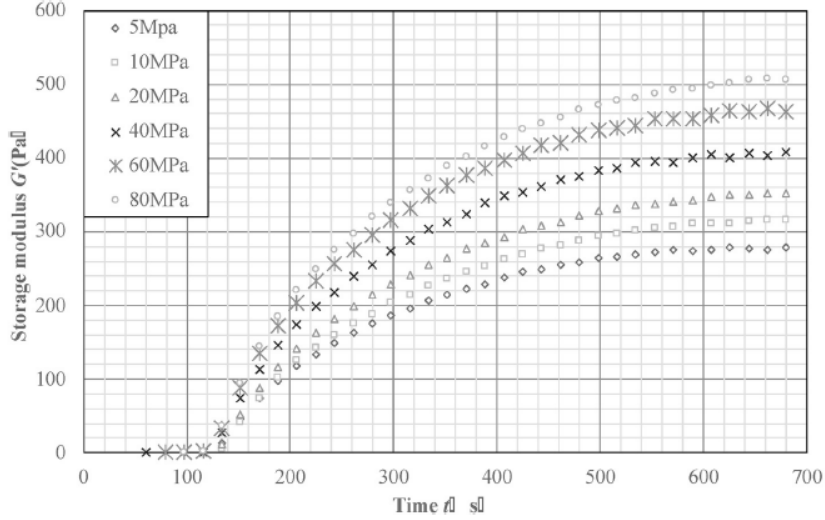


Figure 3.14: Experimental profile of G' with the time at different homogenization pressure for SPI soy oil emulsion gel with 4.5% (w/w) SPI, 4.5% (w/w) soy oil, and 2% GDL. Gelation process was done at frequency of 1 Hz and strain of 0.5% [13]. Permission to use the image was obtained. See Appendix 6.13.

Table 3.9: G'_{sat} , k , and t_0 for SPI soy oil emulsion gels in different homogenization pressure with protein and oil concentration of 4.5% (w/w). 2% GDL was used during gelation process at frequency of 1 Hz and strain of 0.5 [13]. Permission to use the data was obtained.

Homogenization pressure (MPa)	G'_{sat} (Pa)	k (s^{-1})	t_0 (s)
5	292	0.006	123
10	333	0.006	127
20	370	0.006	125
40	426	0.006	120
60	484	0.006	119
80	528	0.006	117

3.4 Conclusion

The investigation of the gelation kinetics, obtained from measurements of the storage modulus, can assist with the selection of ingredients for the creation of soy protein gels and their influence on the gel formation and gel properties. In this chapter, the gelation kinetics for three different sources of soy protein, 11S, SPI, and dry soymilk, different heating temperature conditions, coagulant type and concentration, soybean oil volume fraction, and homogenization pressure were analyzed. According to the analysis, higher heating temperature increased the gelation rate, allowing gels to start and finish faster. So, a coagulation temperature of 95° C may be chosen while keeping in mind that the two major subunits of soy protein are denatured at those conditions. The gelation kinetics for SPI gels were slower than 11S but faster than dried soymilk and produced gels with the highest stiffness and G'_{sat} . As a result, the use of SPI as a source of soy protein can produce stiffer and more elastic gels. This could also make sense as SPI is an isolated soy protein source with more than 90% of protein content. The SPI concentration analysis suggests that increasing the SPI concentration from 2% to 7% could improve the final storage modulus of a gel about 13 times.

A comparison of the gelation kinetics for SPI with two different coagulants, $CaSO_4$ and **GDL**, revealed that $CaSO_4$ -induced gel had much higher gelation rate while having comparable G'_{sat} to the **GDL** induced gel. Finally, the analysis of the gelation kinetics for the creation of SPI emulsion gels, is different from SPI gels. Two important factors affecting the gelation kinetics of SPI-emulsion gels are oil volume fraction and homogenization pressure. Both factors could have a positive effect on the elasticity of a gel and increasing oil volume fraction and homogenization pressure resulted in higher G'_{sat} .

As a consequence of these analyses, SPI was chosen as a source of soy protein and 95° C as a heating and incubation temperature for the experimental work and subsequent steps of the thesis project.

Chapter 4

Citric Acid-Induced SPI Gels

4.1 Overview

In this chapter, the development of a methodology and the associated experimental conditions for the preparation of citric acid-induced Soy Protein Isolate (SPI) gels or curds will be presented. Specifically, heating and coagulation conditions, citric acid state (as liquid or solid) and concentration, and addition method are discussed and related to visual observations of the gels.

4.2 Materials and Methods

4.2.1 Materials

Soy protein isolate (SPI), containing at least 90% protein, was obtained from Archer Daniels Midland company (ADM, product name: PRO-FAM®974, Chicago, USA). Citric acid (purity 99.5%, Product number: A940-500) was purchased from Fisher Scientific company (Ottawa, Canada).

4.2.2 SPI Solution Preparation

The SPI solution was prepared according to Zhao et al. (2020) [68], with some modification. A mass of 40 g SPI was weighted in a balance (Mettler AE 100 Balance) and transferred

to a 1 L beaker. The **SPI** powder was dissolved in ~ 450 ml deionized water and mixed completely using magnetic stirring. Subsequently, the pH of the **SPI** aqueous solution was measured as approximately 7.0 using Mettler Toledo S47 SevenMulti Dual pH and Conductivity Meter. The volume of the aqueous **SPI** solution was adjusted to 500 ml with deionized water to have 8% $w.v^{-1}$ **SPI** solution. The **SPI** solution was stored at 4° C overnight.

4.2.3 Gel Preparation

Prior to the gel preparation, the **SPI** solution was removed from the refrigerator, equilibrated to **Room Temperature (RT)**, and 50 ml of it was poured to a 100 ml beaker. Gel preparation was conducted according to Cao et al. (2017) [9], with minor modifications. The gel preparation consisted of two steps. The first step was the heating of the **SPI** solutions at 95°C using Neslab RTE 111 water bath for 10-30 min. The second step was the coagulation with citric acid addition in different state (powder or liquid) and at different final concentration (0.12 - 0.22% $w.v^{-1}$) and subsequent heating at 80° C for different durations as per Table 4.1 . The citric acid was weighted and added to a **SPI** solution when it was take out from the water bath. Two methods were considered for the citric acid addition:

1. Addition to the **SPI** solution of acid all at once followed by mixing.
2. Addition of citric acid to the **SPI** solution, slowly, while gently mixing the **SPI** solution.

The **SPI** solution containing citric acid was then returned to the water bath and maintained at 80° C for 10 – 30 min. **SPI** citric acid gels were also prepared in which citric acid was added to the **SPI** solution at **RT**, and the **SPI** citric acid solution was heated to 95°C and maintained for 30 - 60 min. All prepared gels were cooled to **RT** for further analysis.

Table 4.1: Composition and naming convention of SPI citric acid gels. Mass and SPI concentration of SPI were 0.4 g and 8% $w.v^{-1}$.

Gel code	Final citric acid concentration ($\%w.v^{-1}$)	Citric acid state	Citric acid addition	Heating step	Coagulation step
DH-0	0.20	powder	added while gently mixing	—	95°C for 30 min
DH-10	0.20	powder	added while gently mixing	95°C for 10 min	80°C for 30 min
DH-20	0.20	powder	added while gently mixing	95°C for 20 min	80°C for 30 min
DH-30	0.20	powder	added while gently mixing	95°C for 30 min	80°C for 30 min
CD-30	0.20	powder	added while gently mixing	—	95°C for 30 min
CD-60	0.20	powder	added while gently mixing	—	95°C for 60 min
P-0	0.20	powder	added while gently mixing	—	95°C for 30 min
L-0	0.20	Liquid	added while gently mixing	—	95°C for 30 min
P-10	0.20	powder	added while gently mixing	95°C for 10 min	80°C for 30 min
L-10	0.20	Liquid	added while gently mixing	95°C for 10 min	80°C for 30 min
MO-0	0.20	powder	added once followed by mixing	—	95°C for 30 min
MG-0	0.20	powder	added while gently mixing	—	95°C for 30 min
MO-10	0.20	powder	added once followed by mixing	95°C for 10 min	80°C for 30 min
MG-10	0.20	powder	added while gently mixing	95°C for 10 min	80°C for 30 min
C-20	0.20	powder	added while gently mixing	—	95°C for 60 min
C-25	0.25	powder	added while gently mixing	—	95°C for 60 min
C-30	0.35	powder	added while gently mixing	—	95°C for 60 min
C-35	0.35	powder	added while gently mixing	—	95°C for 60 min
C-40	0.40	powder	added while gently mixing	—	95°C for 60 min

4.2.4 Visual Observation of the SPI Citric Acid Gels

The visual observation of SPI citric acid gels included the following points:

1. Visual appearance: Based on the visual observation, homogeneity and consistency (e.g. solid-like material, watery, aggregates).
2. Shape retention: A gel sample was placed on a glass surface using a spatula to assess its ability to retain its shape.
3. Holding capacity: A gel sample was placed on a fork to assess its capacity to remain on the fork.

The SPI citric acid gels were analyzed with the descriptors presented in Table 4.2.

Table 4.2: Descriptor of the visual observation of SPI citric acid gels

Descriptor	Detail
Curd	Represents the SPI citric acid sample obtained after thermal treatment (may include heating and coagulation, or may include heating or coagulation only)
Solid mass	Solid mass present in the curd
Liquid	Liquid present in the curd
Lumps	Lumps present in the curd
Aggregates	Aggregates present in the curd
Gel-like	The formed solid-like material were gels
Watery	Solid material was spread in water
Loose	Solid-like material were loose and not continuously and homogeneously connected

4.3 Results and Discussion

4.3.1 Heating Duration

The effect of heating the SPI solution prior to citric acid addition was investigated by conducting the heating at 95°C of the 8% *w.v*⁻¹ SPI for 0, 10, 20, and 30 min followed by

immediate citric acid addition of 0.2% $w.v^{-1}$ (citric acid powder) and subsequent coagulation at 80°C for 30 min as described by Cao et al. (2017) [9]. Details of the SPI citric acid gel composition and preparation are presented in Table 4.1 and images of the gels at room temperature are presented in Figure 4.1.

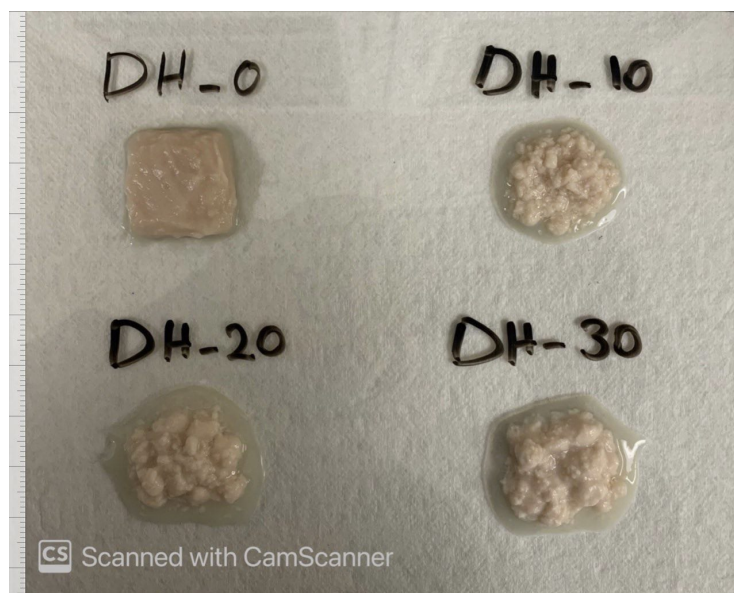


Figure 4.1: SPI citric acid gels obtained with 0.2% $w.v^{-1}$ citric acid according to heating and coagulation conditions in Table 4.1.

The SPI-citric acid gel prepared with no heating (DH-0) consisted of two phases, a liquid phase located on top of a solid mass that could be easily and completely removed. The gel was able to keep its shape and remained on top of the fork (no leaking from the fork). This gel, on the other hand, was a very soft material and weak gel with poor characteristics, and its strength was insufficient compared to commercial soft tofu products. As seen in Figure 4.1, some water leaked out from DH-0, and could not be fully entrapped with the DH-0 gel structure. Furthermore, the DH-0 gel could not be cut into cubic shapes or shaped with an apple cutter; the gel could only be formed with a spatula.

The SPI citric acid gel made by heating SPI solutions (DH-10, DH-20 and DH-30), contained white lumps and aggregates scattered heterogeneously, but not connected with each other. There was no exact boundary between the solid and liquid phases, so the solid part had to be separated from the liquid using cheese cloth. These aggregates could not retain their shape and did not remain on the fork before pressing (pressing will be discussed in section 4.4). The number of aggregates, particle sizes, and compactness appeared to

increase as the heating duration of the SPI solution increased. The DH-10 gel had fewer and finer aggregates in comparison to DH-20 and DH-30 gels.

4.3.2 Coagulation Duration

In this section, the impact of coagulation duration is presented for 8% $w.v^{-1}$ SPI containing 0.20% $w.v^{-1}$ citric acid solution coagulated at 95°C for two duration of 30 or 60 minutes. Citric acid was added to the SPI solution as a powder while gently mixing the solution. Images and characteristics of the gels presented in Figure 4.2 and Table 4.3 indicate gel-like materials that retained their shape.

After 30 minutes of coagulation (CD-30), the gel was somewhat watery and loose. Increasing the coagulation duration to 60 minutes produced a stronger, drier, more compact gel. The solid mass of the CD-60 gel was approximately 20% greater than the CD-30 gel, implying that the longer the coagulation duration, the higher the yield. The smaller amount of liquid for the CD-60 gel could reflect either superior water retention in the gel network or a higher amount of evaporated water.

Table 4.3: Mass of a liquid separated from the solid mass of 8% $w.v^{-1}$ SPI and 0.20% $w.v^{-1}$ citric acid gels with two coagulation durations at 95°C.

Sample	Coagulation duration (min)	Mass of liquid solution on top of the solid mass (g)	Mass of solid portion (g)	Mass of liquid portion (%)	Mass of solid (%)
CD-30	30	21	18.57	53	47
CD-60	60	13	23.36	36	64

Our findings confirm that the CD-60 sample was visually slightly stronger and stiffer than the CD-30 sample. As a result, for making harder samples, a coagulation time of 60 minutes might be chosen.

4.3.3 Citric Acid State

Citric acid is available as citric acid anhydrous, a powder, and as an aqueous solution with various concentrations. In this section, the effect of citric acid state on the visual appearance of SPI gels will be presented. For this purpose, 0.2% $w.v^{-1}$ citric acid as a powder or liquid (the required amount of citric acid was dissolved in less than 1 ml of



Figure 4.2: Gels produced with 8% $w.v^{-1}$ SPI and 0.2% $w.v^{-1}$ citric acid and two coagulation duration at 95°C, as stated in Table 4.3.

deionized water which did not have a considerable effect on the total volume of the SPI solution) was added to 8% $w.v^{-1}$ SPI solution. The SPI solution was heated at 95°C for 0 or 10 minutes prior to citric acid addition followed by coagulation at either 80° or 95°C for 30 minutes (Table 4.1).

As a result of this investigation, prepared gels with anhydrous citric acid were smoother and more homogeneous. When S-10 and L-10 gels are compared, the citric acid solution produced larger aggregates, resulting in higher heterogeneity. The liquid form of citric acid provides hydrated and dissolved citric acid, allowing for rapid interactions with the protein components and fast aggregation rate, resulting in large and heterogeneous aggregates. The inclusion of citric acid powder, on the other hand, necessitates its dissolution in the SPI aqueous solution before interacting with the protein molecules, slowing the rate of aggregation and resulting in more homogenous and compact aggregates.

As illustrated in Figure 4.3, both S-0 and L-0 gels could be formed and retained their shape and had a relatively similar appearance. This similarity could be due to the addition of citric acid to the unheated SPI solution, in which proteins were not unfolded. Therefore, citric acid limited interaction with the protein molecules.

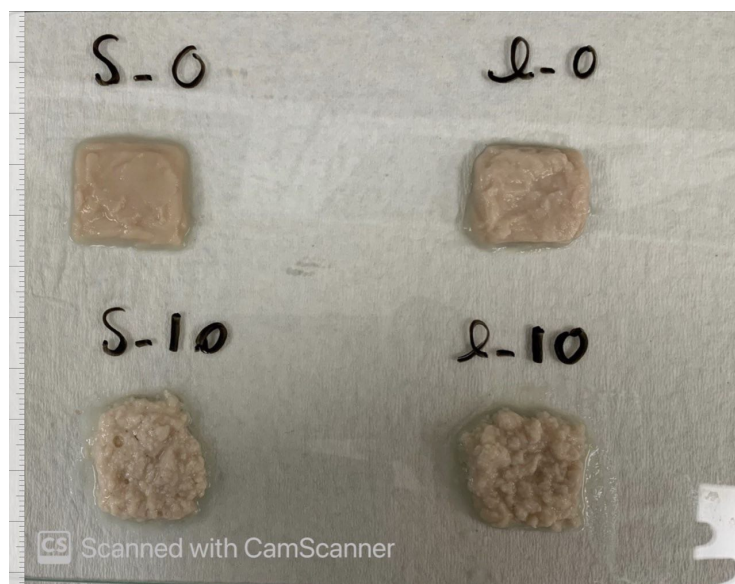


Figure 4.3: Gels produced with 8% $w.v^{-1}$ SPI and 0.2% $w.v^{-1}$ citric acid for citric acid powder or solution, with and without SPI heating and two different coagulation temperatures for 10 minutes (Table 4.1)

4.3.4 Citric Acid Addition Methodology

In this section, the effect of the addition to the 8% $w.v^{-1}$ SPI solution of 0.2% $w.v^{-1}$ citric acid during the coagulation step is described. Samples were prepared as described in section 4.2.2 and 4.2.3 considering conditions summarized in Table 4.1. Citric acid was added as a powder to the SPI solution at once followed by gentle mixing of the solution or added to the solution while gently mixing.

As illustrated in Figure 4.4, the gel obtained when citric acid was added all at once to the SPI solution with no heating (MO-0) was quite loose and spread over the glass surface and could not retain its shape and water was leaking out, while the gel where citric acid was added gradually with gentle mixing of the solution (MG-0) resulted in a stronger gel with increased retention of water. In terms of heating conditions, the MO-10 gel had finer aggregate sizes and a more compact structure; however, less of the SPI solution was converted to aggregates when compared to the gradual addition of citric acid (MG-10).

The addition of citric acid at once may result in a sudden decrease of the pH and could induce uncontrolled aggregation of the SPI. Furthermore, the citric acid may not disperse uniformly and lead to localized pH conditions. Therefore, the addition of citric acid while

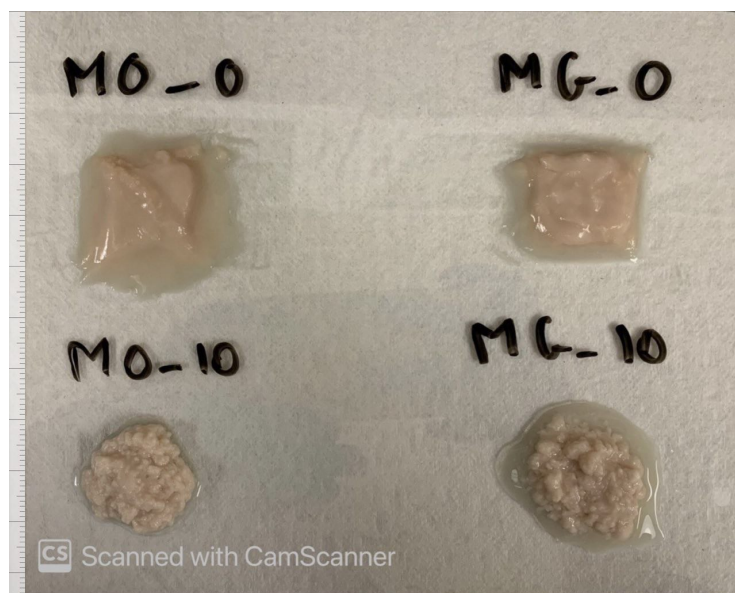


Figure 4.4: Gels produced with 8% $w.v^{-1}$ SPI and 0.2% $w.v^{-1}$ citric acid with and without SPI heating, different coagulation conditions for 30 minutes duration and two methods of citric acid addition (Table 4.1).

gently mixing will be selected for the preparation of SPI citric acid gels.

4.3.5 Citric Acid Concentration

The effect of citric acid concentration on the coagulation step was investigated for 8% $w.v^{-1}$ SPI solution (no heating) at RT. The citric acid powder was added to the SPI solution with a mass giving five different citric acid concentrations: 0.20, 0.25, 0.30, 0.35, and 0.40% $w.v^{-1}$ while gently mixing. After the addition of citric acid, the coagulation step was carried out at 95°C for 60 min. Finally, the beaker was removed from the water bath and let to equilibrate to RT.

The beaker contained two phases, a solid phase at the bottom of the beaker and a liquid phase on top of the solid phase. The liquid was separated from the solid mass, and their corresponding amounts are summarized in Table 4.4. Figure 4.5 represents the visual appearance of the gels.

As illustrated in Figure 4.5, samples containing 0.2, 0.25, and 0.3% $w.v^{-1}$ citric acid retained their shape, did not spread over the glass surface, and did not leak from the fork.

Table 4.4: Mass of the solution separated from the solid mass of 8% $w.v^{-1}$ SPI citric acid mixtures with various citric acid concentration

Sample	Citric acid concentration (% $w.v^{-1}$)	Solid mass (g)	Liquid Mass on top of the solid mas (g)
C-20	0.20	15	25
C-25	0.25	18	28
C-30	0.30	20	28
C-35	0.35	14	25
C-40	0.40	16	26

The gels were smooth and homogeneous with a uniform structure. On the other hand, the gels with higher citric acid concentration, C-35, C-40, were looser and watery which were mostly in liquid form. Increasing citric acid concentration from 0.2% $w.v^{-1}$ to 0.3% $w.v^{-1}$ resulted in the formation of stiffer material with higher strength and solid mass (Table 4.4).

As a consequence of this study, C-30 could be picked as the preferable conditions since this gel could be shaped and was harder, stronger, more compact, and less watery than other gels.



Figure 4.5: SPI samples at 60 min coagulation duration with 0.2 - 0.4% $w.v^{-1}$ citric acid anhydrous.

4.4 Gel Shaping by Pressing

The effect of pressing the gels for shaping was investigated with SPI solutions prepared according to steps proposed in section 4.2.2. For the gel preparation, the water bath was turned on, and its temperature was adjusted to 95° C. SPI solutions were taken out of the refrigerator and brought to room temperature, 50 ml was poured to a 100 ml beaker and then heated in the water bath at 95° C for 30 minutes. Following that, the temperature was decreased to 80° C and 0.15 g citric acid powder was added while gently mixing the solution located in the water bath (final acid concentration: 0.3% $w.v^{-1}$). The solution was left in a water bath at 80° C for 60 min to make protein aggregates (coagulation step). After that, the solid portion was removed and transferred immediately to a container lined up with cheese cloth and subsequently pressed at 10 $g.cm^{-2}$ for 10 min. The citric acid-induced SPI gel, shown in Figure 4.6, was uniform, strong, and homogeneous in structure. It could be cut using a box cutter to a very thin layer (35 mm cube with a thickness of 1-2 mm) for the rheological tests and shaped with an apple cutter, which is an important requirement for uniaxial compression analysis.

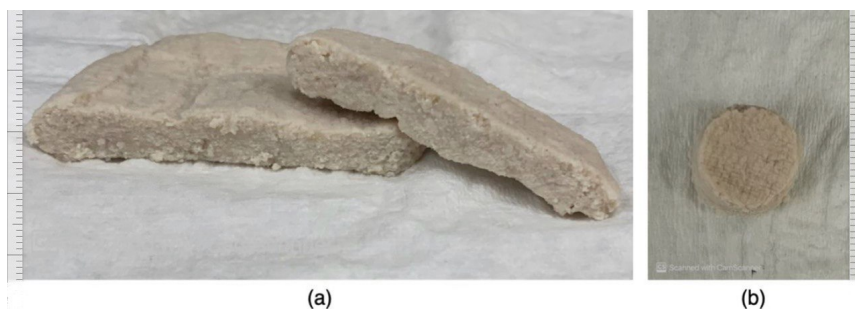


Figure 4.6: 0.3% $w.v^{-1}$ citric acid induced SPI gel, a) sectional view of a gel, b) shaped gel with apple cutter.

4.5 Classification of Gels







The visual appearance of the gels was used to create a classification system consisting of two groups. In the first group, homogeneous, smooth, and solid-like materials were formed which can be called weak gels. In the second group, solid aggregates were created which were dispersed through the protein solution quite heterogeneously. The second group can be called aggregates (Table 4.5).

According to the visual evaluation of the gels, the following conditions were selected for the preparation of citric acid-induced 8% $w.v^{-1}$ SPI gels:

- 0.3% $w.v^{-1}$ citric acid as a powder which should be added to the protein solution while constantly stirring.
- 30 minutes heating at 95°C.
- 60 min coagulation at 80°C.
- Solid recovery with cheese cloth and subsequent pressing at 10 $g.cm^{-2}$ for 10 min.

The conditions above will be used for the preparation of citric acid induced SPI and SPI-polysaccharide gels. The uniaxial and viscoelastic properties of these gels will be evaluated and discussed in chapter 5.

Table 4.5: Classification of citric acid-induced 8% $w.v^{-1}$ SPI gels according to visual observations.

Gel classification	Type	Description	Samples	Photo
Weak Gel	Firm	Uniform and weak gels which retained their shape and remained on the fork (no leaking); Firm and nearly dry in comparison to other samples. Appropriate for test such as rheology, inappropriate for the mechanical testing.	C-30, CD-60	
	Soft	Uniform gels which retained their shape and remained on the fork (no leaking); Softer and more watery than the other gels.	C-20, C-25, CD-30, MG-0, DH-0, S-0, L-0	
	Loose	Very loose and watery that could barely retain their shape. Spread a little over the glass surface.	C-35, C-40, MO-0	
Aggregate	Coarse	Heterogeneous aggregates with large size and higher numbers of aggregation compared with medium and fine coarse. Could not retain shape and were spread over surface and leaked from the fork before pressing; after pressing similar to soft tofu; appropriate for mechanical, and rheological tests	DH-30	
	Medium coarse	Aggregate size between coarse and fine type aggregates; Could not retain shape and were spread over surface and leaked from the fork; after pressing similar to soft tofu	DH-20, L-10	
	Fine	Fine aggregate sizes; Could not retain shape, spread over surface and leaked from the fork, after pressing similar to soft tofu	DH-10, S-10, MO-10, MG-10	

Chapter 5

SPI Gels Containing Polysaccharides

5.1 Overview

This chapter will elaborate on the interpretation and analysis of citric acid induced SPI and SPI-polysaccharide gels. For this purpose, SPI gels containing potato starch, guar gum, inulin, or a combination of those were prepared and their uniaxial compression and viscoelastic properties were evaluated and compared with a citric acid-SPI gel. The characteristics of the SPI-Polysaccharide gels were related to their structure and interactions with protein and water. The Box-Behnken (B-B) method was used to assess the dependence of uniaxial properties (fracture strain, fracture force, Young's modulus) and viscoelastic properties (G' , G'' , $\tan\delta$) on the type and concentration of polysaccharides.

5.2 Materials

Soy protein isolate (SPI) containing at least 90% protein was obtained from Archer Daniels Midland company (ADM, product name: PRO-FAM®974, Chicago, USA). Citric acid (purity 99.5%, Product number: A940-500) was purchased from Fisher Scientific company (Ottawa, Canada). Polysaccharides included Inulin (Fibruline XL, cosucra, Warcoing, Belgium), guar gum (Duinkerken, Ontario, Canada), and starch (Bob's Red Mill, Ontario, Canada).

5.3 Methodology

5.3.1 Gel Preparation

5.3.1.1 SPI or SPI-Polysaccharide Solution

SPI and the selected polysaccharide (P) were weighed on a balance and then placed in a 500 mL beaker. To ensure good solubilization of the SPI and polysaccharide, deionized water was slowly added to the beaker up to a volume of 350 mL. After, the beaker was placed on a magnetic stirrer and mixed for 30 minutes. The pH of the solution was measured with a S47 SevenMulti Dual pH and Conductivity Meter (Mettler Toledo, Mississauga, Canada). The volume of the solution was then adjusted with deionized water (400 ml) before storage at 4° C overnight. Figure 5.1 represents a schematic diagram of SPI and SPI-Polysaccharide (SPI-P) solution preparation.



Figure 5.1: Schematic diagram for the preparation of SPI and SPI-Polysaccharide (SPI-P) solution.

5.3.1.2 SPI or SPI-Polysaccharide Gel

The desired solution, SPI or SPI-P, was taken out of the refrigerator and brought to room temperature. Each SPI-P solution was heated in a water bath pre-heated at 95° for 30 minutes. Following that, the temperature was decreased to 80° and 0.45 g citric acid was added while gently mixing the solution using a spatula (final citric acid concentration: 0.3% w/v). The solution was kept in the water bath at 80° for 60 min to induce protein aggregation. After that, the aggregates were transferred immediately to a square container with a cheese cloth inside. When the aggregates were completely transferred to the container, the aggregates were wrapped and covered with two layers of cheese cloth and pressed at 10 g.cm^{-2} (981 N.m^{-2}) for 10 min to create a solid mass. The pressing was carried out by placing a container with surface area of $\sim 100 \text{ cm}^2$ and mass of 1000 g on top of the wrapped aggregates. Figure 5.2 summarizes the preparation of SPI and SPI-P citric acid gels.

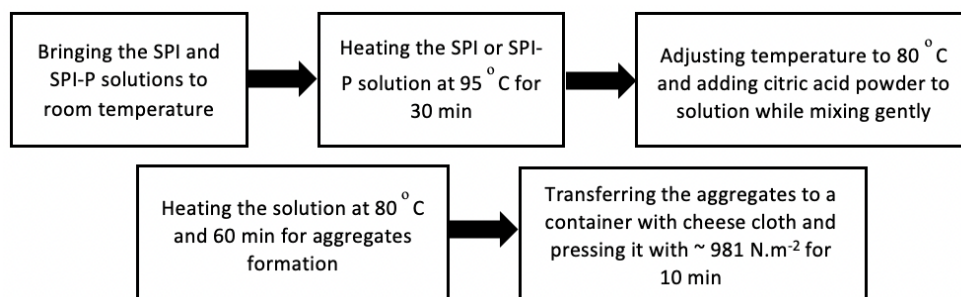


Figure 5.2: Schematic diagram for the preparation of SPI and SPI-P citric acid gels.

5.3.2 Initial Observations

As mentioned in section 5.3.1, the aggregates were cooled to room temperature and pressed at 10 g.cm^{-2} for 10 min to obtain a gel. The mass of the gel and the expelled water caused by the pressing were measured and compared to examine the impact of the polysaccharide on the total solid content and the water retention of the gels. Other observations included cutting of the gels with a box cutter to assess their strength (how soft or firm in comparison to each other). Gels were cut in a cylindrical shape (10 mm in diameter and 10 mm in height) with an apple corer to evaluate their ability to form a self-standing gel, if cutting fractured the gel, and to assess their suitability for mechanical and rheological testing.

5.3.3 Uniaxial Compression Properties

Uniaxial compression measurements were obtained at room temperature with a Shimadzu Autograph AGS-X (Shimadzu, Columbia, Maryland, USA). Immediately after removing the gel from the refrigerator, cylindrical samples from one gel were prepared with an apple corer, 10 mm diameter and 10 mm height. Prior to testing, all samples were allowed to rest for 1 hour at room temperature. A 50 N cell with a compression speed of 40 mm.min^{-1} was used. The compression was continued until the sample was completely fractured at which point it was stopped. Measurements were made for sixteen different types of gel, each with 7 replicates. The fracture point could not be found in results (the fracture point was detected for 5-7 replicates). The Hencky stress, σ (Pa), and strain, ϵ (no unit), were calculated using the Force, F (N), and displacement, ΔL (m), at each time, as shown in Equation 5.1 and 5.2 [111].

$$\sigma(t) = F(t) \times \frac{L_0 - \Delta L(t)}{A_0 \times L_0}, \quad (5.1)$$

$$\epsilon(t) = \ln \frac{L_0 - \Delta L(t)}{L_0}, \quad (5.2)$$

where L_0 (m) and A_0 (m^2) represent the initial height and area of the samples, respectively. In this equation, the changes of the shape of the sample during compression is accounted.

These curves were used to estimate the stress (σ_f) and strain (ϵ_f) at the fracture point corresponding to the maximum point of the stress-strain curve by employing the MAX function of Excel (Appendix A.1). The Stress-Strain relation of SPI and SPI-P gels are curves and non-linear.

In this study, the Young's modulus (E (Pa)) was calculated with two methods: 1) estimation of the slope of a linear region of a curve in a strain range of 0.2-0.3, and 2) estimation of the slope of a curve located between 1/3 and 2/3 of the way to the point of maximum stress [92]. In both methods, the Young's modulus was estimated using the linear regression via Excel (Appendix A.1). Values were expressed as the mean, and error bars indicate the standard deviation of replicates. The median of the stress-strain curve of the replicates were also considered from each gel.

5.3.4 Viscoelastic Behaviour

Viscoelastic measurements were performed using a HAAKE MARS rheometer (ThermoFisher Scientific, Waltham, Massachusetts, USA) with parallel plate geometry (35 mm diameter, 1 mm gap). All samples were cut into 35 mm cubes with a thickness of 1-2 mm using a box cutter immediately after taken out from the refrigerator. Once cut, samples were equilibrated at room temperature for 1 h prior to measurement. Samples were placed in the centre of the plate, and the gap was set to 1 mm. The additional sample height (between 1-2 mm) was pushed by the upper plate which allows for some axial force to squeeze out any trapped air bubbles. To minimize mechanical stress when closing the gap, the lift was set to a lower speed of $1.25 \text{ mm} \cdot \text{min}^{-1}$. The trimming position was used to adjust the sample filling and was set to 0.025 mm higher than the measuring position (1 mm). After fixing the gap distance, lifting speed, and trimming position, the sample was allowed to rest for 10 minutes. One batch of a given gel was split into four 35 mm cubes (thickness = 1-2 mm), one was subjected to strain sweep test and three were subjected to frequency sweep tests.

The amplitude sweep test was conducted in the controlled deformation (CD) mode. A strain range of 0.01–100%, i.e., $\gamma = 0.0001$ –1, was chosen while keeping the frequency and temperature at 1 Hz and 25° C, respectively. For each sample, the Linear Viscoelastic Region (LVR), defined as the strain range for which the storage modulus, G' , remained constant, was determined with the software of the equipment (RheoWin version 4.87.0018, Thermofisher Scientific, Waltham, USA).

The frequency sweep test was conducted in the CD mode. A deformation strain was determined to be within the LVR based on the results of the amplitude sweep test (i.e., strain = 0.01% or $\gamma = 0.000$). A frequency range of 1 – 100 rad.s⁻¹ was used for all samples. All tests were conducted at a temperature of 25° C.

The dependency of G' and G'' according to the angular frequency (ω) was represented by a power law model described by equation 5.3 and 5.4, respectively [112],

$$G' = G'_0 \omega^{n'}, \quad (5.3)$$

$$G'' = G''_0 \omega^{n''}, \quad (5.4)$$

Where G'_0 (Pa) and G''_0 (Pa) are the storage modulus and the loss modulus at 1 rad.s⁻¹, respectively, and exponents n' and n'' (both dimensionless) denote the influence of the angular frequency on the respective modulus. The stronger the interaction in the gel network, the lower will be the dependency of G' and G'' on the frequency. Identical n' and n'' values indicate a gel with strong and good characteristics, whereas non-identical n' and n'' values indicate a weak gel. The G'_0 , G''_0 , n' , and n'' for each sample were estimated using the “Solver Function” of Excel.

5.3.5 Experimental Design

A Box-Behnken (B-B) design of experiments was selected to investigate the effect of the type of polysaccharide, inulin (I), starch (S), and guar gum (G) on SPI citric acid gels. The major advantage of the B-B design of experiments is the ability to generate higher order response surfaces using fewer experimental points than a full factorial design of experiments. The B-B method for three independent factors (I, S, and G) at three levels consists of twelve factorial points and three replicates at the centre point (Table 5.1). Table 5.2 shows the details of each factor, including their levels and the gel composition. The range of the three independent factors was based on preliminary experiments (data not shown). The dependent variables were the uniaxial compression and viscoelastic properties

of the gels (Table 5.3). Between them, stress fracture point, Young’s modulus, and storage modulus are the most important, as they can provide information about the textural attributes, gel strength, hardness, and stiffness, respectively.

Seven replicates of uniaxial compression measurements and three replicates of viscoelastic measurements were performed. Their mean values and standard deviation were used as experimental responses. Experimental runs were randomized to minimize the effects of unexpected variability in the observed responses. The mathematical model corresponding to the B-B design is:

$$Y_i = b_0 + b_1X_1 + b_2X_2 + b_3X_3 + b_{12}X_1X_2 + b_{13}X_1X_3 + b_{23}X_2X_3 + b_{11}X_1^2 + b_{22}X_2^2 + b_{33}X_3^2, \quad (5.5)$$

Where Y_i is the dependent variable (Table 5.3) and $b_0, b_1, b_2, b_3, b_{12}, b_{13}, b_{23}, b_{11}, b_{22}, b_{33}$ are the model coefficients. Results were analysed by one-way ANOVA using the STATISTICA package program (TIBCO Software Inc. (2020). Data Science Workbench, version 14, Palo Alto, California, USA).

Table 5.1: Composition and coded value of the SPI and SPI-P citric acid gels. All gels contained 8% w/v SPI and 0.3% w/v citric acid.

Gel code	Gel composition	X1 coded (I)	I concentration (%w/v)	I mass (g)	X2 coded (S)	S concentration (%w/v)	S mass (g)	X3 coded (G)	G concentration (%w/v)	G mass (g)
C*	SPI	—	—	—	—	—	—	—	—	—
1	SPI-0.05G	-1	0	0	-1	0	0	0	0.05	0.2
2	SPI-4I-0.05G	+1	4	16	-1	0	0	0	0.05	0.2
3	SPI-0.2S-0.05G	-1	0	0	+1	0.2	0.8	0	0.05	0.2
4	SPI-4I-0.2S-0.05G	+1	4	16	+1	0.2	0.8	0	0.05	0.2
5	SPI-0.1S	-1	0	0	0	0.1	0.4	-1	0	0
6	SPI-0.1S-0.1G	-1	0	0	0	0.1	0.4	+1	0.1	0.4
7	SPI-4I-0.1S-0.1G	+1	4	16	0	0.1	0.4	+1	0.1	0.4
8	SPI-4I-0.1S	+1	4	16	0	0.1	0.4	-1	0	0
9	SPI-2I	0	2	8	-1	0	0	-1	0	0
10	SPI-2I-0.2S	0	2	8	+1	0.2	0.8	-1	0	0
11	SPI-2I-0.1G	0	2	8	-1	0	0	+1	0.1	0.4
12	SPI-2I-0.2S-0.1G	0	2	8	+1	0.2	0.8	+1	0.1	0.4
13-15	SPI-2I-0.1S-0.05G	0	2	8	0	0.1	0.4	0	0.05	0.2

* C represents the Control sample which has 8% w/v SPI.

I, S, and G represents Inulin, Starch, and Guar gum, respectively.

Table 5.2: List of the independent factors based on their concentration and mass for a 400 mL solution of SPI-P gels.

Factor	Level -1	Level 0	Level +1
X1 (Inulin) (%w/v) [mass (g)]	0 [0]	2 [8]	4 [16]
X2 (starch) (%w/v) [mass (g)]	0 [0]	0.1 [0.4]	0.2 [0.8]
X3 (guar gum) (%w/v) [mass (g)]	0 [0]	0.05 [0.2]	0.1 [0.4]

Table 5.3: Box-Behnken design dependent variables.

Dependent variable	Gel property
Y1	Fracture stress (σ_f)
Y2	Fracture strain (ϵ_f)
Y3	Young's Modulus (E)
Y4	Storage modulus (G'_0)
Y5	Viscous modulus (G''_0)

5.3.6 Statistical Analysis

Pairwise testing comparison was obtained with the Duncan's test. This statistical test was selected because of its effectiveness in detecting statistical differences while accounting for Type I error which occurs when H_0 is statistically rejected despite being true and in considering the number of treatments and its suitability for small numbers of treatments. A significance level of 0.05 was selected and calculations were achieved with STATISTICA.

5.4 Results and Discussion

5.4.1 Initial Observations

All gels created were strong and stiff enough to be formed and sliced into shapes, with no water leaking out (Figure 5.3). The control sample (SPI citric-acid gel) was crumbly and heterogeneous, while the addition of polysaccharide resulted in more uniform and stiffer gels with smaller visible pores. With the exception of the SPI citric acid gel, all SPI-P citric acid gels resembled soft tofu. The SPI-2I gel (sample 9) and the SPI-2I-0.2S0.1G gel (sample 12) appeared different. The SPI-2I gel appeared stiffer, stronger, and drier. The

presence of 2% w/v inulin made the gel appeared to be a little brittle and fragile. The SPI-2I-0.2S-0.1G gel was, on the other hand, much looser and sticky.

Table 5.4 shows the mass of the gels and the extracted water after 10 minutes of pressing at 981 N.m^{-2} (section 5.3.1). The addition of polysaccharide to the SPI citric acid gel increased the mass, resulting in a 16-51% increase in the final gel mass in comparison with SPI gel. The masses of SPI-P gels is higher than the sum of the mass of SPI gel and polysaccharides. As shown in Table 5.4, the mass of water extracted after pressing was 8-26% lower for the SPI-P citric acid gels compared with SPI citric acid gel, implying that more water was integrated into the gel network in the presence of polysaccharide.

Table 5.4: Mass of SPI and SPI-P citric acid gels and extracted water after pressing at 10 g.cm^{-2} for 10 min. All gels contain 8% w/v SPI and 0.3% w/v citric acid.

Gel code	Gel composition	I (%w/v)	S (%w/v)	G (%w/v)	mass of gel (g)	Mass of water extracted (g)
C*	SPI	0	0	0	92.6	264.4
1	SPI-0.05G	0	0	0.05	120.8	227.3
2	SPI-4I-0.05G	4	0	0.05	133.1	212.8
3	SPI-0.2S-0.05G	0	0.2	0.05	139.5	194.9
4	SPI-4I-0.2S-0.05G	4	0.2	0.05	128.4	211.6
5	SPI-0.1S	0	0.1	0	130.9	209.5
6	SPI-0.1S-0.1G	0	0.1	0.1	132.5	224.5
7	SPI-4I-0.1S-0.1G	4	0.1	0.1	127.5	229.8
8	SPI-4I-0.1S	4	0.1	0	113.3	247.0
9	SPI-2I	2	0	0	117.4	234.1
10	SPI-2I-0.2S	2	0.2	0	114.3	243.9
11	SPI-2I-0.1G	2	0	0.1	112.1	234.5
12	SPI-2I-0.2S-0.1G	2	0.2	0.1	107.6	233.9
13	SPI-2I-0.1S-0.05G	2	0.1	0.05	123.6	225.6
14	SPI-2I-0.1S-0.05G	2	0.1	0.05	124.2	219.0
15	SPI-2I-0.1S-0.05G	2	0.1	0.05	120.5	231.3

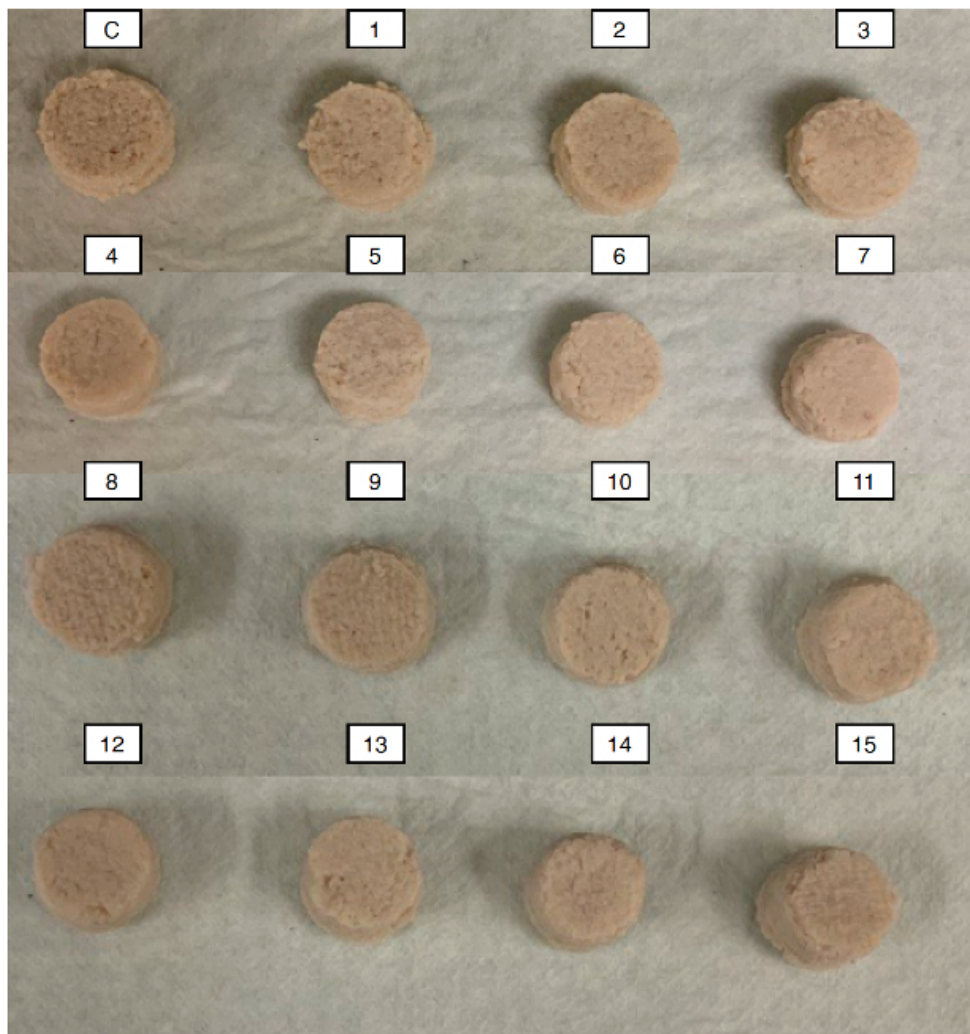


Figure 5.3: *SPI* and *SPI-P* citric acid gels of cylindrical shape with diameter and height of 1 mm (compositions summarized in Table 5.1).

5.4.2 Uniaxial Compression Properties

5.4.2.1 Estimation of Young's Modulus

The SPI-P gels were a viscoelastic and soft gel-like material. As a result, their stress-strain curve was non-linear [91, 90]. This could be due to the behaviour of a soft gels, as their shape and surface area will be changed under the compression, and the strain will not change linearly with stress. A typical stress-strain curve for all sixteen samples is depicted in Figures 5.4-5.6. The median replicate curve of each sample was chosen. The estimation of the Young's modulus for a non-linear stress-strain curve is challenging. Various methods for estimating the Young's modulus have been reported in the literature. The slope of a stress-strain curve at 0.05 strain was calculated as a Young's modulus by Guo et al. (2014) [89]. This estimation is for the onset of the curve, may have a very small value, and cannot capture the true behaviour of a sample prior to fracture. Krupa et al. (2010) [113] used the experimental stress and strain data to fit an exponential model and derive the Young's modulus, as indicated in Equation 5.6 and 5.7.

$$\sigma(\epsilon) = A[\exp(a\epsilon) - 1] \quad (5.6)$$

$$E = \left(\frac{d\sigma}{d\epsilon}\right)_{\rightarrow 0} = Aa, \quad (5.7)$$

where σ and ϵ are true stress and true strain, respectively, which can be determined from Equation 5.1 and 5.2, and E is Young's modulus. Parameters A and a are variables should be determined via a non-linear regression.

Canet et al. (2007) estimated the Young's modulus at higher strain range. In their method, the Young's modulus was estimated in the linear region of the stress-strain curve, located between $\frac{1}{3}$ and $\frac{2}{3}$ of the way to the point of maximum stress [92].

According to Figures 5.4-5.6, the stress-strain curve of all samples was linear in two regions ($R > 0.99$): at the middle of a curve (between strain $\frac{1}{3}$ and $\frac{2}{3}$ of the fracture point) and approximately at the end of a curve (between strains of 0.2-0.3). Therefore, these two regions were used to estimated the Young's modulus, and their values were compared to each other.

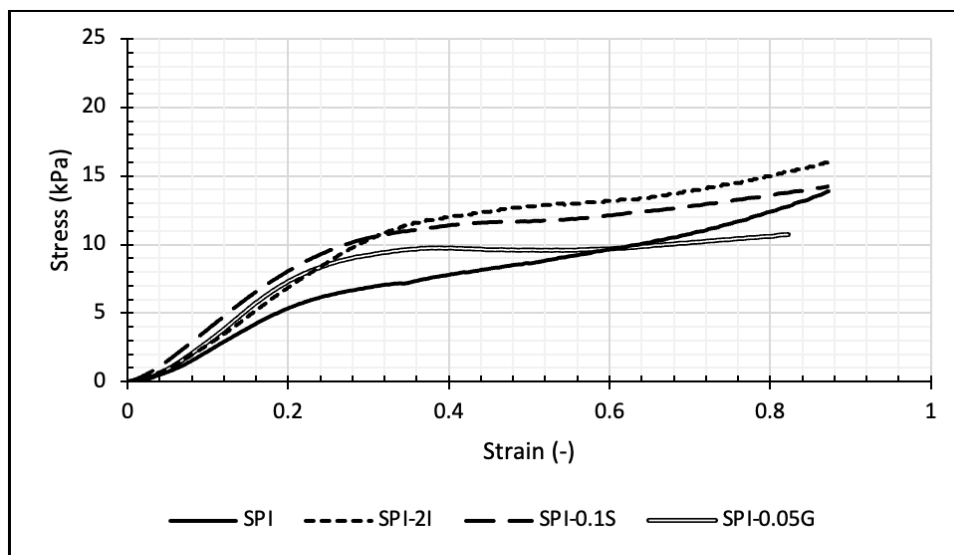
The estimated Young's modulus values are shown in Table 5.5 and expressed as mean and standard deviations. As shown, the estimated Young's modulus was higher in the strain range of 0.2-0.3 compared with the estimated value in the strain range of $\frac{1}{3}$ to $\frac{2}{3}$ of

the fracture strain (this range was below 0.2 strain for all samples), which is due to the convex stress-strain curve (the slope at each point increases as the strain increases). The relative magnitude of the Young's modulus of the gel compared to the control gel (SPI) for a given method and the statistical differences between the samples and the control sample were identical. For each estimation method, the $\frac{\text{Young's modulus}(E_{SPI-P})}{\text{Young's modulus of a control sample}(E_{SPI})}$ was determined and is shown in Table 5.5. It appears that $\frac{E_{SPI-P}}{E_{SPI}}$ was higher when the Young's modulus was estimated between strains of 0.2-0.3.

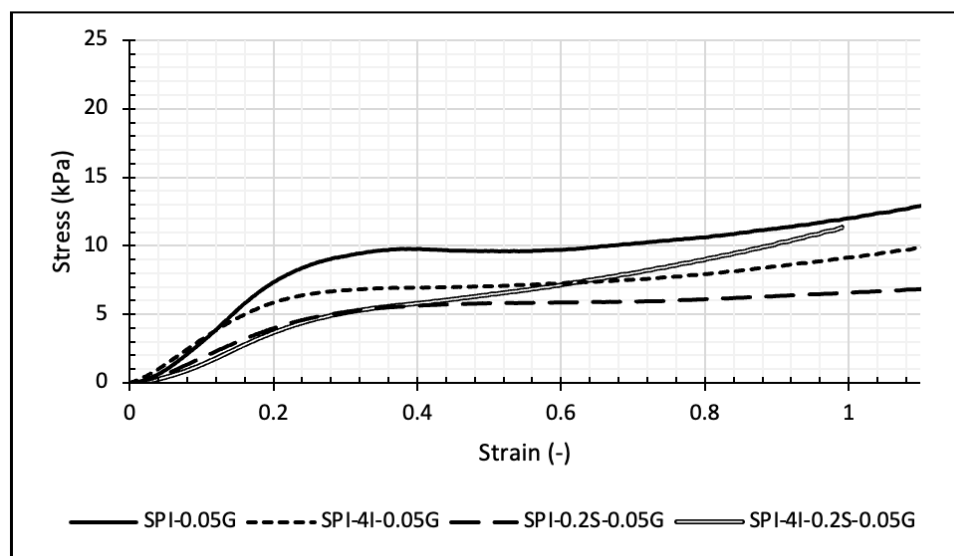
In the next sections, the slope of a linear region of a curve in a strain range between $\frac{1}{3}$ and $\frac{2}{3}$ of the way to the point of maximum stress will be used as an estimation of Young's modulus.

Table 5.5: Estimated Young's modulus. E_1 was estimated as a slope of a linear region of a stress-strain curve in a strain range of 0.2-0.3, E_2 was estimated as a slope of a stress-strain curve in a strain range of 1/3-2/3 of a peak. E_{1SPI} and E_{2SPI} are a modulus value for the control gel (SPI) in each method.

Gel code	Gel composition	I (%w/v)	S (%w/v)	G (%w/v)	E_1 (kPa)	$\frac{E_1}{E_{1SPI}}$	E_2 (kPa)	$\frac{E_2}{E_{2SPI}}$
C*	SPI	0	0	0	25.8 ^a ± 8.3	1	27.7 ^a ± 5.2	1
1*	SPI-0.05G	0	0	0.05	33.6 ^b ± 9.6	1.3	39.6 ^b ± 9.6	1.4
2*	SPI-4I-0.05G	4	0	0.05	23.6 ^a ± 7.4	0.91	27.5 ^a ± 4.3	0.99
3**	SPI-0.2S-0.05G	0	0.2	0.05	22.1 ^a ± 3.0	0.85	26.0 ^a ± 6.5	0.94
4*	SPI-4I-0.2S-0.05G	4	0.2	0.05	22.2 ^a ± 3.9	0.86	25.5 ^a ± 4.4	0.92
5*	SPI-0.1S	0	0.1	0	40.5 ^b ± 3.9	1.6	43.6 ^b ± 1.3	1.6
6***	SPI-0.1S-0.1G	0	0.1	0.1	21.2 ^a ± 4.7	0.85	23.3 ^a ± 3.4	0.84
7***	SPI-4I-0.1S-0.1G	4	0.1	0.1	20.6 ^a ± 3.3	0.80	23.7 ^a ± 3.6	0.86
8***	SPI-4I-0.1S	4	0.1	0	35.4 ^b ± 5.8	1.4	42.2 ^b ± 6.1	1.5
9***	SPI-2I	2	0	0	37.7 ^b ± 3.8	1.5	46.8 ^b ± 9.4	1.7
10*	SPI-2I-0.2S	2	0.2	0	32.6 ^b ± 3.1	1.3	45.4 ^b ± 7.8	1.6
11**	SPI-2I-0.1G	2	0	0.1	18.8 ^a ± 2.8	0.73	21.0 ^a ± 5.1	0.76
12*	SPI-2I-0.2S-0.1G	2	0.2	0.1	13.7 ^c ± 2.6	0.53	15.0 ^c ± 3.1	0.54
13**	SPI-2I-0.1S-0.05G	2	0.1	0.05	18.2 ^a ± 1.4	0.70	21.6 ^a ± 2.1	0.78
14*	SPI-2I-0.1S-0.05G	2	0.1	0.05	22.0 ^a ± 3.1	0.85	27.3 ^a ± 6.8	0.98
15***	SPI-2I-0.1S-0.05G	2	0.1	0.05	21.7 ^a ± 3.8	0.84	24.6 ^a ± 3.9	0.88

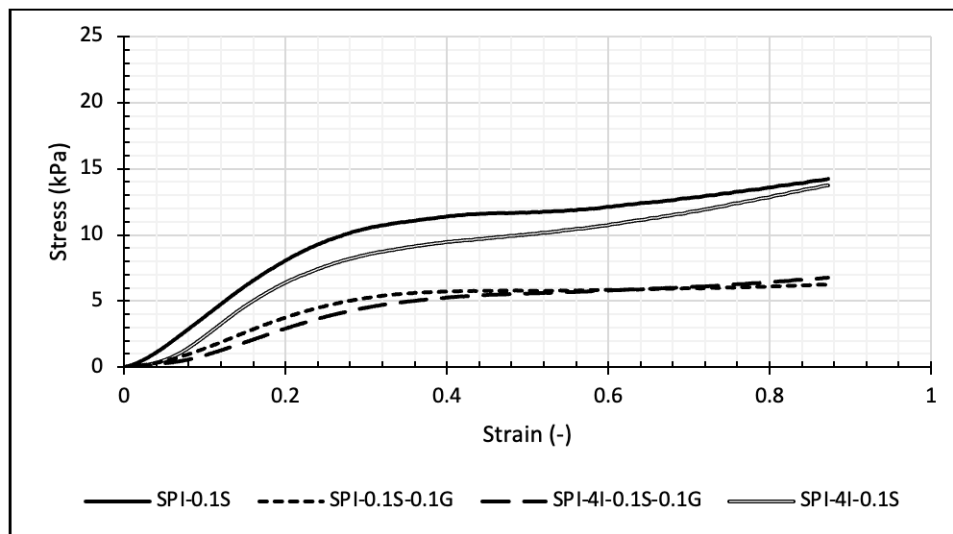


(a)

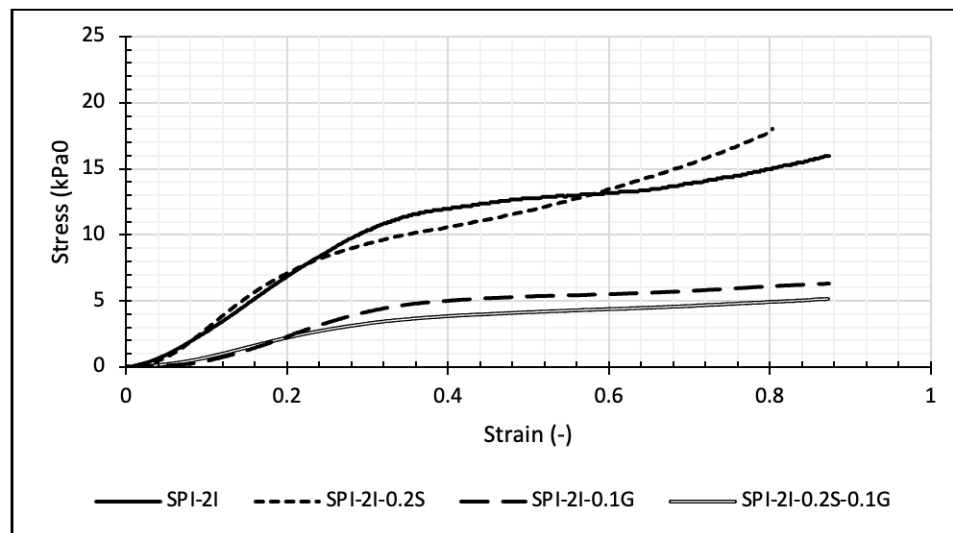


(b)

Figure 5.4: Stress-strain curve for gels (a) SPI, SPI-2I, SPI-0.1S, SPI-0.05G and (b) SPI-0.05G, SPI-4I-0.05G, SPI-0.2S-0.05G, SPI-4I-0.2S-0.05G citric acid gels. The median replicate curve of each gel was selected for Young's modulus, fracture stress, and fracture strain estimation. The average of replicates was also considered for the estimation of Young's modulus, fracture stress, and fracture strain.



(a)



(b)

Figure 5.5: Stress-strain curve for gels (a) SPI-0.1S, SPI-0.1S-0.1G, SPI-4I-0.1S-0.1G, SPI-4I-0.1S and (b) SPI-2I, SPI-2I-0.2S, SPI-2I-0.1G, SPI-2I-0.2S-0.1G citric acid gels. The median replicate curve of each gel was selected for Young's modulus, fracture stress, and fracture strain estimation. The average of replicates was also considered for the estimation of Young's modulus, fracture stress, and fracture strain..

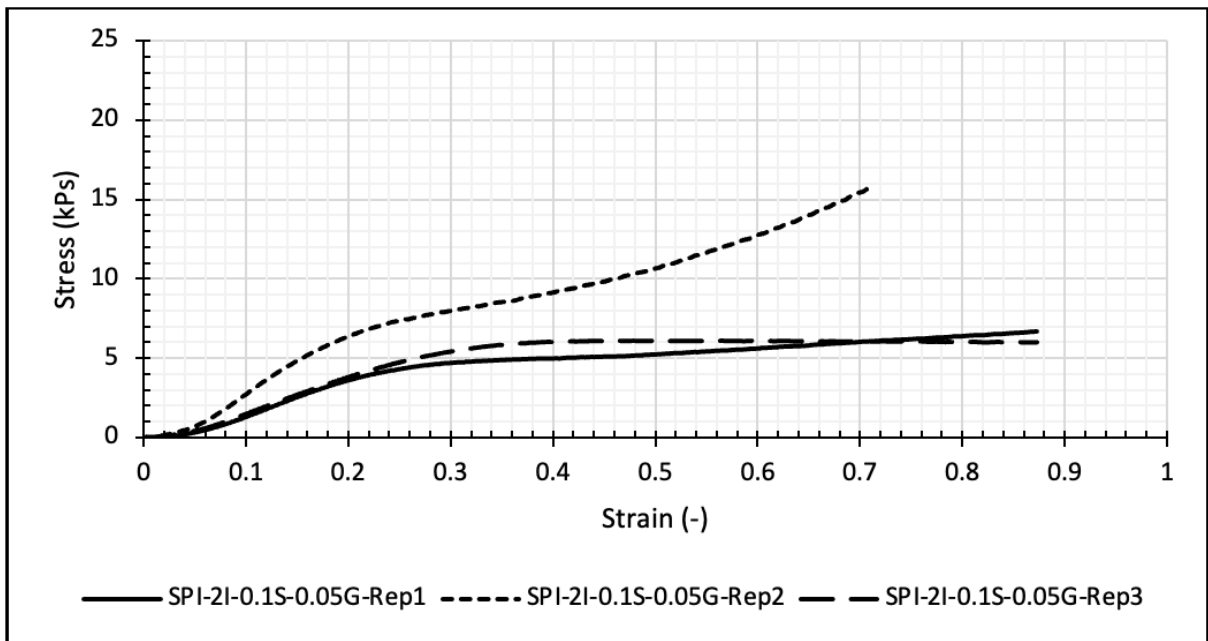


Figure 5.6: Stress-strain curve for SPI-2I-0.1S-0.05G citric acid gel. The median replicate curve of each gel was selected for Young’s modulus, fracture stress, and fracture strain estimation. The average of replicates was also considered for the estimation of Young’s modulus, fracture stress, and fracture strain.

5.4.2.2 Uniaxial Compression Properties of SPI and SPI-P gels-Estimation Method Based on Mean of Replicates

The effect of the individual polysaccharides, inulin, starch and guar gum, on the stress-strain curves obtained under uniaxial compression of SPI citric acid gels will be discussed in this section. The stress strain curves are presented in Figure 5.8a. Figure 5.7-5.11 shows that five out of seven replicates had fracture points that could be detected (all replicates except replicate 6 and 7 in Figure 5.8a), and the curve peak was clearly observed. Hence, only five replicates were used to estimate stress and strain fracture points. This may reflect the aggregated nature of the gels and their gradual fragmentation. For estimation of Young's modulus, the linear portion of the curve between strain $\frac{1}{3}$ and $\frac{2}{3}$ of the fracture strain was employed (details in section 5.4.2.1).

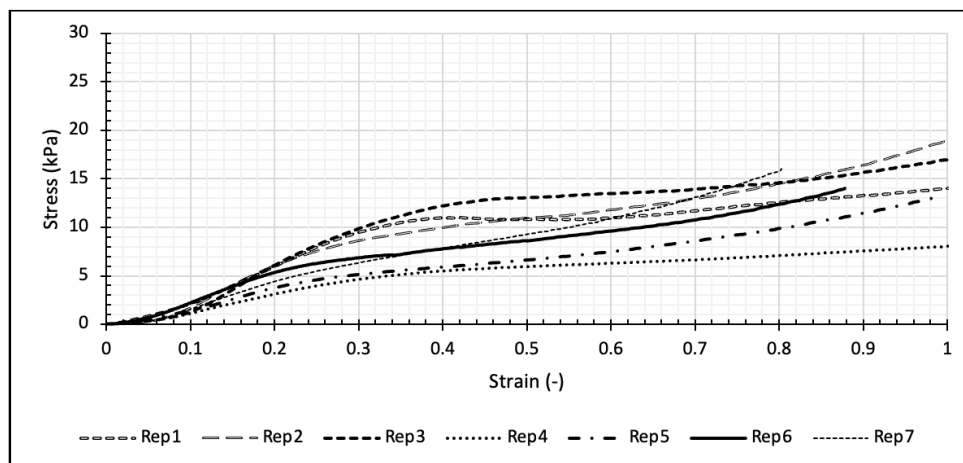


Figure 5.7: The stress-strain curves for SPI citric acid gel.

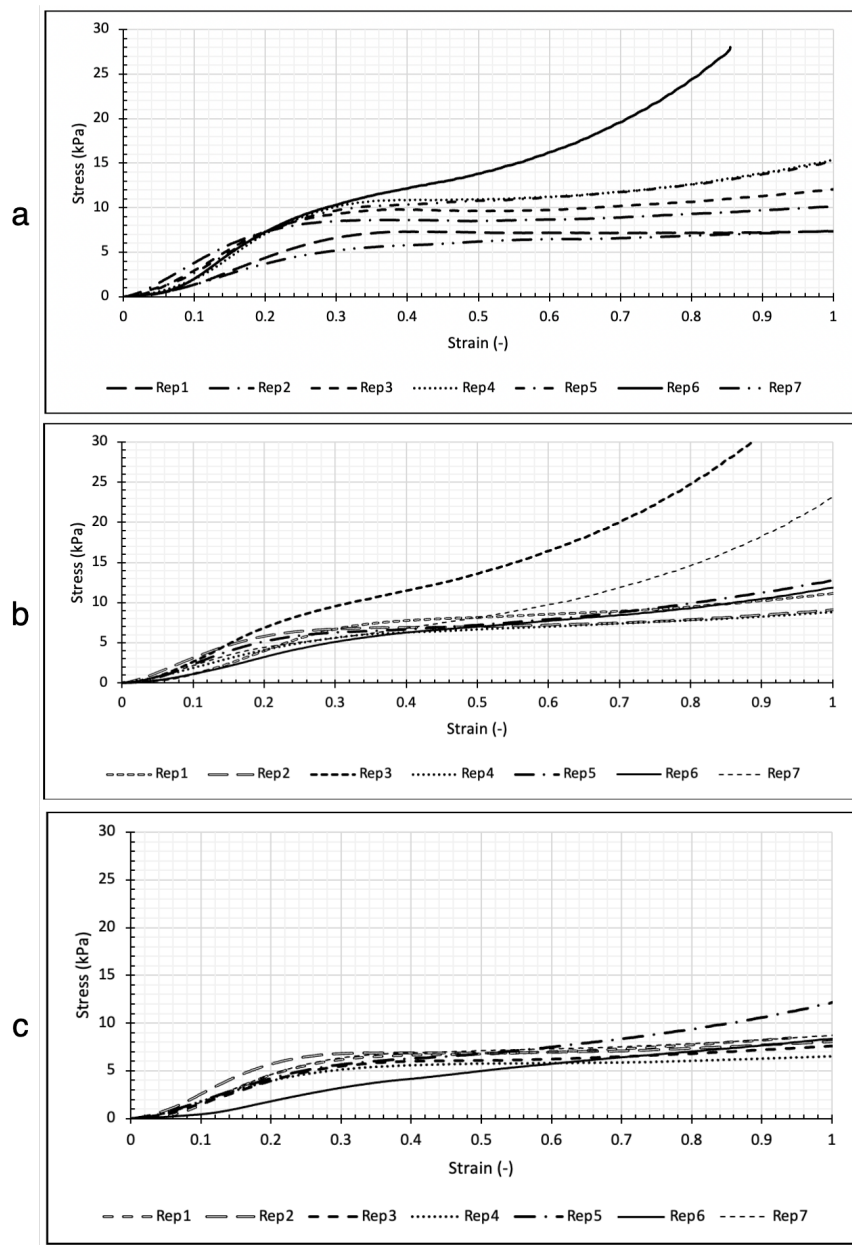


Figure 5.8: The stress-strain curves for a) SPI-0.05G, b)SPI-4I-0.05G, and c) SPI-0.2 S-0.05G citric acid gels.

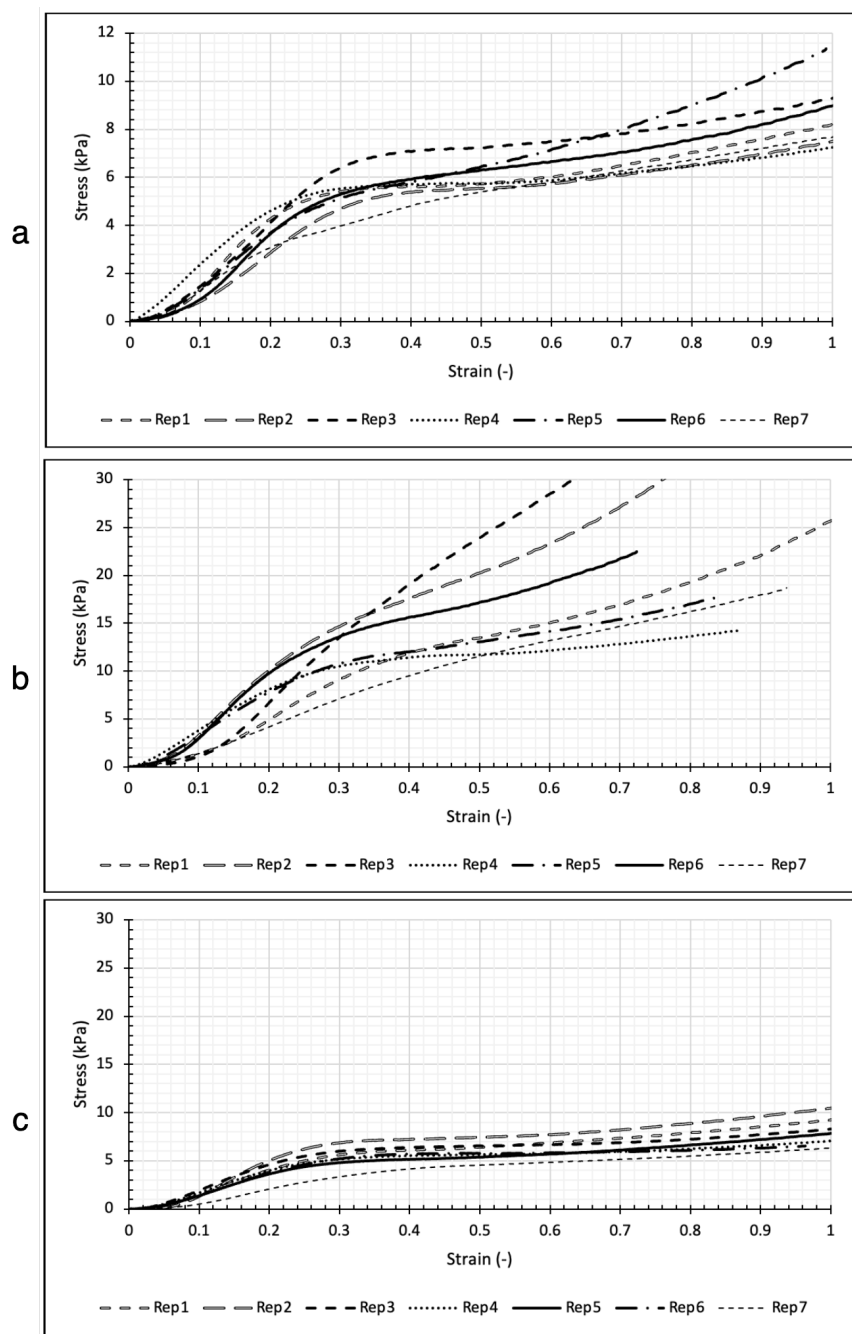


Figure 5.9: The stress-strain curves for a) SPI-4I-0.2S-0.05 G, b) SPI-0.1S , and c) SPI-0.1S-0.1G citric acid gels.

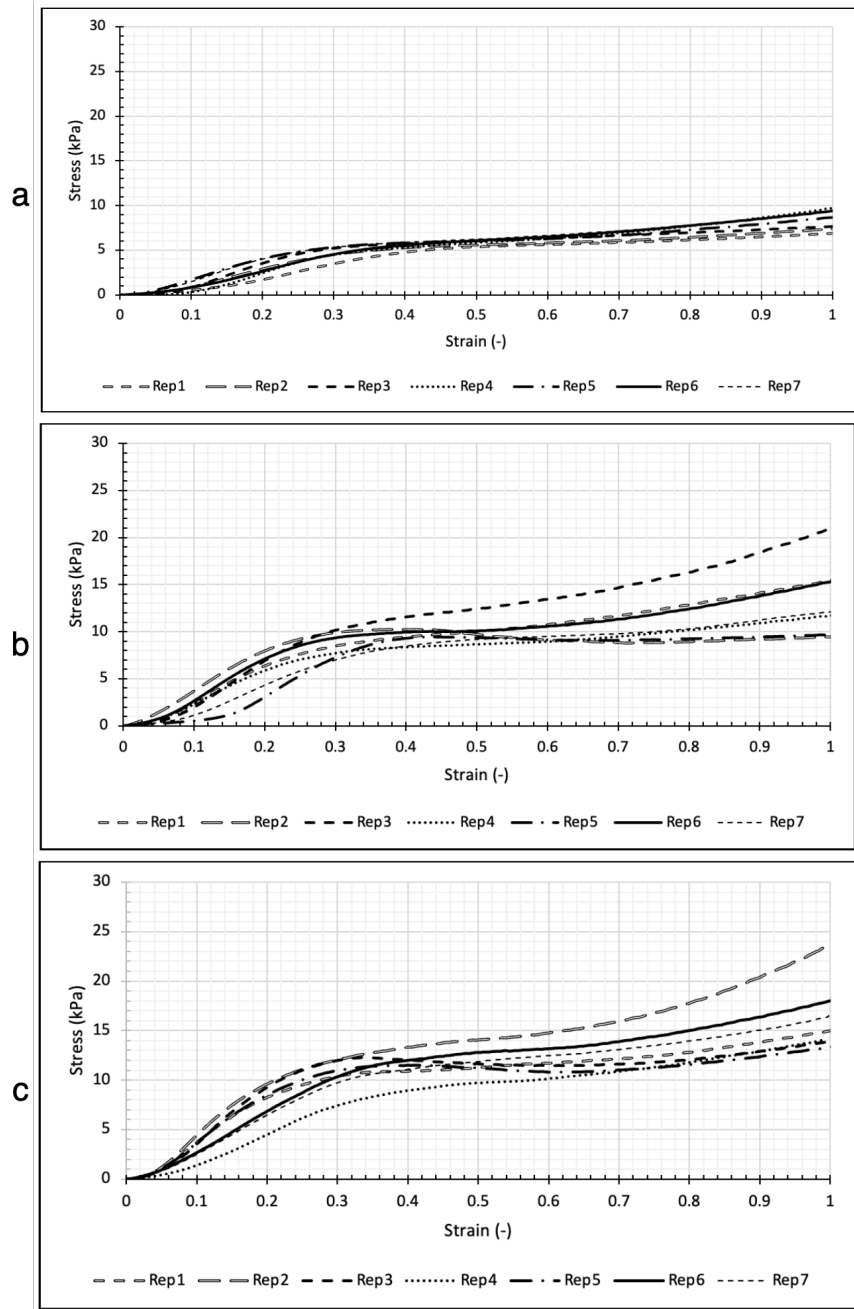


Figure 5.10: The stress-strain curves for a) SPI-4I-0.1S-0.1G, b) SPI-4 I-0.1S , and c) SPI-2I citric acid gels.

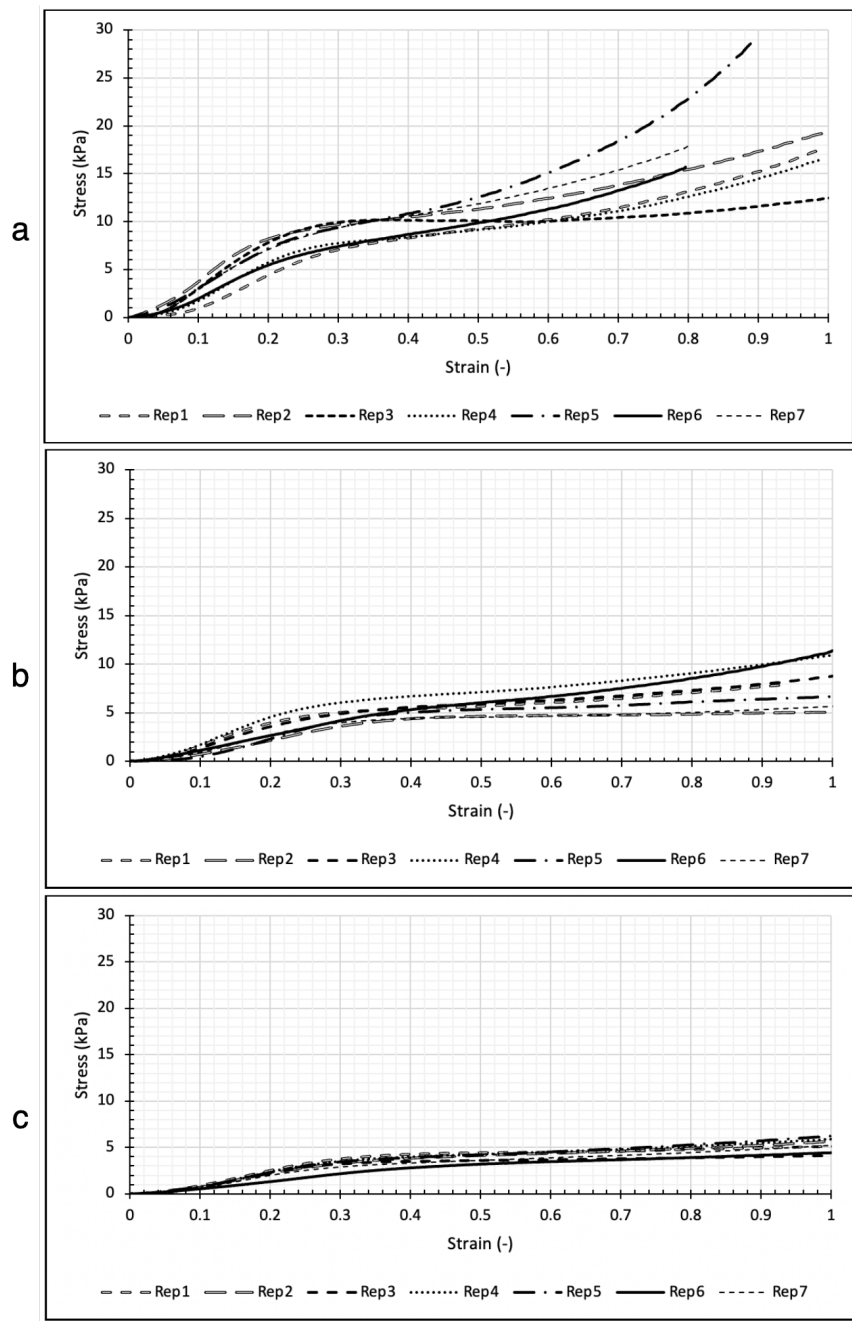


Figure 5.11: The stress-strain curves for a) SPI-2 I-0.2 S, b) SPI-2 I-0.1 G, and c) SPI-2I-0.2S-0.1G citric acid gels.

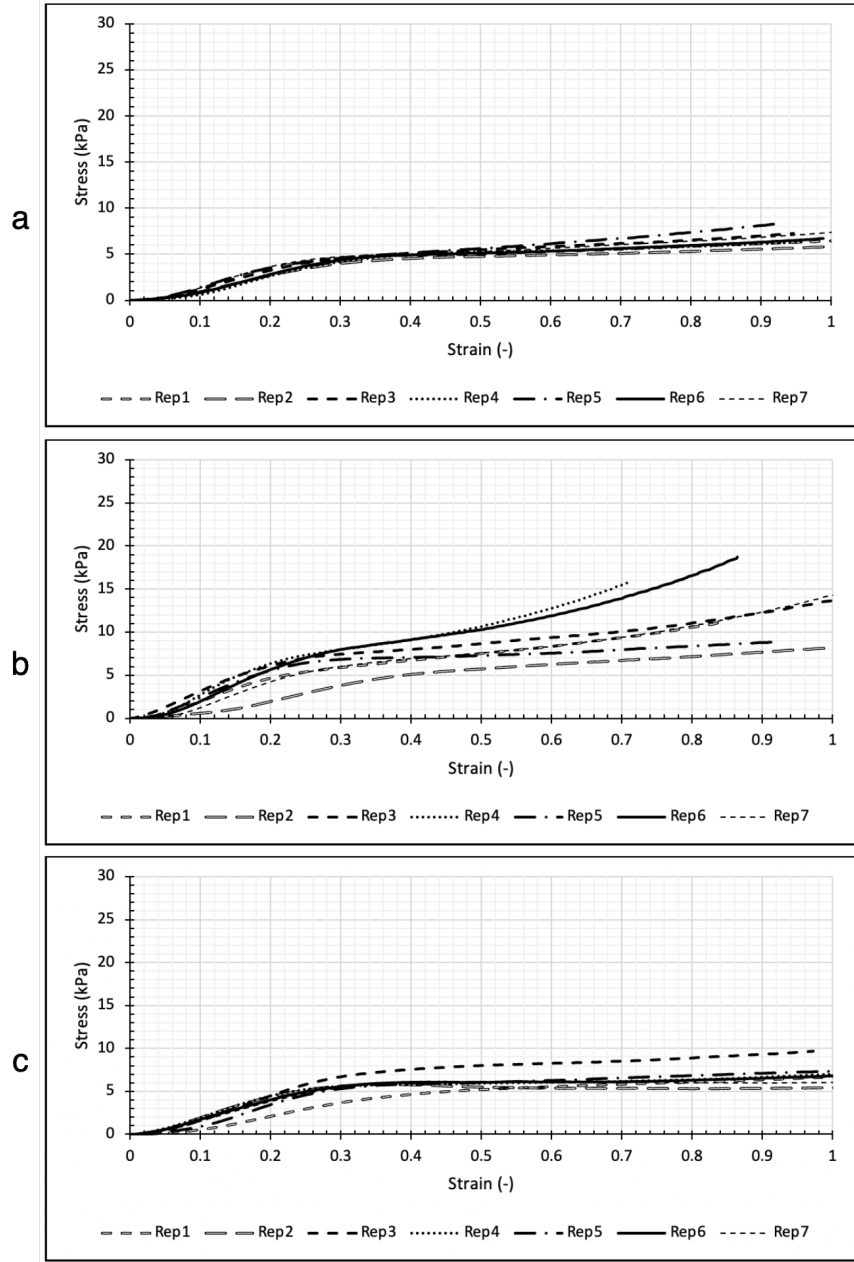


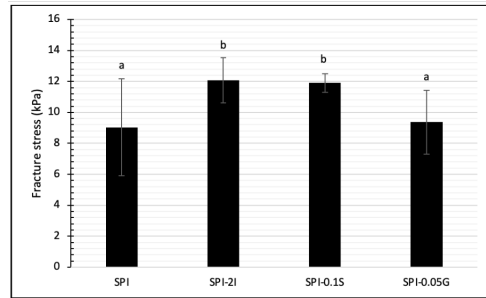
Figure 5.12: The stress-strain curves for SPI-2I-0.1S-0.05G citric acid gel a) first replicate, b) second replicate, and c) third replicate.

The estimated mean and standard deviation of selected replicates of the fracture stress, fracture strain, and Young's modulus for **SPI** (C), **SPI-2I**, **SPI-0.05G**, and **SPI-0.1S** citric acid gels are presented in Figure 5.13. The mean fracture stress of the **SPI** and **SPI-P** citric acid gels was between 9.0 and 12.1 kPa. Considering the mean value and associated standard deviation, the fracture stress of **SPI-2I** and **SPI-0.1S** citric acid gel was statistically higher than the **SPI** and **SPI-0.05G** citric acid gel ($p < 0.05$). The fracture stress increased by around 33% and 32% when 2% w/v inulin (I) or 0.1% w/v starch (S) was present compared to **SPI** citric acid gels. The estimated fracture stress suggest that **SPI-2I** and **SPI-0.1S** citric acid gels have significantly higher toughness than **SPI** citric acid gels, can withstand higher stress, and have a more stable three-dimensional structure that promotes gel strength [16]. This observation could be related to the presence of the hydroxyl groups in inulin and starch that can create hydrogen bonding with protein [16, 20, 17]. Starch and inulin may also lead to hydrophobic interaction with protein, resulting in more protein aggregation and stronger gels [16, 20]. Guar gum, on the other hand, had no significant effect on the fracture stress producing gels that had comparable fracture stress and toughness to the **SPI** citric acid gels.

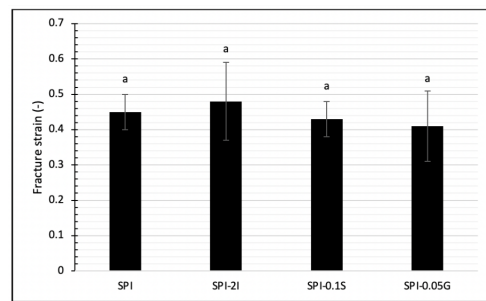
The fracture strain of **SPI** and **SPI-P** citric acid gels were between 0.41-0.48 (Figure 5.13b), which are not statistically significant ($p > 0.05$). The values obtained for the strain fracture point were not as reliable as fracture stress and Young's modulus, as the fracture point in a stress-strain curve was mostly a plateau, and an exact fracture strain point could not be estimated.

The Young's modulus of **SPI** gel, which was estimated as a slope of a linear region of a curve between strain $\frac{1}{3}$ and $\frac{2}{3}$ of the fracture strain and can provide a measure of gel hardness, was affected significantly after the addition of polysaccharide. The Young's modulus was between 25.8 to 40.5 kPa (Figure 5.13c), with **SPI-2I**, **SPI-0.1S**, and **SPI-0.05G** citric acid gels having 46%, 57%, and 30% higher values compared to **SPI** citric acid gel and are statistically different when compared to **SPI** citric acid gel ($p < 0.05$). The estimated experimental error of the Young's modulus was ~ 7.6 - 7.8 kPa for **SPI-2I** and **SPI-0.1S** gels, ~ 16.6 kPa for **SPI** citric acid gel, and ~ 19.2 kPa for **SPI-0.05G** citric acid gel (the highest experimental error was associated to **SPI-G** gels).

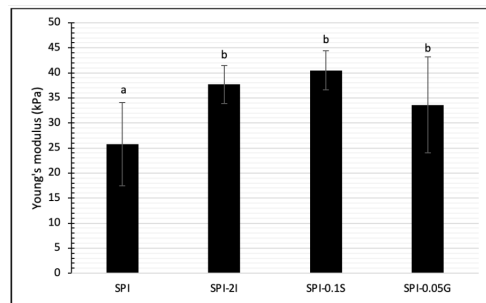
The previous study of Tseng et al. (2009) for **SPI** gel with a different coagulant, glucono-delta-lactone (**GDL**), also reported increased gel hardness with 2% w/v inulin addition [17]. In their study, the texture characteristics of the **SPI-GDL** gels were investigated with TPA, two compression tests, with the height of the force peak (in g) on the first compression cycle being calculated as a gel hardness. The inclusion of 2% w/v inulin increased the hardness of the **SPI GDL** gel from 110 g to 125 g. Although the methodology of estimating gel hardness in their study differed from the current study, the addition of inulin to **SPI**



(a)



(b)



(c)

Figure 5.13: (a) Fracture Stress, (b) Fracture Strain, and (c) Young's modulus for SPI and SPI-2I, SPI-0.1S, and SPI-0.05G citric acid gels. The Young's modulus was estimated as a slope of a linear region of a stress-strain curve between strain $\frac{1}{3}$ and $\frac{2}{3}$ of the fracture strain. All properties were estimated from average and standard deviation of replicates. Data with a and b letters indicate the statistical differences according to Duncan's method ($p < 0.05$). The fracture point was detected for five replicates for SPI and SPI-0.1S citric acid gels, six replicates for SPI-0.05G citric acid gel, and seven replicates for SPI-2I citric acid gel. The error bars represents the standard deviation for the respective numbers of replicates.

GDL or SPI citric acid gels improved the strength and hardness. Another study analyzed the structure of SPI GDL gels with Scanning Electron Microscopy (SEM) and observed that inulin addition altered the aggregation pattern of soy protein by increasing the density of protein cross-linking, hence facilitating the formation of soy protein network [73]. SEM results indicate that SPI-inulin GDL gels resulted in more compact gels with smaller pore sizes [73, 17]. Another study for pea protein isolate emulsion gels reported that the addition of 3% w/v inulin to 9% w/v pea protein isolate emulsion gel increased the gel strength (measured by uniaxial compression test, no details of the estimation of the gel strength were presented) by 23%. The water holding capacity (WHC) increased by 18% while the number of water channels in the protein network was reduced and resulted in a denser microstructure [20]. These findings suggest a synergistic effect between inulin and pea protein isolate and between inulin and water, leading to increased water retention capacity [20].

The effect of the starch, Smilax china L, on the properties of SPI $CaSO_4$ gels was reported by Chu et al. (2019) [16]. Smilax china L. starch contains a variety of active constituents such as saponins, flavonoids, amino acids, polyphenols, organic acids, and polysaccharides, in addition to starch. In their study, the gel hardness, also referred as gel strength, was the maximum force (in g) when the penetration distance of a probe reached 10 mm (size of the sample was not mentioned). The presence of 0.25% w/w starch produced gels with hardness of 70 g which was four times the hardness of SPI $CaSO_4$ gel. According to the gel dissolution method conducted in their study, hydrogen bonding and hydrophobic interaction were two dominant internal forces between starch and SPI. The presence of more hydrogen and hydrophobic interactions in the SPI-starch system resulted in a more stable three-dimensional structure and enhanced gel strength, and altered the microstructure of SPI $CaSO_4$ gel from a loose to a smooth structure was observed [16].

5.4.2.3 Uniaxial Compression Properties of SPI Citric Acid Gels with Combinations of Polysaccharides

Estimation Method Based on Mean of Replicates

In this section, the effect of combination of polysaccharides on the uniaxial compression properties of SPI citric acid gels will be discussed. Their uniaxial compression properties are summarized in Table 5.6. The Young's modulus presented in this table was estimated as the slope of the linear region of the stress-strain curve between strain $\frac{1}{3}$ and $\frac{2}{3}$ of the fracture strain. Data are expressed as mean and standard deviation.

The mean fracture stress of SPI citric acid gels containing various combinations and

levels of inulin, starch, and guar gum could be divided in three groups according to their statistically significant differences ($p < 0.05$).

The first group consists of **SPI** citric acid gels with fracture stress ~ 9 -10 kPa, specifically, **SPI**, **SPI-0.05G**, **SPI-4I-0.1S** and **SPI-2I-0.2S** citric acid gels.

The second group are **SPI** citric acid gels with fracture stress significantly lower when compared to **SPI** citric acid gels ($p < 0.05$), between 21 and 57%. The third group consists of the **SPI-0.1S** and **SPI-2I** citric acid gels with significantly higher fracture stress compared to **SPI** citric acid gel.

The mean fracture strain of **SPI** citric acid gels containing various combinations and levels of inulin, starch and guar gum varied between 0.31 and 0.49, as shown in Table 5.6. The mean fracture strain was not significantly different ($p > 0.05$) for most **SPI** citric acid gels, except the **SPI-2I-0.1S** gel (sample 10) and **SPI-2I-0.1S-0.05G** gel (sample 14). Most polysaccharides do not affect the deformation capacity of **SPI** citric acid gel at the concentrations investigated in this study.

Table 5.6: Fracture stress, fracture strain, and Young's modulus for **SPI** citric acid gels with and without polysaccharides. The Young's modulus was estimated as a slope of a linear region of a stress-strain curve between strain $\frac{1}{3}$ and $\frac{2}{3}$ of the fracture strain. The values are expressed as mean \pm standard deviation, for selected replicates (stress and strain fracture point was detected for: five replicates (*); six replicates (**); seven replicates (***)). Means within a column with different letters are significantly different ($p < 0.05$).

Gel code	Gel composition	I (%w/v)	S (%w/v)	G (%w/v)	Fracture stress (kPa)	Fracture strain (-)	Young's modulus (kPa)
C*	SPI	0	0	0	9.0 ^a \pm 3.1	0.44 ^a \pm 0.05	25.8 ^a \pm 8.3
1*	SPI-0.05G	0	0	0.05	9.4 ^a \pm 2.0	0.41 ^a \pm 0.10	33.6 ^b \pm 9.6
2*	SPI-4I-0.05G	4	0	0.05	7.1 ^b \pm 1.7	0.35 ^a \pm 0.04	23.6 ^a \pm 7.4
3**	SPI-0.2S-0.05G	0	0.2	0.05	6.4 ^b \pm 0.4	0.38 ^a \pm 0.04	22.1 ^a \pm 3.0
4*	SPI-4I-0.2S-0.05G	4	0.2	0.05	5.9 ^b \pm 0.6	0.38 ^a \pm 0.03	22.2 ^a \pm 3.9
5*	SPI-0.1S	0	0.1	0	11.9 ^c \pm 0.6	0.43 ^a \pm 0.05	40.5 ^b \pm 3.9
6***	SPI-0.1S-0.1G	0	0.1	0.1	5.9 ^b \pm 0.7	0.38 ^a \pm 0.03	21.2 ^a \pm 4.7
7***	SPI-4I-0.1S-0.1G	4	0.1	0.1	5.6 ^b \pm 0.2	0.41 ^a \pm 0.04	20.6 ^a \pm 3.3
8***	SPI-4I-0.1S	4	0.1	0	10.1 ^a \pm 1.1	0.49 ^a \pm 0.10	35.4 ^b \pm 5.8
9***	SPI-2I	2	0	0	12.1 ^c \pm 1.5	0.48 ^a \pm 0.11	37.7 ^b \pm 3.8
10*	SPI-2I-0.2S	2	0.2	0	9.4 ^a \pm 1.0	0.35 ^b \pm 0.02	32.6 ^b \pm 3.1
11**	SPI-2I-0.1G	2	0	0.1	4.5 ^b \pm 0.7	0.44 ^a \pm 0.06	18.8 ^a \pm 2.8
12*	SPI-2I-0.2S-0.1G	2	0.2	0.1	3.9 ^b \pm 0.3	0.43 ^a \pm 0.03	13.7 ^c \pm 2.6
13**	SPI-2I-0.1S-0.05G	2	0.1	0.05	5.0 ^b \pm 0.1	0.41 ^a \pm 0.04	18.2 ^a \pm 1.4
14*	SPI-2I-0.1S-0.05G	2	0.1	0.05	6.7 ^b \pm 0.9	0.31 ^b \pm 0.07	22.0 ^a \pm 3.1
15***	SPI-2I-0.1S-0.05G	2	0.1	0.05	5.9 ^b \pm 0.6	0.38 ^a \pm 0.04	21.7 ^a \pm 3.8

The mean Young's modulus of **SPI** citric acid gels containing various combinations and

levels of inulin, starch and guar gum was between 13.7 and 40.5 kPa, as summarized in Table 5.6. As mentioned before, the Young's modulus presented in this table was estimated as the slope of the linear region of the stress-strain curve between strains $\frac{1}{3}$ and $\frac{2}{3}$ of the fracture strain.

These estimates can be classified in three distinct groups according to their statistical differences ($p < 0.05$).

The first group consists of those SPI citric acid gels with a mean Young's modulus ~ 18.2 - 25.8 kPa, similar to the SPI citric acid gel, and includes ten of the fifteen different gel composition.

The second group contains those gels with a mean Young's modulus significantly higher ($p < 0.05$) when compared to the SPI citric acid gel, specifically SPI-0.0G (sample 1), SPI-0.1 S (sample 5), SPI-4I-0.1S (sample 8), SPI-2I (sample 9), and SPI-2I-0.2S (sample 10) citric acid gels which are firmer and harder than the SPI citric acid gel. Thus, the interaction between inulin, starch, and SPI, which is most likely hydrogen bonding and hydrophobic interactions [17, 16, 20], may result in stronger gels with increased firmness/hardness.

The third and smallest group includes those gels with Young's modulus significantly lower ($p < 0.05$) when compared to the SPI citric acid gel, specifically SPI-2I-0.2S-0.1G (sample 12), which is considerably softer.

The combination of guar gum with inulin and starch at the concentrations investigated in this study was not favourable for making firm gels. Therefore, the presence of starch in an SPI-G system could not improve the hardness of SPI citric acid gels.

Previous studies on the addition of guar gum to starch solution have reported its ability to limit the leaching of starch components from starch granules in a starch-guar gum system [114, 115]. Indeed, the increased solution viscosity caused by the addition of guar gum may restrict the diffusion of starch components from the starch granules, preventing starch from efficiently participating in the protein matrix [114, 115]. The same inhibition may have occurred in this study when inulin, guar gum, or SPI were present. The addition of guar gum may have limited the diffusion of inulin in the SPI solution, resulting in less interaction between SPI and inulin. One can envision that the presence of guar gum may have affected the interactions between inulin/starch and the protein molecules or that the interactions between guar gum and soy protein may be affected by the presence of inulin, starch, or both such that guar gum would act as an inactive filler, lowering the strength of the gel.

Figure 5.14 represents the correlation between three uniaxial compression properties. As shown, fracture stress and Young's modulus do not have a correlation with fracture

strain (correlation coefficient between fracture stress and fracture strain = 0.36, correlation coefficient between Young's modulus and fracture strain = 0.26, estimated by Excel). The fracture strains are statistically similar and ranged between 0.3 and 0.5. On the other hand, there is approximately a positive correlation between the fracture stress and Young's modulus (correlation coefficient = 0.94, estimated by Excel).

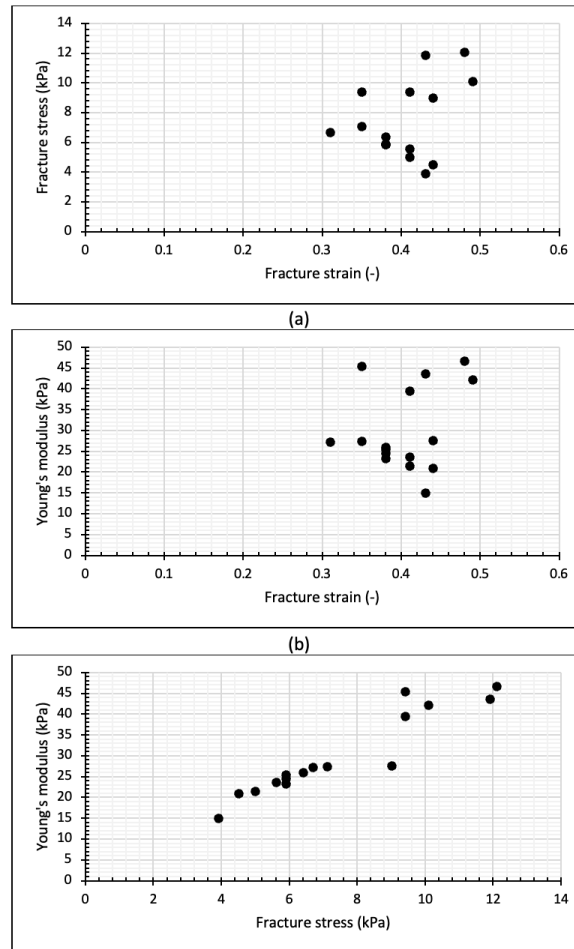


Figure 5.14: The correlation between uniaxial compression properties, a) fracture stress (kPa) vs fracture strain (-), b) Young's modulus (kPa) vs fracture strain (-), c) Young's modulus (kPa) vs fracture stress (kPa).

Estimation Method Based on Median Replicate

In this section, the uniaxial characteristics are computed using the median replicate.

The data related to this approach is summarized in Table 5.7. As shown, the fracture stress, fracture strain, and Young's modulus values differ from what was reported based on the mean of replicates (Table 5.6). The median data could be lower or higher than the mean value.

All gels had fracture stress values in the range of 4-12.7 kPa, which was similar to the previous approach (according to the estimation based on the mean, fracture stress was ranged in 3.9-12.1). Except for SPI-2I that had 16% higher fracture stress than SPI, all gels showed 3-63% lower fracture stress than the SPI citric acid gel, which differed from the prior method's results. It is interesting that based on the estimation method via median, SPI-0.05G and SPI-0.1S represented lower fracture stress than SPI citric acid gel.

The fracture strain could range between 0.30-0.53, which is a wider range than the first method (based on the estimation via mean, the fracture strain was between 0.31 and 0.49). As shown in section 5.4.2.2, when the gel was fractured, the stress-strain curve reached a plateau rather than a maximum point, so determining the fracture strain was challenging and not precise. As a result, the estimated fracture strains were not very reliable either based on the mean value or median replicate.

The results of Young's modulus are quite similar for both methods, the estimated data based on median are between 13.9 and 40.3 kPa, and the estimated data based on mean are between 13.7 and 40.5 kPa. In both methods, SPI-0.05G, SPI-0.1S, SPI-2I, SPI-4I-0.1S, and SPI-2I-0.2S represented 26-62% higher Young's modulus than SPI citric acid gel, while other gels had 16-44% lower Young's modulus than SPI citric acid gel. Similar to the previous method, guar gum, starch, inulin, and starch-inulin can have a positive effect on the Young's modulus, and their addition could increase the SPI gel's hardness.

Table 5.7: Fracture stress, fracture strain, and Young's modulus for SPI citric acid gels with and without polysaccharides. The Young's modulus was estimated as a slope of a linear region of a stress-strain curve between strain $\frac{1}{3}$ and $\frac{2}{3}$ of the fracture strain. The values estimated based on the median replicates were used.

Gel code	Gel composition	I (%w/v)	S (%w/v)	G (%w/v)	Fracture stress (kPa)	Fracture strain (-)	Young's modulus (kPa)
C*	SPI	0	0	0	10.9	0.50	24.9
1*	SPI-0.05G	0	0	0.05	9.8	0.39	34.1
2*	SPI-4I-0.05G	4	0	0.05	6.9	0.35	18.5
3**	SPI-0.2S-0.05G	0	0.2	0.05	5.7	0.44	17.7
4*	SPI-4I-0.2S-0.05G	4	0.2	0.05	5.6	0.39	20.3
5*	SPI-0.1S	0	0.1	0	10.6	0.53	34.1
6***	SPI-0.1S-0.1G	0	0.1	0.1	5.7	0.43	20.5
7***	SPI-4I-0.1S-0.1G	4	0.1	0.1	5.5	0.46	19.7
8***	SPI-4I-0.1S	4	0.1	0	9.7	0.43	31.4
9***	SPI-2I	2	0	0	12.7	0.47	40.3
10*	SPI-2I-0.2S	2	0.2	0	10.4	0.38	32.7
11**	SPI-2I-0.1G	2	0	0.1	5.2	0.46	20.8
12*	SPI-2I-0.2S-0.1G	2	0.2	0.1	4.0	0.45	13.9
13**	SPI-2I-0.1S-0.05G	2	0.1	0.05	5.1	0.43	19.4
14*	SPI-2I-0.1S-0.05G	2	0.1	0.05	8.0	0.30	26.5
15***	SPI-2I-0.1S-0.05G	2	0.1	0.05	6.1	0.42	20.8

5.4.2.4 Quadratic Model Fitting

Estimation Method Based on Mean of Replicates

The fitting of quadratic models to the data is summarized in Table 5.8 for the fracture stress, fracture strain, and Young's modulus as response variables, and inulin, starch, and guar gum concentration as independent variables. According to the ANOVA, the contribution of the quadratic model was significant for the fracture stress and the Young's modulus, but was not significant for the fracture strain. The significance of each factor was determined using the F-test and p-value. The corresponding variables are more significant if the F-value becomes greater and the p-value becomes smaller. As it can be seen, the linear form of the guar gum concentration (X_3) has a significant effect on the fracture stress and the Young's Modulus ($p < 0.05$). All other variables (X_1 , X_1^2 , X_2 , X_2^2 , X_3^2 , X_1X_2 , X_1X_3 , X_2X_3) are not significant ($p > 0.05$).

The R^2 values represent the correlation between experimental and predicted data. The R^2 values for the fracture stress, fracture strain, and Young's modulus are 0.97, 0.56, and 0.94 and the adjusted R^2 values are 0.92, 0, and 0.85. As shown in section 5.4.2.2, when the gel was fractured, the stress-strain curve reached a plateau rather than a maximum point, making the strain fracture point unclear. As a result, the estimated fracture strains were not very reliable, and the quadratic model was unable to provide a precise description of a strain fracture point.

Another way for evaluating the fitted model is to analyze the Predicted Residual Error Sum of Squares (PRESS). PRESS is a form of cross-validation used in regression analysis to assess a model's predictive ability. It provides a summary measure of the fit of a model to a sample of observations that were not themselves used to estimate the model (the PRESS values were not determined in this study).

The lack of fit error indicates if the regression model represents adequately the experimental data. The p value of the lack of fit for the fracture stress, fracture strain, and Young's modulus is 0.73, 0.50, and 0.79, which is not significant ($p > 0.05$). The estimated R^2 and the lack of fit values indicate that the model represents adequately the observed data of the fracture stress and the Young's modulus, while the model is insufficient for the representation of the fracture strain. The dependency of the fracture stress (Y_1) and the Young's Modulus (Y_3) according to the guar gum concentration (X_3), is given by Equations 5.8 and 5.9.

$$Y_1 = 5.86 - 2.95X_3, \quad (5.8)$$

$$Y_3 = 20.63 - 8.99X_3, \quad (5.9)$$

It is worth mentioning that the model was developed from experimental data generated with the B-B experimental design and may have limitations because the experimental data do not include SPI citric acid gel with no polysaccharide, and for a narrow range of polysaccharide concentration. As discussed in the previous section, the comparison of SPI-P citric acid gels containing starch or inulin to SPI citric acid gel indicate that the addition of starch or inulin improved the strength of the gel and produced tougher and harder gel than the SPI citric acid gel. SPI citric acid gels prepared with 2-4% w/v inulin, 0.1-0.2% w/v starch, or a combination of both, as well as with 0.05% w/v guar gum, could produce a tougher and stiffer gel, since they increased the fracture stress and Young's modulus of the gel in comparison to the SPI citric acid gel. The addition of guar gum to the SPI-I-S system is not recommended for producing firm gels, as it produced weaker fracture stress and Young's modulus.

Table 5.8: ANOVA of the quadratic model for the fracture stress(σ_f), fracture strain (ϵ_f), and Young's modulus (E) as response variables and inulin concentration (X_1), starch concentration (X_2), guar gum concentration(X_3) as dependent variables. Estimated data based on the mean of replicates was used.

Source	DF	Fracture stress (σ_f , kPa)				Fracture strain (ϵ_f , -)				Young's modulus (E, kPa)			
		SS	MS	F value	Prob > F	SS	MS	F value	Prob > F	SS	MS	F value	Prob > F
X_1 (I)	1	3.00	3.00	4.14	0.1785	0.0001	0.0001	0.04	0.8553	30.42	30.42	6.81	0.1207
X_2 (S)	1	7.03	7.03	9.72	0.0893	0.0024	0.0024	0.93	0.4365	66.70	66.70	14.94	0.0608
X_3 (G)	1	69.62	69.62	96.24	0.0102	0.0010	0.0010	0.38	0.5984	646.20	646.20	144.78	0.0068
X_1^2	1	4.60	4.60	6.36	0.1276	0.0002	0.0002	0.08	0.7948	66.17	66.17	14.82	0.0613
X_2^2	1	0.17	0.17	0.23	0.6728	0.0001	0.0001	0.04	0.8580	0.95	0.95	0.21	0.6892
X_3^2	1	7.15	7.15	9.88	0.0880	0.0103	0.0103	3.92	0.1860	76.72	76.72	17.18	0.0535
$X_1.X_2$	1	0.81	0.81	1.11	0.4008	0.0009	0.0009	0.34	0.6179	25.50	25.50	5.71	0.1393
$X_1.X_3$	1	0.56	0.56	0.77	0.4708	0.0002	0.0002	0.08	0.7975	5.06	5.06	1.13	0.3984
$X_2.X_3$	1	1.10	1.10	1.52	0.3423	0.0036	0.0036	1.36	0.3628	0	0	0	1.0000
Residual	5	2.44	0.48	-	-	0.0141	0.0028	-	-	13.74	2.74	-	-
Lack of fit	3	1	0.33	0.46	0.7369	0.0088	0.0029	1.12	0.5028	4.82	1.60	0.36	0.7920
Pure error	2	1.44	0.72	-	-	0.0053	0.0026	-	-	8.92	4.46	-	-
Cor total	14	95.52	-	-	-	0.0328	-	-	-	920.40	-	-	-
R ²	-	0.97	-	-	-	0.56	-	-	-	0.98	-	-	-
Adj R ²	-	0.92	-	-	-	0	-	-	-	0.96	-	-	-

Interpretation of the response surface models

The three-dimensional (3D) and contour plots of the fracture stress and the Young's modulus as a function of inulin and starch concentration for different guar gum concentrations are given in Figures 5.15 and 5.16. The fracture stress and the Young's modulus were

highest at all levels of guar gum when no starch and inulin were present. Increasing the guar gum concentration lowered the fracture stress and the Young's modulus. The fracture stress ranged from 8.9 to 13.7 kPa in the absence of guar gum (Fig 5.15a) and dropped to 5.1 to 9.2 at guar gum concentration 0.05% w/v, and 4.0 to 7.1 at guar gum concentration of 0.1% w/v (Fig. 5.15 b-c). A similar effect of the guar gum concentration was observed for the Young's modulus. The Young's modulus was between 31.8 to 47.3 kPa (Fig. 5.16 a) when no guar gum was present and decreased to 18.2-32.7 and 13.9-29.4 kPa with the addition of 0.05% w/v and 0.1% w/v guar gum (Fig. 5.16 b-c). This result could be due to the increased viscosity caused by the guar gum, which consequently, limited the diffusion of starch or inulin into the solution, and inhibit them to effectively participate into the gel network [114, 115].

The 3D and contour plots of the fracture stress and the Young's Modulus with 0.1%w/v starch (level 0) and 2%w/v inulin (level 0), are shown in Figures 5.17 and 5.18. The model estimates indicate that the fracture stress and the Young's Modulus are affected differently by the inulin, starch and guar gum concentration. The fracture stress at 0.1% w/v starch (level 0) and 2% w/v inulin ranged between 4.3-11.5 kPa and 4.1-11.9 kPa, respectively (Figure 5.17 a-b). At constant starch concentration (0.1% w/v), the highest fracture stress was estimated at the lowest inulin concentration and lowest guar gum concentration. The fracture stress decreased more significantly with increasing guar concentration than with increasing inulin concentration. At constant inulin concentration (2% w/v), the highest fracture stress was estimated at the lowest starch concentration and lowest guar gum concentration. The fracture stress decreased more significantly with increasing guar gum concentration than with increasing starch concentration. Similar estimates and behaviour of the fracture stress according to polysaccharide concentration were obtained at other levels of starch and inulin (data not shown).

The estimates of the Young's modulus, shown in Figure 5.18, range between 16.2-39.2 kPa for 0.1% w/v starch (0 level) and 13.8-37.5 kPa for 2% w/v inulin (0 level). At constant starch concentration (0.1% w/v) and constant inulin concentration (2.0% w/v), the highest Young's modulus was estimated at the lowest guar gum concentration. The Young's modulus decreased more significantly with increasing guar gum concentration than with either increasing inulin concentration or increasing starch concentration. Similar estimates of the Young's modulus were obtained at lower or higher amounts of starch and inulin concentration (data not shown).

In summary, the model estimates presented in Figure 5.17 and 5.18 indicate that guar gum has the most effect on the fracture stress and Young's modulus for the guar gum, inulin and starch concentration range investigated in this study. The highest fracture stress and Young's modulus were estimated when guar gum is absent.

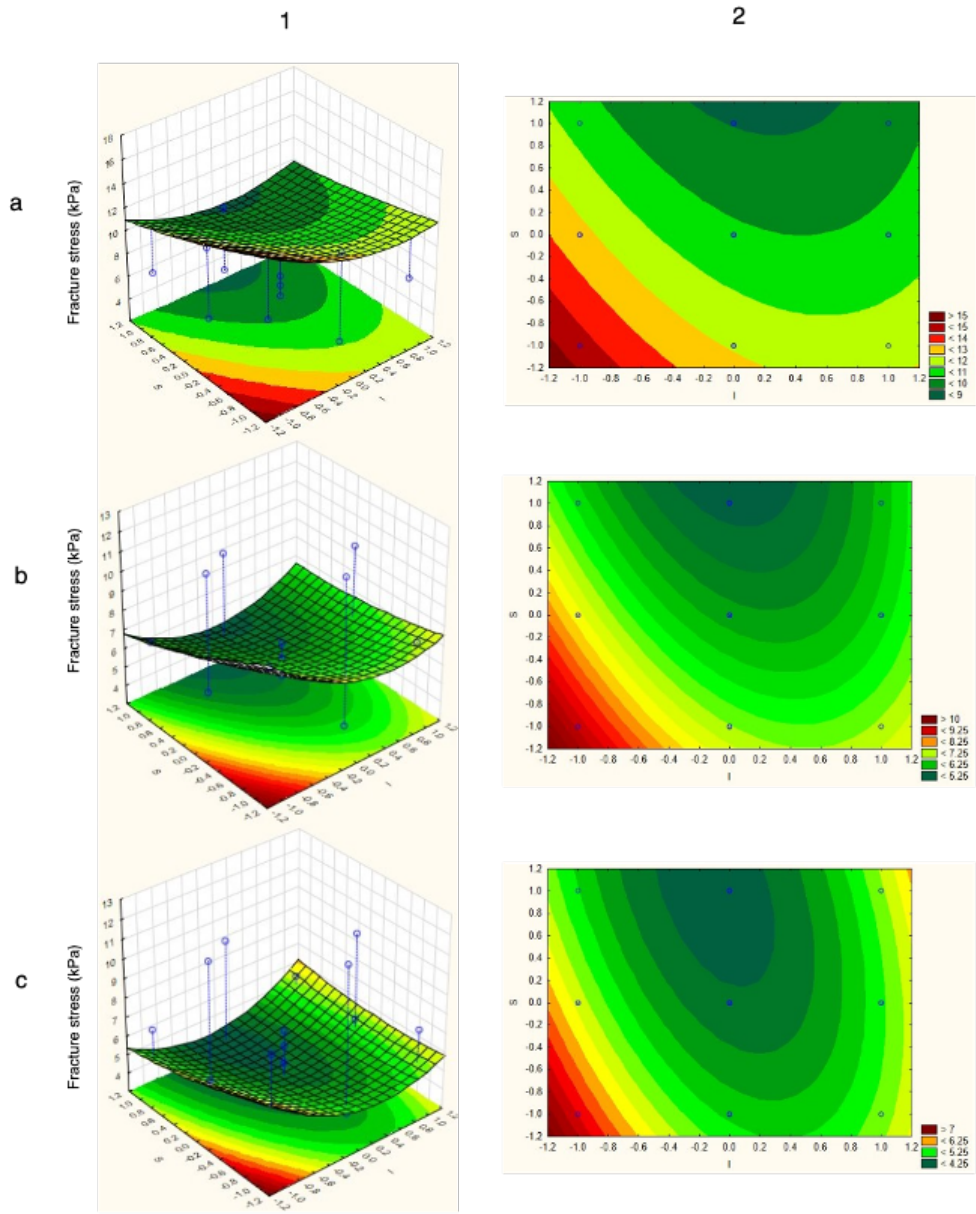


Figure 5.15: Three dimensional (1) and contour (2) plots of fracture stress as a function of inulin concentration (x-axis) and starch concentration (y-axis) for different guar gum concentrations (level): -1 (a), 0 (b), and +1 (c).

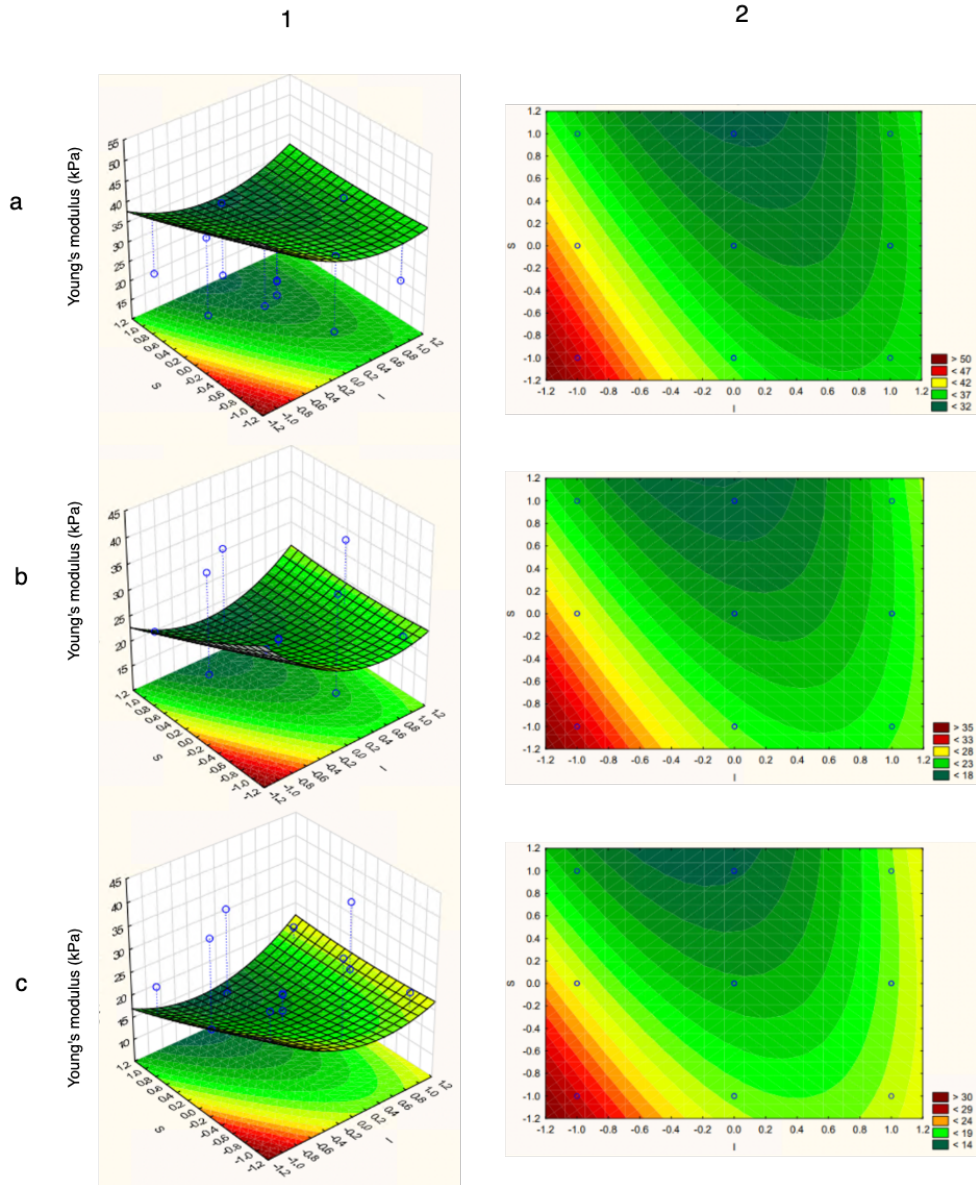


Figure 5.16: Three dimensional (1) and contour (2) plots of Young's modulus as a function of inulin concentration (x-axis) and starch concentration (y-axis) for different guar gum concentrations (level): -1 (a), 0 (b), and +1 (c).

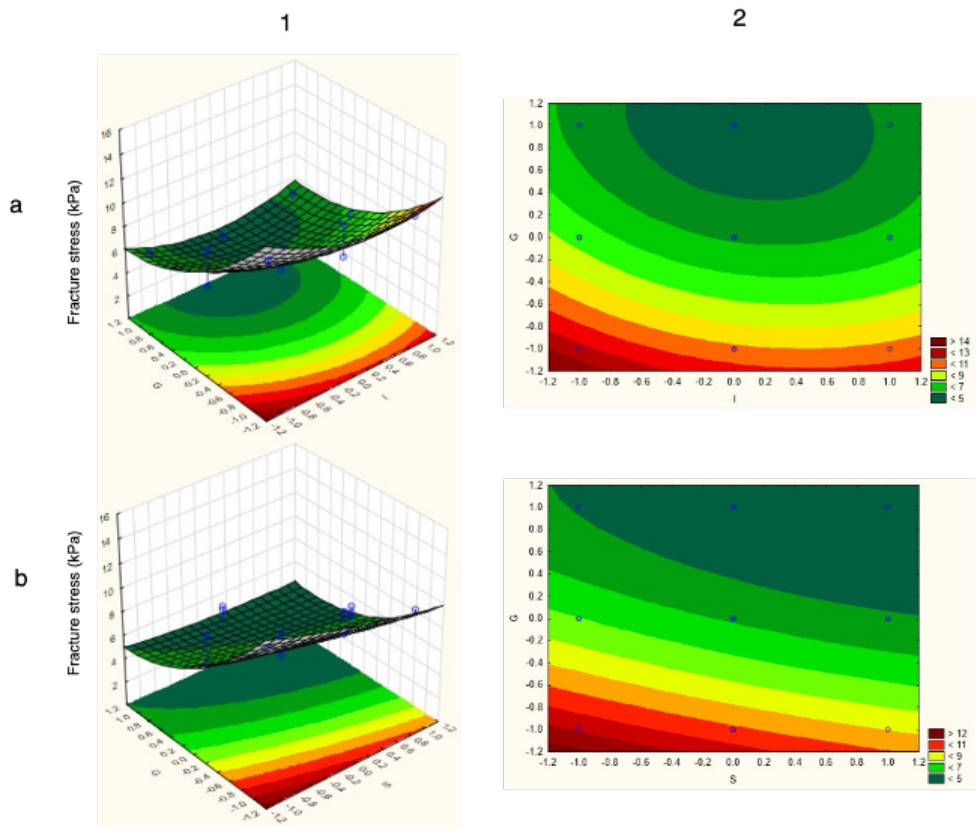


Figure 5.17: Three dimensional (1) and contour (2) plots of fracture stress as a function of (a) inulin concentration (x-axis) and guar gum concentration (y-axis) at 0.1% w/v of starch concentration (level 0) and (b) starch concentration (x-axis) and guar gum concentration (y-axis) at 2% w/v of inulin concentration (level 0).

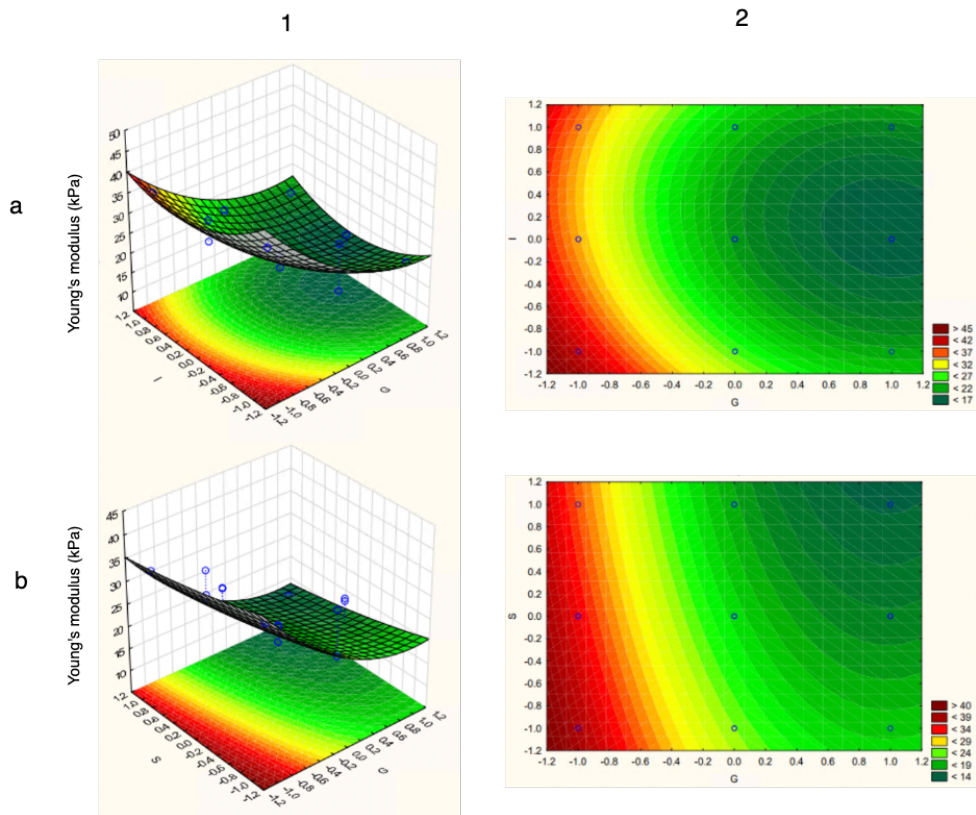


Figure 5.18: Three dimensional (1) and contour (2) plots of Young's modulus as a function of (a) inulin concentration (x-axis) and guar gum concentration (y-axis) at 0.1% w/v of starch concentration (level 0), and (b) starch concentration (x-axis) and guar gum concentration (y-axis) at 2% w/v of inulin concentration (level 0).

Estimation Method Based on Median Replicate

In this section, the quadratic model for describing fracture stress, fracture strain, and Young's modulus was determined based on the estimated data via the median replicate. Table 5.9 is the ANOVA table related to this approach.

According to the results, the associated quadratic model for the median data represented a higher lack of fits and pure error compared with the mean data for fracture stress and Young's modulus. As a result, the R^2 and R_{adj}^2 values were lower when compared to the first method. This result suggests that the estimated quadratic models for the fracture stress and Young's modulus are more valid using the mean data than the median. However, both methods indicate that guar gum (X_3) is the most significant variable, and other variables (X_1 , X_2 , X_1^2 , X_2^2 , X_3^2 , $X_1 \cdot X_2$, $X_1 \cdot X_3$, $X_2 \cdot X_3$) have no statistical effect on the quadratic model related to fracture stress and Young's modulus.

The quadratic models for fracture stress and Young's modulus are represented by Equations 5.10 and 5.11, respectively (Y'_1 and Y'_2 are fracture stress and Young's modulus based on the median data, respectively). In these equations, the intersection coefficients are 6-9% higher, and X_3 coefficients are 3-11% lower than those coefficients derived from the previous method (based on mean of replicates).

$$Y'_1 = 6.40 - 2.87X_3, \quad (5.10)$$

$$Y'_3 = 21.90 - 7.95X_3, \quad (5.11)$$

The quadratic model for describing the fracture strain was not significant for estimation based on either the median replicate or mean of replicates, as the obtained fracture strains were not precise.

Table 5.9: ANOVA of the quadratic model for the fracture stress(σ_f), fracture strain (ϵ_f), and Young's modulus (E) as response variables and inulin concentration (X_1), starch concentration (X_2), guar gum concentration(X_3) as dependent variables. Estimated data based on the median replicate was used.

Source	DF	Fracture stress (σ_f , kPa)				Fracture strain (ϵ_f , -)				Young's modulus (E, kPa)			
		SS	MS	F value	Prob > F	SS	MS	F value	Prob > F	SS	MS	F value	Prob > F
X_1 (I)	1	2.10	2.10	0.97	0.4288	0.0024	0.0024	0.46	0.5644	34.03	34.03	1.96	0.2959
X_2 (S)	1	9.90	9.90	4.56	0.1661	0.0000	0.0000	0.00	0.9310	105.85	105.85	6.11	0.1319
X_3 (G)	1	66.12	66.12	30.47	0.0312	0.0008	0.0008	0.15	0.7335	505.62	505.62	29.20	0.0325
X_1^2	1	0.15	0.15	0.07	0.8185	0.0020	0.0020	0.38	0.5986	0.05	0.05	0.003	0.2959
X_2^2	1	0.59	0.59	0.27	0.6538	0.0010	0.0010	0.19	0.7012	1.44	1.44	0.08	0.8000
X_3^2	1	6.00	6.00	2.76	0.2381	0.0198	0.0198	3.79	0.1907	71.48	71.48	4.12	0.1791
$X_1.X_2$	1	1.96	1.96	0.90	0.4422	0.0001	0.0001	0.02	0.9027	82.81	82.81	4.78	0.1602
$X_1.X_3$	1	0.12	0.12	0.06	0.8343	0.0025	0.0025	0.47	0.5609	0.90	0.90	0.05	0.8406
$X_2.X_3$	1	0.30	0.30	0.14	0.7447	0.0016	0.0016	0.31	0.6358	0.12	0.12	0.007	0.9406
Residual	5	8.12	1.62	-	-	0.0199	0.0039	-	-	67.02	13.40	-	-
Lack of fit	3	3.78	1.26	0.58	0.6822	0.0095	0.0031	0.60	0.6718	32.40	10.80	0.62	0.6638
Pure error	2	4.34	2.17	-	-	0.0104	0.0052	-	-	34.62	17.31	-	-
Cor total	14	95.00	-	-	-	0.0505	-	-	-	868.35	-	-	-
R ²	-	0.91	-	-	-	0.60	-	-	-	0.92	-	-	-
Adj R ²	-	0.76	-	-	-	0	-	-	-	0.78	-	-	-

5.4.3 Viscoelastic Properties

5.4.3.1 Viscoelastic properties of SPI and SPI-P gels-Estimation Method Based on Mean of Replicates

The effect of the individual polysaccharide, inulin, starch and guar gum, on the viscoelastic properties of SPI citric acid gels will be discussed in this section. The first step was to estimate the linear viscoelastic region (LVR) of the gels by conducting strain sweep tests. The LVR (the strain values) of SPI, SPI-2I, SPI-0.1S, and SPI-0.05G gels are 3.5%, 7.1%, 5.2%, and 5.2%, respectively. Therefore, the strain for the frequency sweep test was selected to be 0.01 such that those conditions would ensure that all samples would be located within their respective linear viscoelastic region.

The variation of the storage modulus (G') and loss modulus (G'') as a function of angular frequency at 25° C for citric acid-induced gels, SPI, SPI-2I (sample 9), SPI-0.1S (sample 5), and SPI-0.05G (sample 1) gels are presented in Figure 5.19. Both G' and G'' increased with increasing angular frequency, and are in a range of 0.95-3.1 MPa and

0.2-0.8 MPa, respectively. The errors of this experiment could be related to the sample preparation steps, as all the gels should be cutted to a very thin layar (1 mm thickness), which was challenging.

The G' and G'' values of all SPI-P citric acid gels are significantly greater than SPI citric acid gel ($p < 0.05$), while $\tan\delta$ values are somewhat similar ($p > 0.05$). These results suggest that the network of SPI-P citric acid gels is stronger than the network of SPI citric acid gels [18], which aligns with the observed uniaxial mechanical characteristics. The SPI-2I citric acid gel displayed the highest stiffness with 62-73% higher G' than the SPI citric acid gel. A smaller increase of the G' values was observed for SPI-0.05G and SPI-0.1S citric acid gels compared to SPI citric acid gels, 48-55% and 34-47%. The dependency of $\tan\delta$ according to angular frequency at 25° C for the SPI citric acid gel and the three SPI-P citric acid gels, SPI-2I, SPI-0.1S and SPI-0.05G, is presented in Figure 5.19B. The values of $\tan\delta$ of SPI and SPI-P gels were in a range of 0.21-0.25, which is less than 1 indicating a substantially higher elastic component.

Published viscoelastic properties of various SPI and pea protein isolate gels with and without starch, inulin and guar gum are summarized in Table 5.10. Xu et al. (2021) and Beccard et al. (2019), indicated that inulin alone is unable of forming inulin gel at concentrations below 100 g/L [20, 116]. In contrast, inulin in the presence of pea protein worked synergistically and produced pea protein-inulin emulsion gel with higher storage modulus and lower $\tan\delta$ than pea protein emulsion gel [20]. According to the dissolution behaviour of pea protein inulin emulsion gels in solvents, inulin interactions with pea protein are primarily hydrogen bonding and hydrophobic interactions, with no electrostatic interaction or disulfide bond formed [20]. Inulin is a neutral polysaccharide with no sulfur functional groups but contains a high number of hydroxyl groups that can create hydrogen bonds with the carboxyl and amino groups of the protein [20]. Chu et al. (2019) reported similar results for the interactions between Smilax china L. starch and SPI. It was stated that disulfide bonding was not affected by increasing the concentration of Smilax china L. starch, while hydrogen bonding and hydrophobic interactions increased moderately. Notably, the addition of Smilax china L. starch decreased the electrostatic interactions, which suggests that some electrostatic interactions between the protein side chains may have been replaced by hydrogen bonding or hydrophobic interactions between protein and starch [16].

Guar gum, a galactomannans, will possess intermolecular interactions that are mostly hydrogen bonding between the non-substituted mannan regions [117]. The influence of guar gum on the viscoelastic properties of 8%w/w SPI GDL gel was conducted by Chang et al. (2014) [18]. The instantaneous and retarded elastic moduli estimated from creep and recovery tests were 30% and 5% higher compared to pure SPI GDL gel [18]. These results

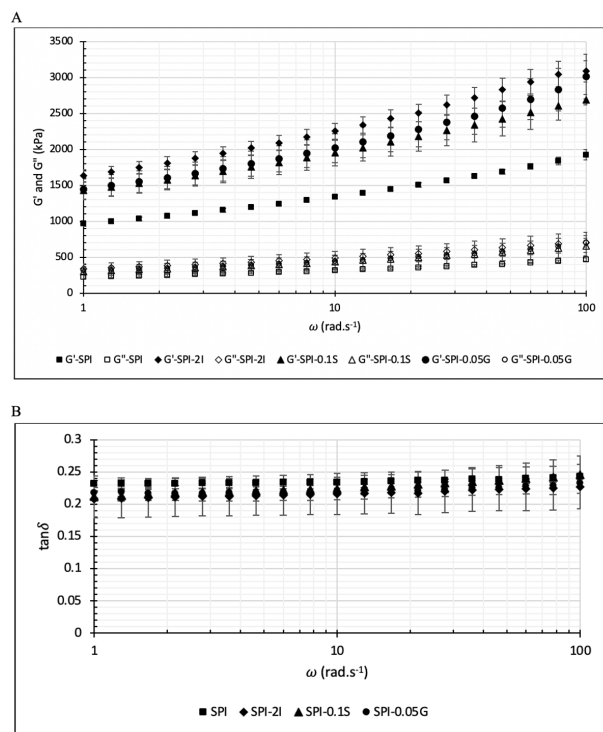


Figure 5.19: A) Storage modulus (G') and loss modulus (G'') and (B) $\tan\delta$ of SPI, SPI-0.05G, SPI-0.1S, and SPI-2I gels at 25° C as a function of angular frequency. All gels contain 8%, w/v and 0.3%w/v citric acid. Three replicates were conducted for each gel type and data are presented as mean of replicates \pm standard deviation.

support the stronger gels obtained in our study when guar gum was added. In contrast, Brito-Oliveira et al. (2020) [117] found that 0.1% w/v guar gum addition to 14% w/v SPI NaCl gels increased the gel heterogeneity, lowered G' by 60%, and increased $\tan\delta$ by 21%, implying that the SPI-guar gum NaCl gel had significantly weaker gel characteristics. These observations contradict our findings for SPI citric acid gels, which could be attributed to the higher guar gum content (0.1-0.3% w/v), the different gel preparation methodology, or the different coagulation mechanism of NaCl and citric acid. Brito-Oliveira et al. (2020) [117] pre-heated the SPI-guar gum solution at 80° C for 30 minutes, cooled it to room temperature with the subsequent addition of NaCl, and stored at 10° C for 12 hours before characterization, with no subsequent heating. NaCl could induce electrostatic interactions with SPI, resulting in the creation of a 3D SPI gel structure. Citric acid, on the other hand, can interact with SPI and guar gum not just by electrostatic interactions but also

Table 5.10: Rheological properties of SPI and pea protein isolate gels containing starch, inulin, or guar gum, as reported in literature.

Protein	Polysaccharide	Coagulant	Frequency range (rad.s ⁻¹)	G' (Pa) at $\omega = 1$ rad.s ⁻¹	G'' (Pa) at $\omega = 1$ rad.s ⁻¹	$\tan\delta$ at $\omega = 1$ rad.s ⁻¹
9% w/w SPI [16]	0% w/w Smilax china L. starch	0.35% w/w $CaSO_4$	0.1-100	200	40	0.2
	0.25% w/w Smilax china L. starch			500	90	0.18
6% w/w SPI [18]	0% w/w guar gum	1.5% w/w GDL	0.1-100	3200	500	0.15
	0.05% w/w guar gum			5600	1100	0.19
14% w/v SPI [117]	0% w/v guar gum	300 mM NaCl	0.01-1	1110	217	0.19
	0.1% w/v guar gum			443	108	0.24
9% w/v PPI* [20]	0% w/v inulin	0.01 M $CaCl_2$	0.1-10	83	15	0.18
	3% w/v inulin			750	113	0.15
7.28% w/w SPI [17]	0% w/v inulin	0.4% w/v GDL	Not done	1290 (at 80° C)	75 (at 80° C)	0.06 (at 80° C)
	2% w/v inulin			1410 (at 80° C)	80 (at 80° C)	0.06 (at 80° C)

* Pea Protein Isolate. The gel contained 7% w/v soybean oil.

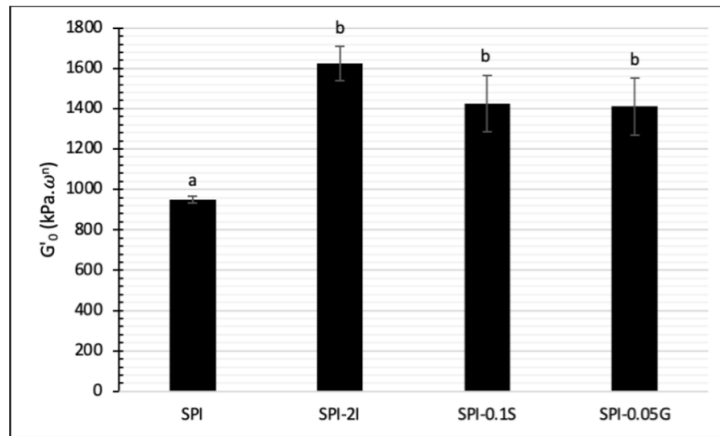
via hydrogen bonding. As a result, citric acid may be substantially more powerful than NaCl at entangling SPI and guar gum. NaCl-induced SPI gel possessed 1000 times lower G' and G'' compared with citric acid-induced SPI gel (G' and G'' of NaCl-SPI gel at 1 rad.s⁻¹ was 1110 and 217 Pa, respectively; G' and G'' of citric acid-SPI gel at 1 rad.s⁻¹ was 1000 and 200 kPa, respectively).

The parameter estimates, G'_0 , G''_0 , n' , and n'' , determined from the fit of the experimental data, G' and G'' according to frequency, with the power law model (Equations 5.3 and 5.4) are presented in Figure 5.20 and Table 5.11. The R^2 values (above 0.98), indicate very good fit of the model to the experimental data. The estimated G'_0 and G''_0 of the SPI-P citric acid gels are significantly higher ($p < 0.05$) than the SPI citric acid gels. In contrast, the estimated n' and n'' of the SPI-P citric acid gels are similar ($p > 0.05$) to the SPI citric acid gels. The magnitude of n' and n'' , is small and similar for all types of SPI-P citric acid gels, 0.14-0.19, which indicates negligible effect of the frequency on the ratio of the storage and loss modulus.

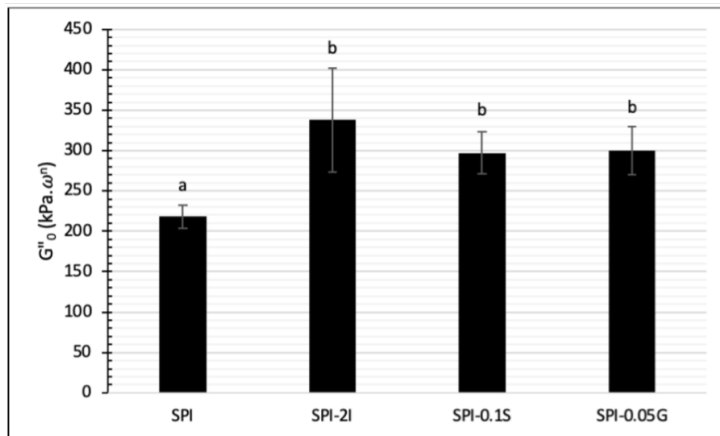
The estimated experimental errors of G'_0 for the SPI gel was ~ 35 kPa. By the addition of polysaccharides, the G'_0 was increased significantly, and the experimental error was estimated as 172 kPa for SPI-2I and 280 kPa for SPI-0.1S and SPI-0.05G gels. Similarly,

the estimated experimental errors for G''_0 was 28 kPa for the **SPI** citric acid gel, 52-60 kPa for **SPI-0.1S** and **SPI-0.05G**, and 128 kPa for **SPI-2I** gel. The estimated G'_0 and G''_0 of **SPI-P** citric acid gels were statistically higher than that of the **SPI** citric acid gel.

The addition of 2% w/v inulin to the **SPI** citric acid gel increased G'_0 and G''_0 , by 71% and 55% and producing gels with higher rigidity and stiffness. The **SPI-0.1S** and **SPI-0.05G** citric acid gels had relatively similar G'_0 and G''_0 with 50% and 37% higher G'_0 and G''_0 , as compared to the **SPI** gel. Thus, 0.1% w/v starch and 0.05% w/v guar gum could be used to create **SPI** gels with comparable gel rigidity. The n' and n'' values are not identical, which implies that they are soft gel material [7]. The n' and n'' values of the **SPI-P** citric acid gels did not differ statistically ($p > 0.05$).



(a)



(b)

Figure 5.20: Power law model parameter estimates of SPI, SPI-2I, SPI-0.1S, and SPI-0.05G citric acid gels. (a) G'_0 and (b) G''_0 . The superscript letters a and b indicate statistical differences ($p < 0.05$). The error bars represent the standard deviation, $n=3$. Estimated data based on the mean of replicates was used.

5.4.3.2 Viscoelastic properties of SPI-Mixed polysaccharide gels

Estimation Method Based on Mean of Replicates

The viscoelastic properties of SPI citric acid gels containing different combinations and levels of inulin, starch and guar gum investigated with a Box-Behnken design of experiments (Table 5.11) are presented in Figures 5.21-5.25. Data used in this section is estimated based on the mean of replicates. The objective of these experiments was to investigate if the addition of a second polysaccharide could alter the interactions between the various constituents of the gel network, using the estimated data based on the mean of replicates. These interactions will be discussed according to polysaccharide type and the corresponding viscoelastic properties of the gel. While the experimental error between replicates was gel composition dependent, the G'_0 and G''_0 of the replicates for SPI-2I-0.1S-0.05G gels, representing the centre point composition, are not statistically different ($p > 0.05$).

The storage and loss modulus of SPI-P citric acid gels containing guar gum and guar gum combinations with starch and inulin, SPI-0.05G, SPI-4I-0.05G, SPI-0.2S-0.05 G, and SPI-4I-0.05G (Figure 5.21) indicate that G'_0 and G''_0 the storage and loss modulus of SPI-0.05G is substantially higher than the other SPI-P citric acid gels ($p < 0.05$). Hence, the interactions between guar gum and inulin or starch disrupt negatively the gel network.

The storage and loss modulus of SPI-P citric acid gels containing starch and starch combinations with guar gum and inulin, SPI-0.1S, SPI-0.1S-0.1G, SPI-4I-0.1S, and SPI-4I-0.1S-0.1G are presented in Figure 5.22. SPI-0.1S gel which contains only starch had a significant higher G'_0 and G''_0 storage and loss modulus than the other gels ($p < 0.05$). The differences in G' and G'' for SPI-0.1S and SPI-4I-0.1S do not follow the observations of the Young's modulus for these gels (section 5.4.2.3). This could be due to the high experimental error of the viscoelastic properties for SPI-4I-0.1S. The experimental error for estimating G'_0 was 696 kPa which is relatively high compared with its mean value, 1397 kPa.

The storage and loss modulus of SPI citric acid gels containing inulin and inulin combinations with starch and guar gum, SPI-2I, SPI-2I-0.2S, SPI-2I-0.1G, and SPI-2I-0.2S-0.1G are presented in Figure 5.23. The storage and loss modulus of SPI-2I is considerably larger than for the other gels ($p < 0.05$).

The parameter estimates, G'_0 , G''_0 , n' , and n'' , determined from the fit of the experimental data using the power law model (Equations 5.3 and 5.4) are summarized in Table 5.11. The R^2 values (above 0.97), indicate very good fit of the experimental data to the model. The estimated G'_0 and G''_0 of the SPI-P citric acid gels are similar for all combinations of polysaccharide except SPI-0.05G, SPI-0.1S and SPI-2I which are higher ($p < 0.05$), and

Table 5.11: Estimated G'_0 , G''_0 , n' for SPI and SPI-P gels and corresponding $\tan\delta$ at angular frequency of 1 rad.s^{-1} . The values are expressed as mean \pm standard deviation, $n=3$. Means within a column with different letters are significantly different ($p < 0.05$).

Gel code	Gel composition	I (%w/v)	S (%w/v)	G (%w/v)	G'_0 (kPa.s ⁿ)	n'	R^2	G''_0 (kPa.s ⁿ)	n''	R^2
C	SPI	0	0	0	950 ^a ±18	0.150 ^a ±0.002	0.994	218 ^a ±14	0.163 ^a ±0.002	0.992
1	SPI-0.05G	0	0	0.05	1411 ^b ±141	0.163 ^a ±0.001	0.993	300 ^b ±30	0.177 ^a ±0.002	0.983
2	SPI-4I-0.05G	4	0	0.05	928 ^a ±50	0.152 ^a ±0.003	0.994	210 ^a ±6	0.169 ^a ±0.002	0.987
3	SPI-0.2S-0.05G	0	0.2	0.05	769 ^a ±142	0.152 ^a ±0.001	0.993	178 ^a ±30	0.175 ^a ±0.011	0.990
4	SPI-4I-0.2S-0.05G	4	0.2	0.05	1121 ^a ±13	0.147 ^a ±0.004	0.991	241 ^a ±52	0.165 ^a ±0.009	0.986
5	SPI-0.1S	0	0.1	0	1427 ^b ±140	0.139 ^a ±0.007	0.989	297 ^b ±26	0.171 ^a ±0.031	0.988
6	SPI-0.1S-0.1G	0	0.1	0.1	1113 ^a ±154	0.153 ^a ±0.014	0.986	238 ^a ±33	0.207 ^a ±0.065	0.984
7	SPI-4I-0.1S-0.1G	4	0.1	0.1	967 ^a ±250	0.154 ^a ±0.016	0.983	213 ^a ±55	0.177 ^a ±0.022	0.981
8	SPI-4I-0.1S	4	0.1	0	1397 ^a ±348	0.170 ^a ±0.028	0.992	372 ^a ±173	0.202 ^a ±0.058	0.971
9	SPI-2I	2	0	0	1624 ^b ±86	0.139 ^a ±0.012	0.991	338 ^b ±64	0.158 ^a ±0.004	0.990
10	SPI-2I-0.2S	2	0.2	0	1171 ^a ±145	0.160 ^a ±0.005	0.992	249 ^a ±19	0.180 ^a ±0.008	0.993
11	SPI-2I-0.1G	2	0	0.1	999 ^a ±123	0.144 ^a ±0.016	0.989	222 ^b ±21	0.163 ^a ±0.006	0.988
12	SPI-2I-0.2S-0.1G	2	0.2	0.1	412 ^c ±90	0.146 ^a ±0.020	0.991	88 ^c ±20	0.188 ^a ±0.017	0.992
13	SPI-2I-0.1S-0.05G	2	0.1	0.05	838 ^a ±48	0.155 ^a ±0.008	0.992	185 ^a ±52	0.177 ^a ±0.014	0.990
14	SPI-2I-0.1S-0.05G	2	0.1	0.05	867 ^a ±134	0.154 ^a ±0.006	0.989	188 ^a ±92	0.177 ^a ±0.004	0.987
15	SPI-2I-0.1S-0.05G	2	0.1	0.05	721 ^a ±59	0.145 ^a ±0.007	0.992	160 ^a ±16	0.170 ^a ±0.012	0.985

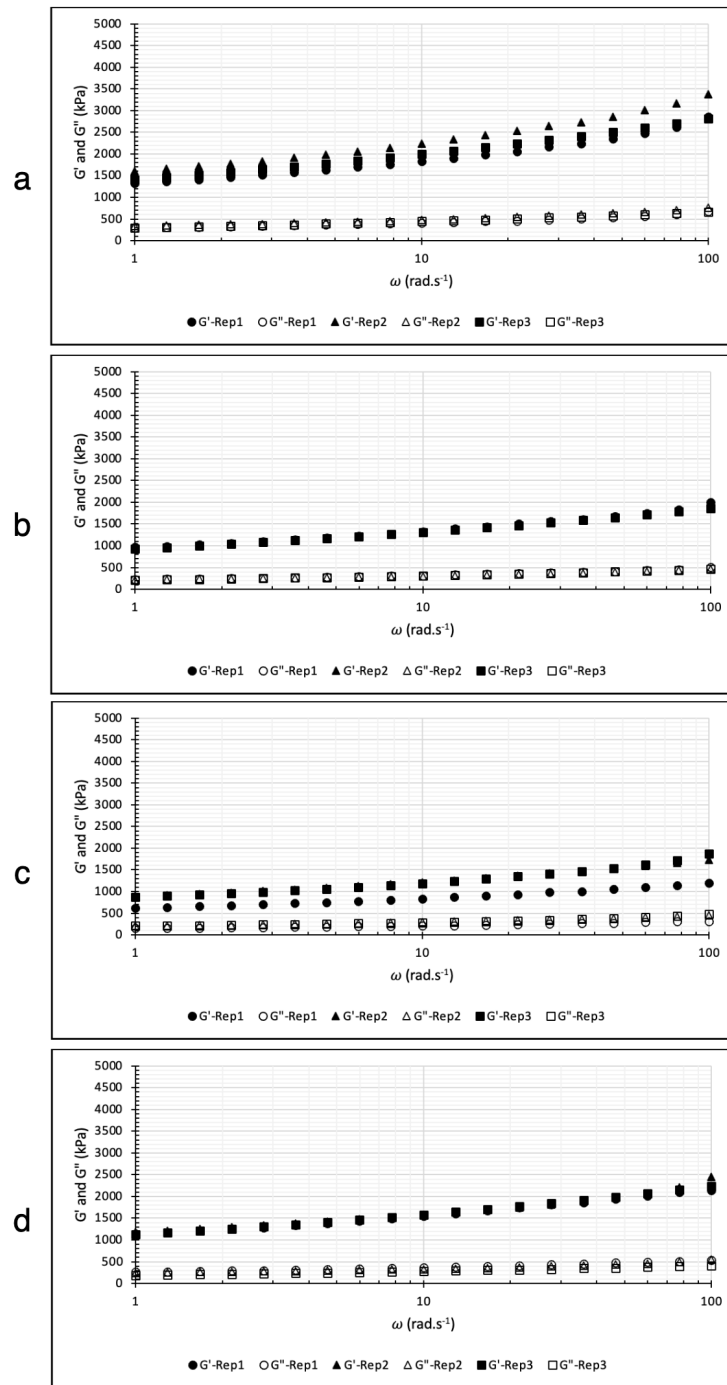


Figure 5.21: Storage modulus (G') and loss modulus (G'') of a) SPI-0.05G, b) SPI-4I-0.05G, c) SPI-0.2S-0.05G, and d) SPI-4I-0.2S-0.05G as a function of angular frequency.

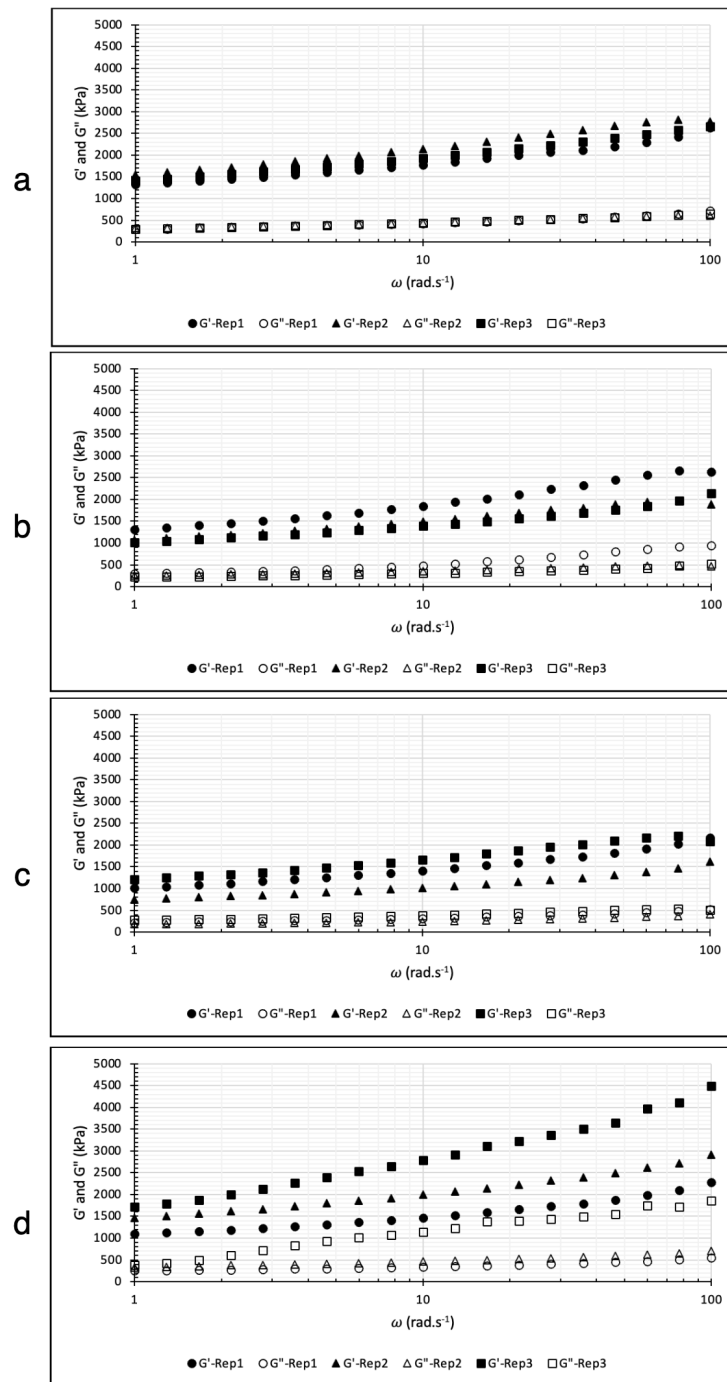


Figure 5.22: Storage modulus (G') and loss modulus (G'') of a) SPI-0.1S, b) SPI-0.1S-0.1G, c) SPI-4I-0.1S-0.1G, and d) SPI-4I-0.1S as a function of angular frequency.

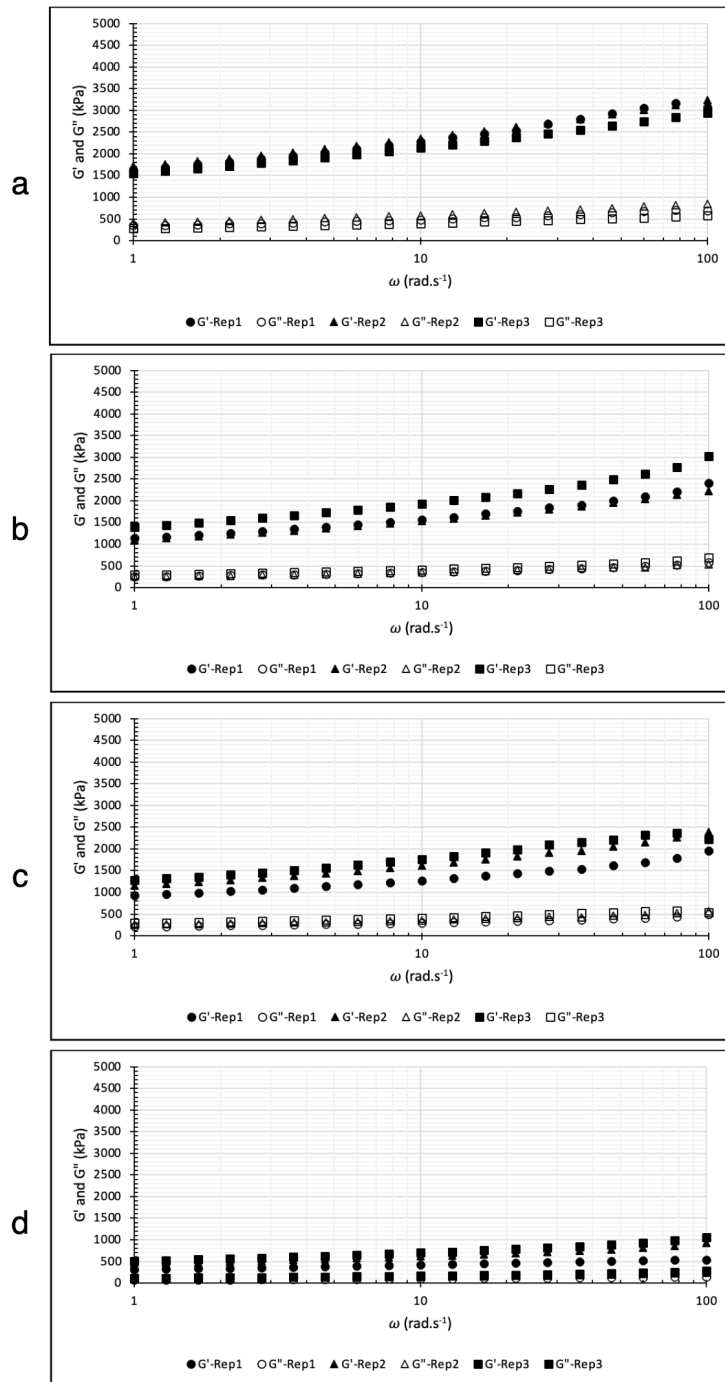


Figure 5.23: Storage modulus (G') and loss modulus (G'') of a) SPI-2I, b) SPI-2I-0.2S, c) SPI-2I-0.1G, d) SPI-2I-0.2S-0.1G as a function of angular frequency.

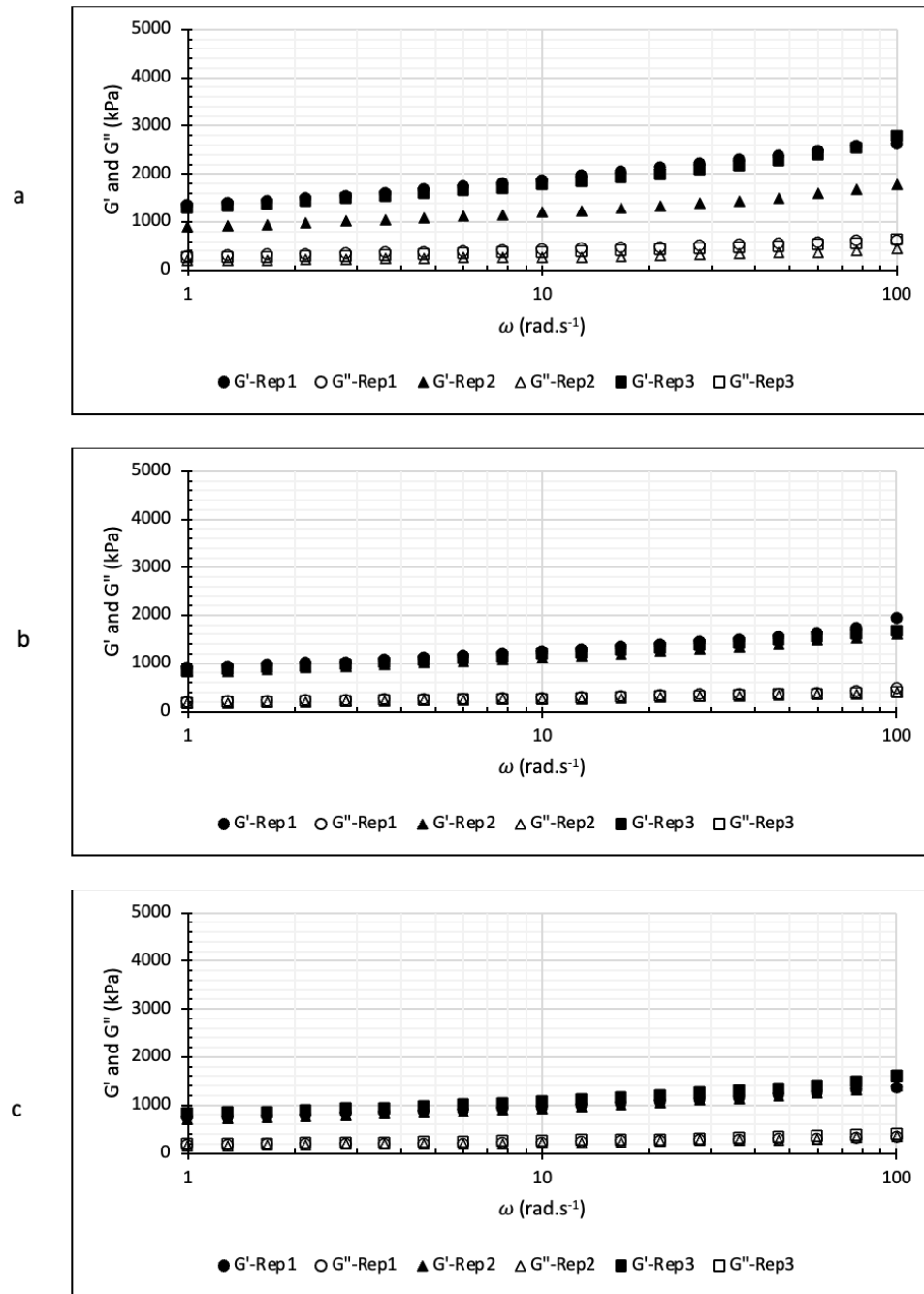


Figure 5.24: Storage modulus (G') and loss modulus (G'') of SPI-2I-0.1S-0.05G citric acid gel a) 1st replicate of centre point, sample 13, b) 2nd replicate of centre point, sample 14, and c) 3rd replicate of centre point, sample 15, as a function of angular frequency.

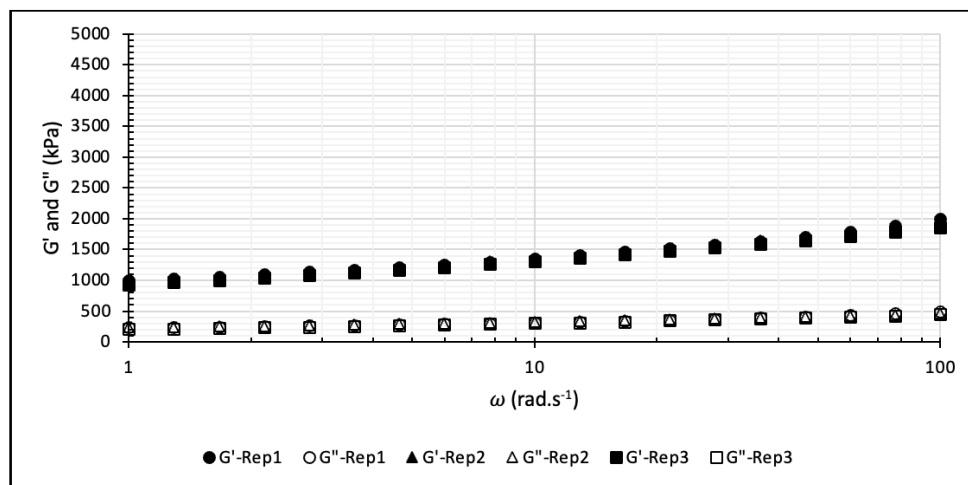


Figure 5.25: Storage modulus (G') and loss modulus (G'') of of control sample, SPI citric acid gel, as function of angular frequency.

SPI-2I-0.2S-0.1G which is lower ($p < 0.05$) when compared to SPI citric acid gels. SPI-2I-0.2S-0.1G had the lowest G'_0 and G''_0 estimates of all SPI-P citric acid gels, with a 56% and 60% decreased in G'_0 and G''_0 compared with SPI citric acid gel, respectively.

The estimated n' , and n'' of the SPI-P citric acid gels are similar for single and combination of polysaccharides ($p > 0.05$) when compared to the SPI citric acid gel. The magnitude of n' , and n'' , is small and is in a range of 0.14-0.18 and 0.16-0.21, respectively, which indicates negligible effect of the frequency on the storage and loss modulus.

Figure 5.26 represents the correlation between viscoelastic properties and viscoelastic-uniaxial compression properties. As shown, G'_0 and G''_0 have a positive correlation with each other with a correlation coefficient of 0.96 (estimated using Excel). Also, there could be a positive correlation between G'_0 and fracture stress or Young's modulus. As estimated by Excel, the correlation coefficient between G'_0 and fracture stress was 0.77, and correlation coefficient between G'_0 and Young's modulus was 0.81.

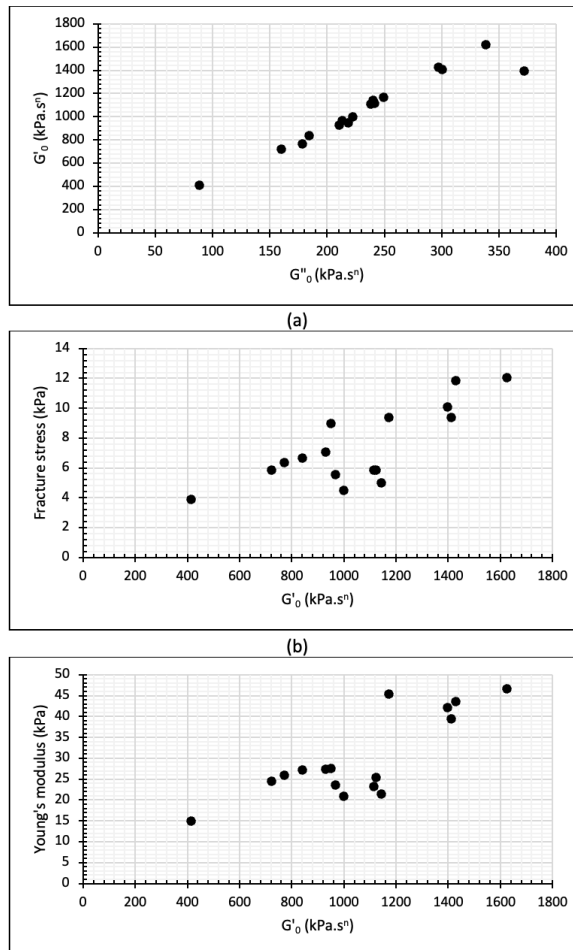


Figure 5.26: The correlation between viscoelastic properties and viscoelastic-uniaxial compression properties, a) G'_0 (kPa.sⁿ) vs G''_0 (kPa.sⁿ), b) Fracture stress (kPa) vs G'_0 (kPa.sⁿ), c) Young's modulus (kPa) vs G'_0 (kPa.sⁿ).

Estimation Method Based on Median Replicates

In this section, the viscoelastic properties are evaluated using the median replicate. The data related to this approach is summarized in Table 5.12. As shown, the storage and loss modulus and their dependency to the frequency (n' and n'') differ from what was reported based on the mean of replicates (Table 5.11). The median data could be lower or higher than the mean value.

All gels had G'_0 values in the range of 433-1637 $kPa.s^n$, which was wider range than the previous approach (according to the estimation based on the mean, G'_0 was ranged from 412 to 1624 $kPa.s^n$). Similar to the previous method, SPI-0.05G, SPI-0.1S, and SPI-2I, which had a single type of polysaccharide, represented 31-70% higher G'_0 and stiffness than SPI citric acid gel. Samples SPI-4I-0.2S-0.05G, SPI-0.1S-0.1G, SPI-4I-0.1S-0.1G, SPI-4I-0.1S, and SPI-2I-0.2S showed 1-48% higher G'_0 than SPI citric acid gel in this method, while they were not statistically different from SPI citric acid gel based on the estimation method via mean of replicates. Other gels showed 1-55% lower G'_0 than SPI citric acid gel.

G''_0 of SPI-P citric acid gels estimated based on the median replicates were between 93-381 $kPa.s^n$, while they were in a range of 88-372 $kPa.s^n$ based on the estimation method via the mean of replicates. Similar to G'_0 results, a single type of polysaccharide could increase the loss modulus by 26-56% which is consistent with the results obtained from the estimation based on the mean method. Also, samples SPI-4I-0.2S-0.05G, SPI-0.1S-0.1G, SPI-4I-0.1S-0.1G, SPI-4I-0.1S, and SPI-2I-0.2S represented 3-72% higher G''_0 than SPI citric acid gel in the estimation method based on median replicate, while they had statistically similar G''_0 to SPI citric acid gel using the mean data. Other gels showed 1-58% lower G''_0 than SPI citric acid gel.

n' and n'' values were in a range of 0.134-0.165 and 0.153-0.195, respectively, which are approximately similar to n' and n'' values obtained from the estimation based on the mean of replicates.

Table 5.12: Estimated G'_0 , G''_0 , n' , and n'' for SPI and SPI-P gels at angular frequency of 1 rad.s^{-1} . Estimated data based on median replicate was used.

Gel code	Gel composition	I (%w/v)	S (%w/v)	G (%w/v)	G'_0 (kPa.s ⁿ)	n'	R^2	G''_0 (kPa.s ⁿ)	n''	R^2
C	SPI	0	0	0	965	0.151	0.996	221	0.165	0.991
1	SPI-0.05G	0	0	0.05	1269	0.164	0.996	278	0.175	0.987
2	SPI-4I-0.05G	4	0	0.05	935	0.155	0.995	217	0.172	0.987
3	SPI-0.2S-0.05G	0	0.2	0.05	830	0.164	0.991	189	0.188	0.993
4	SPI-4I-0.2S-0.05G	4	0.2	0.05	1127	0.151	0.991	228	0.171	0.989
5	SPI-0.1S	0	0.1	0	1323	0.134	0.987	288	0.186	0.992
6	SPI-0.1S-0.1G	0	0.1	0.1	1083	0.137	0.988	249	0.153	0.985
7	SPI-4I-0.1S-0.1G	4	0.1	0.1	977	0.165	0.982	204	0.193	0.981
8	SPI-4I-0.1S	4	0.1	0	1427	0.148	0.994	381	0.163	0.977
9	SPI-2I	2	0	0	1637	0.148	0.994	346	0.161	0.990
10	SPI-2I-0.2S	2	0.2	0	1094	0.161	0.989	236	0.184	0.992
11	SPI-2I-0.1G	2	0	0.1	963	0.157	0.987	219	0.164	0.990
12	SPI-2I-0.2S-0.1G	2	0.2	0.1	433	0.156	0.990	93	0.195	0.993
13	SPI-2I-0.1S-0.05G	2	0.1	0.05	870	0.164	0.992	190	0.193	0.992
14	SPI-2I-0.1S-0.05G	2	0.1	0.05	804	0.147	0.986	176	0.170	0.988
15	SPI-2I-0.1S-0.05G	2	0.1	0.05	770	0.138	0.994	158	0.160	0.986

5.4.3.3 Quadratic model fitting

Estimation Method Based on Mean of Replicates

The ANOVA table of the fitting of the quadratic model for G'_0 and G''_0 and inulin, starch, and guar gum concentration as independent variables with the Box-Behnken design is presented in Table 5.13. According to the ANOVA, the contribution of the quadratic model was significant for both G'_0 and G''_0 . The significance of each factor was determined using the F-test and p-value. The regression coefficients for the inulin concentration (quadratic form, X_1^2), starch concentration (linear form, X_2), guar gum concentration (linear and quadratic form, X_3 , X_3^2), and inulin concentration starch concentration interaction (X_1X_2) are significant ($p < 0.05$). All other effects (X_1 , X_2^2 , X_1X_3 , and X_2X_3) are not significant ($p > 0.05$). The lack of fit error is not significant ($p > 0.05$). The R^2 values for G'_0 and G''_0 are 0.92 and 0.95. As a result, the models are valid and represent accurately G'_0 and G''_0 for the experimental conditions investigated in this study inulin: 0-4% w/v, starch: 0-0.2% w/v, guar gum: 0-0.1% w/v. The dependency of G'_0 (Y_4) and G''_0 (Y_5) according to X_1 (inulin concentration), X_2 (starch concentration), and X_3 (guar gum concentration) is given by equation 5.12 and equation 5.13.

$$Y_4 = 807.67 - 183.5X_2 - 266X_3 + 214X_1X_2 + 214X_1^2 + 203.16X_3^2, \quad (5.12)$$

$$Y_5 = 177.66 - 39.37X_2 - 61.87X_3 + 38X_1X_2 + 55.04X_1^2 + 11.25X_3^2. \quad (5.13)$$

Equation 5.12 and 5.13, indicate that the guar gum concentration (X_3) and the starch concentration (X_2) have a negative effect on G'_0 and G''_0 , whereas the inulin concentration (X_1^2) and the inulin concentration and starch concentration combination (X_1X_2) have a positive impact. As a result, adding inulin or inulin and starch could improve the G'_0 and G''_0 properties of the SPI citric acid gel, possibly due to hydrogen bonding and hydrophobic interaction with protein, water, and starch. Guar gum and starch, on the other hand, lower G'_0 and G''_0 . The addition of guar gum to SPI-starch gels has been reported to prevent the leaching of starch components from starch granules [114, 115], which could explain the negative effect of starch on G'_0 and G''_0 observed in the current study. The combination of guar gum and starch did not create gels with desired G'_0 and G''_0 properties (lower than SPI-guar gum and SPI-starch citric acid gels). While starch or guar gum alone improved the viscoelastic properties of the SPI citric acid gel (section 5.4.3.1).

Interpretation of the response surface models

The three-dimensional (3D) contour plots of the storage modulus (G'_0) and loss modulus (G''_0) estimates as a function of starch and inulin concentration for different guar gum

Table 5.13: ANOVA for quadratic model for G'_0 and G''_0 as response variables and inulin concentration (X1), starch concentration (X2), and guar gum concentration (X3) as independent variables. Estimated data based on the mean of replicates was used.

Source	DF	G'_0				G''_0			
		SS	MS	F value	Prob > F	SS	MS	F value	Prob > F
X_1 (I)	1	10225	10225	1.71	0.3209	60.50	60.50	0.25	0.6631
X_2 (S)	1	269378	269378	45.09	0.0214	12403.13	12403.13	52.48	0.0185
X_3 (G)	1	566048	566048	94.74	0.0103	30628.13	30628.13	129.59	0.0076
X_1^2	1	169356	169356	28.34	0.0335	11186.16	11186.16	47.33	0.0204
X_2^2	1	5810	5810	0.97	0.4280	1.85	1.85	0.01	0.9375
X_3^2	1	152406	152406	25.51	0.0370	8257.85	8258.85	34.94	0.0274
$X_1.X_2$	1	183184	183184	30.66	0.0311	5776.00	5786.00	24.44	0.0385
$X_1.X_3$	1	3364	3364	0.56	0.5312	2500.00	2500.00	10.57	0.829
$X_2.X_3$	1	4489	4489	0.75	0.4774	506.25	506.25	2.14	0.2808
Residual	5	110511	22102.2	-	-	3813.42	762.68	-	-
Lack of fit	3	289600	48266.6	5.49	0.1577	3340.75	1113.58	4.71	0.1800
Pure error	2	11949	5974.3	-	-	472.67	236.33	-	-
Cor total	14	1474771	-	-	-	73999.73	-	-	-
R ²	-	0.92	-	-	-	0.95	-	-	-
Adj R ²	-	0.78	-	-	-	0.85	-	-	-

concentrations are depicted in Figures 5.27 and 5.28. The G'_0 and G''_0 estimates were highest when no starch and no inulin were present for all levels of guar gum (Table 5.14 and 5.15). The G'_0 and G''_0 estimates were lowest at the highest starch concentration and for moderate inulin concentration at all levels of guar gum. The magnitude of G'_0 and G''_0 estimates was affected by the guar gum concentration. In the absence of guar gum ($G = -1$), G'_0 ranged from 1093 to 1888 kPa.sⁿ (Figure 5.27a) and G''_0 estimates ranged from 225 to 282 kPa.sⁿ (Figure 5.28a). At higher guar gum concentration (level 0, 0.05% w/v and level 1, 0.1% w/v), G'_0 estimates decreased to 510-1419 kPa.sⁿ (Figure 5.27b-c). The G''_0 estimates represented maximum value at S = 1 and I = 1 in the absence of guar gum (Figure 5.28a). In the presence of guar gum, the G''_0 estimates ranged from 185 to 310 kPa.sⁿ, and then declined 65 to 239 kPa.sⁿ in the presence of 0.05-0.1% guar gum (Figure 5.28 b-c).

The 3D and contour plots for G'_0 and G''_0 as a function of guar gum and starch concen-

tration for different inulin concentration are shown in Figures 5.30 and 5.29, respectively. The G'_0 and G''_0 estimates differed according to inulin concentration. The highest estimates were predicted when no starch and no guar gum are present when there is no inulin (level -1) and at low inulin concentration (level 0) (Table 5.14 and 5.15). At higher inulin concentration (level +1), G'_0 and G''_0 estimates are the highest in the absence of guar gum but with high starch concentration. The G'_0 and G''_0 were lowest at the highest guar gum concentration and starch concentration when there is no inulin (level -1) and at low inulin concentration (level 0). starch concentration and with moderate inulin concentration for all levels of guar gum. At higher inulin concentration (level +1), G'_0 and G''_0 estimates are the lowest at the highest guar gum concentration and with moderate starch concentration (level 0). The magnitude of G'_0 and G''_0 estimates were affected by the inulin concentration. The G'_0 estimates ranged from 537 to 1888 kPa.sⁿ in level -1 of inulin and declined to 573 to 1460 kPa.sⁿ at level 0 (Figure 5.30b), and was higher at inulin level +1, 935-1521 kPa.sⁿ (Figure 5.30c). In the absence of inulin (level -1), the G''_0 varied from 121 to 361 kPa.sⁿ (Figure 5.29a), decreased to 97 to 267 kPa.sⁿ at level 0 (Figure 5.29b), and was higher, 158-282 kPa.sⁿ at the higher inulin level of +1 (Fig 5.29c).

The 3D and contour plots for G'_0 and G''_0 as a function of inulin and guar gum concentration for different starch concentration are shown in Figures 5.31 and 5.32. The G'_0 and G''_0 estimates differed according to starch concentration where highest estimates were predicted when no inulin and no guar gum are present when there is no starch (level -1) (Table 5.14 and 5.15). At higher starch concentration (level 0 and level +1), G'_0 and G''_0 estimates are the highest in the absence of guar gum but with high inulin concentration. Higher G'_0 and G''_0 values appear to be possible above level +1 inulin and +1 starch with no guar gum present. The lowest G'_0 and G''_0 estimates are somewhat affected by the starch concentration and shift to lower inulin concentration and higher guar gum concentration with increasing starch concentration. The magnitude of G'_0 and G''_0 estimates was affected by the starch concentration. At level -1 of starch (Figure 5.31a), the G'_0 varied from 860 to 1888 kPa.sⁿ, and it decreased to 723 to 1491 kPa.sⁿ at level 0 starch, and 484-1521 kPa.sⁿ at level +1 of starch (Figure 5.31b-c). In the absence of starch, the G''_0 ranged from 163 to 361 kPa.sⁿ and reduced to 129 to 283 kPa.sⁿ and 83-282 kPa.sⁿ with increasing starch concentration.

Table 5.14: Maximum G'_0 estimates derived from equation 5.12.

Estimated maximum G'_0 (kPa.s ⁿ)	I Level	S Level	G Level	Figure number
1356	-1	-1	+1	5.27c
1419	-1	-1	0	5.27b
1460	0	-1	-1	5.30b
1491	+1	0	-1	5.31b
1521	+1	+1	-1	5.30c
1521	+1	+1	-1	5.31c
1888	-1	-1	-1	5.27a
1888	-1	-1	-1	5.30a
1888	-1	-1	-1	5.31a

Table 5.15: Maximum G''_0 estimates derived from equation 5.13.

Estimated maximum G''_0 (kPa.s ⁿ)	I Level	S Level	G Level	Figure number
239	-1	-1	+1	5.28c
268	0	-1	-1	5.29b
282	+1	+1	-1	5.28a
282	+1	+1	-1	5.29c
282	+1	+1	-1	5.32c
283	+1	0	-1	5.32b
310	-1	-1	0	5.28b
361	-1	-1	-1	5.29a
361	-1	-1	-1	5.32a

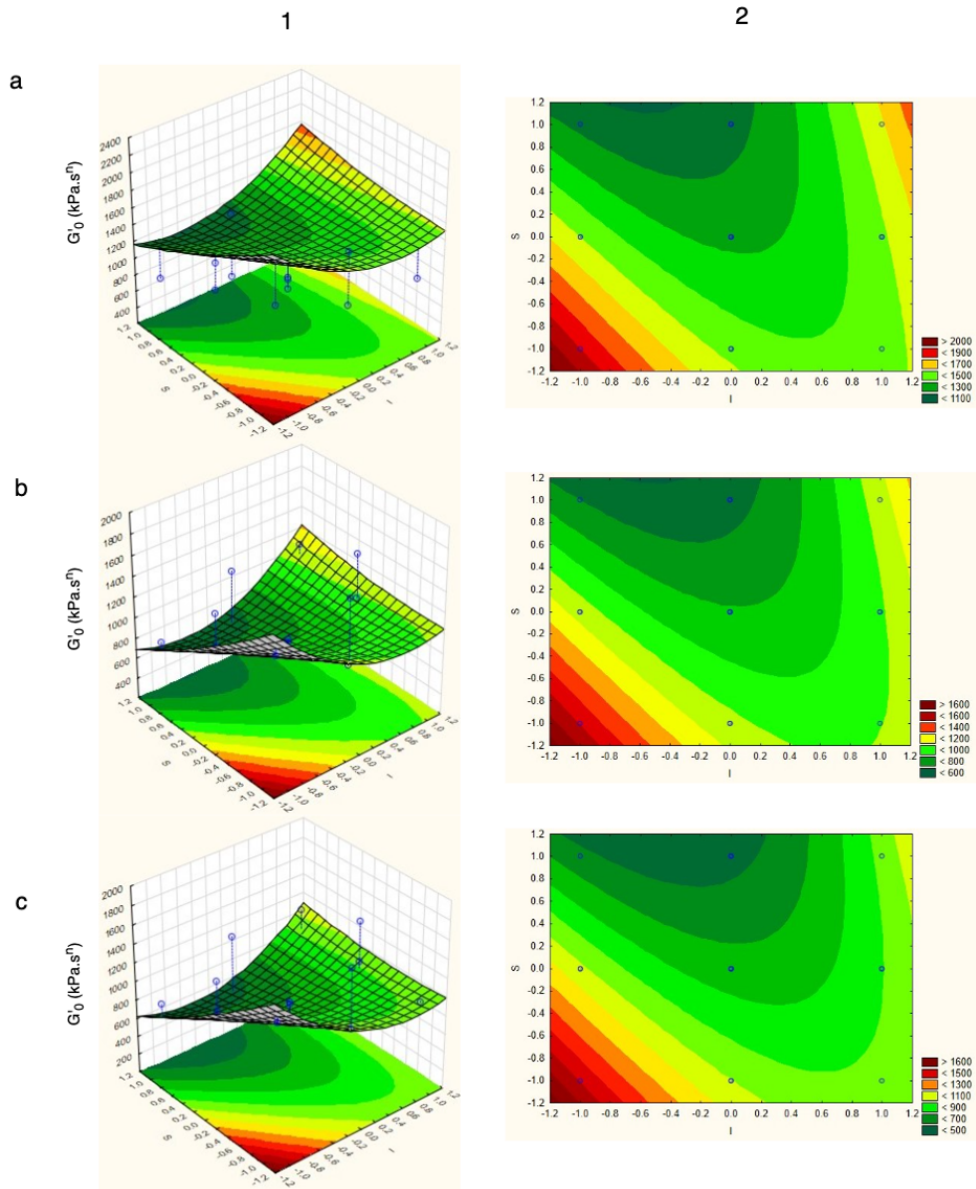


Figure 5.27: Three dimensional (1) and contour (2) plots G'_0 as a function of inulin (x-axis) and starch (y-axis) concentration for different guar gum concentration (level -1 (a), 0 (b), and +1 (c)).

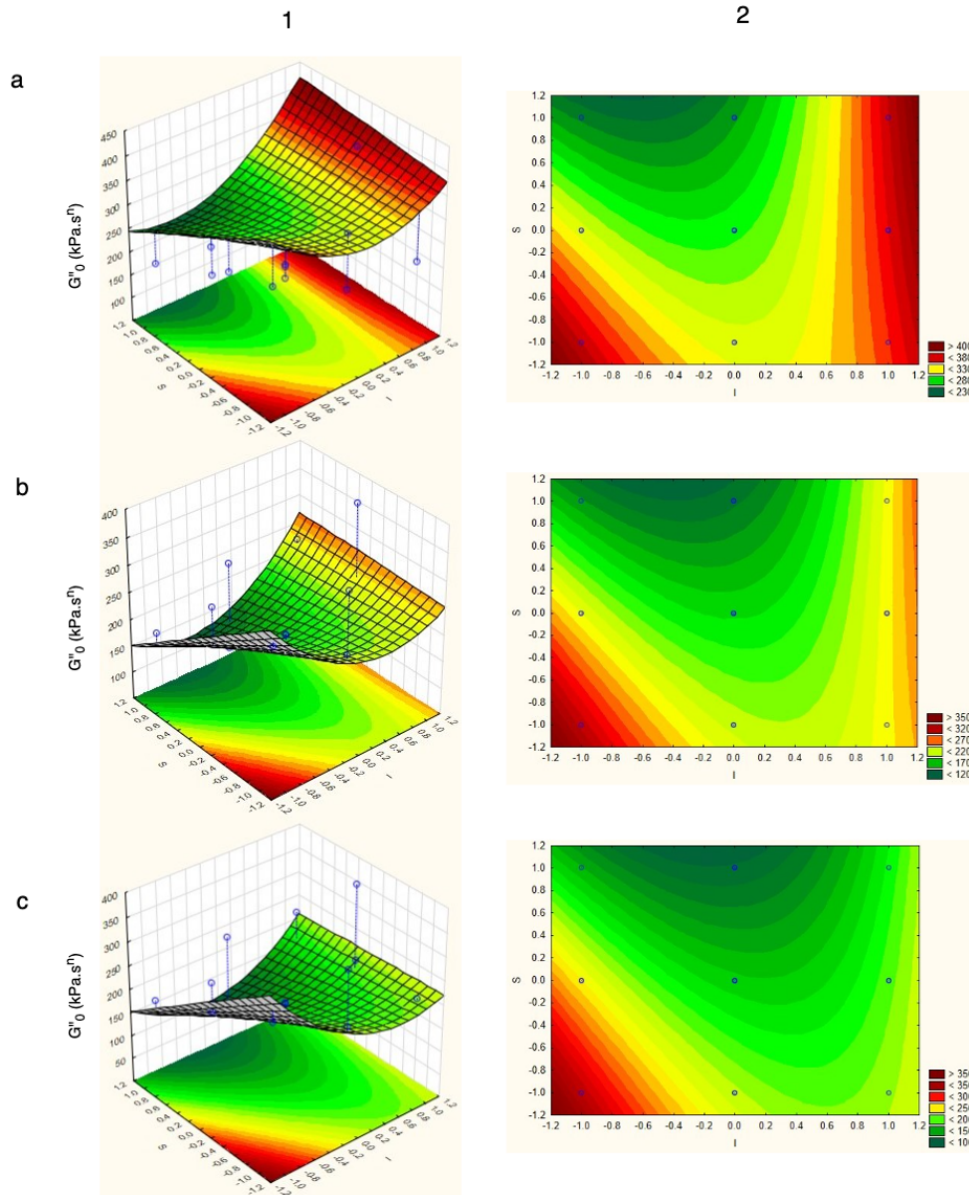


Figure 5.28: Three dimensional (1) and contour (2) plots G''_0 as a function of inulin (x-axis) and starch (y-axis) concentration for different guar gum concentration (level -1 (a), 0 (b), and +1 (c)).

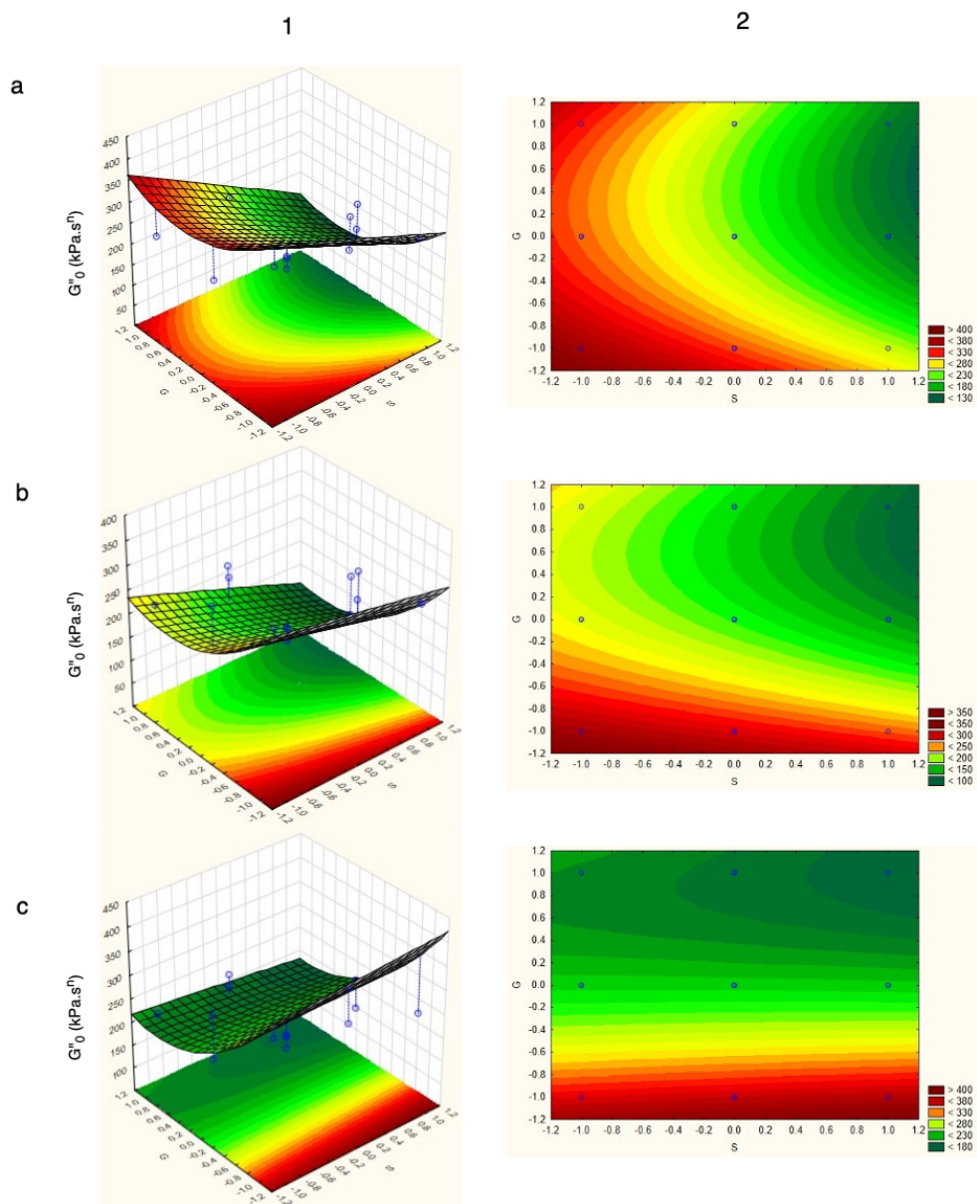


Figure 5.29: Three dimensional (1) and contour (2) plots of G''_0 as a function of starch (x-axis) and guar gum (y-axis) concentration at different inulin concentration (level -1 (a), 0 (b), and +1 (c)).

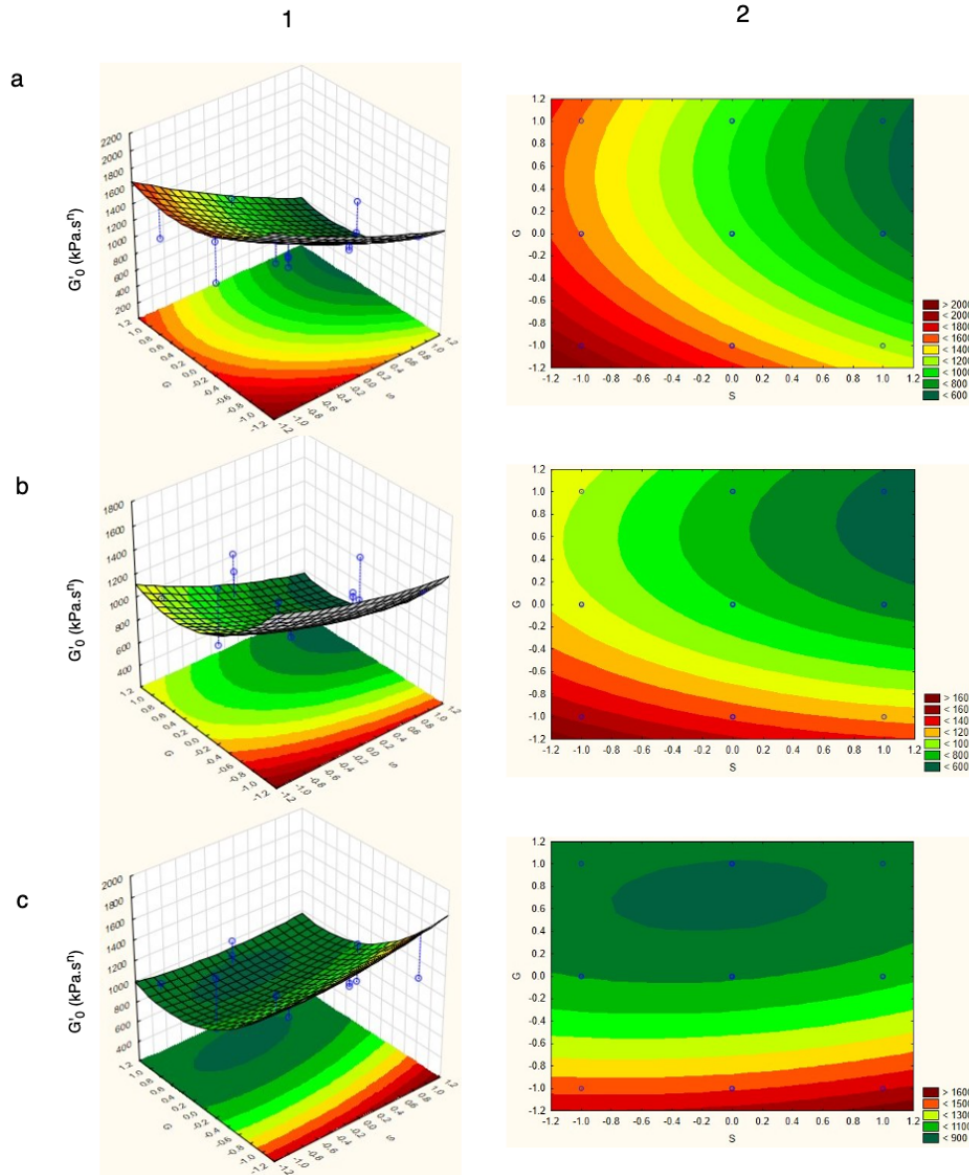


Figure 5.30: Three dimensional (1) and contour (2) plots G'_0 as a function of starch (x-axis) and guar gum (y-axis) concentration for different inulin concentration (level -1 (a), 0 (b), and +1 (c)).

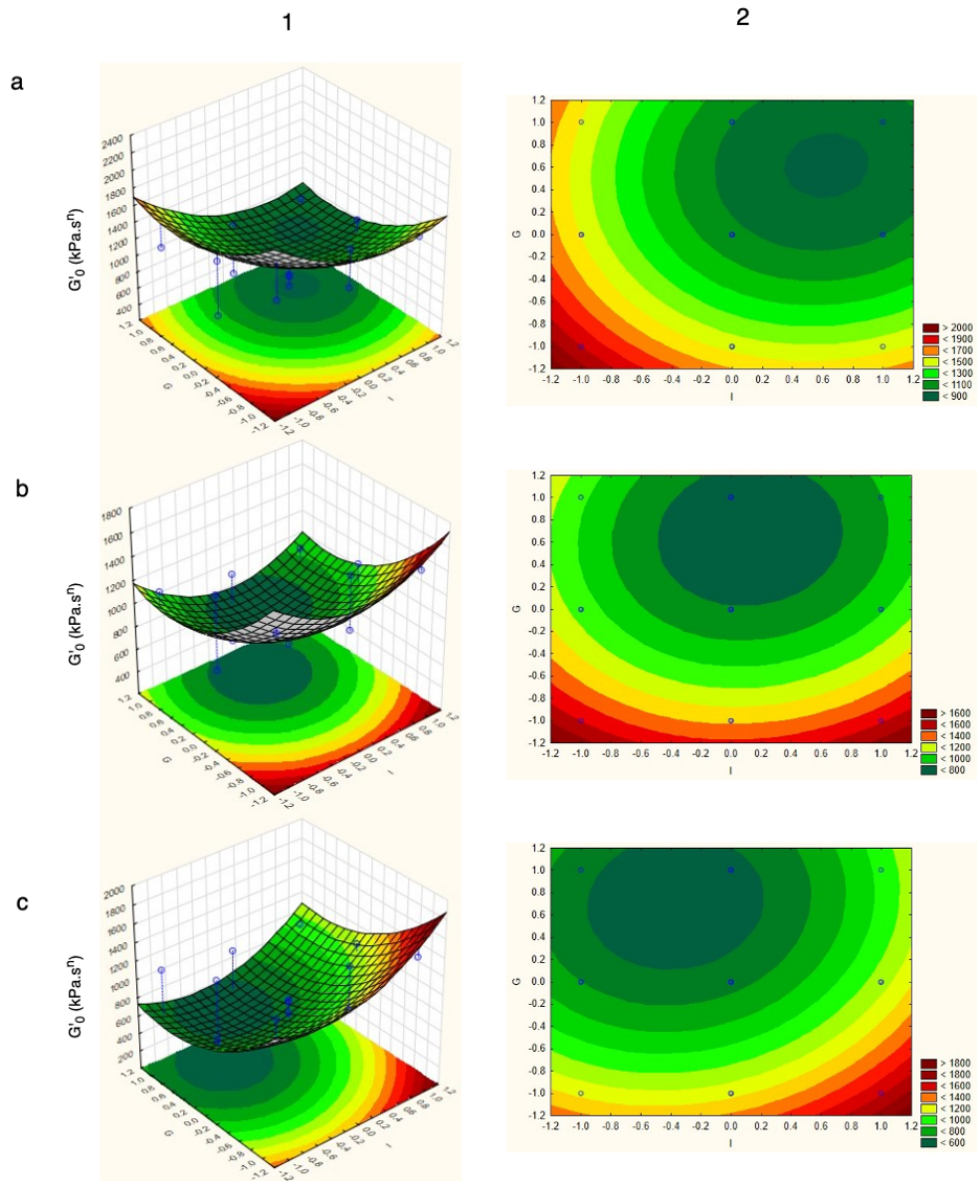


Figure 5.31: Three dimensional (1) and contour (2) plots G'_0 as a function of inulin (x-axis) and guar gum (y-axis) concentration for different starch concentration (level -1 (a), 0 (b), and +1 (c)).

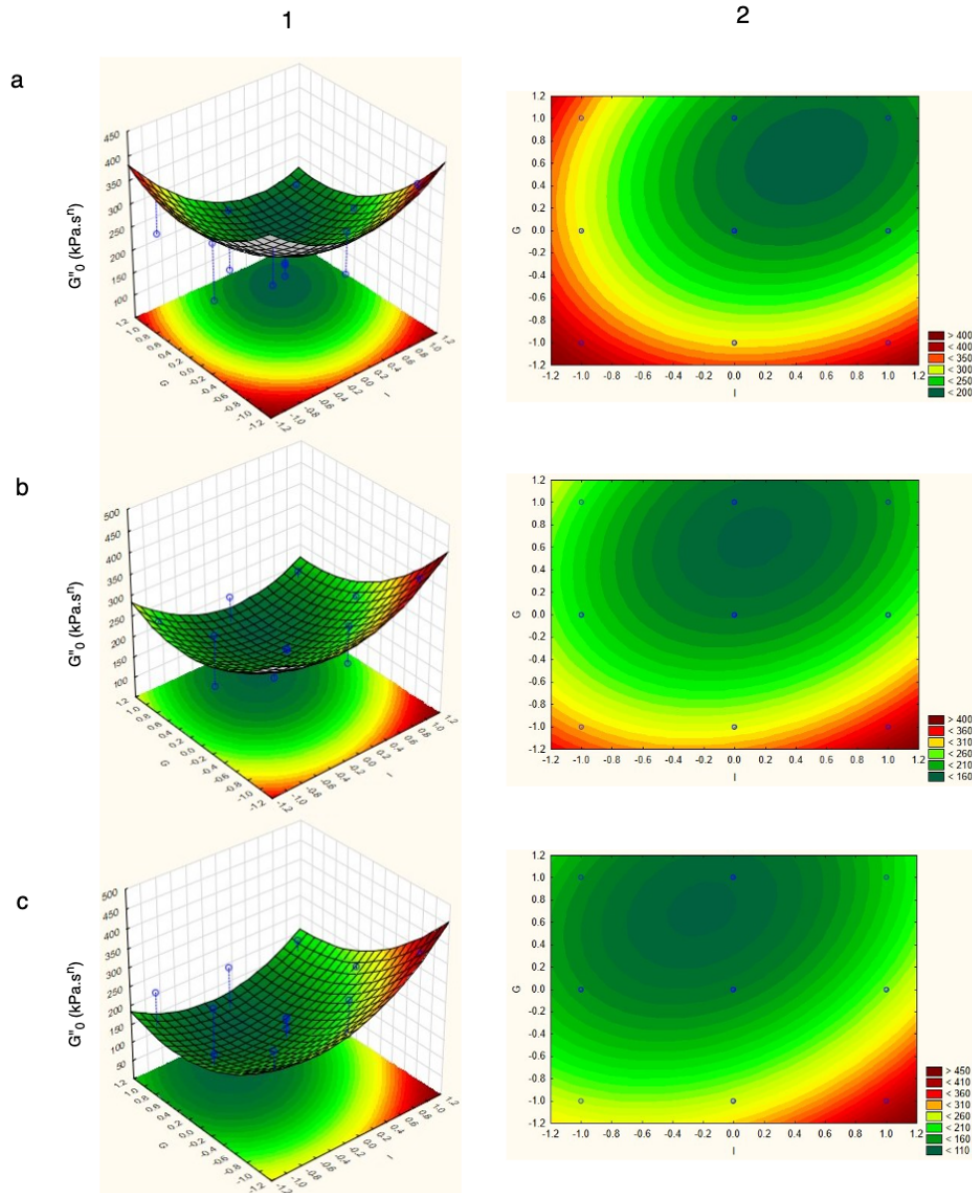


Figure 5.32: Three dimensional (1) and contour (2) plots G''_0 as a function of inulin (x-axis) and guar gum (y-axis) concentration for different starch concentration (level -1 (a), 0 (b), and +1 (c)).

Estimation Method Based on Median Replicates

In this section, the quadratic model for describing storage and loss modulus was determined based on the estimated data via the median replicate. Table 5.16 is the ANOVA table related to this approach.

Similar to the uniaxial compression quadratic model, the associated quadratic model for the median data represented a higher lack of fits and pure error compared with the estimated data via mean of replicates, and had lower R^2 and R_{adj}^2 values. Therefore, the estimated quadratic models for the storage and loss modulus are preciser and more valid for the mean data than the median. Both methods indicate that inulin in a quadratic form (X_1^2), starch in a linear form (X_2), guar gum in a linear and quadratic form (X_3 and X_3^2), and starch-inulin interaction ($X_1.X_2$) are significant variable, and other variables (X_1 , X_2^2 , $X_1.X_3$, $X_2.X_3$) have no statistical effect on the quadratic model of G'_0 . Similar results for G''_0 was obtained, except that the starch-inulin interactions ($X_1.X_2$) was not significant in the G''_0 quadratic model.

The quadratic models for storage and loss modulus are represented by Equations 5.14 and 5.15, respectively (Y'_4 and Y'_5 are storage and loss modulus based on the median data, respectively). The coefficients are approximately 1-26% different from coefficients in Equation 5.12 and 5.13.

$$Y_4 = 868 - 165.2X_2 - 252.8X_3 + 157.7X_1X_2 + 171.2X_1^2 + 163.2X_3^2, \quad (5.14)$$

$$Y_5 = 174.6 - 39.4X_2 - 52.7X_3 + 47X_1^2 + 43.3X_3^2. \quad (5.15)$$

Table 5.16: ANOVA for quadratic model for G'_0 and G''_0 as response variables and inulin concentration (X1), starch concentration (X2), and guar gum concentration (X3) as independent variables. Estimated data based on the median replicates was used

Source	DF	G'_0				G''_0			
		SS	MS	F value	Prob > F	SS	MS	F value	Prob > F
X_1 (I)	1	190	190	0.06	0.8267	171	171	0.66	0.5004
X_2 (S)	1	218460	218460	71.11	0.0137	12403.13	12403.13	48.19	0.0201
X_3 (G)	1	511566	511566	166.52	0.0059	22260	22260	86.50	0.0113
X_1^2	1	108283	108283	35.24	0.0272	8170	8170	31.75	0.0300
X_2^2	1	4	4	0.001	0.9754	134	134	0.52	0.5444
X_3^2	1	98402	98402	32.03	0.0298	6920	6920	25.89	0.0352
$X_1.X_2$	1	99540	99540	32.40	0.0295	2550	2550	9.91	0.0878
$X_1.X_3$	1	11025	11025	3.58	0.1986	1444	1444	5.61	0.1413
$X_2.X_3$	1	30	30	0.01	0.9300	81	81	0.31	0.6312
Residual	5	143676	28735.2	-	-	5388	1077	-	-
Lack of fit	3	137532	45844	14.92	0.0634	4874	1624	6.31	0.1397
Pure error	2	6144	30072	-	-	514	257	-	-
Cor total	14	1178385	-	-	-	58316	-	-	-
R^2	-	0.87	-	-	-	0.90	-	-	-
Adj R^2	-	0.65	-	-	-	0.74	-	-	-

5.5 Effect of Polysaccharide Addition on SPI Citric Acid Gels

The effect of three different polysaccharides, starch, inulin and guar gum, on the uniaxial mechanical and viscoelastic properties of citric acid-induced SPI gels was investigated with a Box-Behnken (B-B) design of experiments to minimize the number of gels while capturing the effect of the three polysaccharides.

The uniaxial properties analysis of the citric acid induced SPI and SPI-P gels suggests that one type of polysaccharide (2% w/v inulin, 0.1% w/v starch, and 0.05% w/v guar gum) could improve the fracture stress and Young's modulus of an SPI gel ($p < 0.05$), while not having a significant effect on the fracture strain point ($p > 0.05$). Therefore, utilizing 2% w/v inulin, 0.1% w/v starch, and 0.05% w/v guar gum combined with 8% w/v SPI could produce a stronger and harder gel than SPI. Gels containing multiple types of polysaccharides demonstrated distinct uniaxial properties. The findings suggest that inulin and starch may have a synergistic effect and that their combination, SPI-4I-0.1S and SPI-2I-0.2S, could produce stiffer and harder gels than SPI gel. The combination of guar gum with either starch or inulin, did not produce firmer, stronger gels than SPI. The quadratic models indicated that guar gum (X_3) in the linear form had the most significant effect on the fracture stress and Young's modulus of a citric acid-induced SPI gel ($p < 0.05$), while all other factors ($X_1, X_1^2, X_2, X_2^2, X_3^2, X_1X_2, X_1X_3, X_2X_3$; X_1 : inulin, X_2 : starch, X_3 : guar gum) were not significant ($p > 0.05$).

Similar observations were obtained for the storage and loss modulus where the addition of one type of polysaccharide significantly increased the storage and loss modulus of the gel while not having a considerable impact on the $\tan\delta$. The storage and loss modulus data were fitted to a power law equation, which showed that G' and G'' of all gels had a dependency on the frequency similar to SPI-citric acid gel. Unlike the uniaxial compression properties, the viscoelastic properties of SPI-4I-0.1S and SPI-2I-0.2S citric acid gels did not differ statistically from those of the citric acid SPI gel ($p > 0.05$). The quadratic models indicate that G'_0 and G''_0 is affected by the concentration of all three polysaccharides (X_1^2, X_2, X_3, X_3^2), and the interaction of starch and inulin ($X_1.X_2$), whereas other factors ($X_1, X_2^2, X_1.X_3, X_2.X_3$) did not have a significant effect.

Stiffer and harder gels could be produced with 0.1-0.2% w/v starch, 2-4% w/v inulin, and their combination compared to citric acid-induced SPI without starch and/or inulin. While SPI-0.05% w/v guar gum could produce stronger gels than SPI, combining guar gum with starch and/or inulin is not recommended.

Chapter 6

Conclusion and Recommendations

6.1 Conclusion

Soy protein gels are gaining popularity as a potential substitute for dairy-based cheeses. A soy protein gel can be made by heating the protein solution and adding a coagulant. One of the coagulants used is citric acid, which can give the soy protein gel a sour taste. Soy protein gel is not strong enough on its own, and its texture characteristics, such as gel strength and hardness, must be modified. For this purpose, other additives such as polysaccharide can be added to the soy protein gel. As reported in the literature, three types of polysaccharides, inulin, guar gum, and starch, were found to improve the soy protein gel's hardness, strength, and viscoelasticity [17, 16, 18].

The purpose of this research was to evaluate and improve the textural qualities of citric acid-induced soy protein gels, with a focus on studying the type (inulin, guar gum, and starch) and concentration of polysaccharide to make harder soy protein gels with improved uniaxial and viscoelastic properties. The uniaxial compression properties, i.e., stress fracture point and Young's modulus, could give insight into the gel strength, firmness, and hardness. On the other hand, viscoelastic properties can provide information about the gel stiffness and the relationship between the viscous and elastic portion of SPI gel. Various studies have been conducted to analyse the textural properties of soy protein gels containing inulin, guar gum, and starch. However, the comparison of the effects of each hydrocolloid on the uniaxial and viscoelastic properties, the evaluation of the feasibility of making an SPI gel containing multiple types of hydrocolloids, and the quantitation of the dependency of the uniaxial and viscoelastic properties of a gel to the type and concentration of hydrocolloids were not investigated.

The goal of this research was accomplished in three steps: 1) gelation kinetics analysis to select proper soy protein type and coagulation temperature, 2) visual evaluation of citric acid-induced SPI gels to develop an appropriate methodology for gel preparation, and 3) uniaxial compression and viscoelastic characterization of SPI-polysaccharide gels.

In the first step, the kinetics of soy protein gelation were quantified with a power law equation and published storage modulus data for three soy protein sources, 11S, SPI, and dried soymilk, under various conditions, the most important of which was heating temperature. According to the findings, increasing the coagulation temperature can greatly improve the rate of gelation, allowing gelation to start earlier and complete faster. So, the highest temperature investigated in the publications, 95° C might be chosen as a heating temperature. When the gelation kinetics of three soy protein sources were compared, SPI gels showed a gelation rate between 11S and dried soymilk, while representing higher gel stiffness and G'_{sat} than both. As a consequence of this analysis, SPI was chosen as a source of soy protein and 95° C as a coagulation temperature for the experimental work and subsequent steps. In the second step, the citric acid-induced 8% w/v SPI gel was generated and the effect of different heating durations (0-30 minutes), citric acid concentrations (0.2-0.4% w/v), coagulation durations (30-60 minutes), citric acid states (liquid or solid), and citric acid addition methods (instantly or continually) on the strength of SPI gel was assessed visually. Citric acid can be added as a coagulant and create a soy protein gel with comparable viscoelasticity and hardness as a conventional tofu product [9]. According to the findings, the highest gel strength was associated to the prepared SPI gel with the following steps:

1. Pre-heating 8% w/v SPI solution in a water bath for 30 min at 95° C.
2. Lowering the temperature to 80° C, and adding 0.3% w/v citric acid as a powder to the pre-heated SPI solution while constantly stirring for 60 minutes.
3. Cooling the prepared aggregates to room temperature, separating aggregates using cheese cloth, and pressing aggregates with 10 $g.cm^{-2}$ for 10 minutes.

In the last step, 0.3% w/v citric acid-induced 8% w/v SPI-polysaccharide gels were made with 0-4% w/v inulin (Inulin (I)), 0-0.2% w/v starch (Starch (S)), 0-0.1% w/v guar gum (G), and a mixture of those applying the Box-Behnken design, based on the approach achieved in step 2. The Box-Behnken design will be used to assess the dependence of gel properties to the type and concentration of polysaccharides.

To evaluate the properties of SPI-polysaccharide gels, uniaxial compression tests were carried out to identify the stress fracture point, strain fracture point, and Young's modulus, whilst also rheological tests were carried out to evaluate the frequency dependence

of storage modulus, loss modulus, and $\tan\delta$. According to the mechanical and rheological characteristics study, **SPI** gels containing only one type of polysaccharide (**SPI-2% I**, **SPI-0.1% S**, and **SPI-0.05% G**) created gels with significantly higher gel strength (higher stress fracture point), hardness (higher Young's modulus), and rigidity (higher storage modulus, as well as enhanced viscoelastic properties compared with **SPI** gels alone. Furthermore, inulin and starch may have a synergistic effect, and their combination (**SPI-4% I-0.1% S** and **SPI-2% I-0.2% S**) could be used to make gels with greater mechanical strength than **SPI** gel, however not statistically different than only **SPI** gel in terms of the viscoelastic properties. Oppositely, combining guar gum with inulin, starch, or both reduced both mechanical and viscoelastic qualities of **SPI** gel, resulting in a gel with much lower gel strength. The quadratic equation obtained from the Box-Behnken analysis revealed that the concentration of guar gum had the most significant and negative effect on the rheological and mechanical properties, which could further confirm that the presence of guar gum combined with starch or inulin is not conducive to the formation of strong gels.

As a conclusion, 0-0.2% w/v starch, 0-4% w/v inulin, or combination of both, as well as 0.05% w/v guar gum could be employed for making 0.3% w/v citric acid-induced 8% w/v **SPI** gel with higher gel strength and hardness and enhanced viscoelastic properties. The prepared gels were visually similar to the soft tofu, and might meet the need of a consumer.

6.2 Recommendations

In this study, **SPI-P** gels were created using three types of polysaccharide, starch, guar gum, and inulin, with various compositions. According to the quadratic model for the uniaxial and viscoelastic properties, there could be an optimum concentration of each polysaccharide for making **SPI** gels with the highest strength and hardness. As a result, one of the potential future works could be focusing on a narrower range of polysaccharide concentrations and determining the optimal gel composition.

Evaluating the interaction of hydrocolloids with soy protein and water could help us to have a better selection of hydrocolloids and, consequently, modify the textural properties of a gel. The gel dissolution method might be used to directly determine the types of interactions. So, another aspect of future works may be to use the gel dissolving method to quantitatively analyze the different types of interactions in **SPI-I**, **SPI-S**, **SPI-G**, and a mixture of them, compare them, and link them to their structure and functional characteristics. In this method, the gel samples could be dissolved in several buffers, most commonly phosphate buffers, containing NaCl, urea, and β -mercaptoethanol, which could disrupt electro-

static interaction, hydrogen bonding and hydrophobic interactions, and disulfide bonds, respectively. We can then determine what interactions exist and which ones predominate in each gel system by measuring the amount of protein dissolved in each buffer.

Analysis of gel microstructure could be another promising future research. Food microstructure can be defined as the spatial arrangement of the cell and the intercellular space in food material [118]. Food microstructure can influence sensory perception, oral processing, rheology, and mechanical properties of a food, which can assist manufacturers in developing their product [119]. Microstructure measurements can be performed using a variety of methods, including SEM. Conventional SEM, Variable Pressure (VP)-SEM, and Cryo-SEM are all examples of SEM. The VP-SEM and Cryo-SEM techniques could be used to analyze the microstructure of SPI gels, since they have various benefits over conventional SEM. Both VP and Cryo-SEM need fewer sample preparation steps and may provide more exact results for hydrated samples while causing less degradation and deformation, and could preserve gel samples from high vacuum.

Finally, sensory testing could be performed to use the human senses to objectively analyse foods – for properties such as taste, flavour and texture, and improving those properties to meet customer expectations.

Letters for Copyright Permission

9/2/2021 RightLink Printable License

ELSEVIER LICENSE
TERMS AND CONDITIONS

Sep 02, 2021

This Agreement between University of Waterloo – Haniye Abdi Kotdilar ("You") and Elsevier ("Elsevier") consists of your license details and the terms and conditions provided by Elsevier and Copyright Clearance Center.

License Number	5140880365496
License date	Sep 02, 2021
Licensed Content Publisher	Elsevier
Licensed Content Publication	Trends in Food Science & Technology
Licensed Content Title	Particle formation and gelation of soy milk: Effect of heat
Licensed Content Author	Xingyun Peng, Chengang Ren, Shuntang Guo
Licensed Content Date	Aug 1, 2016
Licensed Content Volume	54
Licensed Content Issue	n/a
Licensed Content Pages	10
Start Page	138
End Page	147

9/2/2021 RightLink Printable License

Type of Use	reuse in a thesis/dissertation
Portion	figures/tables/illustrations
Number of figures/tables/illustrations	2
Format	electronic
Are you the author of this Elsevier article?	No
Will you be translating?	No
Title	Analyzing the Gelation and Gelation Kinetics of Soy Gel Material
Institution name	University of Waterloo
Expected presentation date	Dec 2021
Portions	Fig. 1: Schematic of an oil body, which includes a matrix of triglyceride enclosed by a layer of phospholipids and oleosins. Fig. 5: Mechanism of soy milk gel formation
Requestor Location	University of Waterloo 280 Phillip St. Fenwick Apt. unit 518 Waterloo, ON N2L 3X1 Canada Attn: University of Waterloo
Publisher Tax ID	GB 494 6272 12
Total	0.00 CAD

Figure 6.1: The copyright permission from Copyright Clearance Center for reusing figures/tables/data from reference [42].

9/2/2021

RightLink Printable License

ELSEVIER LICENSE
TERMS AND CONDITIONS

Sep 02, 2021

This Agreement between University of Waterloo -- Haniye Abdi Kordlar ("You") and Elsevier ("Elsevier") consists of your license details and the terms and conditions provided by Elsevier and Copyright Clearance Center.

License Number 5140880643922

License date Sep 02, 2021

Licensed Content Publisher Elsevier

Licensed Content Publication Food Hydrocolloids

Licensed Content Title Soy proteins: A review on composition, aggregation and emulsification

Licensed Content Author K. Nishinari, Y. Fang, S. Guo, G.O. Phillips

Licensed Content Date Aug 1, 2014

Licensed Content Volume 39

Licensed Content Issue n/a

Licensed Content Pages 18

Start Page 301

End Page 318

9/2/2021

RightLink Printable License

Type of Use reuse in a thesis/dissertation

Portion figures/tables/illustrations

Number of figures/tables/illustrations 1

Format electronic

Are you the author of this Elsevier article? No

Will you be translating? No

Title Analyzing the Gelation and Gelation Kinetics of Soy Gel Material

Institution name University of Waterloo

Expected presentation date Dec 2021

Portions Fig. 1: Schematic diagram of glycimin molecule consisting of acidic, A, and basic, B, subunits.

Requestor Location University of Waterloo
280 Phillip St.
Fenwick Apt. unit 518
Waterloo, ON N2L 3X1
Canada
Attn: University of Waterloo

Publisher Tax ID GB 494 6272 12

Total 0.00 CAD

Figure 6.2: The copyright permission from Copyright Clearance Center for reusing figures/tables/data from reference [45].

9/4/2021 RightLink Printable License

JOHN WILEY AND SONS LICENSE
TERMS AND CONDITIONS

Sep 04, 2021

This Agreement between University of Waterloo -- Haniye Abdi Korrlar ("You") and John Wiley and Sons ("John Wiley and Sons") consists of your license details and the terms and conditions provided by John Wiley and Sons and Copyright Clearance Center.

License Number	5142221067885
License date	Sep 04, 2021
Licensed Content Publisher	John Wiley and Sons
Licensed Content Publication	JOURNAL OF THE AMERICAN OIL CHEMISTS' SOCIETY
Licensed Content Title	Current Knowledge in Soybean Composition
Licensed Content Author	Jelena Medic, Christine Atkinson, Charles R. Hurburgh
Licensed Content Date	Jan 20, 2014
Licensed Content Volume	91
Licensed Content Issue	3
Licensed Content Pages	22
Type of use	Dissertation/Thesis

9/4/2021 RightLink Printable License

Requestor type	University/Academic
Format	Electronic
Portion	Figure/table
Number of figures/tables	1
Will you be translating?	No
Title	Analyzing the Gelation and Gelation Kinetics of Soy Gel Material
Institution name	University of Waterloo
Expected presentation date	Dec 2021
Portions	Table 2: Amino acid composition for different subunits of glycinin and β -conglycinin.
Requestor Location	University of Waterloo 280 Phillip St. Fenwick Apt. unit 518 Waterloo, ON N2L 3X1 Canada Attn: University of Waterloo
Publisher Tax ID	EU826007151
Total	0.00 CAD

Figure 6.3: The copyright permission from Copyright Clearance Center for reusing figures/tables/data from reference [35].

9/2/2021	RightLink Printable License
ELSEVIER LICENSE TERMS AND CONDITIONS	
Sep 02, 2021	
<hr/>	
This Agreement between University of Waterloo – Haniye Abdi Kondlar ("You") and Elsevier ("Elsevier") consists of your license details and the terms and conditions provided by Elsevier and Copyright Clearance Center.	
License Number	5140880984046
License date	Sep 02, 2021
Licensed Content Publisher	Elsevier
Licensed Content Publication	Current Opinion in Food Science
Licensed Content Title	Heat-induced gelation of plant globulins
Licensed Content Author	Taco Nicolai, Christophe Chassenieux
Licensed Content Date	Jun 1, 2019
Licensed Content Volume	27
Licensed Content Issue	n/a
Licensed Content Pages	5
Start Page	18
End Page	22

9/2/2021	RightLink Printable License
Type of Use	reuse in a thesis/dissertation
Portion	figures/tables/illustrations
Number of figures/tables/illustrations	1
Format	electronic
Are you the author of this Elsevier article?	No
Will you be translating?	No
Title	Analyzing the Gelation and Gelation Kinetics of Soy Gel Material
Institution name	University of Waterloo
Expected presentation date	Dec 2021
Portions	Fig 1: Proposed schematic representation of four steps of gelation of SPI during heating in an aqueous environment
Requestor Location	University of Waterloo 280 Phillip St. Fenwick Apt. unit 518 Waterloo, ON N2L 3X1 Canada Attn: University of Waterloo
Publisher Tax ID	GB 494 6272 12
Total	0.00 CAD

Figure 6.4: The copyright permission from Copyright Clearance Center for reusing figures/tables/data from reference [55].

9/4/2021 <https://marketplace.copyright.com/cs-us-web/cgi/checkout/confirmation-details/?tabid33a=1aab-4c12-b690-06610430661f>

CCC Marketplace™

Order Confirmation

Thank you, your order has been placed. An email confirmation has been sent to you. Your order license details and printable licenses will be available within 24 hours. Please access Manage Account for final order details.

This is not an invoice. Please go to manage account to access your order history and invoices.

CUSTOMER INFORMATION

Payment by invoice: You can cancel your order until the invoice is generated by contacting customer service.

Billing Address	Customer Location
Haniye Abdi Kordilar University of Waterloo 518-280 Philip Street Waterloo, ON N2L 3X1 Canada +1 (519) 778-7173 haidkior@uwaterloo.ca	Mrs. Haniye Abdi Kordilar University of Waterloo 518-280 Philip Street Waterloo, ON N2L 3X1 Canada
PO Number (optional) N/A	Payment options Invoice

PENDING ORDER CONFIRMATION

Confirmation Number: Pending
Order Date: 04-Sep-2021

1. Soft matter	0.00 CAD
-----------------------	----------

Article: Salting-out and salting-in: competitive effects of salt on the aggregation behavior of soy protein particles and their emulsifying properties.

Order License ID	Pending	Publisher	ROYAL SOCIETY OF CHEMISTRY
ISSN	1744-6848	Portion	Chart/graph/table/figure
Type of Use	Republish in a thesis/dissertation		

9/4/2021 <https://marketplace.copyright.com/cs-us-web/cgi/checkout/confirmation-details/?tabid33a=1aab-4c12-b690-06610430661f>

LICENSED CONTENT

Publication Title	Soft matter	Publication Type	e-Journal
Article Title	Salting-out and salting-in: competitive effects of salt on the aggregation behavior of soy protein particles and their emulsifying properties.	Start Page	5926
		End Page	5932
		Issue	29
		Volume	11
Author/Editor	Royal Society of Chemistry (Great Britain)	URL	http://www.rsc.org/Publishing/journals/smf/index.asp
Date	06/01/2005		
Language	English		
Country	United Kingdom of Great Britain and Northern Ireland		
Rightsholder	Royal Society of Chemistry		

REQUEST DETAILS

Portion Type	Chart/graph/table/figure	Distribution	Canada
Number of charts / graphs / tables / figures requested	1	Translation	Original language of publication
Format (select all that apply)	Electronic	Copies for the disabled?	No
Who will republish the content?	Publisher, not-for-profit	Minor editing privileges?	No
Duration of Use	Current edition and up to 5 years	Incidental promotional use?	No
Lifetime Unit Quantity	Up to 499	Currency	CAD
Rights Requested	Main product		

NEW WORK DETAILS

Title	Analyzing the gelation and gelation kinetics of soy gel material	Institution name	University of Waterloo
Instructor name	Haniye Abdi Kordilar	Expected presentation date	2021-12-31

ADDITIONAL DETAILS

Order reference number	N/A	The requesting person / organization to appear on the license	Haniye Abdi Kordilar
-------------------------------	-----	--	----------------------

REUSE CONTENT DETAILS

Title, description or numeric reference of the portion(s)	Fig. 10: Schematic representation of the influence of NaCl concentration on the particle aggregation of SPI in the emulsion	Title of the article/chapter the portion is from	Salting-out and salting-in: competitive effects of salt on the aggregation behavior of soy protein particles and their emulsifying properties.
Editor of portion(s)	Xu, Hua-Neng; Liu, Yang; Zhang, Lianfu	Author of portion(s)	Xu, Hua-Neng; Liu, Yang; Zhang, Lianfu
Volume of serial or monograph	11	Issue, if republishing an article from a serial	N/A
Page or page range of portion	5931	Publication date of portion	2015-08-07

Total Items: 1 **Total Due: 0.00 CAD**

Accepted: All Publisher and CCC Terms and Conditions

Figure 6.5: The copyright permission from Copyright Clearance Center for reusing figure/tables/data from reference [54].

9/2/2021

RightLink Printable License

ELSEVIER LICENSE
TERMS AND CONDITIONS

Sep 02, 2021

This Agreement between University of Waterloo -- Haniye Abdi Kordlar ("You") and Elsevier ("Elsevier") consists of your license details and the terms and conditions provided by Elsevier and Copyright Clearance Center.

License Number	5140881450292
License date	Sep 02, 2021
Licensed Content Publisher	Elsevier
Licensed Content Publication	Trends in Food Science & Technology
Licensed Content Title	An overview on preparation of emulsion-filled gels and emulsion particulate gels
Licensed Content Author	Toktam Farjami,Ashkan Madadlou
Licensed Content Date	Apr 1, 2019
Licensed Content Volume	86
Licensed Content Issue	n/a
Licensed Content Pages	10
Start Page	85
End Page	94

9/2/2021

RightLink Printable License

Type of Use	reuse in a thesis/dissertation
Portion	figures/tables/illustrations
Number of figures/tables/illustrations	1
Format	electronic
Are you the author of this Elsevier article?	No
Will you be translating?	No
Title	Analyzing the Gelation and Gelation Kinetics of Soy Gel Material
Institution name	University of Waterloo
Expected presentation date	Dec 2021
Portions	Fig. 1: Schematic representation of two emulsion-filled gels. a) oil droplets behave as active filler particles, b) oil droplets behave as inactive filler particles
Requestor Location	University of Waterloo 280 Phillip St. Fenwick Apt. unit 518 Waterloo, ON N2L 3X1 Canada Attn: University of Waterloo
Publisher Tax ID	GB 494 6272 12
Total	0.00 CAD

Figure 6.6: The copyright permission from Copyright Clearance Center for reusing figures/tables/data from reference [69].

9/2/2021

RightLink Printable License

SPRINGER NATURE LICENSE
TERMS AND CONDITIONS

Sep 02, 2021

This Agreement between University of Waterloo -- Haniye Abdi Kordlar ("You") and Springer Nature ("Springer Nature") consists of your license details and the terms and conditions provided by Springer Nature and Copyright Clearance Center.

License Number	5140940932044
License date	Sep 02, 2021
Licensed Content Publisher	Springer Nature
Licensed Content Publication	Journal of Food Science and Technology
Licensed Content Title	Modifications of nutritional, structural, and sensory characteristics of non-dairy soy cheese analogs to improve their quality attributes
Licensed Content Author	Renda Kankanange Chaturika Jeewanthi et al
Licensed Content Date	Sep 1, 2018
Type of Use	Thesis/Dissertation
Requestor type	academic/university or research institute
Format	electronic
Portion	figures/tables/illustrations
Number of figures/tables/illustrations	1

9/2/2021

RightLink Printable License

Will you be translating?	no
Circulation/distribution	1 - 29
Author of this Springer Nature content	no
Title	Analyzing the Gelation and Gelation Kinetics of Soy Gel Material
Institution name	University of Waterloo
Expected presentation date	Dec 2021
Portions	Fig. 1: Curd formation process in soy cheese
Requestor Location	University of Waterloo 280 Phillip St. Fenwick Apt. unit 518 Waterloo, ON N2L 3X1 Canada Attn: University of Waterloo
Total	0.00 CAD

Figure 6.7: The copyright permission from Copyright Clearance Center for reusing figures/tables/data from reference [120].

9/2/2021	RightLink Printable License
ELSEVIER LICENSE TERMS AND CONDITIONS	
Sep 02, 2021	
<hr/> <hr/>	
This Agreement between University of Waterloo -- Haniye Abdi Kordlar ("You") and Elsevier ("Elsevier") consists of your license details and the terms and conditions provided by Elsevier and Copyright Clearance Center.	
License Number	5140890243877
License date	Sep 02, 2021
Licensed Content Publisher	Elsevier
Licensed Content Publication	International Dairy Journal
Licensed Content Title	Cheese analogues: a review
Licensed Content Author	Hans-Peter Bachmann
Licensed Content Date	Jul 11, 2001
Licensed Content Volume	11
Licensed Content Issue	4-7
Licensed Content Pages	11
Start Page	505
End Page	515
Type of Use	reuse in a thesis/dissertation

9/2/2021	RightLink Printable License
Portion	figures/tables/illustrations
Number of figures/tables/illustrations	1
Format	electronic
Are you the author of this Elsevier article?	No
Will you be translating?	No
Title	Analyzing the Gelation and Gelation Kinetics of Soy Gel Material
Institution name	University of Waterloo
Expected presentation date	Dec 2021
Portions	Fig. 1: Different types of cheese substitutes
Requestor Location	University of Waterloo 280 Phillip St. Fenwick Apt. unit 518 Waterloo, ON N2L 3X1 Canada Attn: University of Waterloo
Publisher Tax ID	GB 494 6272 12
Total	0.00 CAD

Figure 6.8: The copyright permission from Copyright Clearance Center for reusing figures/tables/data from reference [82].

The screenshot displays the CCC RightsLink interface. At the top, the logo 'CCC RightsLink' is visible on the left, and navigation links for Home, Help, Live Chat, and a user profile (Haniye Abdi Kordlar) are on the right. The main content area features a white box with the following information:

Rheological Characteristics and Gelation Mechanism of Tofu (Soybean Curd)
 Author: Kaoru Kohyama, Yoh Sano, Etsushiro Doi
 Publication: Journal of Agricultural and Food Chemistry
 Publisher: American Chemical Society
 Date: Jul 1, 1995
 Copyright © 1995, American Chemical Society

Below this, a section titled 'PERMISSION/LICENSE IS GRANTED FOR YOUR ORDER AT NO CHARGE' contains the following text:

This type of permission/license, instead of the standard Terms and Conditions, is sent to you because no fee is being charged for your order. Please note the following:

- Permission is granted for your request in both print and electronic formats, and translations.
- If figures and/or tables were requested, they may be adapted or used in part.
- Please print this page for your records and send a copy of it to your publisher/graduate school.
- Appropriate credit for the requested material should be given as follows: "Reprinted (adapted) with permission from (COMPLETE REFERENCE CITATION). Copyright (YEAR) American Chemical Society." Insert appropriate information in place of the capitalized words.
- One-time permission is granted only for the use specified in your RightsLink request. No additional uses are granted (such as derivative works or other editions). For any uses, please submit a new request.

If credit is given to another source for the material you requested from RightsLink, permission must be obtained from that source.

At the bottom of this section are two buttons: 'BACK' and 'CLOSE WINDOW'. The footer of the page includes copyright information: © 2021 Copyright - All Rights Reserved | Copyright Clearance Center, Inc. | Privacy statement | Terms and Conditions, and a contact email: customer@copyright.com.

Figure 6.9: The copyright permission from Copyright Clearance Center for reusing figures/tables/data from reference number [102].

9/2/2021

RightLink Printable License

ELSEVIER LICENSE
TERMS AND CONDITIONS

Sep 02, 2021

This Agreement between University of Waterloo -- Haniye Abdi Kordlar ("You") and Elsevier ("Elsevier") consists of your license details and the terms and conditions provided by Elsevier and Copyright Clearance Center.

License Number 5140890562145

License date Sep 02, 2021

Licensed Content Publisher Elsevier

Licensed Content Publication LWT - Food Science and Technology

Licensed Content Title Improvement of calcium sulfate-induced gelation of soy protein via incorporation of soy oil before and after thermal denaturation

Licensed Content Author Haibo Zhao, Bin Yu, Yacine Hemar, Jie Chen, Bo Cui

Licensed Content Date Jan 1, 2020

Licensed Content Volume 117

Licensed Content Issue n/a

Licensed Content Pages 1

Start Page 108690

End Page 0

9/2/2021

RightLink Printable License

Type of Use reuse in a thesis/dissertation

Portion figures/tables/illustrations

Number of figures/tables/illustrations 1

Format electronic

Are you the author of this Elsevier article? No

Will you be translating? No

Title Analyzing the Gelation and Gelation Kinetics of Soy Gel Material

Institution name University of Waterloo

Expected presentation date Dec 2021

Portions Fig. 3: Temperature-sweep test results for the storage modulus as a function of time containing different soy oil during CaSO₄ induced gelation at frequency of 1 Hz and strain of 1%.

Requestor Location University of Waterloo
280 Phillip St.
Fenwick Apt. unit 518
Waterloo, ON N2L 3X1
Canada
Attn: University of Waterloo

Publisher Tax ID GB 494 6272 12

Total 0.00 CAD

Figure 6.10: The copyright permission from Copyright Clearance Center for reusing figures/tables/data from reference [68].

CCC | RightsLink®

Home Help Live Chat Haniye Abdi Kordlar

Rheological study on gelation of soybean 11S protein by glucono- δ -lactone

Author: Kaoru. Kohyama, Makoto. Yoshida, Katsuyoshi. Nishinari
Publication: Journal of Agricultural and Food Chemistry
Publisher: American Chemical Society
Date: May 1, 1992

ACS Publications
Most Trusted. Most Cited. Most Read.

Copyright © 1992, American Chemical Society

PERMISSION/LICENSE IS GRANTED FOR YOUR ORDER AT NO CHARGE

This type of permission/license, instead of the standard Terms and Conditions, is sent to you because no fee is being charged for your order. Please note the following:

- Permission is granted for your request in both print and electronic formats, and translations.
- If figures and/or tables were requested, they may be adapted or used in part.
- Please print this page for your records and send a copy of it to your publisher/graduate school.
- Appropriate credit for the requested material should be given as follows: "Reprinted (adapted) with permission from {COMPLETE REFERENCE CITATION}. Copyright {YEAR} American Chemical Society." Insert appropriate information in place of the capitalized words.
- One-time permission is granted only for the use specified in your RightsLink request. No additional uses are granted (such as derivative works or other editions). For any uses, please submit a new request.

If credit is given to another source for the material you requested from RightsLink, permission must be obtained from that source.

BACK CLOSE WINDOW

© 2021 Copyright - All Rights Reserved | Copyright Clearance Center, Inc. | Privacy statement | Terms and Conditions
Comments? We would like to hear from you. E-mail us at customercare@copyright.com

Figure 6.11: The copyright permission from Copyright Clearance Center for reusing figures/tables/data from reference [101].

9/2/2021 RightLink Printable License

ELSEVIER LICENSE
TERMS AND CONDITIONS

Sep 02, 2021

This Agreement between University of Waterloo -- Haniye Abdi Kordlar ("You") and Elsevier ("Elsevier") consists of your license details and the terms and conditions provided by Elsevier and Copyright Clearance Center.

License Number	5140961472688
License date	Sep 02, 2021
Licensed Content Publisher	Elsevier
Licensed Content Publication	Food Chemistry
Licensed Content Title	Rheological and textural characteristics of black soybean tofuu (soft soybean curd) prepared with glucono- δ -lactone
Licensed Content Author	Yung-Ho Chang,Hui-Jen Su,Sy-Yu Shiao
Licensed Content Date	Jul 15, 2009
Licensed Content Volume	115
Licensed Content Issue	2
Licensed Content Pages	7
Start Page	585
End Page	591

9/2/2021 RightLink Printable License

Type of Use	reuse in a thesis/dissertation
Portion	figures/tables/illustrations
Number of figures/tables/illustrations	2
Format	electronic
Are you the author of this Elsevier article?	No
Will you be translating?	No
Title	Analyzing the Gelation and Gelation Kinetics of Soy Gel Material
Institution name	University of Waterloo
Expected presentation date	Dec 2021
Portions	Fig. 3. Temperature-dependencies of the gelation time (t ₀), the saturated storage modulus (G' sat), and rate constant (k) of tofuu prepared with 4% solids content
Requestor Location	University of Waterloo 280 Phillip St. Fenwick Apt. unit 518 Waterloo, ON N2L 3X1 Canada Attn: University of Waterloo
Publisher Tax ID	GB 494 6272 12
Total	0.00 CAD

Figure 6.12: The copyright permission from Copyright Clearance Center for reusing figures/tables/data from reference [15].

ELSEVIER LICENSE
TERMS AND CONDITIONS

Sep 02, 2021

This Agreement between University of Waterloo -- Haniye Abdi Kordlar ("You") and Elsevier ("Elsevier") consists of your license details and the terms and conditions provided by Elsevier and Copyright Clearance Center.

License Number 5140950615211

License date Sep 02, 2021

Licensed Content
Publisher ElsevierLicensed Content
Publication Journal of Food Engineering

Licensed Content Title Effect of high-pressure homogenization on gelling and rheological properties of soybean protein isolate emulsion gel

Licensed Content Author Chong-hao Bi, Peng-lin Wang, Dong-yu Sun, Zi-ming Yan, Yi Liu, Zhi-gang Huang, Fei Gao

Licensed Content Date Jul 1, 2020

Licensed Content Volume 277

Licensed Content Issue n/a

Licensed Content Pages 1

Start Page 109923

End Page 0

Type of Use reuse in a thesis/dissertation

Portion figures/tables/illustrations

Number of
figures/tables/illustrations 2

Format electronic

Are you the author of this
Elsevier article? No

Will you be translating? No

Title Analyzing the Gelation and Gelation Kinetics of Soy Gel Material

Institution name University of Waterloo

Expected presentation
date Dec 2021Portions Fig. 1: Experimental profile of G' with the time at different homogenization pressure for SPI-emulsion gel. Table 1: G' vs. k , and to for SPI-emulsion gels in different homogenization pressure with protein and oil concentration of 4.5% (w/w).Requestor Location University of Waterloo
280 Phillip St.
Fenwick Apt. unit 518Waterloo, ON N2L 3X1
Canada
Attn: University of Waterloo

Publisher Tax ID GB 494 6272 12

Total 0.00 CAD

Figure 6.13: The copyright permission from Copyright Clearance Center for reusing figures/tables/data from reference [13].

This Agreement between University of Waterloo -- Haniye Abdi Kordlar ("You") and Elsevier ("Elsevier") consists of your license details and the terms and conditions provided by Elsevier and Copyright Clearance Center.

License Number	5239010057541
License date	Jan 30, 2022
Licensed Content Publisher	Elsevier
Licensed Content Publication	Journal of Food Engineering
Licensed Content Title	Effect of freeze-thaw treatment on the structure and texture of soft and firm tofu
Licensed Content Author	Yangzi Xu, Yukun Tao, Satya Shivkumar
Licensed Content Date	Dec 1, 2016
Licensed Content Volume	190
Licensed Content Issue	n/a
Licensed Content Pages	7
Start Page	116
End Page	122

Figure 6.14: The copyright permission from Copyright Clearance Center for reusing figures/tables/data from reference [90]

This Agreement between University of Waterloo -- Haniye Abdi Kordlar ("You") and Elsevier ("Elsevier") consists of your license details and the terms and conditions provided by Elsevier and Copyright Clearance Center.

License Number	5239011132579
License date	Jan 30, 2022
Licensed Content Publisher	Elsevier
Licensed Content Publication	Elsevier Books
Licensed Content Title	Food Texture and Viscosity
Licensed Content Author	Malcolm C. Bourne
Licensed Content Date	Jan 1, 2002
Licensed Content Pages	82
Start Page	107
End Page	188
Type of Use	reuse in a thesis/dissertation
Portion	figures/tables/illustrations

Figure 6.15: The copyright permission from Copyright Clearance Center for reusing figures/tables/data from reference [87]

References

- [1] Reza Farahmandfar, M Mazaheri Tehrani, Seyed Mohammad Ali Razavi, and MB Habibi Najafi. (2011). Effect of trisodium citrate concentration and soy cheese on meltability of pizza cheese. *International Journal of Food Properties*, 14(4):697–707.
- [2] Ana N Rinaldoni, Diana R Palatnik, Noemi Zaritzky, and Mercedes E Campderros. (2014). Soft cheese-like product development enriched with soy protein concentrates. *LWT-Food Science and Technology*, 55(1):139–147.
- [3] R. K. C. Jeewanthi and H. D. Paik. (2018). Modifications of nutritional, structural, and sensory characteristics of non-dairy soy cheese analogs to improve their quality attributes. *Journal of Food Science and Technology*, 55 (11):4384–4394.
- [4] PMMI. (2013). dairy industry market assessment, industry reports. the association for packaging and processing technologies, reston, va.
- [5] Jeelani Raja, Hillal A Punoo, and Farooq A Masoodi. (2014). Comparative study of soy paneer prepared from soymilk, blends of soymilk and skimmed milk. *Journal of Food Process Technology*, 5(301):2.
- [6] Bahareh Hajirostamloo and P Mahastie. Comparison of nutritional and chemical parameters of soymilk and cow milk. (2009). *World Academy of Science, Engineering and Technology*, 57(9):436–438.
- [7] N. Murekatete, Y. F. Hua, M. V. M Chamba, O. Djakpo, and C. M. Zhang. (2014). Gelation behavior and rheological properties of salt or acid-induced soy proteins soft tofu-type gels. *Journal of Texture Study*, 45:62–73.
- [8] Wendy MY Lo, Edward R Farnworth, and Eunice CY Li-Chan. (2006). Angiotensin i-converting enzyme inhibitory activity of soy protein digests in a dynamic model system simulating the upper gastrointestinal tract. *Journal of Food Science*, 71(3):S231–S237.

- [9] F-H. Cao, X-J. Li, S-Z. Luo, D-D. Mu, X-Y. Zhong, S-T. Jiang, Z. Zheng, and Y-Y. Zhao. (2017). Effects of organic acid coagulants on the physical properties of and chemical interactions in tofu. *LWT-Food Science and Technology*, 85:58–65.
- [10] Ramy M Khoder, Tao Yin, Ru Liu, Shanbai Xiong, Juan You, Yang Hu, and Qilin Huang. (2020). Effects of nano fish bone on gelling properties of tofu gel coagulated by citric acid. *Food Chemistry*, 332:127401.
- [11] X. Wang, K. Luo, S. Liu, B. Adhikari, and J. Chen. (2006). Improvement of gelation properties of soy protein isolate emulsion induced by calcium cooperated with magnesium. *Journal of Food Engineering*, 244:32–39.
- [12] N. Murekatete, C. Zhang, J. Hategekimana, E. Karangwa, and Y. Hua. (2016). Soybean oil volume fraction effects on the rheology characteristics and gelation behavior of glucono-delta-lactone and calcium sulfate-induced tofu gels. *Journal of Texture Studies*, 47:112–130.
- [13] C. h. Bi, P. l. Wang, D. y. Sun, Z. m. Yan, Y. Liu, Z. g. Huang, and F. Gao. (2020). Effect of high-pressure homogenization on gelling and rheological properties of soybean protein isolate emulsion gel. *Journal Food Engineering*, 109923.
- [14] J. Zhang, L. Liang, Z. Tian, L. Chen, and M. Subirade. (2012). Preparation and in vitro evaluation of calcium-induced soy protein isolate nanoparticles and their formation mechanism study. *Food Chemistry*, 133:390–399.
- [15] Y. H. Chang, H. J Su, and S. Y. Shiau. (2009). Rheological and textural characteristics of black soybean touhua (soft soybean curd) prepared with glucono-d-lactone. *Food Chemistry*, 115:585–591.
- [16] Lulu Chu, Licong Yang, Jingen Li, Lezhen Lin, and Guodong Zheng. (2019). Effect of smilax china l. starch on the gel properties and interactions of calcium sulfate-induced soy protein isolate gel. *International Journal of Biological Macromolecules*, 135:127–132.
- [17] Yen-Chang Tseng and Youling L Xiong. (2009). Effect of inulin on the rheological properties of silken tofu coagulated with glucono- δ -lactone. *Journal of Food Engineering*, 90(4):511–516.
- [18] Yuan-yuan Chang, Dong Li, Li-jun Wang, Chong-hao Bi, and Benu Adhikari. (2014). Effect of gums on the rheological characteristics and microstructure of acid-induced spi-gum mixed gels. *Carbohydrate Polymers*, 108:183–191.

- [19] T. Wüstenberg. (2015). General overview of food hydrocolloids. *Cellulose and Cellulose Derivatives in the Food Industry Fundamentals and Applications*; Wüstenberg, T., Ed, pages 1–68.
- [20] Qingqing Xu, Baokun Qi, Lu Han, Diqiong Wang, Shuang Zhang, Lianzhou Jiang, Fengying Xie, and Yang Li. (2021). Study on the gel properties, interactions, and ph stability of pea protein isolate emulsion gels as influenced by inulin. *LWT- Food Science and Technology*, 137:110421.
- [21] Andrew J Gravelle, Shai Barbut, and Alejandro G Marangoni. (2017). Food-grade filler particles as an alternative method to modify the texture and stability of myofibrillar gels. *Scientific Reports*, 7(1):1–16.
- [22] Mathias Johansson, Epameinondas Xanthakis, Maud Langton, Carolin Menzel, Francisco Vilaplana, Daniel P Johansson, and Patricia Lopez-Sanchez. (2021). Mixed legume systems of pea protein and unrefined lentil fraction: Textural properties and microstructure. *LWT- Food Science and Technology*, 144:111212.
- [23] Ángela Bravo-Núñez, Raquel Garzón, Cristina M Rosell, and Manuel Gómez. (2019). Evaluation of starch–protein interactions as a function of ph. *Foods*, 8(5):155.
- [24] Zhong-Qing Jiang, Jing Wang, Frederick Stoddard, Hannu Salovaara, and Tuula Sontag-Strohm. (2020). Preparation and characterization of emulsion gels from whole faba bean flour. *Foods*, 9(6):755.
- [25] Mahdiyar Shahbazi, Henry Jäger, Jianshe Chen, and Rammile Ettelaie. (2021). Construction of 3d printed reduced-fat meat analogue by emulsion gels. part ii: Printing performance, thermal, tribological, and dynamic sensory characterization of printed objects. *Food Hydrocolloids*, 121:107054.
- [26] Carla Arancibia, Sara Bayarri, and Elvira Costell. (2015). Effect of hydrocolloid on rheology and microstructure of high-protein soy desserts. *Journal of Food Science and Technology*, 52(10):6435–6444.
- [27] Meng Li, Fusheng Chen, Bao Yang, Shaojuan Lai, Hongshun Yang, Kunlun Liu, Guanhao Bu, Caili Fu, and Yun Deng. (2015). Preparation of organic tofu using organic compatible magnesium chloride incorporated with polysaccharide coagulants. *Food Chemistry*, 167:168–174.

- [28] Yanting Shen and Yonghui Li. (2021). Acylation modification and/or guar gum conjugation enhanced functional properties of pea protein isolate. *Food Hydrocolloids*, 117:106686.
- [29] Paweł Glibowski and Anna Bukowska. (2011). The effect of pH, temperature and heating time on inulin chemical stability. *Acta Scientiarum Polonorum Technologia Alimentaria*, 10(2):189–196.
- [30] Alan Imeson. (2011). *Food stabilisers, thickeners and gelling agents*. John Wiley & Sons.
- [31] Ho-Kyung Ha, Na-Eun Jeon, Jin Wook Kim, Kyoung-Sik Han, Sung Seob Yun, Mee-Ryung Lee, and Won-Jae Lee. (2016). Physicochemical characterization and potential prebiotic effect of whey protein isolate/inulin nano complex. *Korean Journal for Food Science of Animal Resources*, 36(2):267.
- [32] PJ Hennelly, PG Dunne, M O’sullivan, and ED O’riordan. (2006). Textural, rheological and microstructural properties of imitation cheese containing inulin. *Journal of Food Engineering*, 75(3):388–395.
- [33] Emiliane A Araújo, Antônio F de Carvalho, Eliana S Leandro, Mauro M Furtado, and Célia A de Moraes. (2010). Development of a symbiotic cottage cheese added with lactobacillus delbrueckii ufv h2b20 and inulin. *Journal of Functional Foods*, 2(1):85–89.
- [34] Talina Vanessa Nieto-Nieto, Yi Xiang Wang, Lech Ozimek, and Lingyun Chen. (2015). Inulin at low concentrations significantly improves the gelling properties of oat protein—a molecular mechanism study. *Food Hydrocolloids*, 50:116–127.
- [35] J. Medic, C. Atkinson, and C.R. Hurburgh. (2014). Current knowledge in soybean composition. *Journal of the American Oil Chemists’ Society*, 91:363–384.
- [36] Lawrence A Johnson. (2008). Oil recovery from soybeans. In *Soybeans*, pages 331–375. Elsevier.
- [37] A Garcia Serrato. (1981). Extraction of oil from soybeans. *Journal of the American Oil Chemists’ Society*, 58(3Part1):157–159.
- [38] X. Gu, L. J. Campbell, and S. R. Euston. (2009). Effects of different oils on the properties of soy protein isolate emulsions and gels. *Food Research International*, 42:925–932.

- [39] S. Guatam, B. Sharma, and P. Jain. (2020). Green natural protein isolate based composites and nanocomposites: A review. *Polymer Testing*, 106626.
- [40] Jobie Kirkwood, David Hargreaves, Simon O’Keefe, and Julie Wilson. (2015). Using isoelectric point to determine the ph for initial protein crystallization trials. *Bioinformatics*, 31(9):1444–1451.
- [41] M. Guo. (2009). *Functional Foods: Principles and Technology*. CRC Press, Woodhead, Cambridge, UK. 358 p.
- [42] X. Peng, C. Ren, and S. Guo. (2016). Particle formation and gelation of soymilk: Effect of heat. *Trends in Food Science and Technology*, 54:138–147.
- [43] Hari B Krishnan. (2000). Biochemistry and molecular biology of soybean seed storage proteins. *Journal of New Seeds*, 2(3):1–25.
- [44] E Derbyshire, DJ Wright, and D. Boulter. (1976). Legumin and vicilin, storage proteins of legume seeds. *Phytochemistry*, 15(1):3–24.
- [45] K. Nishinari, Y. Fang, S. Guo, and G. O. Phillips. (2014). Soy proteins: A review on composition, aggregation and emulsification. *Food Hydrocolloids*, 39:301–318.
- [46] F. A. Perrechil, V. A. Ramos, and R. L. Cunha. (2015). Synergistic functionality of soybean 7s and 11s fractions in oil-in-water emulsions: Effect of protein heat treatment. *International Journal of Food Properties*, 18(11):2593–2602.
- [47] Raj Rajagopalan and Paul C Hiemenz. (1997). Principles of colloid and surface chemistry. *Marcel Dekker, New-York*, 8247:8.
- [48] C. Liu, X. Q. Yang, M. G. Lin, R. Y. Zhao, C. H. Tang, L. Luo, and L. Liu. (2011). Complex coacervation of chitosan and soy globulins in aqueous solution: a electrophoretic mobility and light scattering study. *International Journal of Food Science and Technology*, 46 (7):1363–1369.
- [49] S. Y. Hsia, Y. H. Hsiao, W. T Li, and J. F. Hsieh. (2016). Aggregation of soy protein isoflavone complexes and gel formation induced by glucono- δ -lactone in soymilk. *Scientific Reports*, 6:35718.
- [50] D. B. Yuan, W. Min, X. Q. Yang, C. H. Tang, K. L. Huang, J. Guo, J. M. Wang, N. N. Wu, H. G. Zheng, and J. R. Qi. (2010). An improved isolation method of soy β -conglycinin subunits and their characterization. *Journal of the American Oil Chemists’ Society*, 87:997–1004.

- [51] L. J. Campbell, X. Gu, S. J. Dewar, and S. R. Euston. (2009). Effects of heat treatment and glucono- δ -lactone-induced acidification on characteristics of soy protein isolate. *Food Hydrocolloids*, 23:344–351.
- [52] N. Chen, M. Zhao, F. Niepceron, T. Nicolai, and C. Chassenieux. (2017). The effect of the ph on thermal aggregation and gelation of soy proteins. *Food Hydrocolloids*, 66:27–36.
- [53] N. Chen, M. Zhao, C. Chassenieux, and T. Nicolai. (2017). The effect of adding *nacl* on thermal aggregation and gelation of soy protein isolate. *Food Hydrocolloids*, 70:88–95.
- [54] H. Xu, Y. Liu, and L. Zhang. (2015). Salting-out and salting-in: competitive effects of salt on the aggregation behavior of soy protein particles and their emulsifying properties. *Soft Matter*, 11:5926–5932.
- [55] T. Nicolai and C. Chassenieux. (2019). Heat-induced gelation of plant globulins. *Current Opinion in Food Science*, 27:18–22.
- [56] C. Ren, L. Tang, M. Zhang, and S. Guo. (2009). Structural characterization of heat-induced protein particles in soy milk. *Journal of Agricultural and Food Chemistry*, 57:1921–1926.
- [57] H. Zhao, W. Li, F. Qin, and J. Chen. (2016). Calcium sulphate induced soya bean protein tofu-type gels: influence of denaturation and particle size. *International Journal of Food Science and Technology*, 51:731–741.
- [58] J. Guo, X. Q. Yang, X. T. He, N. N. Wu, J. M. Wang, W. Gu, and Y. Y. Zhang. (2012). Limited aggregation behavior of β -conglycinin and its terminating effect on glycinin aggregation during heating at ph 7.0. *Journal of Agricultural and Food Chemistry*, 60:3782–3791.
- [59] X. T. He, D. B. Yuan, J. M. Wang, and X. Q. Yang. (2016). Thermal aggregation behaviours of soy protein: Characteristics of different polypeptides and subunits. *Journal of the Science of Food and Agriculture*, 96:1121–1131.
- [60] G. Shun-Tang, T. Ono, and M. Mikami. (1999). Incorporation of soy milk lipid into protein coagulum by addition of calcium chloride. *Journal of Agriculture Food Chemistry*, 47:901–905.

- [61] S. L. Tay, H. Y. Tan, and C. Perera. (2006). The coagulating effects of cations and anions on soy protein. *International Journal of Food Properties*, 9:317–323.
- [62] E. Dickinson. (2012). Emulsion gels: The structuring of soft solids with protein-stabilized oil droplets. *Food Hydrocolloids*, 28(1):224–241.
- [63] M. Zhang, P. Wang, M. Zou, R. Yang, M. Tian, and Z. Gu. (2019). Microbial transglutaminase-modified protein network and its importance in enhancing the quality of high-fiber tofu with okara. *Food Chemistry*, 289:169–176.
- [64] X. S. Qin, S. S. Chen, X. J. Li, S. Z. Luo, X. Y. Zhong, S. T. Jiang, Y. Y Zhao, and Z. Zheng. (2017). Gelation properties of transglutaminase-induced soy protein isolate and wheat gluten mixture with ultrahigh pressure pretreatment. *Food and Bioprocess Technology*, 10 (5):866–874.
- [65] C. H. Tang, H. Wu, H. P. Yu, L. Lin, Z. Chen, and X. Q. Yang. (2006). Coagulation and gelation of native soy protein isolates induced by microbial transglutaminase. *Journal of Food Biochemistry*, 30:35–55.
- [66] C. Tang, L. Li, J. Wang, and X. Yang. (2007). Formation and rheological properties of ‘cold-set’tofu induced by microbial transglutaminase. *LWT-Food Science and Technology*, 40 (4):579–586.
- [67] CHANTAL R STAMPANONI and AC Noble. (1991). The influence of fat, acid, and salt on the temporal perception of firmness, saltiness, and sourness of cheese analogs. *Journal of Texture Studies*, 22(4):381–392.
- [68] H. Zhao, B. Yu, Y. Hemar, J. Chen, and B. Cui. (2020). Improvement of calcium sulfate-induced gelation of soy protein via incorporation of soy oil before and after thermal denaturation. *LWT-Food Science and Technology*, 117:108690.
- [69] T. Farjami and A. Madadlou. (2019). An overview on preparation of emulsion-filled gels and emulsion particulate gels. *Trends in Food Science and Technology*, 86:85–94.
- [70] L Yang. (2015). Fundamentals of nanotechnology and orthopedic materials. *Nanotechnology-Enhanced Orthopedic Materials; Elsevier BV: Amsterdam, The Netherlands*, pages 1–25.
- [71] G. O. Phillips and P. A. Williams. (2009). *Handbook of Hydrocolloids (2nd Edition)*. Woodhead Publishing.

- [72] VE Sánchez, GB Bartholomai, and AMR Pilosof. (1995). Rheological properties of food gums as related to their water binding capacity and to soy protein interaction. *LWT-Food Science and Technology*, 28(4):380–385.
- [73] Y-C Tseng, YL Xiong, and WL Boatright. (2008). Effects of inulin/oligofructose on the thermal stability and acid-induced gelation of soy proteins. *Journal of Food Science*, 73(2):E44–E50.
- [74] Canadian dairy information centre. national dairy code, 2005 - part ii and iii. [https://agriculture.canada.ca/sites/default/files/legacy/resources/prod/dairy/pdf/National_Dairy_Code_Part_II-III_\(2005\)_e.pdf](https://agriculture.canada.ca/sites/default/files/legacy/resources/prod/dairy/pdf/National_Dairy_Code_Part_II-III_(2005)_e.pdf).
- [75] M. Alinovi and G. Mucchetti. (2020). Effect of freezing and thawing processes on high-moisture mozzarella cheese rheological and physical properties. *LWT-Food Science and Technology*, 124:109137.
- [76] AK Chawla, S Singh, and SK Kanawjia. (1985). Development of low fat paneer. *Indian Journal of Dairy Science*.
- [77] AK Chawla, S Singh, and SK Kanawjia. (1987). Effect of fat levels, additives and process modifications on composition and quality of paneer and whey. *Asian Journal of Dairy Research*, 6(2):87–92.
- [78] M Ashraf Pal and PL Yadav. (1991). Effect of blending buffalo and cow milk on the physico-chemical and sensory quality of paneer. *Indian Journal of Dairy Science*, 44:327–327.
- [79] Shahnawaz Umer Khan, Mohammad Ashraf Pal, Sarfaraz Ahmad Wani, and Mir Salahuddin. (2014). Effect of different coagulants at varying strengths on the quality of paneer made from reconstituted milk. *Journal of Food Science and Technology*, 51(3):565–570.
- [80] DC Bhattacharya, ON Mathur, MR Srinivasan, and O Samlik. (1971). Studies on the method of production and shelf life of paneer (cooking type of acid coagulated cottage cheese). *Journal of Food Science and Technology (Mysore)*.
- [81] G. K. Deshwal, R. Ameta, H. Sharma, A. K. Singh, N. R. Panjagari, and B. Baria. (2020). Effect of ultrafiltration and fat content on chemical, functional, textural and sensory characteristics of goat milk-based halloumi type cheese. *LWT-Food Science and Technology*, 126:109341.

- [82] H. P. Bachman. (2001). Cheese analogues: a review. *International Dairy Journal*, 11:505–515.
- [83] S Kumar and YK Jha. (1997). Soymilk substitution on quality attributes of mozzarella cheese made from buffalo milk. *Journal of Food Science and Technology (Mysore)*, 34(2):113–118.
- [84] Renda Kankanamge Chaturika Jeewanthi, Na-Kyoung Lee, Kyung Ah Lee, Yoh Chang Yoon, and Hyun-Dong Paik. (2015). Comparative analysis of improved soy-mozzarella cheeses made of ultrafiltrated and partly skimmed soy blends with other mozzarella types. *Journal of Food Science and Technology*, 52(8):5172–5179.
- [85] K Gaan, S Dabir, E Ignaszewski, N Manu, S Murray, and Z Weston. (2020). State of the industry report: Plant-based meat, eggs, and dairy.
- [86] Tonávan Vliet et al. (1995). Large deformation and fracture behaviour of gels. *Faraday Discussions*, 101:359–370.
- [87] Malcolm Bourne (2002). *Food texture and viscosity: concept and measurement*. Elsevier.
- [88] Jun KangII, Yasuki Matsumura, and Tomohiko Mori. (1991). Characterization of texture and mechanical properties of heat-induced soy protein gels. *Journal of the American Oil Chemists' Society*, 68(5):339–345.
- [89] Jian Guo, Yong-Chuang Liu, Xiao-Quan Yang, Yu-Cong Jin, Shu-Juan Yu, Jin-Mei Wang, Jun-Jie Hou, and Shou-Wei Yin. (2014). Fabrication of edible gellan gum/soy protein ionic-covalent entanglement gels with diverse mechanical and oral processing properties. *Food Research International*, 62:917–925.
- [90] Yangzi Xu, Yukun Tao, and Satya Shivkumar. (2016). Effect of freeze-thaw treatment on the structure and texture of soft and firm tofu. *Journal of Food Engineering*, 190:116–122.
- [91] Nicolaas Westerhof, Nikolaos Stergiopoulos, Mark IM Noble, and Berend E Westerhof. (2019). Elasticity. In *Snapshots of Hemodynamics*, pages 57–64. Springer.
- [92] Wenceslao Canet, M Dolores Álvarez, and MJ Gil. (2007). Fracture behaviour of potato samples (cv. desiree) under uniaxial compression. *Journal of Food Engineering*, 82(4):427–435.

- [93] Peineng Zhu, Weijuan Huang, and Lingyun Chen. (2022). Develop and characterize thermally reversible transparent gels from pea protein isolate and study the gel formation mechanisms. *Food Hydrocolloids*, 125:107373.
- [94] Qi-Hui Chen, Xiao-Yin Li, Chun-Lan Huang, Peng Liu, Qing-Zhu Zeng, Xin-Quan Yang, and Yang Yuan. (2021). Development and mechanical properties of soy protein isolate-chitin nanofibers complex gel: The role of high-pressure homogenization. *LWT*, 150:112090.
- [95] Haibo Zhao, Jie Chen, Yacine Hemar, and Bo Cui. (2020). Improvement of the rheological and textural properties of calcium sulfate-induced soy protein isolate gels by the incorporation of different polysaccharides. *Food Chemistry*, 310:125983.
- [96] Takahiro Funami. (2011). Next target for food hydrocolloid studies: Texture design of foods using hydrocolloid technology. *Food Hydrocolloids*, 25(8):1904–1914.
- [97] TA Instruments Germany A. Franck. Viscoelasticity and dynamic mechanical testing. http://tainstruments.com/pdf/literature/AAN004_Viscoelasticity_and_DMA.pdf.
- [98] L. J. Struble and X. Ji. (2001). *Rheology. Handbook of Analytical Techniques in Concrete Science and Technology*.
- [99] Shinya Ikeda and Katsuyoshi Nishinari. (2001). Weak gel-type rheological properties of aqueous dispersions of nonaggregated κ -carrageenan helices. *Journal of Agricultural and Food Chemistry*, 49(9):4436–4441.
- [100] TA Instruments. Understanding rheology of structured fluids. http://www.tainstruments.com/pdf/literature/AAN016_V1_U_StructFluids.pdf.
- [101] K. Kohyama, M. Yoshida, and K. Nishinari. (1992). Rheological study on gelation of soybean 11s proteins by glucono-delta-lactone. *Journal of Agricultural and Food Chemistry*, 40:740–744.
- [102] K. Kohyama, Y. Sano, and E. Doi. (1995). Rheological characteristics and gelation mechanism of tofu (soybean curd). *Journal of Agriculture Food Chemistry*, 43:1808–12.
- [103] Yan-Yan Zhao, Feng-Hong Cao, Xing-Jiang Li, Dong-Dong Mu, Xi-Yang Zhong, Shao-Tong Jiang, Zhi Zheng, and Shui-Zhong Luo. (2020). Effects of different salts on the gelation behaviour and mechanical properties of citric acid-induced tofu. *International Journal of Food Science and Technology*, 55(2):785–794.

- [104] Z. Xi, W. Liu, D. J. McClements, and L. Zou. (2019). Rheological, structural, and microstructural properties of ethanol induced cold-set whey protein emulsion gels: Effect of oil content. *Food Chemistry*, 291:22–29.
- [105] Sangseok Lee and Dong Kyu Lee. (2018). What is the proper way to apply the multiple comparison test? *Korean Journal of Anesthesiology*, 71(5):353.
- [106] Dave J Saville. (1990). Multiple comparison procedures: the practical solution. *The American Statistician*, 44(2):174–180.
- [107] Mary L McHugh. (2011). Multiple comparison analysis testing in anova. *Biochemia medica*, 21(3):203–209.
- [108] Paulina Zheng. (2018). An overview of methods to address the multiple comparison problem. *Towards Data Science, Toronto, ON*.
- [109] Webplotdigitizer. <https://apps.automeris.io/wpd/>.
- [110] D. W. Ningtyas, B. Tam, B. Bhandari, and S. Prakash. (2021). Effect of different types and concentrations of fat on the physico-chemical properties of soy protein isolate gel. *Food Hydrocolloids*, 111:106226.
- [111] VD Truong and CR Daubert. (2000). Comparative study of large strain methods for assessing failure characteristics of selected food gels. *Journal of Texture Studies*, 31(3):335–353.
- [112] María Dolores Alvarez and Wenceslao Canet. (2013). Dynamic viscoelastic behavior of vegetable-based infant purees. *Journal of Texture Studies*, 44(3):205–224.
- [113] Igor Krupa, Tomáš Nedelčev, Dušan Račko, and Igor Lacík. (2010). Mechanical properties of silica hydrogels prepared and aged at physiological conditions: testing in the compression mode. *Journal of Sol-Gel Science and Technology*, 53(1):107–114.
- [114] Takao Nagano, Eri Tamaki, and Takahiro Funami. (2008). Influence of guar gum on granule morphologies and rheological properties of maize starch. *Carbohydrate Polymers*, 72(1):95–101.
- [115] Yayuan Zhang, Zhengbiao Gu, Ling Zhu, and Yan Hong. (2018). Comparative study on the interaction between native corn starch and different hydrocolloids during gelatinization. *International Journal of Biological Macromolecules*, 116:136–143.

- [116] Steffen Beccard, Jörg Bernard, Rudy Wouters, Karin Gehrich, Birgitta Zielbauer, Markus Mezger, and Thomas A Vilgis. (2019). Alteration of the structural properties of inulin gels. *Food Hydrocolloids*, 89:302–310.
- [117] Thais C Brito-Oliveira, Ana Clara M Cavini, Leticia S Ferreira, Izabel CF Moraes, and Samantha C Pinho. (2020). Microstructural and rheological characterization of nacl-induced gels of soy protein isolate and the effects of incorporating different galactomannans. *Food Structure*, 26:100158.
- [118] Jose Miguel Aguilera. (2005). why food microstructure? *Journal of Food Engineering*, 67(1-2):3–11.
- [119] Xinmiao Wang and Jianshe Chen. (2019). food sensory perception influenced by structure and/or food–saliva interactions.
- [120] R. K. C. Jeewanthi, N. K. Lee, K. A. Lee, Y. C. Yoon, and H. D. Paik. (2015). Comparative analysis of improved soy-mozzarella cheeses made of ultrafiltrated and partly skimmed soy blends with other mozzarella types. *Journal of Food Science and Technology*, 52 (8):5172–5179.

APPENDICES

Appendix A

A.1 Calculation of Stress, Strain, and Young Modulus

The stress value at each time ($\sigma(t)$) can be calculated by knowing the force ($F(t)$) and surface area ($A(t)$) in each time:

$$\sigma(t) = \frac{F(t)}{A(t)},$$

By considering the initial surface area, A_0 , we have:

$$\sigma(t) = \frac{F(t)}{A(t)} = \frac{F(t)}{A(t)} \times \frac{A_0}{A_0} = \frac{F(t)}{A_0} \times \frac{A_0}{A(t)}, \quad (1.1)$$

Considering the constant volume for our shape during the compression process:

$$\begin{aligned} V_0 &= V_t \\ A_0 \times l_0 &= A(t) \times l(t) \\ \frac{A_0}{A_t} &= \frac{l(t)}{l_0}, \end{aligned} \quad (1.2)$$

Where A_0 and l_0 are the initial surface area and initial shape height, respectively. By applying equation 1.2 into equation 1.1, we will have:

$$\sigma(t) = \frac{F(t)}{A_0} \times \frac{A_0}{A(t)} = \frac{F(t)}{A_0} \times \frac{l(t)}{l_0},$$

$$\sigma(t) = \frac{F(t)}{A_0} \times \frac{l(t)}{l_0}, \quad (1.3)$$

The strain value at each time ($\epsilon(t)$) can be calculated by knowing the displacement ($\Delta l(t)$) and the initial shape height (l_0) in each time:

$$\begin{aligned} \Delta\epsilon(t) &= \frac{\Delta l(t)}{l_0} \\ d\epsilon &= \frac{dl}{l_0} \\ \int d\epsilon &= \int \frac{dl}{l_0} = \ln\left(\frac{l(t)}{l_0}\right), \\ l(t) &= l_0 - \Delta l(t) \end{aligned} \quad (1.4)$$

Using equation 1.3 and 1.4, we can calculate the stress, $\sigma(t)$, and strain, $\epsilon(t)$, values at each time by having Force, $F(t)$, displacement, $\Delta l(t)$, and initial height, l_0 .

Now, by calculating the stress and strain values, the stress-strain curve could be obtained (Figure A.1). The fracture point is the point of strain where the material physically separates. At this point, the strain reaches its maximum value and the material actually fractures. Young's modulus was estimated using two different strain regions: 1) calculating the slope of a linear region of a curve in a strain range of 0.2-0.3, and 2) calculating the slope of a curve located between 1/3 and 2/3 of the way to the point of maximum stress [92]. For this purpose, the data obtained from the measurement and calculations using Equation 1.3 and 1.4 were used as the experimental data. In the "Data analysis" toolbar of Excel, by selecting the "Regression", and then choosing the calculated strain as a "input X" and the calculated stress as a "input Y", the Young's modulus was obtained for each sets of data.

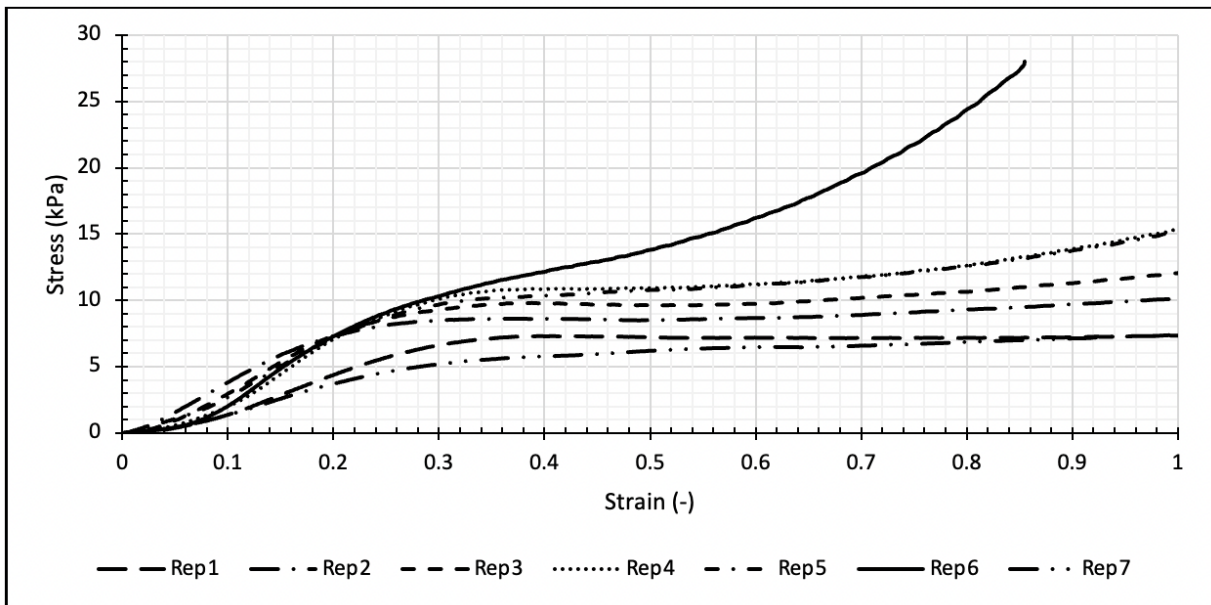


Figure A.1: The stress-strain curve for replicate 2 of control sample. The stress and strain fracture points are shown with long dash line, and the Young's modulus could be calculated as a slope of a linear part of a curve before fracture (short dash line).